UNIVERSITY OF
CAMBRIDGE

Biofuels & Atmospheric Chemistry:

What can a global model tell us about our future decisions?

Rachel Catherine Pike
Emmanuel College

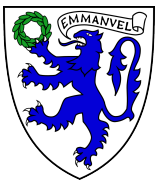

This dissertation is submitted for the degree of Doctor of Philosophy

Declaration

This dissertation is the result of my own work and includes nothing which is the outcome of work done in collaboration except where specifically indicated in the text.

This dissertation has not been submitted, in whole or in part, for any other degree, diploma or other qualification at any other university, and is less than 60,000 words in length.

Rachel Pike

December 2009

Abstract

Biofuels & Atmospheric Chemistry:
What can a global model tell us about our future decisions?

Rachel Pike
Emmanuel College, University of Cambridge

Biomass energy is the oldest form of energy harnessed by humans. Currently, processed biofuels, which are derived from biomass, are being pursued as a possible route to decarbonize the transport sector—a particularly difficult task for both technological and sociological reasons. In this thesis I explore the impacts that large scale biofuel use could have on atmospheric chemistry.

I review the current state of biofuels politically and technologically, focusing on ethanol and biodiesel. I discuss the salient features of tropospheric chemistry and in particular the oxidation of isoprene, an important biogenic volatile organic compound. I examine the impact that including isoprene oxidation has in a new chemistry-climate computer model, UKCA; the response of ozone turns out to depend on local chemical conditions. To evaluate the global model, I use data from the OP3 field campaign in Malaysia and compare it with output from the model chemical mechanism. The mechanism is able to reproduce $\mathrm{NO_x}$ and ozone measurements well, though is more sensitive to representations of physical rather than chemical processes. I also perform a simple sensitivity study which examines crop changes in the region of Southeast Asia.

In the final two chapters, I turn to two distinct phases of the biofuel life cycle. I characterize a potential future atmosphere through an ozone attribution study, then examine the impact of future cropland expansion (phase I of a biofuel life cycle) on tropospheric chemistry. I find that land use change has a large impact on ozone, and that it is more acute than another perturbation ($\mathrm{CO_2}$ suppression) to isoprene emissions. I then move to phase III of the life cycle—combustion—and look at the sensitivity of the model chemistry to surface transport emissions from biofuels as a replacement for conventional fuels. I find that biodiesel reduces surface ozone, while ethanol increases it, and that the response has both a linear and nonlinear component.

Acknowledgments

Writing a PhD is an intense and solitary process. Without the support of colleagues, friends, and family, I'm not sure how anyone finishes one of these things.

I have first to thank Professor John Pyle for his guidance and advice over the last three years; I couldn't have asked for a better supervisor. Thank you to Paul Young, for humoring (humouring?) countless questions; he actually taught me how a global model works, what isoprene is, and how to design a set of experiments. To G6 members, past and present, thank you for debugging advice and office olympics. I owe a particular note of gratitude to Luke Abraham for his help with UKCA. Thank you to Juliette Lathière for collaborating on the isoprene crop experiments, and for being enthusiastic throughout the process. I need to acknowledge James Lee for his patience with the box model work, and to say that the entire OP3 team are fantastic. We all miss Kate Furneaux; may she be in peace.

Thank you to the Gates Trust for funding.

I had a number of moments of panic while writing, and I am desperately grateful to my friends in Cambridge for rescuing me from myself. Thank you to my friends at Emma, fellow Gates Scholars, the residents of Earl Street, and a certain northeastern chemist. To my friends further away: some of those phone calls were the best distraction I could have asked for—thank you. Finally, to my family: Mom, Dad, and Max. This PhD would never have been submitted without occasional respite in California and many phone calls around the world. I love you.

Rachel Pike
December 2009

for granny

Contents

List of Figures

List of Tables

Acronyms, Abbreviations & Symbols

BD20	A fuel blend of 20% biodiesel and 80% conventional diesel
BD100	100% biodiesel fuel
BL	Boundary layer
BVOC	Biogenic volatile organic compound
CCM	Climate composition model
DGVM	Dynamic global vegetation model
DM8H	Daily 8-hour ozone maximum
E85	A fuel blend of 85% ethanol and 15% petrol
ETS	Emissions trading scheme
GCM	General circulation model
GHG	Greenhouse gas
HDV	Heavy duty vehicle
IPCC	Intergovernmental Panel on Climate Change
LCA	Life cycle assessment
LDV	Light duty vehicle
MIM	Mainz isoprene mechanism [*Pöschl et al.*, 2000]
NO_x	Nitrogen oxides = NO + NO_2
OP3	Oxidation and Particle Photochemical Processes; a NERC-funded field campaign
PAN	Peroxyacyl nitrate
PAR	Photosynthetically active radiation
PFT	Plant functional type
SOA	Secondary organic aerosol
SST	Sea surface temperature
STE	Stratosphere-troposphere exchange
Tg	Teragram (= 1 x 10^{12} g)
UKCA	United Kingdom Chemistry & Aerosol Model (a CCM)
UNFCCC	United Nations Framework Convention on Climate Change
VOC	Volatile organic compound

h	Planck's constant
λ	Wavelength
ν	Frequency

Prologue

Biofuels could form an important part of our future energy supply. Although the impact of biofuels on the carbon budget and greenhouse gas emissions has been previously studied, the air quality implications of large scale biofuel use have not yet been well characterized. The goal of this thesis is to explore some of the potential feedbacks between biofuels and tropospheric chemistry, and to address this question, I use the concept of a life cycle assessment and a new global climate composition computer model. A model is a good place to test the sensitivities of the system before any sweeping decisions are made.

In **Chapter 1**, I describe the political agreements which relate to decarbonization and fuel standards, the Earth's potential to grow biomass, and state of technology in biofuel growth and production. I also introduce the concept of a life cycle assessment, and posit some types of emissions that could impact the atmosphere. Due to its climatic, health, and chemical importance, I examine ozone frequently throughout the thesis, and in **Chapter 2** the chemistry of ozone production and destruction is introduced. I also spend parts of further chapters examining the impact of isoprene (an important biogenic volatile organic compound) emissions on tropospheric chemistry, so the background to isoprene emission, chemistry, and global flux estimation is also included.

Chapter 3 is the first full description of the tropospheric version the United Kingdom Chemistry and Aerosol model (UKCA) which is used at the University of Cambridge. In addition to a brief background to the dynamical core of the model, I describe the chemistry and emissions in detail. The second half of the

chapter focuses on how including isoprene in the model impacts the model results, particularly for ozone. In **Chapter 4**, I use a number of measurements from the OP3 field campaign in Borneo, Malaysia, to assess the ability of the model chemical mechanism. Can this mechanism represent data, and therefore, is it useful? I also perform two sensitivity studies which examine the impact of changing isoprene emissions in the region; these changes in emissions could be due to growth of biofuel feedstock crops.

Chapter 5 begins with an ozone attribution study of a potential future atmosphere. I also ask: how could phase I of the biofuel life cycle impact tropospheric chemistry through changing isoprene emissions? I compare the impact of land use change to the influence of CO_2 suppression of isoprene emission on ozone, HO_x, and certain reaction fluxes. In **Chapter 6**, I move to the third phase of the life cycle, combustion. How would air quality change if all the cars in the world ran on ethanol (biodiesel)? I examine the impacts of these fuels on surface ozone in particular.

The thesis closes in **Chapter 7** with a summary of the novel work and conclusions gained from my research. I then present some further work (short term) which could be directly related to the experiments I conducted. Finally, I briefly describe the outlook (long term) for this type of biofuel-atmosphere research.

Chapter 1

Biofuels: A Solution?

Past, present, and projected changes in the Earth System have been unequivocally linked to anthropogenic activity [*Solomon et al.*, 2007b]. The majority of positive radiative forcing resulting from human activity has occurred due to increasing atmospheric concentrations of carbon dioxide [*Solomon et al.*, 2007b], a product of using petroleum-derived hydrocarbon fuels to power the world's economies. A number of other radiatively active greenhouse gases have also increased due to anthropogenic activity: notably, methane, nitrous oxide, halocarbons, and tropospheric ozone. In order to reduce the probability of large changes in the climate system, atmospheric concentrations of greenhouse gases, and therefore emissions of these gases, will have to be reduced. In this light, a number of technologies which reduce carbon emissions have been proposed.

In the beginning part of this chapter, I explain why biofuels could form part of this renewable energy mix. In particular, I review a brief history of climate agreements (section 1.1) that have codified emissions reductions, and I explain why transportation is a particularly difficult sector to decarbonize (section 1.2). Section 1.3 is concerned with an overview of biofuels, including the various types of fuels and the differences between them. In section 1.4, I describe the life cycle assessment of two biofuels, ethanol and biodiesel, which are currently the most likely contenders to replace conventional fuels in the short term. This chapter

closes with a description of the potential atmospheric impacts of each phase of the biofuel life cycle.

1.1 A brief history of climate agreements

The first international conference on climate change was sponsored by the World Meteorological Organization and held in Geneva in 1979 [*World Meteorological Organization*, Geneva, February 1979]. Nearly a decade later, the Intergovernmental Panel on Climate Change (IPCC) was set up by the United Nations; the Panel released its first assessment report in 1990 [*Houghton et al.*, 1990]. In 1992, the United Nations Framework Convention on Climate Change (UNFCCC) was completed, which committed signatory parties to voluntarily reductions in emissions. The stated aim was that in the year 2000, emissions levels were to equal 1990 levels [*United Nations Framework Convention on Climate Change*, 1992]. In 1997, the Kyoto Protocol was adopted [*United Nations Framework Convention on Climate Change*, 1997], which shifted the reductions from voluntary to mandatory. It wasn't until Russia ratified the Protocol in 2004, however, that it was able to come into force [*Hopkin*, 30 September, 2004]. The next Conference of the Parties (COP-15) to the UNFCCC is to be held in Copenhagen in December, 2009, at which a new emissions reduction scheme may be introduced.

Although international agreements exist at the macro scale, regional and national commitments have been ratified as well. The European Union has set a goal of reducing emissions by 20% below 1990 levels by the year 2020 [*Communication from the commission to the European Parliamant*, 23 January 2008], which is amendable to 30% if other nations commit to similar reductions [*European Commission*, 23April 2009]. The main tool through which they are encouraging emissions control is the carbon emissions trading scheme (ETS). The EU ETS is the largest cap-and-trade system in the world, in which total carbon emissions are 'capped', and emissions permits are 'traded'; the goal is to create both a price

for carbon and a functioning carbon market. Individual European countries have set additional targets, separate from the regulation of carbon emissions required under the EU ETS. For example, the UK has set reduction targets of 26 per cent by 2020 and at least 60 per cent by 2050, compared to 1990 levels [*United Kingdom Parliament*, 2007-2008 Session].

Another national level agreement is the energy bill currently under review in the United States Congress. The targets are set to 3% by 2012, and 85% by 2050, using 2005 as the base year. The renewable energy requirement would begin at 6% in 2012 and gradually rise to 25% in 2025, and a national lower carbon fuel standard would also come into effect. In addition to federal legislation, individual states have recently been allowed to regulate their greenhouse gas (GHG) emissions under the Clean Air Act. In 2006, California legislated that greenhouse gas emissions must be reduced to 1990 levels by the year 2020 [*California Congress*, 2005-2006 Session]. Obtaining energy from renewable sources has become a legislative priority in individual states—twenty four states have renewable portfolio standards, in which a certain percentage of electricity is required to be sourced renewably [*U.S. Department of Energy: Energy efficiency and renewable energy*, 2009]. The obligations range from 10% (Michigan, North Dakota, South Dakota, Wisconsin and Vermont) to 33% (California).

Within the larger framework of decarbonizing the energy sector, specific targets and regulations have recently been passed concerning transportation, some of which affect biofuels. In the EU, a biofuels directive was passed in 2003, which mandated 5.75% of fuel be replaced by biofuels by 2010, and 10% by 2020 [*European Commission*, 8 May 2003]. Recently, these volumetric requirements were repealed concurrent with the implementation of 'sustainability criteria' for biofuels. A life cycle assessment (LCA) mechanism has been adopted to assess the full greenhouse gas benefits of particular biofuels and pathways, and using the formula described in *European Commission* [23 April 2009], greenhouse gas savings for biofuels must be at least 35% in comparison with conventional fuels. This value

will scale to 50% savings by 2017 [*European Commission*, 23 April 2009].

In the United States, both volumetric and GHG requirements have been adopted. The total renewable fuel requirement in 2008 was 9.0 billion gallons [*United States Environmental Protection Agency*, 2009]. Over the course of the regulation, which falls under the Energy Independence and Security Act [*One Hundred Tenth Congress of the United States of America*, 4 January, 2007], the total renewable requirement increases to 36 billion gallons by 2022. The 'advanced' biofuel requirement (comprised of cellulosic ethanol and biodiesel) is 21 billion gallons in the same year. All renewable fuels are required to reduce GHG emissions by 20% compared to their conventional fuel counterparts. Advanced biofuels are required to have a 50% savings and cellulosic biofuels are required to have even greater savings of 60%. Individual states have also enacted and regulated fuel carbon standards. For example, the Governor of California issued an Executive Order which mandated a low carbon fuel standard [*Office of the Governor of California*, 18 January 2007]. The low carbon standard requires a reduction in carbon intensity of fuels by 10% by 2020 [*California Environmental Protection Agency: Air Resources Board*, Accessed 15 September 2009]. The fuels will be assessed using a life cycle assessment model, GREET [*Wang*, 2009].

In the UK, the Renewable Transport Fuels Obligation (RTFO), which requires a small percentage of fuel to be renewable, was passed in 2007 [*United Kingdom Statutory Instrument No. 3072*, 26 October, 2007]. The RTFO requires renewable fuel to comprise 2.5% of supply in 2008-2009, which has been met, growing to 3.5% in 2010-2011. For these fuels, reductions in GHG emissions, which are output using a 'carbon calculator', are supposed to be 40% below conventional fuels in 2008-2009 and 50% below in 2010-2011 [*Renewable Fuels Agency*, Accessed 21 October, 2009].

1.2 The transport sector

Reaching political agreements for emissions reductions is only one challenge in the decarbonization process. Each sector requires its own technological solutions, and not all sectors consume energy, or even types of energy, equally. The transport sector proves a particular challenge because its growth rate has been high during the last 35 years. Figure 1.1 shows the global end use consumption of oil by sector. In terms of oil consumption, the transport sector has grown by the largest amount of any sector in recent decades [*International Energy Agency*, 2008]. In terms of total energy consumption (not just oil), during the same period, growth globally (206%) and in OECD countries (182%) has also been high.

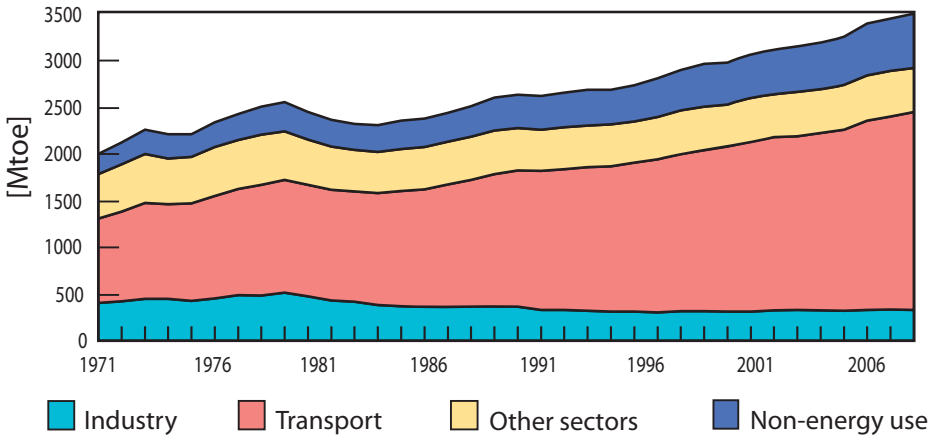

Figure 1.1. Global end use oil consumption [Mt oil equivalent] by sector from *International Energy Agency* [2008]. Other sectors includes agriculture, public services, and residential use.

A high growth rate is one of four factors which make the transport sector particularly difficult to decarbonize. A second contributing feature is the complicated infrastructure which is required to support a vehicle fleet. If future fuels differ widely from their current analogues, both the fleet itself (the cars and trucks) may need to be replaced, and the distribution network (the pipelines, tankers, storage systems, and refueling stations) may also need to be changed. Both would require

time, capital investment, and energy. These costs—temporal, financial, and energetic—are the second reason that the transport sector is hard to change.

The sociological barriers for decarbonizing transport are especially challenging. A centralized sector such as power generation is rather easier to transition; as long as electricity continues to flow with minimal change in cost, the end user is generally satisfied. In contrast, the requisites for maintaining status quo in the transport sector are more stringent, and include rapid refueling, certain power and speed expectations, and maintenance of a 300-500 mile driving range. The power and driving range both rely on energy density; that is, a fuel system must supply enough energy in a small enough volume to be carried on board individual vehicles. These phenomena contribute to the technological barriers in creating the future transport systems.

Large growth, the cost of infrastructure change, and sociological expectations are three parts of the challenge that faces the transport sector. In addition, a solution must be technologically feasible. This question of technical capability and feasibility was addressed in a study by *Pacala and Socolow* [2004], in which the authors proposed that stabilisation of atmospheric CO_2 concentrations would require a suite of carbon-reducing technologies. Figure 1.2 shows their 'stabilization triangle'. Each of the 'wedges' shown in the bottom of Figure 1.2 represent a type of technology that could, by 2054, reduce carbon emissions by one Gt per annum. The authors proposed 15 wedges, of which seven are required in order to stabilise CO_2 concentrations at 500 ± 50 ppmv. Only *two* of these proposals relate to the transportation sector: hydrogen fuel derived from wind power used in fuel cell vehicles, and biofuels. With both hydrogen technology [*Solomon and Banerjee*, 2006] and fuel cells [*Romm*, 2006] still not ready for large scale production or use, not to mention infrastructure development costs, biofuels are one of the only potential options for reducing carbon emissions from the transport sector in the short to medium term. Biofuels can be carbon neutral, but only if the carbon absorbed during cultivation equals the carbon emitted during combustion [*Tilman*

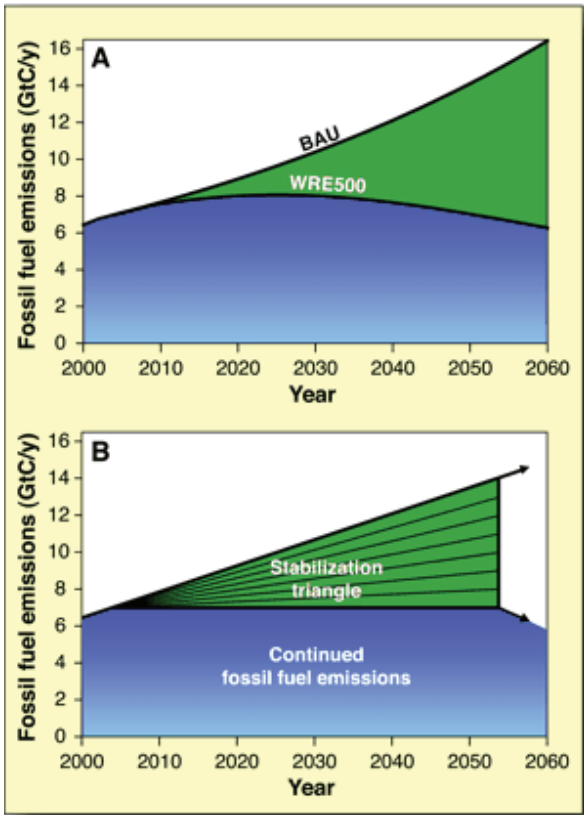

Figure 1.2. Stabilisation wedges from *Pacala and Socolow* [2004]. A) The top curve represents a business as usual path, and the lower curve represents an emissions stabilisation path at 500 ppmv CO_2. The green area represents the area of avoided carbon required in order to stabilise. B) The stabilisation triangle is divided into seven 'wedges', each of which reaches 1 Gt C yr^{-1} by 2054.

et al., 2009; *Sustainable biofuels: prospects and challenges*, 2008]. *Pacala and Socolow* [2004] also described another possible wedge for future carbon savings: increased afforestation and decreased deforestation. Because the carbon storage capacity of agricultural land is lower than forests [e.g. *Foley et al.*, 2005; *Jain and Yang*, 2005], if we cut down the forest to plant biofuel crops, the carbon savings are lost.

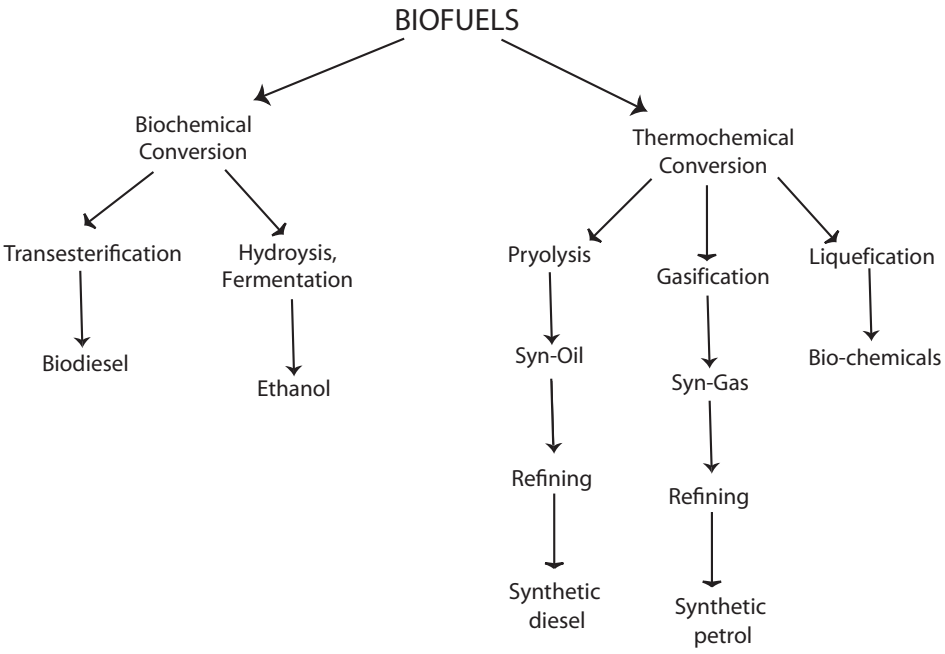

Figure 1.3. Schematic of biofuel production through biological and thermochemical processing, after *Demirbas* [2007a].

1.3 An introduction to biofuels

Biomass energy is the oldest form of energy harnessed by humans. Primary biomass, such as charcoal or wood, is still used throughout a large portion of the developing world for energy. This type of primary biomass energy contributed more than 10% to global energy supply in 2005 [*Anderson et al.*, 2004]. In Sub-Saharan Africa, combustion of primary biomass and waste comprises 61.5% of energy supply [*Anderson et al.*, 2004]. Combustion of this type of primary biomass energy has a strong effect on the atmosphere [e.g. *Crutzen and Andreae*, 1990; *van der Werf et al.*, 2004; *Jain et al.*, 2006; *Aghedo et al.*, 2007; *Ziemke et al.*, 2009, and references therein]. These types of fuels, however, cannot fuel transportation.

On the other hand, secondary, or processed, biofuels are viable liquid fuels for transport. The potential efficacy and uses of a particular biofuel depend both on its feedstock and its conversion method. Biomass converts approximately 1%

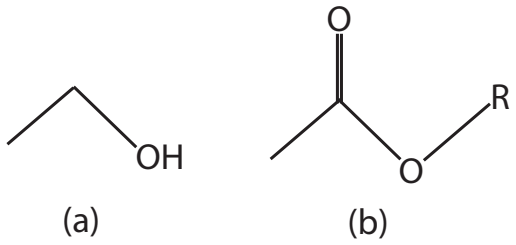

Figure 1.4. Chemical structure of a) ethanol and b) biodiesel.

of incoming solar radiation into usable energy [*Schiermeier et al.*, 2008]. After biomass cultivation, two major branches of conversion methods exist [*Demirbas*, 2007a]: biochemical and thermochemical. Figure 1.3 summarises the branching and families of biofuel production. Biological processes usually deliver a fairly pure product, although the process may be slow; alternatively, thermochemical processes are more rapid but yield heterogenous products that can be difficult to distill or refine [*Sustainable biofuels: prospects and challenges*, 2008]. Thermochemical products are molecularly similar to their conventional fuel analogues, while biological products are different. Because currently the most common biofuels for the transportation sector are produced biologically, they are the focus of this thesis. The chemical structure of the two main biologically produced biofuels, ethanol and biodiesel, and shown in Figure 1.4. In biodiesel, the R group is a chain of 14-24 carbons, depending on feedstock, and has between 0 and 3 double bonds [*Ma and Hanna*, 1999; *Pinzi et al.*, 2009].

1.3.1 Biomass potential

The feasibility of large scale biofuel deployment depends not only on the vehicle technologies and distribution pathways, but also on the amount of biomass that could be produced. *Berndes et al.* [2003] reviewed a number of studies of global biomass potential; Table 1.1 shows a summary of biomass potential estimates for a range of years from *Berndes et al.* [2003] and *Moreira* [2006]. The range of po-

Table 1.1. Estimates of future energy supply [EJ (10^{18} joules) yr^{-1}] from biomass summarized from *Berndes et al.* [2003] and *Moreira* [2006].

Year	1990	2020-30	2050	2100
Hall et al. [1993]	31			
Johansson et al. [1993]		62	78	
Battjes [1994]			47	
Williams [1995]		30	38	46
Fujino et al. [1999]	88			
Houghton et al. [2001]			441	
Fischer and Schrattenholzer [2001]			350-450	
Yamamoto et al. [2001]	84			265

tential biomass estimates is large, from 31 to 88 EJ (10^{18} joules) yr^{-1} in 1990, and from 38 to 450 EJ yr^{-1} in 2050. The large majority of the variability in projections is due to differences in estimates for global land cover and the potential yield or production capacity from a unit of land [*Berndes et al.*, 2003]. In addition, assumptions about food productivity and availability, degraded land availability, and competing land use types contribute to variability in potential biomass estimates. The total global energy demand in 2004 was 308.8 EJ yr^{-1} , and the global transportation demand was 82.4 EJ yr^{-1} [*Sims and Schock*, 2007]. From the estimates listed in Table 1.1, it is clear that biomass could supply a significant part of the transportation energy demand; by some estimates, biomass could cover the energy required by the entire global fleet.

I should note that the energy harnessed from biomass does not have to take the form of liquid fuel for transport. A number of studies have suggested that using biomass to generate combined heat and power (CHP) would be more efficient than producing liquid fuels for transport. The use of this type of energy by the transport sector would require development of electric vehicles and therefore advanced battery technology. Estimates of the increase in efficiency for the CHP-electric fuel system compared to liquid fuel production range from 33% [*Sims et al.*, 2006], to 100% [*Ohlrogge et al.*, 2009] and 112% [*Campbell et al.*, 2009].

1.3.2 Ethanol

1.3.2.1 Introduction

The use of ethanol as a liquid fuel for transport is as old as the motor vehicle; Henry Ford outfitted the Model T to be a flex fuel vehicle that could run on alcohol-based fuels [*Solomon et al.*, 2007a]. For most of the twentieth century, however, mineral fuels proved to be cheaper and easier to produce, and alcohol-based fuels never took a significant part of the market. The first country to revive the ethanol market was Brazil, which developed their 'Proalcool' program in 1975 in the wake of the 1973 OPEC oil embargo [*Solomon et al.*, 2007a]. Today, all liquid transport fuel in Brazil contains at least 24% ethanol [*Moreira*, 2000; *Solomon et al.*, 2007a] and ethanol comprises approximately 40% of all transport fuel used in the country [*Solomon et al.*, 2007a].

Ethanol production in the United States, the other major world producer, has grown somewhat more gradually, aided by a series of tax exemptions beginning in 1978 [*Solomon et al.*, 2007a]. Ethanol forms a relatively small percent of the liquid fuel for transport used in the United States—E85 forms 1% of the alternative fuel market, and 0.02% of the entire market. E85 is a mixture of 85% ethanol and 15% conventional gasoline. Ethanol in 'gasohol' (a mixture of 10% ethanol and 90% gasoline by volume, or E10) forms a slightly larger section of the total end use market for transport fuel (2%), but it is still relatively small. Despite this, the United States is the world's largest producer of fuel ethanol, producing 9 billion gallons in 2008 [*Renewable Fuels Association*, Accessed 15 September, 2009]. In the same year, Brazil produced 6.5 billion gallons of ethanol for transport.

1.3.2.2 Feedstocks

Sugar- and starch-producing crops comprise the main feedstocks of most current ethanol production. The main sugar crops are sugarcane, sugar beet, and sweet sorghum [*Demirbas*, 2007a; *Sustainable biofuels: prospects and challenges*,

Table 1.2. Energy balance of ethanol fuel-feedstock systems, as in *Goldemberg* [2007]. Energy balance is the renewable output energy divided by the fossil fuel input energy, such as transport, fertilizer, and industrial processing.

Feedstock	Energy Balance
Sugarcane	10.2
Sugar beet	2.1
Corn	1.4
Cellulose	10.0

2008]. Starchy crops include corn, sorghum, and wheat, of which corn is the most prevalent in present day production [*Demirbas*, 2007a].

Cellulosic ethanol is derived from the sugars within the cell walls of the entire biomass of a plant (see section 1.3.2.3). Instead of optimizing growth and crop choice for maximum sugar output, cellulosic ethanol crops are chosen for their total biomass output. Perennial grasses (either single species or polycultures) and fast growing trees (short rotation coppice) are examples of dedicated energy crops that could be used to produce cellulosic ethanol [*Tilman et al.*, 2006; *Sustainable biofuels: prospects and challenges*, 2008]. Cellulosic ethanol could also be extracted from waste or co-products, such as the extra biomass from cereal production, forestry waste, or municipal biomass waste [*Sustainable biofuels: prospects and challenges*, 2008]. Because development of the sugar extraction techniques from cell walls is still underway, cellulosic ethanol is sometimes referred to as 'second generation' ethanol.

Each of these feedstocks differs in its energy balance, or total output of renewable energy per unit of input energy. Table 1.2 lists a summary of common ethanol feedstocks and their energy balances. Ethanol derived from sugarcane, for example, is very favorable in its energy balance and produces over 10 times the amount of energy required as inputs. One reason for this is that a high proportion of the input production is powered from the waste products within the sugarcane production cycle, called bagasse [*Moreira*, 2000; *Wang et al.*, 2008]. Bagasse, because

it is also grown during the cultivation period (and pulls down atmospheric carbon) does not count as an energy input. Although sugar beet and corn have positive energy balances, they are not as positive as sugarcane; one reason for this is the starch and sugar can only be extracted from the fruit of the plant. Cellulosic ethanol also shows a high return on energy inputs, partly because the entire biomass of the plant is used.

1.3.2.3 Production

Currently, the most established method of ethanol production is biological fermentation. For sugar-producing crops, the production process involves four or five steps: milling, pressing, fermentation, distillation, and possibly denaturing [*Solomon et al.*, 2007a]. A starchy crop, such as corn, requires seven steps: milling, liquefaction, saccharification, fermentation, distillation, dehydration, and denaturing [*Solomon et al.*, 2007a]. The increased number of steps, particularly the need for a hydrolysis reaction, decreases the energy balance significantly for starchy crops versus those which produce sugar directly [*Lin and Tanaka*, 2006]. Saccharification, the hydrolysis of long starch polymers, is necessary because the yeast which produces ethanol can only digest sugars. Distillation is also a very energy intensive step, which would be improved by increasing the concentration of ethanol produced during the fermentation process. The obstacle to this is the alcohol tolerance of the bacteria used in fermentation, which is currently approximately 18% [*Sustainable biofuels: prospects and challenges*, 2008].

A crop is only a small part of the entire biomass of a plant. Sugar polymers exist throughout the entire plant; cellulose is a polymer of six-carbon glucose sugars that constructs the majority of cell walls. It is intertwined both with hemicellulose, which is a branched, shorter polymer of five-carbon sugars, and with lignin, a stiff polymer which crosslinks the former two [*Service*, 2007]. In order to use the full biomass of a plant as a feedstock for ethanol production, lignin must be removed before fermentation can begin. This difficult deconvolution is currently the subject

of much research [*Service*, 2007; *Weng et al.*, 2008].

1.3.3 Biodiesel

1.3.3.1 Introduction

In an early public display of the compression ignition engine, Robert Diesel used peanut oil as fuel [*Shay*, 1993]. Despite early testing of a variety of vegetable oils in diesel engines [*Shay*, 1993; *AltIn et al.*, 2001], concentrated interest in generating fuel from vegetable oils did not occur until the 1970s, in response to the OPEC oil embargo [*Shay*, 1993]. Reducing carbon emissions has sparked renewed interest in diesel derived from biomass. In the United States, biodiesel constitutes 5.3% of alternative fuels, and 0.14% of total transport fuel. Biodiesel production in the United States sums to 1.8 billion litres in 2008 [*Sims et al.*, 2008]. In the same year, the EU produced 5.8 billion litres [*Sims et al.*, 2008].

1.3.3.2 Feedstocks

Biodiesel can be derived from a number of oil-producing crops. The most commonly used feedstocks are soybean, palm, sunflower, safflower, cottonseed, rapeseed (canola), and peanut [*Demirbas*, 2007b]. Because of many centuries of use in the food industry, the oil produced per hectare from these crops has been optimized to maximize output. A more recently cultivated plant, Jatropha, which produces the physic nut, is also a potential feedstock for biodiesel production [*Sims et al.*, 2008]. Jatropha growth has not been fully optimized for maximum production, and its successful use in biodiesel production is therefore considered to be 'second generation', similar to cellulosic ethanol. Microalgal production of oils is early in the development process, and is also considered to be a 'second generation' biofuel. There are no commercial algal biodiesel production facilities [*Lardon et al.*, 2009], although the energy company ExxonMobile has recently funded Craig Venter at

Table 1.3. Energy balance of biodiesel fuel-feedstock systems. Energy balance is the renewable output energy divided by the fossil fuel input energy.

Feedstock	Energy Balance	Source
Soybean	1.93	*Hill et al.* [2009]
Palm	4.8	*Yáñez Angarita et al.* [2009]
Microalgae	0.98-3.5	*Lardon et al.* [2009]
Rapeseed	1.93	*Patterson et al.* [2008]

Synthetic Genomics to build one [*Service*, 2009][1]. The most common feedstock for biodiesel production in the United States is soybean [*Hill et al.*, 2006], while in Europe it is rapeseed [*Sustainable biofuels: prospects and challenges*, 2008].

As with ethanol, each biodiesel feedstock and each pathway has its own energy balance. Table 1.3 shows some example energy balances for soybean, palm, and microalgae derived biodiesel. The most positive energy balance is for palm derived biodiesel, followed by microalgae. The range for microalgae estimates is large primarily because of energy consumption levels for the different oil extraction techniques [*Lardon et al.*, 2009]. The total net energy balance for biodiesel, no matter what the input feedstock, is never as high as for ethanol. One of the reasons for this is that only the fruit of a plant can be used to extract oils, while the entire biomass of a plant can contain sugars (e.g. sugarcane).

1.3.3.3 Production

There are four main stages in biodiesel production: extraction, transesterification, phase separation, and distillation [*Demirbas*, 2007b; *Sims et al.*, 2008]. Oil-producing crops produce triglycerides. The main transformation step for biodiesel is the removal of the glycerin backbone and replacement with a methyl group. For one molecule with three different fatty acid chains, this will produce three different fatty acid methyl esters (see Figure 1.4). The removal of glycerin is the bulk of the

[1] Confirmed by personal communication with Juan Enriquez, co-founder of Synthetic Genomics; July, 2009 in Oxford, UK.

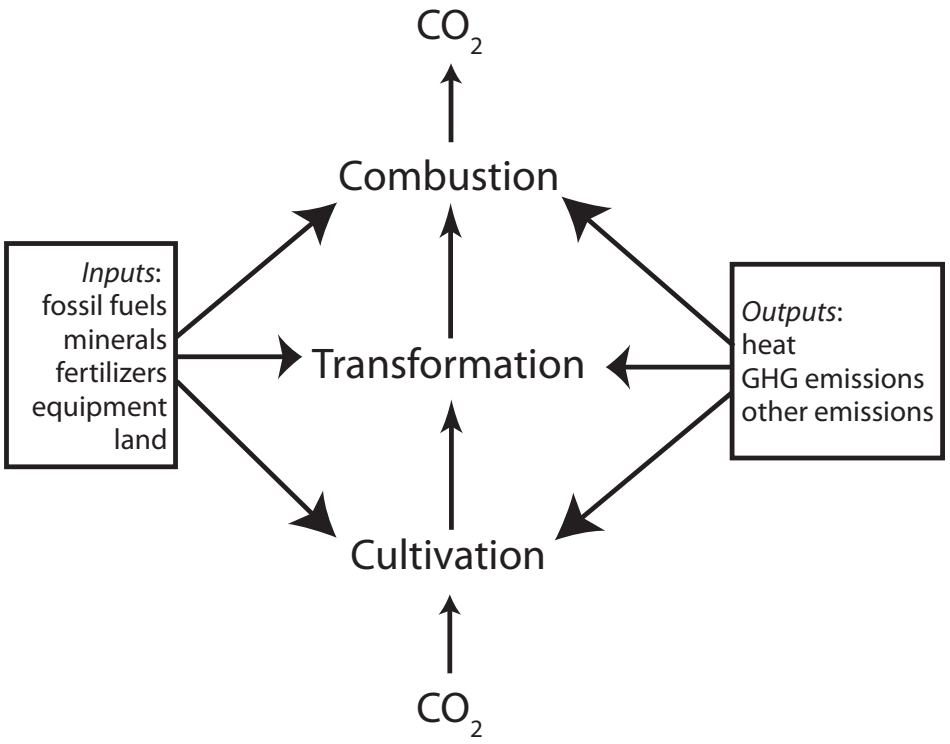

Figure 1.5. Schematic of the three stages of a biofuel life cycle including inputs and outputs, adapted from *Sustainable biofuels: prospects and challenges* [2008].

phase separation step [*Ma and Hanna*, 1999]; glycerol is also a valuable coproduct used in household products such as cosmetics and soap.

1.4 Life cycle of a biofuel

The life cycle of a biofuel can be broken down into three distinct stages: cultivation, transformation, and combustion. Figure 1.5 shows a schematic of the inputs and outputs from a biofuel life cycle, each phase of which will have a unique environmental and atmospheric footprint. A typical life cycle assessment attempts to quantify the energy and environmental inputs and outputs over the entire lifetime of a product. For fuel-feedstock systems, LCA is also sometimes described as

'well-to-wheels' analysis.

The full analysis of a fuel-system life cycle is complex, and depends both on the fuel pathway and the vehicle technology (sometimes also known as a 'propulsion system'). A number of LCA studies were reviewed by *MacLean and Lave* [2003], who reported ranges of energy balance and GHG estimates from the literature. The authors found that for fuel pathways and vehicle propulsion systems that have been around for a long period of time, both the energy and greenhouse balance are well constrained to a fairly small range. Newer and future fuels and systems, however, have a much broader range; for example, ethanol derived from cellulose is reported to have a range of greenhouse gas emissions of -85 to +14 g CO_2 equivalent per MJ of fuel energy [*MacLean and Lave*, 2003].

1.4.1 Phase I: Cultivation

There are two main types of feedstock for biofuels: dedicated energy crops and waste products [*Sustainable biofuels: prospects and challenges*, 2008]. The technology to use waste products (especially sugar extraction from cellulose) efficiently is not yet available, so I will focus on dedicated energy crops.

The growth and cultivation of crops requires both energy and equipment, and releases a particular set of emissions into the atmosphere. Life cycle analyses have considered the energy and GHG cost of fertilizer production, machinery manufacturing, and direct energy needed to cultivate and store the feedstock crop [*Wu et al.*, 2006]. For an oily crop, the cultivation stage can also include crude oil extraction on site, and yield from this extraction process [*Huo et al.*, 2008]. Trace gas emissions associated with the cultivation stages include soil NO_x and volatile organic compounds (VOC) emitted by the plant species themselves. Biogenic VOC emissions from the cultivation step are a focus in chapters 4 and 5.

Although emissions of reactive trace gases are not usually considered in phase I of the biofuel life cycle, agricultural emissions of the greenhouse gas N_2O emissions often are [*MacLean and Lave*, 2003]. *Crutzen et al.* [2008] considered the

impact of increasing N_2O emissions resulting from large scale biofuel use on the atmosphere by using an fertilizer application/atmospheric release rate of 3-5%, which was higher than previous estimates. The authors found that the increased emission of N_2O, which is a greenhouse gas (and also destroys stratospheric ozone), outweighed any carbon savings gained by converting to biofuels. Soybean biodiesel and corn ethanol were the fuels considered.

While energy, greenhouse gas emissions, and some trace gas emissions have been considered in LCAs to date, these factors do not necessarily include all of the potential environmental impacts of biofuel cultivation. For example, cultivating energy crops would require water [*Schilling et al.*, 2008]. On the other hand, positive effects could include improved soil health and increased biodiversity [*Rowe et al.*, 2009].

1.4.2 Phase II: Transformation

The transformation step involves the conversion of a feedstock (in the case of ethanol) or crude mixture (in the case of biodiesel) into a fuel that is usable in vehicle engines. Calculating the contribution of the second stage of a biofuel life cycle to the entire LCA requires the inclusion of a number of smaller steps. These include the energy to make and transport needed solvents and chemicals, wet or dry milling (for ethanol), feedstock transportation, fuel transportation, and the energy to carry out industrial chemical reactions [*Wu et al.*, 2006; *Huo et al.*, 2008]. *Wang et al.* [2007] examined the impact of the processing plant used to transform corn to ethanol, and found that the energy balance and GHG emission were affected significantly. The total life cycle can also be influenced by the production of coproducts at the transformation stage. For ethanol, a common coproduct is animal feed [*Wang et al.*, 2007; *Sims et al.*, 2008], while for biodiesel, a common coproduct is glycerol [*Huo et al.*, 2008]. Phase II of a life cycle assessment also usually includes emissions of criteria air pollutants, whose calculation usually depends on reported emissions factors [e.g. *Wu et al.*, 2006]. These trace gases may

include a number of typical anthropogenic industrial emissions such as CO, NO_x, anthropogenic VOCs, and toxic aromatic compounds.

1.4.3 Phase III: Combustion

The end use, or Phase III, of the biofuel life cycle is combustion in a vehicle engine. This stage usually encompasses transport from a distribution centre to a refueling station, vehicle operation, and sometimes vehicle service. This stage also includes the evaporative emissions that occur due to leaks and errors in the distribution process [*Jacobson*, 2007; *Huo et al.*, 2009]. Trace gas emissions linked to the combustion stage may include CO, NO_x, and vehicle tailpipe VOCs. Because of the widespread nature of mobile vehicle emissions, the footprint of combustion is the largest of the three phases. A more in depth exploration of the reason for the different emissions profile of ethanol and biodiesel versus their conventional counterparts can be found in section 6.1.2.

As I describe further in the next chapter, the presence of NO_x is often a determining factor in whether a local chemical regime produces or destroys ozone [e.g. *Liu et al.*, 1987, and section 2.1.2]. The emission of NO_x during the biofuel lifecycle is therefore an important aspect of their potential impact on the atmosphere. Variations in fuel quality and combustion characteristics lead to changes in tailpipe NO_x emissions. NO formation in a combustion engine normally proceeds through thermal formation by the Zeldovich mechanism [*Zeldovich*, 1946]. The reactions proceed at very high temperatures (2000+ °C) [*Hanson and Saliman*, 1984], and are initiated by reaction of atomic oxygen with molecular nitrogen:

$$O + N_2 \rightarrow N + NO \tag{1.1}$$

which is the rate limiting step. This leads to reaction of atomic nitrogen with molecular oxygen:

$$N + O_2 \rightarrow O + NO, \tag{1.2}$$

or reaction with OH:

$$\mathrm{N} + \mathrm{OH} \rightarrow \mathrm{H} + \mathrm{NO} \tag{1.3}$$

both of which form a second molecule of NO. High engine temperatures are highly correlated to changes in NO formation and emission [*Hanson and Saliman*, 1984]. A much smaller fraction of tailpipe $\mathrm{NO_x}$ emission can also arise from 'prompt $\mathrm{NO_x}$' (a mechanism which proceeds through the formation of hydrogen cyanide) or from 'fuel $\mathrm{NO_x}$' (from combustion of nitrogen within the fuel content) reactions [*Fernando et al.*, 2006].

1.5 Summary

In this chapter I have explored the potential for biofuels to form part of a future renewable energy mix. This has been recognized in a series of political agreements, which I documented in the first section of this chapter. I then described the particular difficulties of solving the transportation energy problem: high growth rates in the transport sector, inertia in the infrastructure of the system, sociological requirements, and technological feasibility.

After introducing biofuels, I described the concept of biomass potential for which there is currently a high level of uncertainty in the literature. I also went through the two major types of biofuels, ethanol and biodiesel, and documented their major feedstocks and production pathways. I finished this chapter with a discussion of the three phases of a biofuel life cycle—cultivation, transformation, and combustion—and the potential trace gas emissions profile of each.

In the next chapter, I describe the atmospheric chemistry that these emissions have the potential to perturb.

Chapter 2

Biofuels: Potential Atmospheric Impacts

Emissions of NO_x, CO, and VOC from the biofuel life cycle could have implications for air quality and tropospheric chemistry. In section 2.1, I explore the initiation, propagation, and termination steps of radical chemistry in both a polluted and unpolluted environment, focusing on the formation and destruction of ozone. I then describing the nonlinearities of the chemical system, and the differences between a VOC-sensitive and a NO_x-sensitive chemical regime. In section 2.2, I turn to isoprene, the focus of Chapters 3 and 5. The second half of this chapter examines the chemistry and emission of isoprene into the atmosphere.

2.1 Tropospheric chemistry

The troposphere is the lowermost part of the atmosphere which extends from the surface to between eight and eighteen kilometres, depending on latitude. It is characterized by rapid meteorological processes which create a well-mixed environment, significant presence of water vapour, and high temperatures. The principal components of the troposphere are nitrogen (78%) and oxygen (21%), but a number of trace gas constituents play important chemical roles.

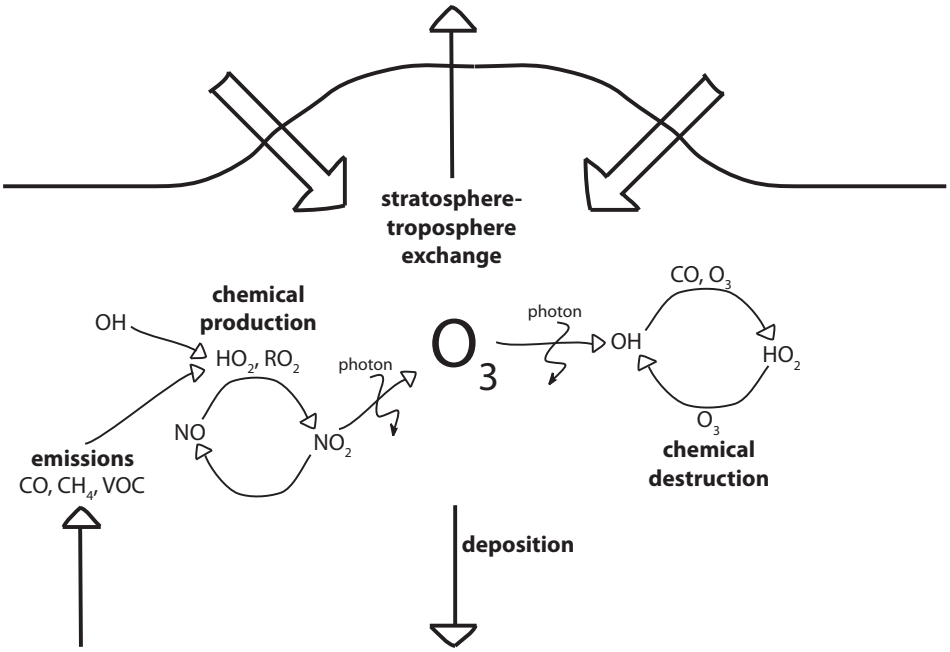

Figure 2.1. Schematic of the tropospheric ozone budget, showing the two production processes (stratosphere-troposphere exchange and chemical production) and the two loss processes (deposition and chemical destruction). Based on *Fowler et al.* [2008] and *Young* [2007].

Ozone is of particular importance because of its role in initiating the radical oxidation chemistry that dominates in the troposphere. Besides its chemical role (described below in sections 2.1.1 and 2.1.3), ozone is also a radiatively active gas [e.g. *Gauss et al.*, 2003; *Shindell et al.*, 2006a], and can be detrimental to both human [e.g. *Wilkins et al.*, 2001; *Jerrett et al.*, 2009] and crop health [e.g. *Long et al.*, 2005; *Hayes et al.*, 2007; *Mills et al.*, 2007; *van Dingenen et al.*, 2009]. Figure 2.1 shows a schematic representation of the ozone budget in the troposphere. Ozone production is dominated by the chemical term, the model mean of which was between 3448 and 5110 Tg yr^{-1} in a number of recent model intercomparisons [see *Wild*, 2007, and references therein]. Ozone production depends on relative concentrations of NO_x and VOC, which I describe further in section 2.1.3. An additional source of ozone is the flux from the stratosphere, which has been modelled be-

tween 552 and 765 Tg yr^{-1} [*Wild*, 2007]. Destruction of ozone is also dominated by chemical processes, and has been estimated to be between 3435 and 4668 Tg yr^{-1} [*Wild*, 2007]. The final term in the ozone budget is deposition, or physical loss of ozone to the surface of the earth. Deposition has been modelled at between 818 and 1003 Tg yr^{-1} [*Wild*, 2007].

The chemistry of ozone and other tropospheric constituent gases is complex and nonlinear; Figure 2.2 presents a visual summary of this chemistry. What follows is a descriptive summary of the key reactions that govern the chemistry and composition of trace gases the troposphere.

2.1.1 Initiation

The troposphere constitutes a sort of low temperature oxidation chamber which proceeds by radical chemistry. The generation of radicals arises from the photochemical lability of a number of trace gases. The major source of radicals in the troposphere is the photolysis of ozone, which proceeds through two channels:

$$O_3 + h\nu(\lambda \leq 1150\text{nm}) \rightarrow O(^3P) + O_2, \tag{2.1}$$

$$O_3 + h\nu(\lambda \leq 310\text{nm}) \rightarrow O(^1D) + O_2. \tag{2.2}$$

The ground state $O(^3P)$ generated from the longer wavelength photolysis channel reforms O_3 by:

$$O(^3P) + O_2 + M \rightarrow O_3 + M. \tag{2.3}$$

A large portion of the $O(^1D)$ formed through the short wavelength photolysis channel is collisionally quenched:

$$O(^1D) + M \rightarrow O(^3P) + M \tag{2.4}$$

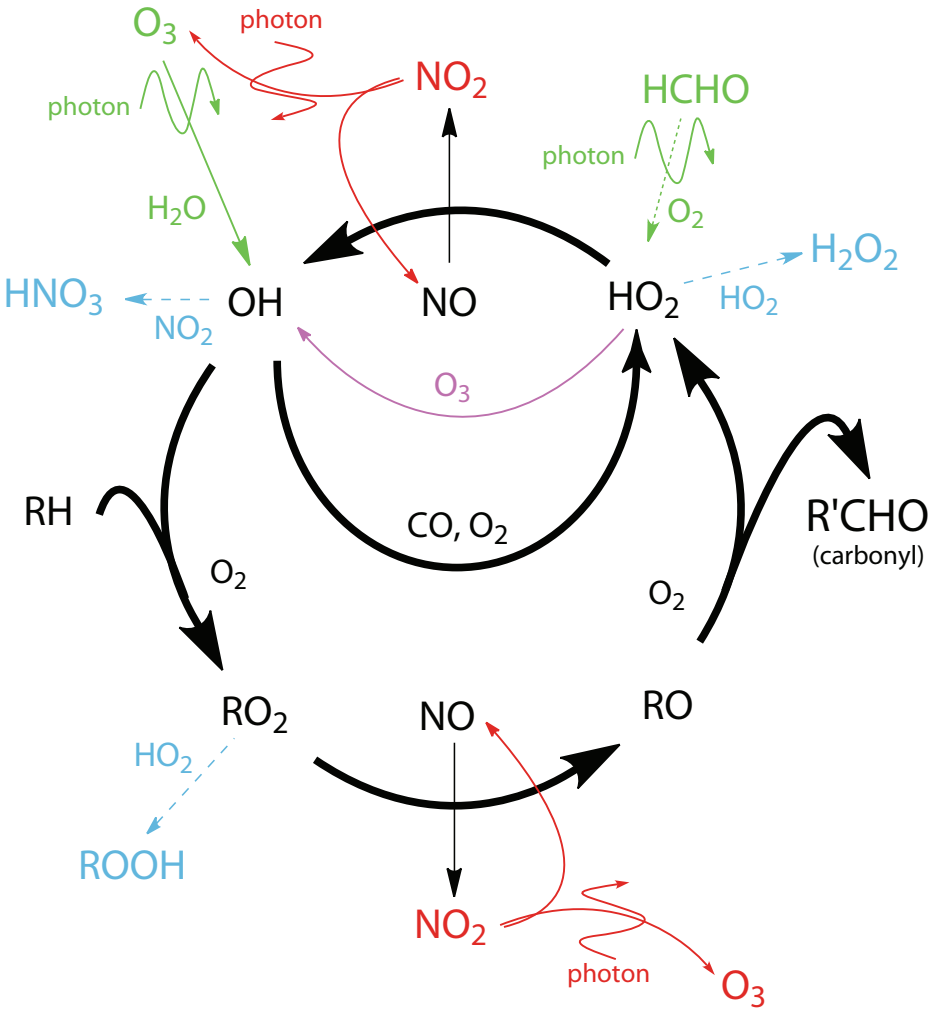

Figure 2.2. A visual summary of tropospheric chemistry as described in the text, adapted from *Jenkin and Clemitshaw* [2000] and *Young* [2007]. Radicals are produced through two main initiation steps (green), and cycle through the main oxidation radical propagation steps (black). In the absence of NO_x, ozone is consumed (purple), whereas in the presence of NO_x, ozone is produced (red). The cycle ends with radical-radical chain termination reactions (blue).

after which the $O(^3P)$ reforms ozone as in reaction 2.3. The small fraction of $O(^1D)$ remaining can react with water vapour to generate the hydroxyl radical:

$$O(^1D) + H_2O \rightarrow 2OH. \tag{2.5}$$

The formation of OH is therefore dependent on the concentration of water vapour, (which is linked to temperature and therefore climate), the concentration of ozone, and the photolysis frequency.

A more minor channel of radical production results from the photochemical lability of carbonyl species. The main radical-producing channel of photolysis of formaldehyde, the most abundant carbonyl in the atmosphere [*Levy II*, 1971; *Carlier et al.*, 1986], is:

$$HCHO + h\nu(\lambda \leq 338\text{nm}) \rightarrow H + HCO \tag{2.6}$$

after which the radicals H and HCO go on to form HO_2 by:

$$H + O_2 + M \rightarrow HO_2 + M \tag{2.7}$$

$$HCO + O_2 \rightarrow CO + HO_2 \tag{2.8}$$

HO_2 and OH are rapidly interconverted; the two together comprise the HO_x family. Once generated, these radical species can participate in a host of reaction cycles in the troposphere.

2.1.2 Propagation

Once formed, the hydroxyl radical can react with numerous trace gases. Principally, OH is consumed by the oxidation of CO:

$$CO + OH \rightarrow CO_2 + H \tag{2.9}$$

which accounts for 70% of OH reactivity in the troposphere [e.g. *Wayne*, 2000]. The H atom then goes on to form HO_2 by:

$$H + O_2 + M \rightarrow HO_2 + M \tag{2.7}$$

A second major fate for the hydroxyl radical is reaction with a volatile organic compound (VOC). Though there are numerous VOCs in the atmosphere, each with a separate oxidation mechanism, a number of salient features are common to all. For this reason, I take the most abundant and simple VOC, methane, as a representative example. The oxidation of methane by hydroxyl begins with hydrogen abstraction:

$$CH_4 + OH \rightarrow CH_3 + H_2O, \tag{2.10}$$

after which oxygen rapids adds to the methyl radical to form methylperoxy:

$$CH_3 + O_2 + M \rightarrow CH_3O_2 + M. \tag{2.11}$$

The formation of methylperoxy from methane oxidation can lead to the oxidation of NO, if it is present:

$$CH_3O_2 + NO \rightarrow CH_3O + NO_2. \tag{2.12}$$

The resulting methoxy radical can react with O_2 to regenerate HO_x by:

$$CH_3O + O_2 \rightarrow HCHO + HO_2 \tag{2.13}$$

where the production of formaldehyde can lead to further radical production through photolysis. Methylperoxy is a representative radical product of VOC, from which NO oxidation is common. Using R to represent a generic hydrocarbon, this process can be written as:

$$RO_2 + NO \rightarrow RO + NO_2. \tag{2.14}$$

An analogous reaction exists for HO_2 (formed during CO oxidation, reaction 2.9), from which OH is recycled:

$$HO_2 + NO \rightarrow OH + NO_2; \tag{2.15}$$

though in the absence of NO, HO_2 can react with O_3:

$$HO_2 + O_3 \rightarrow OH + 2O_2. \tag{2.16}$$

The two reactions above (2.14 and 2.15), in which NO_2 is generated from the oxidation of NO, form the basis for ozone formation in the troposphere, as NO_2 is rapidly photolysed:

$$NO_2 + h\nu(\lambda \leq 400\text{nm}) \rightarrow NO + O(^3P) \tag{2.17}$$

from which $O(^3P)$ goes on to form ozone via reaction 2.3.

The oxides of nitrogen have a particularly important role in the atmosphere because of their role in reducing peroxy radical species. During this process, NO_2 is formed (reactions 2.14 and 2.15), which leads to the formation of ozone (reactions 2.17 and 2.3). In the absence of these conversion processes, NO will react with ozone by:

$$NO + O_3 \rightarrow NO_2 + O_2. \tag{2.18}$$

The sum of reactions 2.3, 2.18, and 2.17 forms the photostationary state, which is a null cycle. The presence of radical species, such as RO_2 and HO_2, perturb this cycle and lead to the production of ozone. This ozone producing regime proceeds as:

$$CO + OH \rightarrow CO_2 + H \tag{2.9}$$

$$H + O_2 + M \rightarrow HO_2 + M \tag{2.7}$$

$$HO_2 + NO \rightarrow OH + NO_2 \tag{2.15}$$

$$NO_2 + h\nu \rightarrow NO + O(^3P) \quad (2.17)$$

$$O(^3P) + O_2 + M \rightarrow O_3 + M \quad (2.3)$$

with the net reaction:

$$CO + 2O_2 \rightarrow CO_2 + O_3. \quad (2.19)$$

In contrast, in a cleaner environment with lower concentrations of NO_x, ozone destruction may occur by:

$$CO + OH \rightarrow CO_2 + H \quad (2.9)$$

$$H + O_2 + M \rightarrow HO_2 + M \quad (2.7)$$

$$HO_2 + O_3 \rightarrow OH + 2O_2 \quad (2.16)$$

with the net reaction:

$$CO + O_3 \rightarrow CO_2 + O_2 \quad (2.20)$$

The determining factor between these two regimes is the presence or absence of the oxides of nitrogen [e.g. *Liu et al.*, 1987; *Chameides et al.*, 1992].

2.1.3 Chain termination

The radical chemistry that prevails in the troposphere is terminated through two main routes. These chain terminating (radical-radical) steps either form hydroperoxides:

$$HO_2 + HO_2 \rightarrow H_2O_2, \quad (2.21)$$

and other peroxides:

$$HO_2 + RO_2 \rightarrow ROOH, \quad (2.22)$$

or nitric acid:

$$OH + NO_2 + M \rightarrow HNO_3 + M. \quad (2.23)$$

A more minor channel of nitric acid formation was recently reported by *Butkovskaya et al.* [2005, 2007], in which HO_2 reacts with NO:

$$HO_2 + NO \rightarrow HNO_3 \tag{2.24}$$

which competes with the recycling of NO_2 in reaction 2.15, but is more important in the upper troposphere [*Cariolle et al.*, 2008]. Both hydroperoxides [*Zhang et al.*, 2003b] and nitric acid are extremely soluble in water and are rapidly and permanently removed by wet or dry deposition [e.g. *Wesely and Hicks*, 2000, and references therein]. Nitric acid is also subject to attack by OH, a more minor channel, and photolysis, which is more important in the upper troposphere.

Ozone production depends on the concentrations of both NO_x and VOC in the local environment. Figure 2.3 shows an ozone production map for a range of NO_x and VOC emission rates.[1] This 'topography' of ozone production shows that as both NO_x and VOC increase, ozone production also increases (along the dark blue line, the maximum 'ridge' of ozone production). When emissions of either NO_x or VOC are particularly high, increasing the emissions of the same species *decreases* ozone production. This occurs largely through the chain termination processes, formation of nitric acid or peroxides, described above. The dominating chain termination step occurring in a particular location can be indicative of the type of chemical regime [*Sillman*, 1995].

In a 'NO_x-sensitive' environment, the addition of NO_x to the chemical system increases ozone production; this is depicted on the bottom half of Figure 2.3. In these environments, concentrations of peroxy radicals are high, and the formation of peroxides (reactions 2.21 and 2.22) competes with recycling of NO by reactions 2.14 and 2.15. High fluxes through the reactions which form peroxides are therefore indicative of a NO_x-sensitive regime.

In contrast, in a 'VOC-sensitive' chemical regime, the addition of VOC in-

[1] Although a version of this graphic appears in *Sillman and He* [2002], the slightly edited version shown here was accessed from Sanford Sillman's website: http://www-personal.umich.edu/ sillman/ozone.htm.

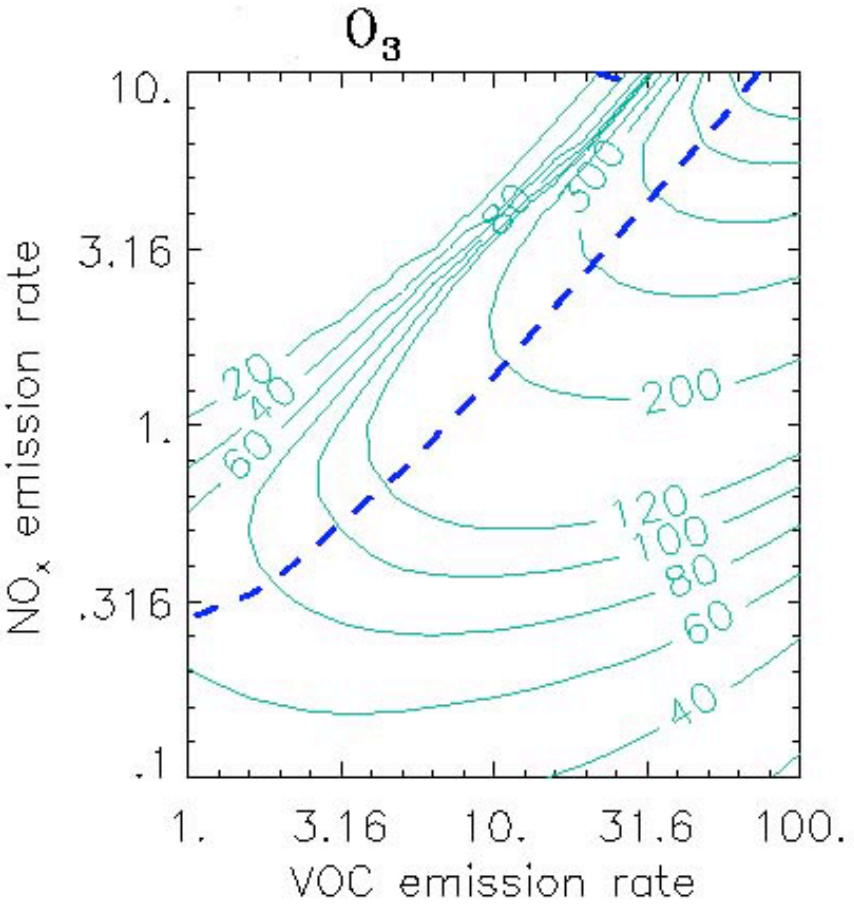

Figure 2.3. Topography of ozone based on NO_x and VOC emission rates, from *Sillman and He* [2002]. Ozone isopleths are shown in light blue [ppbv], and the maximum 'ridge' of ozone production is shown in the dark blue dashed line.

creases ozone production, and this is depicted on the top half of Figure 2.3. In these areas, high concentrations of NO_x lead to HO_x loss via the formation of nitric acid (reactions 2.23 and 2.24). It is the formation of nitric acid which is indicative of a VOC-sensitive chemical regime. It is noteworthy that in the ozone production topography shown in Figure 2.3, the way to increase ozone production most rapidly is to add VOC to a VOC-sensitive environment.

2.1.4 PAN chemistry

In addition to these loss processes, the formation of reservoir species such as PAN can also play a role in the temporary loss of HO_x and NO_x [*Sillman et al.*, 1990; *Sillman and He*, 2002]. The most abundant of these is peroxyacetyl nitrate (PAN) [*Crutzen*, 1979], which is formed by the addition of NO_2 to the acetyl radical. PAN is thermally labile and is in equilibrium with acetyl and NO_2:

$$CH_3C(O)O_2 + NO_2 \rightleftharpoons CH_3C(O)OONO_2. \tag{2.25}$$

The thermal dependence of the lifetime of PAN is in the range of typical tropospheric temperatures. PAN becomes particularly stable higher up in the troposphere [*Singh and Hanst*, 1981; *Talukdar et al.*, 1995; *Moxim et al.*, 1996], where thermal decomposition does not occur but photolysis may. The increased lifetime of PAN at these high altitudes allows for the transport of NO_x around the globe; as PAN descends into the warmer regions of the troposphere, NO_2 is released as the equilibrium shifts towards the left side of reaction 2.25.

2.1.5 Nighttime chemistry

Once the sun sets, the formation of OH by photolysis of ozone ceases. At night, NO_3 can abstract a hydrogen, usually from alkenes, producing nitric acid, and providing an initiation step for radical chemistry. NO_3 is photolytically labile, and as such does not exist during the day. At night, it can be formed from the reaction

between ozone and NO_2:

$$O_3 + NO_2 \rightarrow NO_3 + O_2. \tag{2.26}$$

Once formed, NO_3 and NO_2 are in equilibrium with dinitrogen pentoxide:

$$NO_3 + NO_2 \rightarrow N_2O_5 \tag{2.27}$$

which can be hydrolysed on aerosol surfaces to form nitric acid; this provides a nocturnal sink for NO_x. Ozonolysis of VOCs is an additional initiation step that can occur at night.

2.2 Isoprene

Isoprene, or 2-methyl-1,3-butadiene, is particularly important for tropospheric chemistry because of its high levels of emission and fast reactivity. In this section I describe the atmospheric chemistry of isoprene, a number of observations of its emission, and three types of studies that have attempted to estimate its global flux into the atmosphere.

2.2.1 Isoprene chemistry

Isoprene is a very reactive trace gas. Its reactivity arises from double unsaturation as well as methyl substitution, which stabilizes the formation of radical products. Table 2.1 lists the lifetimes of several common VOCs found in the troposphere, and shows that propane, ethene, and formaldehyde have lifetimes on the order of days. The isoprene lifetime for reaction with OH is the lowest of any of these VOCs, with a value of 1.4 hours only.

Initial reaction between one of isoprene's two π bonds and OH, plus addition of molecular oxygen yields a hydroxyperoxy radical (RO_2). In the presence of NO, this can be reduced to a hydroxyalkoxy radical (RO). The formation of HO_2 by

Table 2.1. Tropospheric lifetimes of various hydrocarbon species for reaction with the hydroxyl and nitrate radicals. Data are from *Atkinson and Arey* [2003].

VOC	Lifetime OH	Lifetime NO_3
Propane	10 day	7 yr
Ethene	1.4 day	225 day
Formaldehyde	1.2 day	80 day
α-pinene	2.6 h	5 min
Isoprene	1.4 h	50 min

hydrogen abstraction yields formaldehyde and a first generation carbonyl product; the highest molar yields of this carbonyl are for the formation of methacrolein (MACR) and methyl vinyl ketone (MVK) [e.g. *Ruppert and Heinz-Becker*, 2000, and references therein]. These first generation carbonyl products are then subject to attack by OH, particularly because of the presence of a second double bond, which begins the cycle again. The relative ratio of MVK to MACR can be indicative of the surrounding chemistry, owing to differences in the rate of removal of each by reaction with OH and ozone [see e.g. *Kuhn et al.*, 2007]. In addition, the ratio of the sum of MVK+MACR to isoprene has been shown to correlate to NO_x [*Biesenthal et al.*, 1998] and OH concentrations [*Kuhn et al.*, 2007].

A second and much smaller reaction pathway for isoprene is direct reaction with ozone through ozonolysis. Ozone can add to either of isoprene's double bonds to form an ozonide, which rapidly decomposes to a Criegee intermediate. This intermediate can then form formaldehyde, methacrolein, and methyl vinyl ketone [*Grosjean et al.*, 1993; *Aplincourt and Anglada*, 2003].

2.2.1.1 Isoprene nitrates

Another possible fate for a hydroxyperoxy radical along the isoprene oxidation chain is the formation of chain terminating species. Most important for ozone chemistry is the formation of isoprene nitrates, which occurs by collisional stabilization of the peroxy-NO intermediate [*Zhang et al.*, 2003a]. The first step is

formation of the excited intermediate:

$$\mathrm{RO_2 + NO \rightarrow ROONO*} \tag{2.28}$$

which either forms $\mathrm{NO_2}$ and the hydroxyalkoxy radical,:

$$\mathrm{ROONO* \rightarrow RO + NO_2,} \tag{2.29}$$

or is collisionally stabilized to form the nitrate:

$$\mathrm{ROONO* + M \rightarrow RONO_2 + M.} \tag{2.30}$$

These nitrates are formed in yields between 4% and 12% [see *Horowitz et al.*, 2007, and references therein]. Isoprene nitrates act as a reservoir species for $\mathrm{NO_x}$, which can be reversed by chemical reaction with hydroxyl, or which can form a permanent loss if dry or wet deposition occurs [*Horowitz et al.*, 2007]. These rates and are still subject to further research, as isoprene nitrate measurements in the field are few. The role of isoprene nitrates has also been identified as a weakness in global tropospheric chemistry modelling [e.g. *Wu et al.*, 2007].

2.2.1.2 Isoprene and aerosol formation

The existence of aerosol derived from natural organic carbon-containing compounds was first noted by *Went* [1960]. *Carlton et al.* [2009] reviewed laboratory findings and model experiments for isoprene secondary organic aerosol (SOA), and reported that estimates of isoprene SOA remain highly uncertain, with a range of 6 to 30 Tg $\mathrm{yr^{-1}}$. Global SOA has been found to be 27% [*Hoyle et al.*, 2007] to 78% [*Heald et al.*, 2008] resultant from isoprene oxidation. *Paulot et al.* [2009] recently proposed that reaction between the hydroxyhydroperoxide (a product of the first cycle of isoprene oxidation) and OH can form an epoxide whilst also recycling OH. The epoxides measured by *Paulot et al.* [2009] demonstrated rapid uptake

onto aerosol seeds. More remains to be done in order to reduce the uncertainty in isoprene derived SOA formation, but this is an important impact of isoprene on the atmosphere, as aerosol has consequences for both climate [e.g. *Bellouin et al.*, 2005; *Kanakidou et al.*, 2005] and human health [*Englert*, 2004].

2.2.2 Observations of isoprene emission

Discoveries of biogenic isoprene emission occurred in both the United States [*Rasmussen and Went*, 1965] and the former Soviet Union [*Sanadze*, 1957]. Early flux measurements confirmed that isoprene is emitted from specific taxa common to forest ecosystems; early on, these were documented in North America [e.g. *Rasmussen*, 1970] and the tropics [e.g. *Rasmussen and Khalil*, 1988]. In conjunction with these early flux measurements, inventories of VOC and isoprene emission were calculated for the United States [*Zimmerman*, 1979; *Lamb et al.*, 1987] and the globe [*Müller*, 1992].

Thousands of measurements of isoprene emission have been made for various plant species. A summary of relevant measurements of species-specific isoprene fluxes can be found Table 2.2 as reviewed by *Kesselmeier and Staudt* [1999]. The data presented are for plants whose emission rates are notably high; also listed are common crop species that are of potential interest for biofuel production. More recently, an electronic database of biogenic VOC measurements has also been established [*Wiedinmyer et al.*, 2004][2].

The biosynthetic pathway of many of the biogenic VOCs emitted into the troposphere are similar, and most monoterpenes and isoprene share the same precursor compound dimethylallyl pyrophosphate (DMAPP) [*Fuentes et al.*, 2000]. Isoprene synthesis is carried out by an enzyme, isoprene synthase, whose activity is correlated with isoprene emission [*Kuzma and Fall*, 1993]. Isoprene escapes from a plant through its stomata [*Sharkey*, 1996], though the physiological reason for isoprene emission still remains unknown. It has been noted that many less evolved

[2]Enclosure measurements are available online: http://bai.acd.ucar.edu/Data/BVOC/index.shtml

Table 2.2. Isoprene flux rates for high-emitting and biofuel relevant species. Emission factors are standardized to 1000 μ mol^{-1} s^{-1} incoming photosynthetically active radiation (PAR) and 30 °C and are given in units of μg LDW^{-1} h^{-1}, or μg isoprene emitted per gram of leaf dry weight per hour. Data are summarized from *Kesselmeier and Staudt* [1999].

Species	Familiar Name	Flux Rate $\mu g \cdot LDW^{-1}\ h^{-1}$
Mucuna Pruriens	Velvet Bean	317
Eleais guineesis	Palm Oil Tree	172.9
Acacia Nigrescens	African Acacia	110
Salix Babylonica	Weeping Willow	115
Populus Balsamifera	Southern Poplar	100±46
Quercus Alba	White Oak	7.8-120
Querus Coccinea	Scarlet Oak	40-130
Querus Velutina	Black Oak	60-100
Liquidambar styraciflua	Sweetgum	63-99
Securinega Virosa	Securinega	81
Eucalyptus Globulus	Blue Gum Eucalyptus	15-49
Arundo Donax	Giant Reed	38.6
Oryza Sativa	Rice	0
Secale Cereale	Rye	0
Sorghum Bicolor	Sorghum	0
Triticum Aestivum	Wheat	0
Glycine Max	Soy Bean	0

plants emit isoprene [*Fuentes et al.*, 2000, and references therein]. Emission for thermal protection has been proposed [*Sharkey and Singsaas*, 1995], as well as protection from ozone [e.g. *Loreto et al.*, 2001].

2.2.2.1 Isoprene emission, light, and temperature

Although the physiological reason for isoprene emission remains unknown, the relationship between isoprene emission and light and temperature has been documented for over thirty years.

The relationship between isoprene emissions and temperature was recorded by both *Rasmussen and Jones* [1973] and *Tingey et al.* [1979]. That emission is correlated to the activity of isoprene synthase rather than stomatal conductance was first reported by *Jones and Rasmussen* [1975]. The activity of isoprene synthase

is temperature dependent [*Fall and Wildermuth*, 1998; *Logan et al.*, 2000], and isoprene emission generally increases strongly with increased temperature. This relationship holds until a threshold temperature is reached (approximately 40 °C), when isoprene synthase begins to denature [*Fall and Copley*, 2000].

The correlation of isoprene emission with radiation was first recognized by *Sanadze* [1964], and was clarified by *Rasmussen and Jones* [1973]. Isoprene emission requires light to be emitted [*Lerdau and Gray*, 2003], and increases with increased incident radiation, though the physiological reasons behind this dependence remain unknown. In addition to the correlation between laboratory measurements of emissions and light and temperature, correlation of *in situ* flux measurements and light and temperature have been reported [e.g. *Rinne et al.*, 2002].

2.2.2.2 Isoprene suppression by CO_2

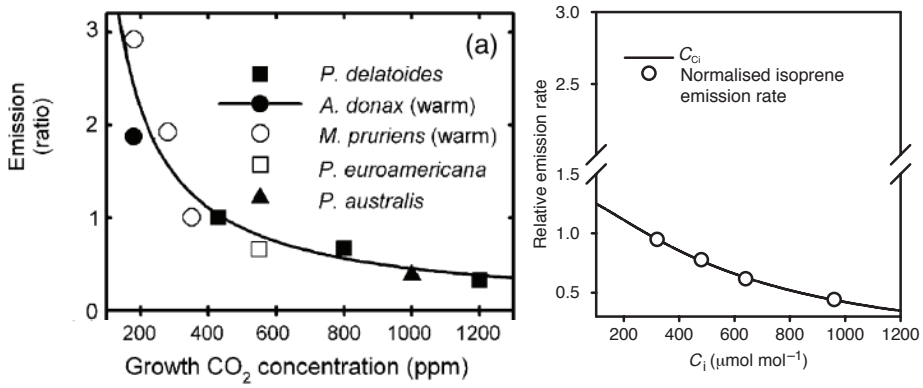

Figure 2.4. Empirically deduced relationships between CO_2 and isoprene emission from *Possell et al.* [2005] (left) and *Wilkinson et al.* [2009] (right).

That CO_2 concentration levels impact emission of isoprene was reported as early as 1973 by *Rasmussen and Jones*. The suppression of emission at high CO_2 was measured in leaf cuvettes by both *Monson and Fall* [1989] and *Loreto and Sharkey* [1990]. More recently, isoprene emission has been found to be suppressed when CO_2 concentrations were artificially raised in an otherwise open environ-

ment [*Rosenstiel et al.*, 2003]. The study of *Possell et al.* [2005] compiled the reported values in the literature with new measurements to deduce a simple empirical relationship between CO_2 concentration and leaf-scale isoprene emission; this relationship is shown in Figure 2.4. The inhibition of emission from present day values (300-400 ppbv) of CO_2 to potential future values (600-800 ppbv) was also reported by *Wilkinson et al.* [2009], whose emission relationship is also shown in Figure 2.4. The stimulation of emission at lower ambient concentrations was not supported by *Wilkinson et al.* [2009], who linked the relationship between CO_2 and isoprene emission to competing processes occurring at the cellular level for pyruvate, an important molecule in isoprene production. *Arneth et al.* [2007a] conducted a review of the potential explanations for CO_2 inhibition of isoprene emission at the plant physiological level.

2.2.3 Estimations of isoprene emissions

Three types of modelling studies have attempted to estimate the global flux of isoprene into the atmosphere. In this section, I review the empirical, process based, and satellite studies and the resulting estimations of global isoprene emission.

2.2.3.1 Empirical

The first empirical attempt to estimate global VOC emission was undertaken by *Rasmussen and Went* [1965]. The authors reported a value of 438 Tg VOC yr^{-1} using a simple methodology; they multiplied four factors together which accounted for above-forest concentration of VOC, the height of the boundary layer, the total land area covered by VOC-emitting vegetation, and the season of emission. Much lower estimates for the contiguous United States were reported by *Zimmerman* [1979] (65 Tg yr^{-1}) and *Lamb et al.* [1987] (31 Tg VOC yr^{-1}). In the latter, the estimate accounted for land use, the temperature dependence of emission, and light and seasonal dependence. The parameterizations were simple: isoprene emissions were not allowed after the first frost and before spring, and emission was also not

allowed at night.

Global isoprene emission estimates increased in their complexity throughout the following decade. *Rasmussen and Khalil* [1988] considered land area, leaf surface area, percent of emitters in an ecosystem type, rate of emission, number of emission days, and the length of days in their calculation of global isoprene emission. The authors estimated global isoprene emission to be 397 Tg C yr^{-1} (450 Tg isoprene yr^{-1}). *Turner et al.* [1991] used foliar biomass instead of percentage of emitters, and the exponential temperature dependence of *Tingey et al.* [1981] to calculate a value of 251 Tg C yr^{-1} (285 Tg isoprene yr^{-1}). Using the future distribution of vegetation from a climate-vegetation model, *Turner et al.* [1991] also calculated a future isoprene emission of 318 Tg C yr^{-1} (360 Tg isoprene yr^{-1}). A similar estimate was calculated by *Müller* [1992], who used vegetation type, the exponential temperature dependence of *Lamb et al.* [1987], and leaf biomass density to estimate total global isoprene emission of 221 Tg C yr^{-1} (250 Tg isoprene yr^{-1}). The authors included a calculation of net primary productivity which include parameterizations for precipitation and temperature, which was then taken to be proportional to leaf biomass density.

The algorithm of *Guenther et al.* [1995] improved on these existing methodologies. The authors included more accurate emission factors, more nuanced parameterizations of the emission dependence on light and temperature, and a greater horizontal ($0.5^\circ \times 0.5^\circ$) and temporal (monthly) resolution of input parameters than previous estimates. Their flux estimations were calculated according to:

$$F = D \cdot \epsilon \cdot C_T \cdot C_L \tag{2.31}$$

where F is the flux, D is the foliar density (kg dry matter m^{-2}), ϵ is an emission factor dependent on the ecosystem type, and C_T and C_L are empirically derived activity adjustment factors which account for the emission dependence on temperature and light, respectively. The foliar density, D, was calculated using net primary productivity, which was dependent on temperature and precipitation. ϵ was nor-

Table 2.3. Literature estimates of total present day global isoprene flux [Tg C yr^{-1}] from a number of models.

Source	Emissions estimate [Tg C yr^{-1}]
Rasmussen and Khalil [1988]	397
Turner et al. [1991]	251
Müller [1992]	221
Guenther et al. [1995]	503
Wang and Shallcross [2000]	530
Adams et al. [2001]	495
Potter et al. [2001]	559
Levis et al. [2003]	507
Sanderson et al. [2003]	484
Naik et al. [2004]	454
Lathière et al. [2005]	402
Shim et al. [2005]	566
Tao and Jain [2005]	601
Lathière et al. [2006]	460
Guenther et al. [2006]	529
Arneth et al. [2007b]	410
Lathière et al. [2009]	413

malized to incoming photosynthetically active radiation (PAR) of 1000 μmol m^{-2} s^{-1} and a temperature of 303.15 K. Five possible ϵ values were assigned according to the ecosystem type; these emission factors were derived from analysis of twelve separate measurement studies. The algorithm developed by *Guenther et al.* [1995] is the basis for most of the global isoprene flux estimates listed in Table 2.3.

Although the original empirical equation (2.31) remains the basis for the estimates listed in Table 2.3, a number of additional factors have been added over subsequent years. Examples include plant growth stage [*Potter et al.*, 2001], leaf age [*Lathière et al.*, 2005; *Tao and Jain*, 2005], and the percentage of an emission flux which escapes from the canopy [*Tao and Jain*, 2005]. Some amount of the variability between estimates is due to difference input datasets. The distribution of ecosystem types has also been estimated from dynamical global vegetation models (DGVMs) [e.g. *Sanderson et al.*, 2003; *Naik et al.*, 2004; *Lathière et al.*,

2005].

The emission model of *Lathière et al.* [2009] is based on the Model of Emissions of Gases and Aerosols from Nature (MEGAN), which was described by *Guenther et al.* [2006]. The MEGAN scheme made improvements on the work of *Guenther et al.* [1995] by including the impacts of soil moisture, leaf age, and canopy loss processes on isoprene fluxes. Although *Guenther et al.* [2006] implemented emission factors (ϵ) which vary spatially, *Lathière et al.* [2009] use mean emission factors due to long integration periods. Six ecosystems, or plant functional types (PFTs) were used. The impact of CO_2 according to *Possell et al.* [2005] was included in the model calculations. The isoprene emission distributions used throughout this thesis are from the model of *Lathière et al.* [2009].

2.2.3.2 Process based

A second method for bottom-up estimations of isoprene emission is process based. These models use the cellular processes which control isoprene emission to calculate their estimates rather than ecosystem level empirical data. So far, three process based models have been developed to estimate isoprene emission fluxes [*Niinemets et al.*, 1999; *Martin et al.*, 2000; *Zimmer et al.*, 2003], and their differences are reviewed in *Arneth et al.* [2007a]. *Arneth et al.* [2007b] used the algorithm of *Niinemets et al.* [1999] to calculate global isoprene emission of 410 Tg C yr^{-1} using 10 ecosystem types.

Keenan et al. [2009] used the model of *Guenther et al.* [1995] as well as the processed based models of *Niinemets et al.* [1999] and *Martin et al.* [2000] to estimate isoprene fluxes from European forests. The authors found that for the present day calculation, the choice of emissions model did not significantly affect the results; they reported 1.03 Tg C yr^{-1} isoprene emission from European forests. For the future, however, the models diverged in their projections of total isoprene emissions; the model of *Martin et al.* [2000] calculated an isoprene flux (2.36 Tg C yr^{-1}) almost 50% higher than the model of *Niinemets et al.* [1999] (1.58 Tg C

yr^{-1}).

2.2.3.3 Satellite derived

Finally, a top-down method for isoprene flux calculations has been achieved using satellite data. Formaldehyde is a product of isoprene oxidation and is detectable by remote sensors. Using the yield of formaldehyde, which is calculated using a model chemical mechanism, and the formaldehyde data as measured by the Global Ozone Monitoring Experiment (GOME) satellite, *Palmer et al.* [2003] calculated summertime isoprene fluxes over North America. Their results (5.7 Tg C in July) were lower than an analogous calculation from the *Guenther et al.* [1995] method (7.1 Tg C in July). *Shim et al.* [2005] extended this method to calculate a global isoprene emission flux of 566 Tg C yr^{-1}.

A second top-down estimation, using the satellite data retrieved by the Ozone Monitoring Instrument (OMI), was undertaken by *Millet et al.* [2008]. In the method which is most directly comparable to the results described in *Palmer et al.* [2003], *Millet et al.* [2008] reported 8.2 Tg C yr^{-1} emitted by North America in the period June-August. This compared with 10.6 Tg C yr^{-1} predicted by *Guenther et al.* [2006].

2.2.3.4 Magnitude & range of estimates

The total emission of isoprene is roughly equal to that of methane (582 Tg yr^{-1} in *Solomon et al.* [2007b]). Generally, biogenic VOC comprises a large fraction of total VOC emissions; in my control run (BASE, in chapters 3, 5, and 6) anthropogenic VOC was only 22% of the total global flux. Since the development of the original empirical model by *Guenther et al.* [1995], the range of estimates has been relatively small, between 400 and 600 Tg C yr^{-1}. This appears to be well constrained, though *Arneth et al.* [2008a] argued that this was due to proliferation of a few algorithm types rather than low levels of scientific uncertainty. The range that does occur can be explained by variations in input data; *Pfister et al.* [2008a]

noted that a 28% change in their emissions calculation arose from changing the input land cover characteristics.

2.3 Summary

In this chapter, I introduced the salient features of tropospheric chemistry. I described the initiation of the radical oxidation processes that occur in the atmosphere, followed by the propagation of these reactions. This included the separation between ozone-producing and ozone-destroying chemical regimes. I described the chain termination reactions which can be used to describe a NO_x-sensitive or VOC-sensitive chemical environment.

After explaining the basics of PAN chemistry and nighttime chemistry, I turned to isoprene. The lifetime of isoprene in the atmosphere was discussed, as well as a series of observations of isoprene emission and its correlation to light, temperature, and CO_2 concentration. I devoted the last section of this chapter to a discussion of global isoprene flux estimations, describing empirical, process based, and satellite based methods.

In the next chapter, I describe the atmospheric model that is used in this thesis, and the impact that including isoprene has on model chemistry.

Chapter 3

The Impact of Isoprene in UKCA

In this chapter, I introduce the global climate composition model UKCA (the United Kingdom Chemistry and Aerosol model). In section 3.2, I describe the basic model dynamics, chemistry, and emissions used in my experiments. After a short model evaluation (section 3.3) and experimental description (section 3.4), I explore the impact of including isoprene oxidation in UKCA in a present day atmosphere (section 3.5).

3.1 Introduction

Numerical approaches to weather prediction and meteorology were first proposed by Cleveland Abbe in the early twentieth century [*Abbe*, 1901]. His suggestions were realized in part by Vilhelm Bjerknes, the first scientist to propose the diagnostic-prognostic system for weather prediction [see the review of *Lynch*, 2008, and references therein]. Bjerknes also put forward the first set of independent mathematical equations to describe the present and future states of the atmosphere from a set of initial conditions [*Bjerknes*, 1904]. Solving these equations was emboldened by the vision of Lewis Fry Richardson, the advent of the modern computer, and the leadership of John von Neumann [*Richardson*, 1922; *Tribbia and Anthes*, 1987; *Lynch*, 2008]. The first computational predictions of weather occurred in the early

1950's [*Platzman*, 1979; *Tribbia and Anthes*, 1987].

Simultaneously, the importance of atmospheric chemistry for air quality was being established; in 1952, *Haagen-Smit* described the effects of photochemical smog. The nature of tropospheric photochemistry has been elucidated and characterized in more depth since [e.g. *Crutzen*, 1970; *Liu et al.*, 1987; *Atkinson*, 2000], through the use of a number of tools, one of which is computer models. Global modelling has been approached in two distinct ways: first, with the use of chemistry-transport models (CTMs) [see e.g. *Logan et al.*, 1981; *Brasseur et al.*, 1998; *Wild and Prather*, 2000; *Bey et al.*, 2001; *Park et al.*, 2004; *Savage et al.*, 2004; *Teyssèdre et al.*, 2007] which are externally forced, and second with general circulation models (GCMs) [see e.g. *Roelofs and Lelieveld*, 1995; *Johnson et al.*, 1999; *Horowitz et al.*, 2003; *Zeng and Pyle*, 2003; *Hauglustaine et al.*, 2004; *Schmidt et al.*, 2006], which generate their own meteorological fields. Tropospheric chemistry modelling has historically been approached through the lens of air quality.

The inclusion of isoprene oxidation, which is particularly important for tropospheric chemistry, is a more recent addition to global models [e.g. *Fehsenfeld et al.*, 1992; *Pfister et al.*, 2008b]. Isoprene chemistry is complex, and involves hundreds of intermediates; for this reason, its chemistry is represented in models in a number of condensed schemes. The particular mechanism which represents isoprene oxidation has been shown to influence model results [e.g. *Archibald et al.*, in press]. *von Kuhlmann et al.* [2004] found a large differences (up to 60%) in ozone when the various lumped mechanisms were used in their model. The production of PAN is also cited as a reason for the differences in isoprene modelling, with global PAN concentrations varying by over 50% in several sensivity studies in *von Kuhlmann et al.* [2004]. Differences in model representations of isoprene degradation has also been identified as one of the key areas of uncertainty in model intercomparisons. *Wu et al.* [2007] found that the yield of organic nitrates from isoprene oxidation plays a large role in the differences between model ozone budgets.

Pfister et al. [2008a] described the contribution of representing isoprene oxidation in a CTM chemical budget by implementing a tracer tagging scheme. Over hot-spot emitting regions in the southern hemisphere, column PAN was found to be up to 70% resultant from isoprene degradation. Global ozone burden decreased by 3% when isoprene was removed from the model calculations, and regional changes in ozone of up to 4 Dobson units occurred over high NO_x-emitting regions. Over the Amazon, a reduction in ozone was calculated when isoprene was included in their model, which the authors attributed to ozonolysis. 9-16% of the CO burden was derived from isoprene oxidation [*Pfister et al.*, 2008a], similar to the estimate of *Granier et al.* [2000], in which isoprene contributed 10% to the tropospheric CO burden.

The photooxidation of isoprene is important for air quality on both global [e.g. *Fehsenfeld et al.*, 1992; *Houweling et al.*, 1998; *Folberth et al.*, 2006] and regional [e.g. *Pierce et al.*, 1998; *Tao et al.*, 2003] scales, though precise results seem to be sensitive to the configuration of the base model. The inclusion of isoprene in one model led to a 250% increase in ozone in the northern hemisphere [*Houweling et al.*, 1998]. *Wang and Shallcross* [2000] found that isoprene chemistry increased ozone by 4 ppbv over oceans and 8-12 ppbv over land and across northern midlatitudes in August. *Folberth et al.* [2006] reported somewhat higher values between 8-25 during northern hemisphere summer due to isoprene. Isoprene is also important for the ozone budget, as reported by *Wild* [2007], in which isoprene emissions were found to be one of the leading causes for budget variability. In the work of *Roelofs and Lelieveld* [2000] net chemical production increased by 110 g yr^{-1} due to isoprene, while the annually averaged burden increased by 23 Tg.

One of the most important ways in which isoprene impacts ozone concentrations is through interaction with NO_x. There is some uncertainty in the chemistry of PAN and other nitrates that are formed during the degradation of isoprene (e.g. isoprene nitrates, higher peroxy nitrates, or nitroxy-aldehydes). The yield of isoprene nitrates from reaction between isoprene peroxy radicals and NO remains

uncertain, and has been reported at 4.4% [*Chen et al.*, 1998], 8% [*Carter and Atkinson*, 1996], and even 8-12% [*Sprengnether et al.*, 2002]. The fate of these nitrates is also uncertain, including the rate of potential recycling of NO_x through reaction with OH [see *Horowitz et al.*, 2007, and references therein] and rates of deposition [*Shepson et al.*, 1996]. The sensitivity of models to these parameters has been tested in *Horowitz et al.* [1998], *Fiore et al.* [2005], and *von Kuhlmann et al.* [2004]. The maximum relative changes in ozone burden in *von Kuhlmann et al.* [2004] were found to arise from variations in deposition velocity as opposed to the chemical mechanism, total isoprene emission, or treatment of nitrates. *Fiore et al.* [2005] did not test the deposition sensivity, but did report that a change in the yield and recycling of NO_x from isoprene nitrates altered ozone maxima by over 10 ppbv.

In this chapter, my aim is describe UCKA and to quantify the impact that isoprene has on model results.

3.2 UKCA

UKCA has both a stratospheric version, which has been described in *Morgenstern et al.* [2009], and a tropospheric version, which has been described briefly in *O'Connor et al.* [2009]. The stratospheric version of the model runs with a different chemistry and is more often used with interactive chemistry-climate feedbacks [e.g. *Morgenstern et al.*, 2008]. What follows is the first description of the tropospheric version of the model which is run in Cambridge.

3.2.1 Dynamics

UKCA is a chemistry module embedded in the unified model (UM), which is developed by the UK Met Office for both research and numerical weather prediction. UM6.1 (the version used here) is a non-hydrostatic model which uses a semi-Lagrangian tracer transport scheme [*Priestley*, 1993]. The horizontal resolution is

3.75 by 2.5 degrees. The model has semi-implicit timestepping, and is inherently mass conserving. The dynamical core of the model is described in *Davies et al.* [2005]. Gravity wave drag has both an orographic [*Webster et al.*, 2003] and a spectral component [*Scaife et al.*, 2002]. The radiation scheme of *Edwards and Slingo* [1996] is used, and for the BASE run, carbon dioxide was set to 345 ppmv and was methane set to 1655 ppbv. In addition, the mixing ratios of N_2O, CFC-11, and CFC-12 were set to 207 ppbv, 230 pptv, and 382 pptv, respectively. Ozone can interact on-line with the radiation scheme [e.g. *Morgenstern et al.*, 2008], but in these experiments values are set by the climatology of *Li and Shine* [1995] to reduce variability between simulations. Cloud microphysics are represented as in *Wilson and Ballard* [1999] and cloud top height for convection is parameterized using *Gregory and Rowntree* [1990].

3.2.2 Chemistry

UKCA uses the ASAD chemistry package [*Carver et al.*, 1997], which has been used in the CTM TOMCAT [*Law et al.*, 1998; *Cook et al.*, 2007; *Hamilton et al.*, 2008] and the GCM UM_CAM [*Zeng and Pyle*, 2005, 2003; *Zeng et al.*, 2008]. The chemistry is solved by a Newton-Raphson solver derived from *Wild and Prather* [2000]. It is a medium-sized chemistry, simulating the O_x, HO_x, and NO_x chemical cycles and the oxidation of CO, methane, ethane, propane, and isoprene. The mechanism without isoprene chemistry has been described in *Arnold et al.* [2005]. The model has 55 chemical tracers, 114 bimolecular reactions, 15 termolecular reactions, and 35 species are photolysed. Isoprene oxidation is parameterized using the condensed Mainz isoprene mechanism (MIM).

The MIM is described in *Pöschl et al.* [2000] and its implementation into the ASAD chemistry package is discussed in *Young* [2007] and *Young et al.* [2009]. The MIM performed favourably in comparison with a much more complex mechanism (the Master Chemical Mechanism, or MCM, [*Jenkin et al.*, 1997; *Saunders et al.*, 1997]). It varied from the MCM by less than 10% in most cases for compar-

Table 3.1. Tracers involved in the MIM representation of isoprene oxidation, after *Pöschl et al.* [2000].

Tracer	Description
C_5 compounds	
C_5H_8	isoprene
ISO_2	peroxy radicals from C_5H_8 + OH
ISOOH	β-hydroxyhydroperoxides from ISO_2 + HO_2
ISON	β-hydroxy alkylnitrates from ISO_2 + NO and alkyl nitrates from C_5H_8 + NO_3
C_4 compounds	
MACR	methacrolein, methyl vinyl ketone, and other C_4 carbonyls
$MACRO_2$	peroxy raicals from MACR + OH
MACROOH	hydroperoxides form $MACRO_2$ + HO_2
MPAN	peroxymethacrylic nitric anhydride and other higher peroxyacyl nitrates
C_3 compounds	
HACET	hydroxyacetone and other C_3 ketones
MGLY	methylglyoxal and other C_3 aldehydes
C_2 and C_1 compounds	
$CH_3C(O)O_2$	peroxyacetyl radical
PAN	peroxyacetyl nitrate
$CH_3C(O)OOH$	peroxy acetic acid
$CH_3C(O)OH$	acetic acid
NALD	nitrooxy acetaldehyde
HCOOH	formic acid

isons with O_3, OH, CO, and PAN among other species [*Pöschl et al.*, 2000]. Table 3.1 shows a list of the 16 tracers involved in the representation of isoprene chemistry, which go through 44 chemical reactions. The main oxidation pathway of isoprene is via reaction with OH, from which ISO_2 is produced in the MIM. This can either form a peroxide (ISOOH), resulting from reaction with either HO_2 or another ISO_2 molecule, or can react with NO. The ISO_2 + NO reaction forms either a nitrate species (ISON), or a representative C_4 species (MACR), and formaldehyde; from the latter reaction, other tracers are formed in much smaller quantities. The MACR tracer can produce MPAN or hydroxyacetone, which can be oxidized by OH to form methylglyoxal; oxidation of methylglyoxal by OH yields the peroxyacetyl radical. The peroxyacetyl radical can form PAN (see section 2.1.4) or formaldehyde and methylperoxy, followed by final oxidation to carbon dioxide and water.

Photoysis is calculated using the off-line scheme of *Law and Pyle* [1993a], which relies on tabulated values for photolysis as calculated by the Cambridge 2D model [*Harwood and Pyle*, 1975]. Photolysis rates are adjusted for solar zenith angle and have a diurnal variation. 32 species are dry deposited, and dry deposition is calculated from tabulated velocities [*Ganzeveld and Lelieveld*, 1995; *Zhang et al.*, 2003b] and is adjusted for season, time of day, and surface roughness as described by *Giannakopoulos et al.* [1999]. Five surface types are accounted for: snow/ice, water, forest, desert, and savannah/grassland. The deposition velocity is then extrapolated into the middle of the lowermost model level using the method of *Sorteberg and Hov* [1996]. Wet deposition is described as a first order loss using rainfall rates as calculated by the dynamics of the UM [*Giannakopoulos et al.*, 1999] and is calculated for 24 species.

Concentrations of ozone, NO_y, and CH_4 are overwritten in the stratosphere above approximately 30 hPa with zonal mean concentrations generated by the Cambridge 2D model [*Harwood and Pyle*, 1975; *Law and Pyle*, 1993b,a]. This allows for representative seasonal changes in tracer concentrations without running a

Table 3.2. Present day emissions of NO_x, CO, and non-methane VOCs in UKCA.

Species	Amount
NO_2, Tg N yr^{-1}	
Domestic	1.5
Industrial	10.3
Traffic	16.1
Soil	7.0
Biomass Burning	10.2
Total	*45.0*
CO, Tg CO yr^{-1}	
Domestic	238.3
Industrial	37.6
Traffic	194.6
Biogenic	89.0
Ocean	11.0
Biomass Burning	507.5
Total	*1078.0*
VOC, Tg VOC yr^{-1}	
Domestic	28.8
Industrial	39.3
Traffic	47.7
Natural (acetone)	48.3
Natural (isoprene)	468.1
Biomass Burning	31.3
Total	*663.5*

full stratospheric chemistry. Carbon dioxide (345 ppmv) and methane (1655 ppbv) are set at a fixed value in the chemistry to avoid excessively long spin-up periods.

3.2.3 Emissions

Eight chemical species are emitted in UKCA: nitrogen dioxide (NO_2), carbon monoxide (CO), formaldehyde (HCHO), ethane (C_2H_6), propane (C_3H_8), acetaldehyde (CH_3CHO), acetone ($CH_3C(O)CH_3$), and isoprene (C_5H_8). Tracers are emitted into the lowermost model level, and emissions are updated every five model days. Isoprene is the only species emitted with diurnal variation. Geographic distributions of the emissions of the first seven species were compiled by

Dentener et al. [2005]. These emissions were used by the model intercomparisons of *Stevenson et al.* [2006] and *Shindell et al.* [2006b], as well as in the fourth assessment of the Intergovernmental Panel on Climate Change (IPCC) [*Solomon et al.*, 2007b]. Emissions of NO_x, CO, and total non-methane VOCs are summarized in Table 3.2 and are broken down by source sector. Anthropogenic emissions are based on the Edgar3.2 dataset [*Olivier and Berdowski*, 2001], which includes ship emissions estimated for 1995 and assumes a 1.5% growth rate per annum. Biomass burning emissions are distributed according to *van der Werf et al.* [2003], with totals derived from the 1997-2002 average. Ecosystem-specific biomass burning emission factors were used from *Andreae and Merlet* [2001].

Soil NO_x emissions are distributed according to the GEIA emissions inventory [*Global Emissions Inventory Activity*, Accessed 21 October, 2009] based on the model of *Yienger and Levy II* [1995] and are scaled to 7 Tg N yr^{-1} as recommended by *Stevenson et al.* [2006]. Aircraft emissions are from AERO2K [*Eyers et al.*, 2004]. Lightning NO_x emission is based on the parameterization of [*Price and Rind*, 1992] and is scaled to 5 Tg N yr^{-1} based on an idealized five year model run. Natural CO emissions (biogenic and oceanic) are distributed as recommended by *Stevenson et al.* [2006], according to the POET project [*POET Inventory*, Accessed 21 October, 2009], based on *Müller and Brasseur* [1995] and are scaled to 100 Tg CO yr^{-1}. Table 3.3 shows the breakdown of VOC emissions. Non-methane non-isoprene hydrocarbons are scaled to 116 Tg VOC yr^{-1} for anthropogenic sources, as suggested by the fourth assessment report of the IPCC [*Solomon et al.*, 2007b]. Speciation is provided by the third assessment of the IPCC *Prather et al.* [2001]. Not all the species listed in *Prather et al.* [2001] are initialized in UKCA, so after speciation the total is re-scaled to 100%. Biogenic acetone emissions of 30.1 Tg C yr^{-1} are added to this using the spatial and temporal distribution of the GEIA database.

Table 3.3. Present day emissions of ethane, propane, formaldehyde, acetaldehyde, acetone, and isoprene in UKCA [Tg VOC yr^{-1}].

Species	Amount
Ethane	
Domestic	9.5
Industrial	13.0
Traffic	15.8
Biomass burning	12.8
Total	*51.1*
Propane	
Domestic	11.2
Industrial	15.2
Traffic	18.5
Biomass burning	3.7
Total	*48.5*
Formaldehyde	
Domestic	1.0
Industrial	1.4
Traffic	1.7
Biomass burning	2.2
Total	*6.3*
Acetaldehyde	
Domestic	3.2
Industrial	4.4
Traffic	5.4
Biomass burning	11.1
Total	*24.2*
Acetone	
Domestic	3.9
Industrial	5.3
Traffic	6.4
Biomass burning	1.5
Natural	48.3
Total	*65.3*
Isoprene	
Total	*468.1*

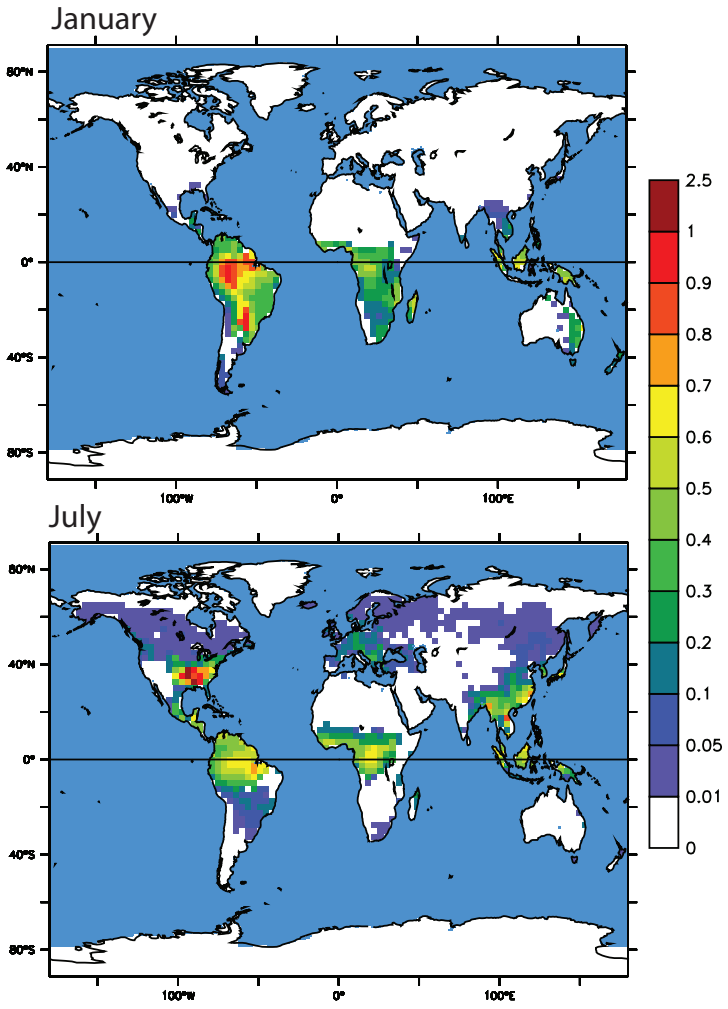

Figure 3.1. January (top) and July (bottom) isoprene emissions [μg m^2 s^{-1}] modelled by the SDVGM and a BVOC emission model.

3.2.4 Isoprene emissions

Isoprene emissions were derived using a BVOC emissions model[1]. The emissions model is based on the empirical parameterizations of *Guenther et al.* [1995], which were updated in *Guenther et al.* [2006] and have been described in Chapter 2. In the version used here, parameterizations were adjusted from their original form

[1]Isoprene emissions were calculated by Juliette Lathière at the University of Sheffield. Our collaboration is part of the QUEST project.

and did not include geographic variation in emissions factors from various plant functional types (PFTs). The distribution of PFTs was calculated by the Sheffield Dynamic Global Vegetation Model (SDGVM) [*Woodward et al.*, 1995; *Beerling et al.*, 1997]. The vegetation model was forced with meteorological fields output from the UM, which was run without chemistry. The present-day global vegetation map is based on *Loveland et al.* [2000] and accounts for crops by using *Ramankutty and Foley* [1999] and anthropogenic grasses from *Klein Goldewijk* [2001][1].

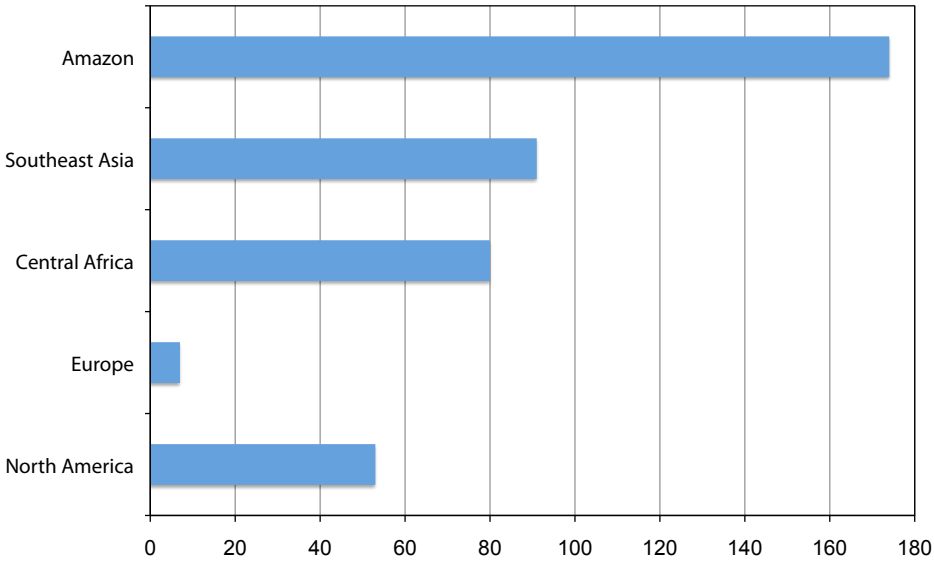

Figure 3.2. Regional isoprene emissions [Tg C yr^{-1}].

Figure 3.1 shows the geographical location and magnitude of present day isoprene emissions for January and July, when emissions are at their peak in the southern and northern hemisphere, respectively. A meridional seasonality appears in the emissions that follows the path of the sun, as emissions of isoprene are closely correlated to radiation and temperature (see section 2.2.2.1). Tropical and sub-tropical forests are notably high emitting, and key emission regions include the Amazon, central Africa, Southeast Asia and in July, the southeastern United States. The total

[1]The crop map was compiled by Nathalie du Noblet-DuCoudré and Jean-Yves Peterschmitt in collaboration with Juliette Lathière [*Lathière et al.*, 2009].

global emissions of isoprene are 413 Tg C yr^{-1} (468 Tg isoprene yr^{-1}), which is 78% of total flux of VOC into the atmosphere in the BASE experiment.

Figure 3.2 shows isoprene emissions for high emitting regions. The Amazon emits the most of any region, at 174 Tg C yr^{-1}. Central Africa and Southeast Asia emit 80 and 91 Tg C yr^{-1}, respectively. Annual isoprene emissions in North America are lower than the other hot-spot areas, but the numbers are slightly misleading due to the seasonality of emissions. In January, North American emissions are as low as 1.9 Tg C $month^{-1}$, and in July, this value rises to 9.35 Tg C $month^{-1}$. If this high level of emission was maintained, the annual emission would come to 112.2 Tg C yr^{-1}, higher than Southeast Asia and central Africa.

3.3 Model evaluation

3.3.1 Stratosphere-troposphere exchange

Initially, a 38-level version of the model was developed. This version is still employed at the UK Met Office, and is described briefly in *O'Connor et al.* [2009]. I found ozone concentrations that were too high in remote marine areas when using this version of the model, especially in the northern hemisphere during March-April and the southern hemisphere during September-October. This seasonal cycle is suggestive of too strong stratosphere-troposphere exchange (STE), which is a result of the Brewer-Dobson circulation [*Dobson et al.*, 1946; *Brewer*, 1949]. The seasonality of the circulation leads to a strengthening of the downward motion in the winter hemisphere [*Holton et al.*, 1995]. The Brewer-Dobson circulation is stronger in the northern hemisphere, due to to increased wave activity in the region, and this may contribute to observed maxima in spring concentrations of ozone in the region [e.g. *Monks*, 2000].

The introduction of an on-line STE diagnostic[1] reinforced our hypothesis. Seasonally varying annual STE [Tg O_3 yr^{-1}] is shown in Figure 3.3 for two model

[1]The diagnostic was implemented by Dr. N. Luke Abraham.

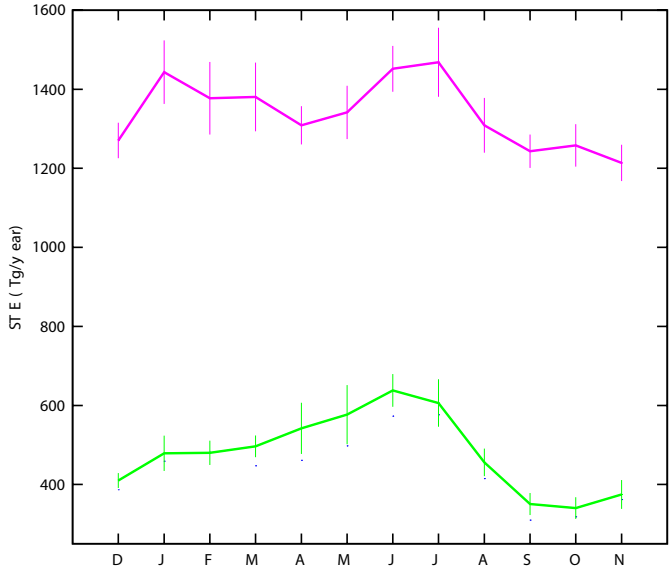

Figure 3.3. Stratosphere-troposphere exchange [Tg O_3 yr^{-1}] for two model runs. The 38 level version is shown in pink, and the 60 level version is shown in green (the 'BASE' run).

runs. The 38-level version of the model simulates the atmosphere up to 56 km, while the 60-level version captures the whole stratosphere and simulates up to 84 km. This extension into the mesosphere meant that the Brewer-Dobson overturning could be fully and more accurately modelled. Indeed, the 60-level version has an average annual STE is 424 Tg yr^{-1}, which lies within the first standard deviation of the model average from the recent comprehensive model assessment by *Stevenson et al.* [2006] of 556 $\pm$ 154 Tg yr^{-1}. This was a marked improvement over the 38 level version, which had an average annual STE of 1324 Tg yr^{-1}. The estimate from the 60-level version of the model is similar to that reported in *Murphy and Fahey* [1994], who used observed ratios to estimate the flux of ozone from the stratosphere to be 450 Tg yr^{-1}. *Gettelman et al.* [1997] estimated STE to be 450-590 Tg yr^{-1} from satellite data.

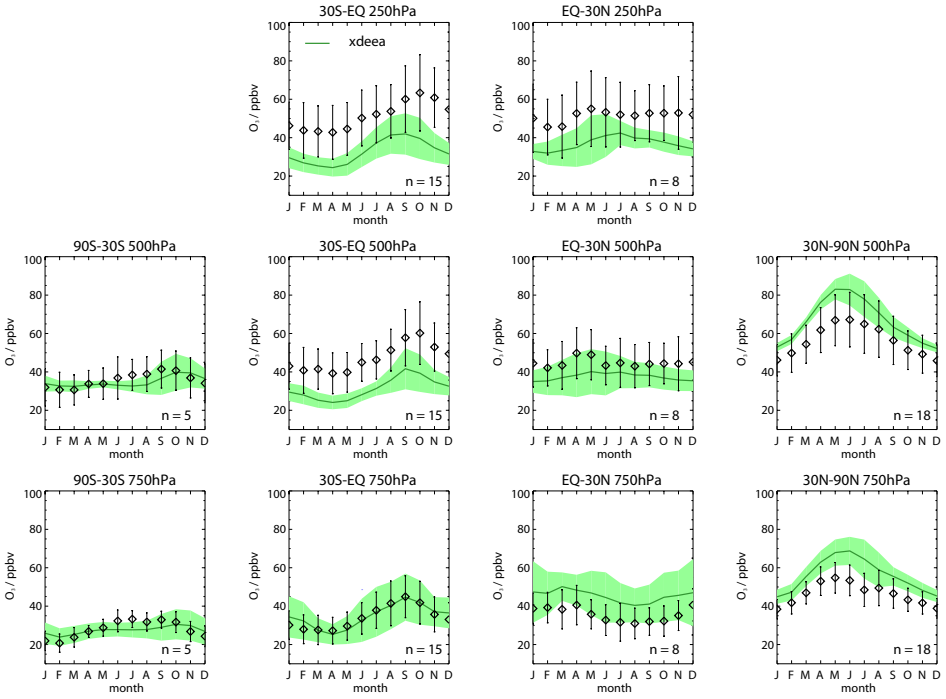

Figure 3.4. Comparison of climatological ozone (black diamonds) as described in [*Stevenson et al.*, 2006] with the BASE model run (green line). Lines show the standard deviation of the measurements and the lighter green shows the standard deviations for the model. Both model and measurements are sampled for a series of latitude bands and three pressure levels identically. Data are from *Logan* [1999] and *Thompson et al.* [2003].

3.3.2 Comparison to measurements

Ozone is of particular chemical importance for tropospheric chemistry (see section 2.1.1), and also has an impact on the radiative balance of the atmosphere, human health, and crop health. Throughout this thesis, I use ozone as a sort of exemplar trace constituent in the troposphere, and examine the sensitivity of ozone to various perturbations. Though a more exhaustive analysis of the model's performance can be found in a forthcoming paper by Fiona O'Connor (to be submitted as Part II of *Morgenstern et al.* [2009]), here I briefly describe the model's ability to simulate ozone. Chapter 4 elaborates on the model chemical mechanism's ability to reproduce measurements.

Figure 3.4 shows the performance of UKCA against the climatological ozone fields described in *Logan* [1999] and *Thompson et al.* [2003] as shown in *Stevenson et al.* [2006]. Data are broken down into four latitude bands—the southern high latitudes, the southern tropics, the northern tropics, and the northern high latitudes—and three pressure levels—750 hPa, 500 hPa, and 250 hPa. Near the surface, UKCA compares well with measurements, capturing both the seasonal variation and the magnitude of the climatologies. One key weakness is apparent: the northern tropics and northern high latitudes are slightly overestimated in magnitude (by approximately 8 and 6 ppbv, respectively). The overprediction is also evident in the multi-model assessment of *Stevenson et al.* [2006], which uses the same emissions, and could be an artefact thereof.

In the middle of the troposphere at 500 hPa, the seasonal variation in the climatology continues to be reproduced by the model, though the tropical measurements are slightly underestimated in magnitude. The opposite occurs in the northern high latitudes, where the model slightly overpredicts ozone concentrations; this is visible in the multimodel comparison, and again could be an artefact of the emissions [*Stevenson et al.*, 2006]. The comparison is poorest in the the upper tropical troposphere, where the underprediction is exacerbated and reaches up to 15 ppbv. This is not the case for the multi-model average of *Stevenson et al.* [2006], where upper troposphere ozone is overpredicted by approximately 7 ppbv in the northern hemisphere during winter. The negative bias is only partially (up to -2 ppbv) explained by the positive bias in the model humidity in the same region [*O'Connor et al.*, 2009]. It could also be linked to lightning NO_x, for which the uncertainty has recently been estimated at 60% [*Schumann and Huntrieser*, 2007]; perturbations to lightning NO_x led to up to 10% changes in the ozone burden in the work of *Wild* [2007]. Another contributing factor could be the underestimation of HO_x from the photolysis of formaldehyde, for which the absorption cross section has recently been found to be greater than previously thought [*Carbajo et al.*, 2008].

3.4 Experimental setup

I ran two experiments: BASE, in which isoprene was included, and NOISOP, in which isoprene emissions were set to zero. Although in older work [e.g. *Zeng and Pyle*, 2003] the lack of biogenic VOC emissions was often compensated for by increasing CO emissions, here I kept CO emissions constant in both experiments to minimize the variable differences between the two runs. I employed the 60 level version of UKCA. Model meteorology in the atmosphere-only version is forced using sea surface temperatures (SSTs) and sea ice distribution. For these two present day runs, SSTs were constructed using a two stage interpolation of observations [*Rayner et al.*, 2003]. Both simulations were run for five years and four months between 1999 and 2005, with the first sixteen months taken as spin up.

3.5 Impact of isoprene in UKCA

3.5.1 Ozone

3.5.1.1 The global impact

Figure 3.5 shows the impact of including isoprene on near-surface monthly mean ozone in January and July. Isoprene reduces ozone by 5-10 ppbv in the Amazon, Southern Africa, and Southeast Asia in January. These three regions also displayed decreases in ozone when a similar sensitivity study was carried out by *Young* [2007], although the absolute magnitude of the change was higher in that study (-20 to -40 ppbv), which is likely a result of differing distributions in emissions. In January, only one region shows a large increase in ozone concentrations due to the inclusion of isoprene in model runs, which is central Africa. Central Africa has strong NO_x emissions from biomass burning in January, enough so that the local chemical environment is VOC-sensitive in terms of ozone production. Thus the inclusion of isoprene increases ozone production by providing VOC to the system (see section 2.1.3).

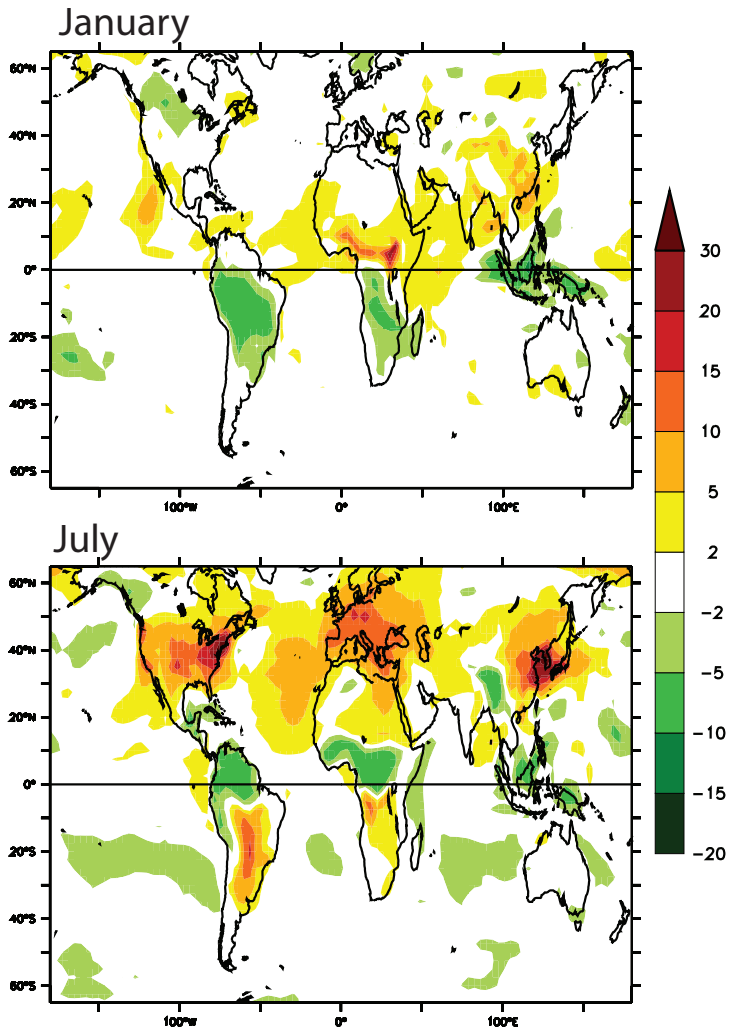

Figure 3.5. Change [ppbv] in five year average near-surface (600 m and below) ozone January (left) and July (right) between the BASE and NOISOP simulations.

In July, the reduction in ozone is limited to a smaller area of the Amazon, central Africa, and Southeast Asia to a lesser degree. The more noteworthy feature in boreal summer is the dramatic increase in ozone production throughout the northern hemisphere, which is particularly strong in the eastern United States, Europe, and eastern Asia. The strength of the signal over terrestrial areas is between 10-30 ppbv, which is higher than the values of 8-12 ppbv reported in *Wang and Shallcross*

[2000], though similar values are described in the work of *Folberth et al.* [2006] (8-25 ppbv) and *Young* [2007] (5-20+ ppbv). Over the oceans, smaller changes were noted in all three studies, and have been modelled here as well. Increases in the summer ozone concentrations with the inclusion of 'higher' (non-methane) hydrocarbons are also reported in *Roelofs and Lelieveld* [2000] and *Houweling et al.* [1998]. Variations in the exact magnitude of the changes in ozone resulting from representing isoprene could be due to variations in emissions used in each model, and to variations in the number and reactivity of hydrocarbons in the base chemistry.

Ozone concentrations also increase in the southern part of South America and in southern Africa in July, though the two hemispheric signals have separate and distinct causes. The increase in ozone in the northern hemisphere is due to the seasonality of isoprene emissions (see Figure 3.1). In the NO_x-rich environment of the more polluted northern hemisphere, the addition of VOC increases ozone production by altering the balance between NO_x and VOC. In the southern hemisphere, the signal is more closely linked to seasonal increases in NO_x (as opposed to increases in VOC), as shown in Figure 3.6. The southern hemisphere elevations in NO_x emissions are due to biomass burning emissions.

Table 3.4 shows the impact of isoprene on the global tropospheric ozone budget. The greatest absolute impact on the ozone budget is the increase in production of 129 Tg yr^{-1} (4.2%) when isoprene is included, although the greatest relative change is seen for net chemical production. A similar increase in total ozone production (93 Tg yr^{-1}) was reported in *Wu et al.* [2007]. Loss also increases as ozonolysis (O_3 + isoprene) is introduced and as elevated HO_2 concentrations increase the rate of the HO_2 + O_3 reaction (section 2.1.2). The ozone lifetime decreases by a day and a half when isoprene is included in the model (-4.5%), which is the same as the relative difference described in *Pfister et al.* [2008a], although the absolute values are very slightly higher here. The lifetime was also reduced in the study of *Wild* [2007] by 1.1 days. The burden is nearly unchanged, similar to

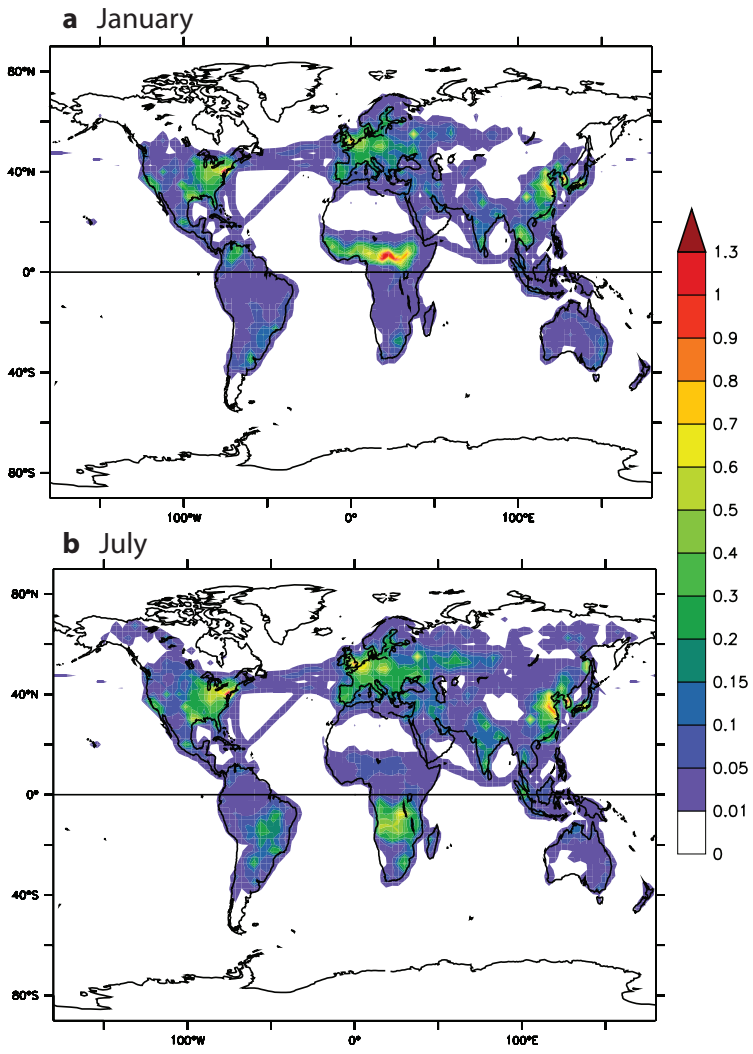

Figure 3.6. NO_2 [g m^{-2} $month^{-1}$] emissions in the BASE simulation for UKCA.

the result (-0.4%) in an earlier version of the model [*Young*, 2007]. Low changes in the ozone burden resulting from isoprene oxidation have also been reported by *Wu et al.* [2007] and *Pfister et al.* [2008a].

Once isoprene is included in the model, the total chemical production of ozone is 3215 Tg yr^{-1}, which is lower than the mean of 3984 reported in *Wild* [2007] (which includes the ACCENT study of *Stevenson et al.* [2006]). The net chemical production in UKCA of 402 Tg O_3 yr^{-1} is closer to the multi-model mean in *Wild*

Table 3.4. Annual ozone budgets with and without isoprene included in UKCA. Each term is given in Tg O_3 yr^{-1} except the burden [Tg] and the lifetime [days].

Experiment	NOISOP	BASE	Difference	Relative change
Production	3086	3215	129	4.2%
Loss	2748	2813	65	2.4%
Net Chem. Production	338	402	64	18.9%
Deposition	762	795	33	4.3%
Inferred STE	424	397	27	-6.4%
O_3 τ	33.1	31.6	1.5	-4.5%
O_3 Burden	323	317	6	-1.9%

[2007] of 245 Tg yr^{-1}. Both terms have a significant range in their estimations (761 and 346 Tg yr^{-1}, respectively). Deposition of 795 Tg yr^{-1} and STE of 397 Tg yr^{-1} are also lower in UKCA than in the multi-model mean, which were 902 and 636 Tg yr^{-1}. Despite these underestimations, the atmospheric burden of ozone in UKCA (317 Tg yr^{-1}) is close to the mean estimate reported in *Wild* [2007] of 307 Tg yr^{-1}. These values are lower than those reported by a previous implementation of the model chemistry, for which production was found to be 4025 Tg yr^{-1} and loss was 3225 Tg yr^{-1} [*Young*, 2007]. A value of 3620 Tg yr^{-1} for chemical production was also reported using a similar chemical mechanism with an older version of the dynamics [*Zeng et al.*, 2008]. The values in UKCA could be partially resultant from the lumped isoprene oxidation mechanism, which has been shown to underpredict ozone in both high and low isoprene conditions [*Archibald et al.*, in press].

3.5.1.2 The chemical impact

Figure 3.7 shows the change in annual average chemical production of ozone in the troposphere resulting from the addition of isoprene oxidation to UKCA. Three of the world's isoprene hot-spots show a reduction in chemical production: the Amazon, central Africa, and Southeast Asia/the maritime continent. Terrestrially, the notable exception to this is the southeastern United States, where the introduc-

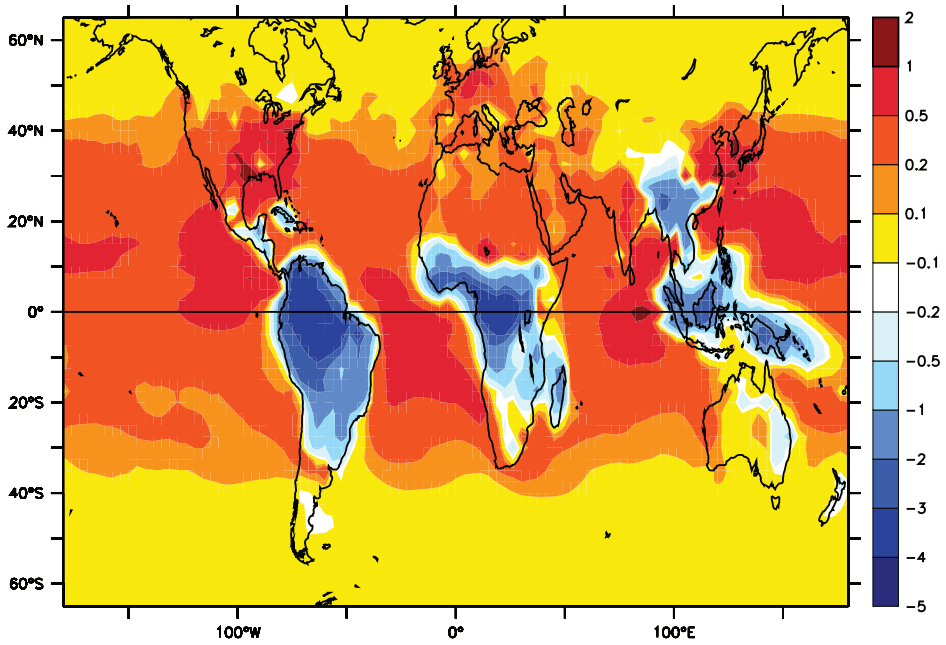

Figure 3.7. Annual average tropospheric chemical production of ozone (8500 m and below) between BASE and NOISOP runs [kg O_3 gridbox month^{-1}]

tion of isoprene instead leads to an increase in ozone production. This is a region where NO_x emissions are high, and the same is true for Europe and eastern Asia, areas that also show an increase in ozone production when isoprene is included in the model. In addition, ozone production increases over the oceans downwind of regions of high emission (the equatorial Pacific near South America, the tropical Atlantic between central Africa and the Amazon, the Indian ocean adjacent to the maritime continent, and the Pacific east of Southeast Asia.) The formation of nitrates, notably PAN, allows NO_x to be transported to these remote areas. There is also a widespread increase in ozone production over all of the tropical oceans. The production of ozone in southern South America and central Africa due to biomass burning emissions, described earlier, are not evident in this annual average picture. A very similar distribution in the change of ozone production has been found previously, using the same chemical mechanism in a predecessor model [*Young*,

2007].

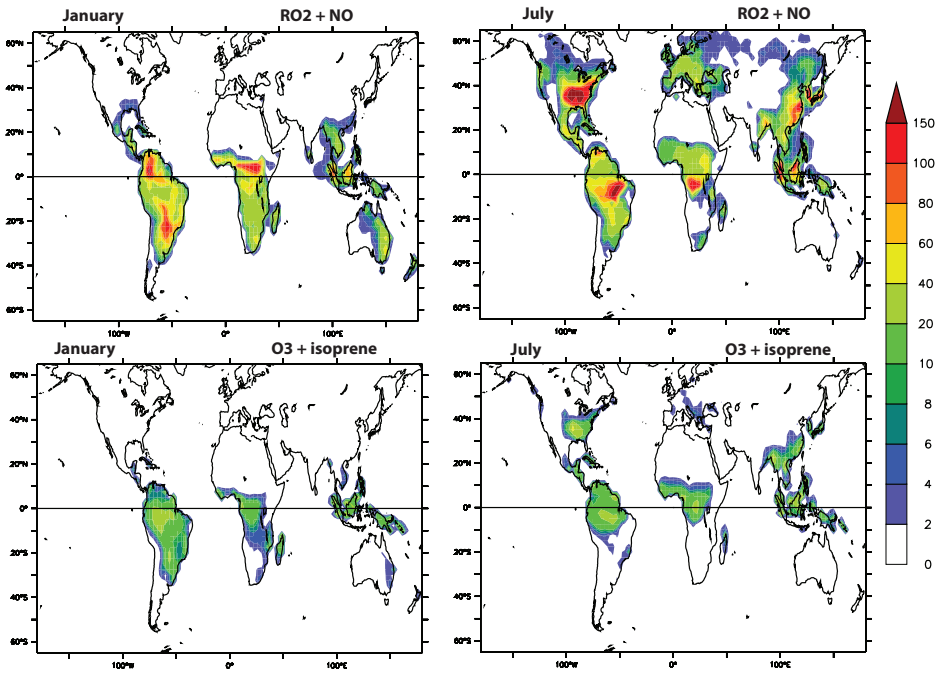

Figure 3.8. Key reaction fluxes [moles gridbox^{-1} second^{-1}] between the BASE and NOISOP simulations.

One of the ways in which isoprene impacts the ozone budget is through the increased regeneration of NO_2 by reaction of NO with RO_2. The top panels in Figure 3.8 show the flux through the reaction RO_2 + NO in January and July. This leads to the formation of ozone via photolysis of NO_2 (see section 2.1), but depends both on RO_2 radical concentrations (to which isoprene contributes), and NO concentrations. The strongest signal is modelled over the southeastern United States, where NO_x emissions are high and background concentrations of NO are elevated. Other strong signals appear in areas of high NO_x emission such as central Africa in January, and the central Amazon in July. In contrast, isoprene also leads directly to ozone loss via ozonolysis. The flux through this reaction is shown in the bottom panels of Figure 3.8.

Another way in which isoprene chemistry influences ozone is through the for-

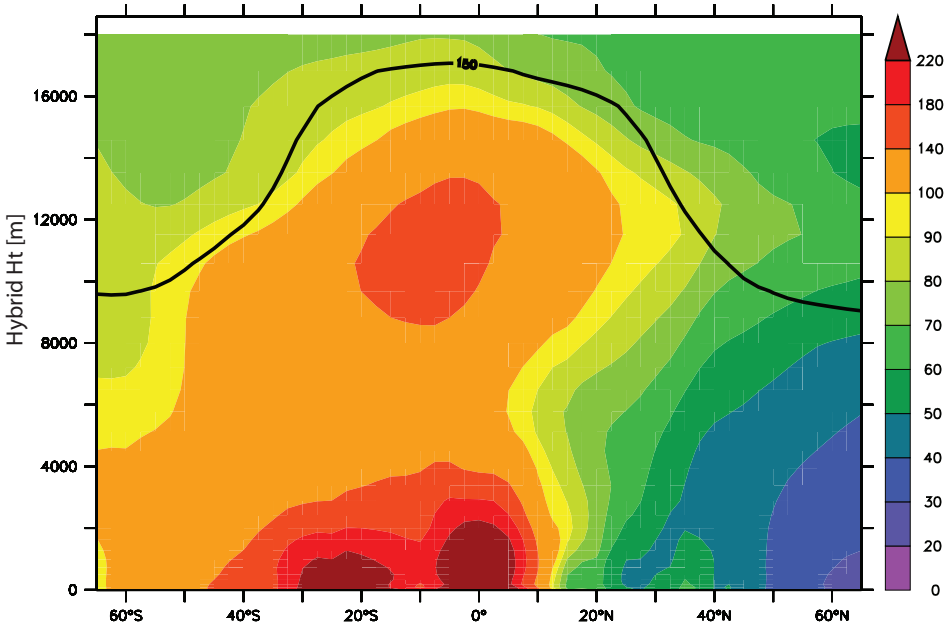

Figure 3.9. Annual average relative increase [%] in tropospheric zonal mean PAN between BASE and NOISOP runs.

mation of PAN, a reservoir species for NO_x. The lifetime of PAN has a strong dependence on temperature, so that when PAN is lofted into the higher, colder altitudes of the troposphere, it can exist for up to one month in winter, and approximately 10 days in summer [*Crutzen*, 1979; *Moxim et al.*, 1996]. In warmer, surface regions it dissociates with a lifetime of hours, releasing NO_x, which can then participate in further radical reactions. The formation of nitrates during isoprene oxidation is stabilized by a feedback loop involving OH. Reaction with OH can destroy nitrates, though this is slow in comparison with thermal degradation for PAN. In regions of high isoprene emission, where nitrate formation can be high, isoprene reacts with OH, reducing the potential sink of nitrates by chemical destruction. This small feedback loop is an additional reason why nitrate formation is marked when isoprene is added to UKCA. The stabilization of nitrate species is particularly important for ISON, a lumped isoprene nitrate species (formed both by reaction of first generation hydroxyalkoxy RO with NO_2, and by reaction of

isoprene with the NO_3 radical).

The relative difference in zonal mean PAN between the BASE and NOISOP simulations is shown in Figure 3.9. A strong hemispheric gradient appears, arising from the the fact that the majority of isoprene is emitted in the southern hemisphere and tropics (up to 10°N, see Figure 3.1). The seasonal emissions of the southeastern United States appear as an area of 50-70% increase in PAN between 30°N and 40°N. Because the PAN lifetime is strongly dependent on temperature, the increase (140%) in PAN at high altitudes is due to low temperatures in this region. In contrast, the rise nearer to the surface is due to the very high concentrations of isoprene, where PAN is produced in high quantities despite the shorter lifetime.

Young [2007] also found a high change in PAN burden due to isoprene oxidation, with increases of up to 900%. The largest relative changes were also over the southern tropics, similar to what is modelled by UKCA. Large changes in PAN were also reported by *Wang and Shallcross* [2000].

3.5.1.3 Relationships between emission and ozone changes

In order to understand the ozone changes shown in Figure 3.5, I attempted to delineate different chemical regimes by correlation to levels of isoprene or NO_x emission. The two regimes of 'VOC-sensitive' and 'VOC-rich' become apparent when the change in ozone is plotted as a scatter function against isoprene emission, as shown in Figure 3.10. The VOC-sensitive regime appears as a dense, positive correlation on the left side of the plot and is highlighted by the orange box. These points represent gridboxes in which the addition of isoprene has increased ozone concentrations. A number of gridboxes show increases in ozone of up to 20 ppbv, with some showing an even higher response. The longer, less dense correlation that corresponds to a VOC-rich environment extends through to the right side of the plot, and is highlighted in the blue box. These are points for which the inclusion of isoprene oxidation has decreased ozone concentrations. The addition of VOC to a VOC-sensitive regime results in a larger change in ozone concentrations (0-20+

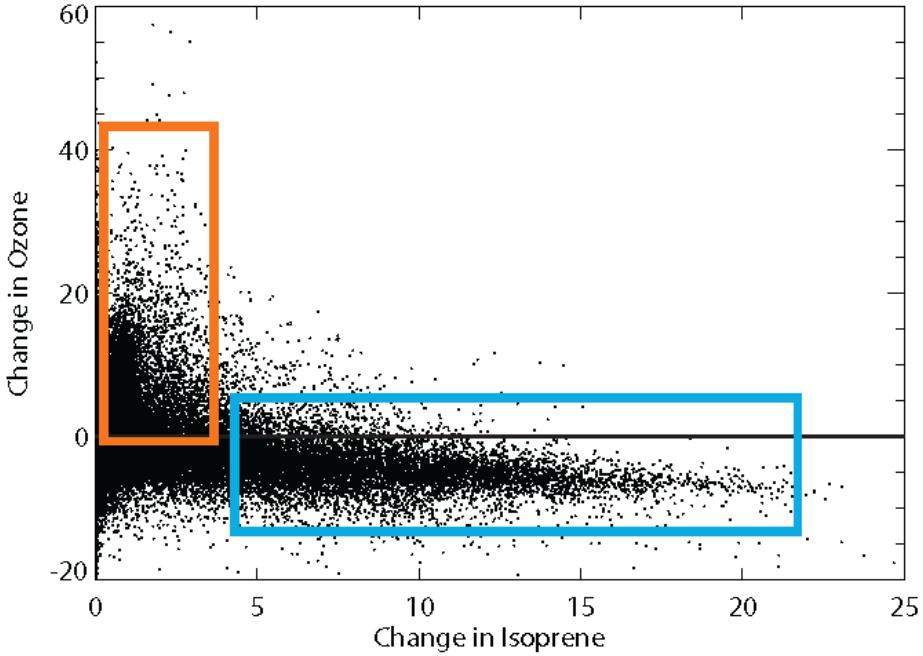

Figure 3.10. Scatter plot of the change in ozone [ppbv] versus the change in isoprene [ppbv] for all surface gridpoints in the BASE and NOISOP model runs. The VOC-sensitive regime is highlighted in orange, and the VOC-rich regime is highlighted in blue.

ppbv), while changes in the VOC-rich regions are relatively smaller in magnitude (-10-0 ppbv). In VOC-sensitive locations, the sinks of HO_x are lower than the sinks of NO_x, and the radical concentrations are not sufficient to oxidize all the NO in a gridbox [*Sillman and He*, 2002]. This creates the sharp gradient in the upper right of Figure 2.3, and the greater response in VOC-sensitive regions (orange box).

The addition of VOC to a VOC-sensitive chemical environment can stimulate ozone production by promoting NO_2 regeneration through reaction of NO with RO_2 (see the ozone production topography in section 2.1.3). It can also promote the formation of nitrate species, which remove NO_x from the chemical system and reduce ozone production. These two competing effects are evident in Figure 3.11. In gridboxes with low NO_x emission (shown in the orange box), which can be either NO_x- or VOC-sensitive, isoprene does not have a definitive effect, in

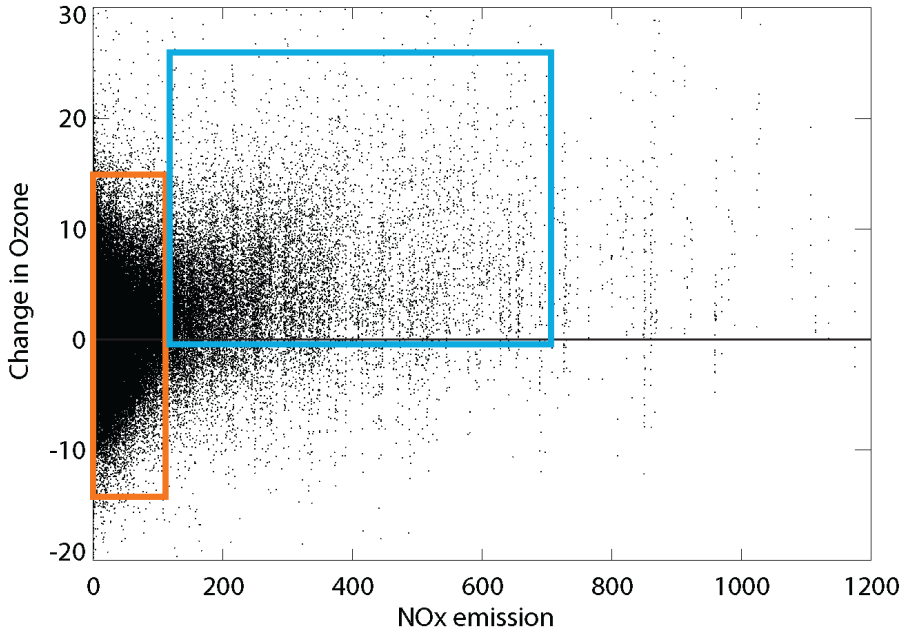

Figure 3.11. Scatter plot of the change in ozone [ppbv] versus NO_x emission [mg m^2 $month^{-1}$] for all surface gridpoints in the BASE and NOISOP model runs. The NO_x-sensitive regime is highlighted in orange, and the NO_x-rich regime is highlighted in blue.

some areas reducing ozone, and in some areas increasing it. The response even shows a sort of Gaussian distribution around zero. In a remote forest location, for example, low NO_x emissions in one box could be sequestered as PAN or ISON (reducing ozone production), but downwind upon the release of NO_x, ozone production could increase. In areas of higher NO_x emission (shown in the blue box), however, the inclusion of isoprene nearly always results in elevated ozone levels. In most cases increases of up to 15 ppbv ozone are modelled, with exceptional values above 20 ppbv shown for a fewer number of gridboxes. The correlation shows a wide spread, though a similar relationship and spread has been described in *Sillman et al.* [1990]. A positive NO_x-O_3 correlation in response to isoprene was also modelled in relation to the PROPHET field campaign [*Barket Jr. et al.*, 2004].

3.5.2 Methane

3.5.2.1 The impact on OH

Another way in which isoprene alters the chemistry of the troposphere is through its chemical relationship with HO_x. The direct impacts of isoprene on surface OH can be seen in Figure 3.12. Surface OH decreases everywhere in the model when isoprene oxidation is included, though the high-emitting regions (Figure 3.2) exhibit the strongest reductions in OH concentrations. The seasonality of emissions appears in the fluctuation of OH reductions from south to north. The largest changes are modelled over South America and Asia, with values of up to -4.5 $\times$ 10^6 molec cm^{-3}. Slightly lower changes between 2-4 $\times$ 10^6 molec cm^{-3} are modelled over other hot-spot regions. These changes in OH in UKCA are similar to work in a predecessor version of the model [*Young*, 2007], and have also been shown in a number of other global models [*Houweling et al.*, 1998; *Jöckel et al.*, 2006; *Folberth et al.*, 2006]. Away from areas of very high emission, OH concentrations change by a smaller magnitude of 0-1 $\times$ 10^6 molec cm^{-3}. Reduced OH arises from an increase in the formation of peroxides (section 2.1.3) which can form a permanent sink for HO_x. Secondly, the recycling of OH from HO_2 (a product of VOC oxidation) by ozone, which proceeds as:

$$HO_2 + O_3 \rightarrow OH + 2O_2 \tag{2.16}$$

is less efficient than recycling by NO:

$$HO_2 + NO \rightarrow OH + NO_2 \tag{2.15}.$$

Isoprene oxidation therefore reduces the OH/HO_2 ratio [*Young*, 2007] in a low NO_x environment.

The chemical relationship between isoprene and OH is complex. In high NO_x environments, the oxidation of VOC leads to the formation of HO_2 which reacts

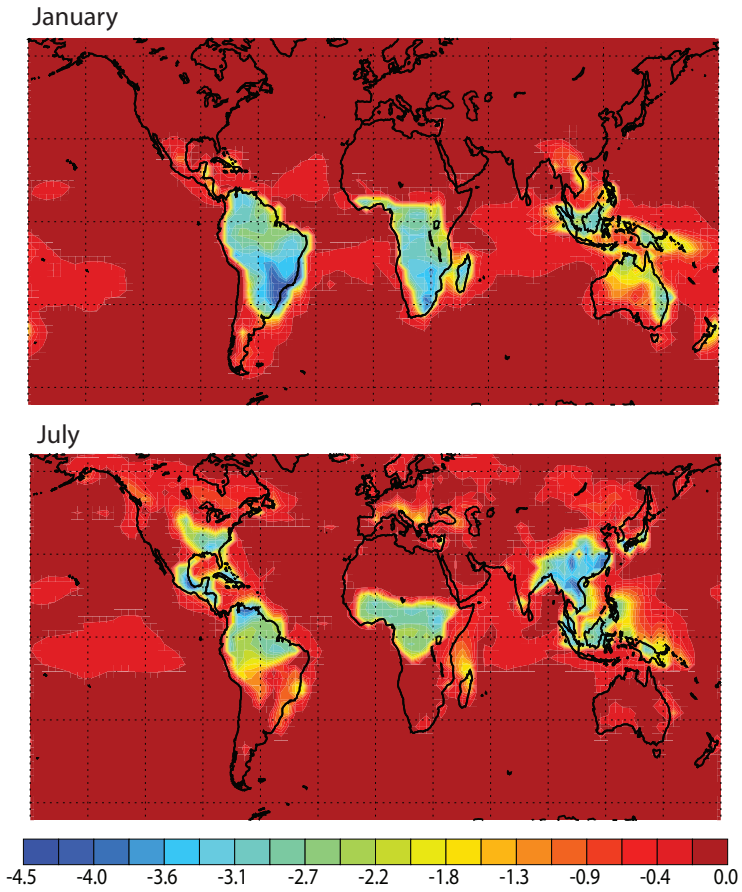

Figure 3.12. Difference in surface OH [10^6 molec cm^{-3}] between BASE and NOISOP runs for January (top) and July (bottom).

with NO to form OH. This generally maintains a high concentration of OH. In low NO_x environments, the chemistry is more complex, though depletion of OH has been reported by a number of global models [*Houweling et al.*, 1998; *Jöckel et al.*, 2006; *Folberth et al.*, 2006]. Recent work has suggested that high measured concentrations of OH in low NO_x environments [e.g. *Ren et al.*, 2008; *Hofzumahaus et al.*, 2009] indicate a missing OH source that models fail to consider [*Lelieveld et al.*, 2008; *Butler et al.*, 2008]. OH is also a byproduct of ozonolysis reactions between ozone and terpenes, including isoprene [*Atkinson et al.*, 1992]. The inclusion of the O_3 + isoprene reaction was not enough to account for measured concentra-

tions of OH in the work of *Biesenthal et al.* [1998] or *Carslaw et al.* [2001]. Future discoveries of the 'missing OH source' may shift our understanding of the VOC-HO_x chemical relationship. Future work will perhaps model decreases in OH (and the resultant increase in methane lifetime) of a reduced magnitude in response to evolving scientific understanding of isoprene oxidation in low NO_x environments [see e.g. *Karl et al.*, 2009].

3.5.2.2 Methane lifetime

Although changes in OH are especially important for the oxidizing capacity of the troposphere, they are also important because reaction with OH forms the main sink for methane, a radiatively active greenhouse gas [*Solomon et al.*, 2007b]. Figure 3.13 shows the average annual seasonal cycle of methane lifetime in the atmosphere for simulations with and without isoprene emissions. Two things are notable: first is the seasonal cycle of methane lifetime, arising from the fact that OH concentrations are elevated in the northern hemisphere summer due to the presence of anthropogenic pollution [e.g. *Spivakovsky et al.*, 2000]. Second, there is a large difference between the runs with and without isoprene. The average annual methane lifetime for these runs is 10.2 years (without isoprene) and 12.5 years (with). These values are higher than those reported in *Stevenson et al.* [2006] of 8.7 $\pm$ 1.3 years. The methane lifetime decresed 4.2% when the negative bias in humidity in the tropics in UKCA was removed [*O'Connor et al.*, 2009], where OH concentrations are high, and by inference, so is the methane sink, [e.g. *Thompson et al.*, 1989; *Lelieveld et al.*, 1998; *Bousquet et al.*, 2006]. Despite this, the methane lifetime in UKCA remained high (9.61 years). *Wild* [2007] found that humidity, temperature, and treatment of wet deposition were the largest reasons for methane lifetime variability in global model budgets.

Through increasing the sink for OH, isoprene chemistry accounts for a 22.5% increase in the methane lifetime. *Young* [2007] found that isoprene accounted for a 28% rise in the methane lifetime of UKCA's predecessor model, UM_CAM. Simi-

lar results have been reported for a halving of isoprene emissions, where resulting OH concentrations increased by 7.2% and methane lifetime decreased by 7 months [*Young et al.*, 2009]. Consistent with this picture, a 7.3% decrease in global OH due to isoprene was also reported in *Pfister et al.* [2008a].

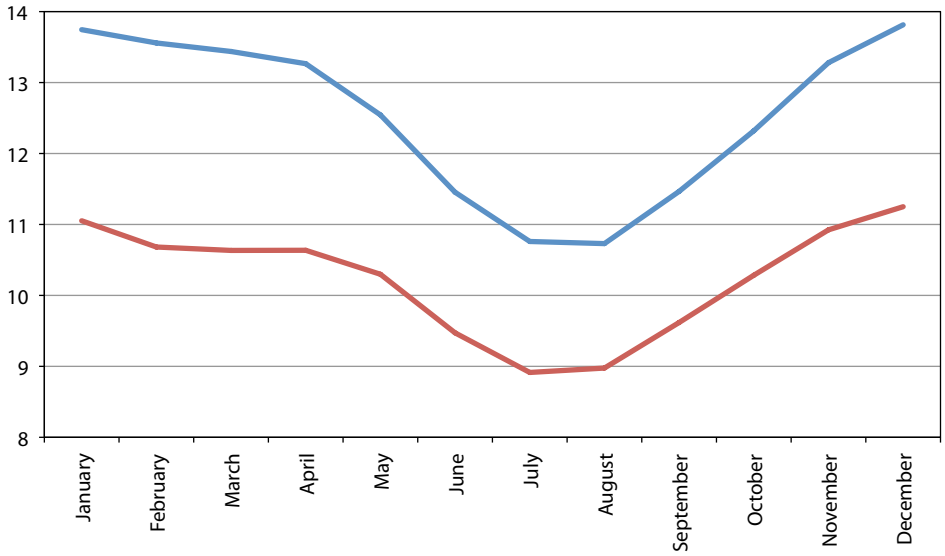

Figure 3.13. Seasonal variation of tropospheric methane lifetime with respect to OH [years] for simulations with (blue) and without (red) isoprene emissions.

The magnitude of the seasonal cycle in methane lifetime also increases (from 2.3 years to 3.1 years, a change of 32%) when isoprene is included in model calculations. Two competing factors are at play: first, the direct interaction between OH and isoprene, and second, the indirect effect of isoprene in the formation of ozone, which in turn leads to elevated concentrations of OH. As isoprene emissions are concentrated in the southern hemisphere (see Figures 3.1 and 3.2), the removal of OH due to chemical reaction is more marked than in the northern hemisphere, thus the first effect dominates during December, January, and February. In the northern hemisphere summer, (June, July, and August) ozone increases strongly with the inclusion of isoprene. Increased ozone, along with increasing radiation due to the season leads to higher values of OH. The seasonal difference in the effects of these

two signals leads the larger magnitude in the methane lifetime seasonal cycle. This change was also reported in *Young* [2007], in which isoprene led to a 36% increase in the seasonal cycle of the methane lifetime.

3.6 Summary

In this chapter, I described the CCM UKCA in a tropospheric configuration. I began with a description of the dynamical core of the model (the Unified Model), and the representation of chemistry used (the ASAD chemistry package), and the the emissions used in the BASE and NOISOP present-day model simulations. The model's vertical top was considered in the discussion of STE, which showed that a full representation of the stratosphere was necessary in order to model STE accurately. A short model comparison was done against ozone climatologies similar to the work of *Stevenson et al.* [2006], which showed that the model performs well at the surface but underestimates ozone in the tropical upper troposphere. After describing the emissions modelling, geographical distribution, and seasonality of isoprene emissions worldwide, I examined the impact that isoprene has model results.

As expected, the change in surface ozone resulting from isoprene oxidation was closely correlated to the local chemical environment into which isoprene was emitted. The largest increases in ozone were modelled throughout the northern hemisphere in summer, while decreases were modelled over most of the high emitting regions in the tropics, though this was dependent on season. I showed NO_x emissions to help identify the environment into which isoprene emission occurred, and I was able to separate the chemical regime of the ozone change through correlations with both isoprene and NO_x emissions. Finally, I described the impact that isoprene has on methane lifetime and OH in UKCA, which was to increase methane lifetime by 2.3 years and to increase its seasonal cycle. Consistent with other models, OH concentrations were reduced substantially over high emitting

regions.

In the next chapter, I describe a set of regional and local experiments in Southeast Asia, an area of high isoprene emission.

Chapter 4

Case Study: South East Asia

In this chapter, Southeast Asia is used as a case study for two types of model experiments. In section 4.1, I perform experiments in connection with data from the OP3 field campaign. I use a box model to assess the ability of the UKCA chemical mechanism to reproduce NO, $\mathrm{NO_2}$, and $\mathrm{O_3}$ measurements from a remote tropical rainforest field site in Malaysian Borneo. Section 4.2 is comprised of two simple sensitivity studies performed at the regional scale; in the first of these isoprene emissions are doubled in Southeast Asia, and in the second they are reduced by twenty five percent.

4.1 OP3

4.1.1 Introduction

A four month field campaign, part of the NERC-funded 'Oxidant and Particle Photochemical Processes' (OP3) [*OP3*, Accessed 11 November, 2009], was conducted in the Malaysian state of Sabah, on the island of Borneo (the location is shown in Figure 4.9), between April and July of 2008 [*Hewitt et al.*, 2009a]. There were two intensive periods of observation, the first between 8 April and 3 May, and the second between 25 June and 23 July. A key goal of the project is to assess our understanding of photochemical processes above a rainforest and their impacts on

various scales; to this end, the campaign utilised simultaneous ground, airborne, and satellite measurements [a full list of instrumentation can be found in *Hewitt et al.*, 2009a]. A further aim is to understand the scale relationships of these measurements as they are used by and contribute to mesoscale, regional, and global models.

Atmospheric oxidation above a tropical rainforest is complex [e.g. *Kuhn et al.*, 2007; *Lelieveld et al.*, 2008], and it is therefore beyond current computational resources to represent it explicitly in a global model. Furthermore, the horizontal resolution of the current generation of global models is 2-5° [*Stevenson et al.*, 2006] (approximately equivalent to 220 and 550 km at the equator), which limits their ability to model sub-grid scale processes such as emissions variability. At the same time, these models attempt to simulate the production and destruction of ozone, which is dependent on local chemical conditions [*Crutzen*, 1973; *Sillman et al.*, 1990; *Jenkin and Clemitshaw*, 2000]. Our understanding of the future impacts of ozone often relies on the output of global models [*Forster et al.*, 1996; *Fuglestvedt et al.*, 1999; *Stevenson et al.*, 2006, e.g.] and it is therefore essential to understand how global chemical mechanisms perform in relation to the local measurements which help to constrain them.

NO and NO_2 act as catalysts in many oxidation cycles in the atmosphere due to their rapid interconversion; the availability of NO_x largely determines whether ozone production or destruction dominates in a specific region of the tropical boundary layer [*Liu et al.*, 1987]. Nitrogen oxides are emitted both by natural processes and human activities. Of the biogenic sources, emission from soils [*Yienger and Levy II*, 1995; *Delon et al.*, 2008] and formation during lightning storms [*Franzblau and Popp*, 1989; *Schumann and Huntrieser*, 2007] are the major contributors. Fossil fuel combustion, biomass burning and aircraft emissions are the major anthropogenic sources [*Kasibhatla*, 1993; *Levy II et al.*, 1999; *Toenges-Schuller et al.*, 2006]. Though fluxes from tropical areas are not yet well quantified, the work of *Bakwin et al.* [1990] suggested significant NO_x emissions from

tropical forested areas. *Jaeglé et al.* [2004] reported that soil emissions of NO_x could be as large as biomass burning emissions in Africa. In these remote tropical areas the potential for NO_x species to influence local chemistry is significant, due to low background NO_x and high concentrations of both the hydroxyl radical and biogenic VOC [*Hewitt et al.*, 2009b; *Steinkamp et al.*, 2009]. An increase in the frequency and spatial distribution of tropical NO_x measurements will help quantify local tropical fluxes and sources. But global models will largely play the role of quantifying the impact of these fluxes on a regional and global scale. For this reason, it is important to understand how global models relate to local measurements.

To this end, I use the chemical mechanism incorporated in the global CCM UKCA, and study what alterations are required to match measured NO, NO_2, and O_3. In this section, my aim is to assess the ability of UKCA's chemical mechanism.

4.1.2 The measurements

4.1.2.1 Methods

Nitrogen oxides and ozone measurements were taken at the Bukit Atur Global Atmospheric Watch (GAW) station (04°58'53", 117°50'37", and elevation 426 m) the location of which is shown in Figure 4.9[1]. NO measurements were made by chemiluminescence using an Ecophysics CLD 780 TR nitric oxide analyser, with an Ecophysics PLC 762 NO_2 photolytic converter connected to allow conversion of NO_2 to NO. NO and NO_2 concentrations were measured from an inlet situated at 5 m above ground level. Each measurement cycle lasted for 1 minute and consisted of 12 seconds of NO measurement, 12 seconds of NO_2 measurement and 24 seconds of interference determination. The remaining 12 seconds allowed for switching between the different modes and purging of the reaction cell. The 1σ limit of detection for 10 minute frequency data was approximately 2.8 pptv for NO and 7 pptv for NO_2. Ozone concentrations were measured using a Thermo

[1]Measurements were made by James Lee and Sarah Moller from the University of York. Our collaboration in this measurement-model comparison is part of the NERC OP3 project.

Environmental Instruments (TEI) 49i UV absorption ozone analyser. The data was internally averaged to one minute frequency and the detection limit was 0.6 ppbv.

On board the FAAM BAe 146 aircraft, NO and NO_2 were measured using the the University of East Anglia (UEA) NOxy instrument, which employed the same technique as the ground based instrument described above[2]. Zeros were carried out at the beginning of level runs during the flights and calibrations took place during transit to and from the airport. Detection limits of the UEA NOxy are of the order of 3 pptv for NO and 15 pptv for NO_2 for 10s data, with estimated accuracies of 10% for NO at 1 ppbv and 10% for NO_2 at 1 ppbv. The instrument is described in detail by *Brough et al.* [2003]. Ozone was measured on board the aircraft using a TEI 49C UV absorption analyser.

Isoprene fluxes, used in the box modelling experiments, were measured using a PTR-MS instrument at the Bukit Atur site[3]. Its response was optimized to achieve the best compromise between the optimal detection limit for VOCs and the minimization of the impact of high relative humidity. The operational details of the instrument have been presented elsewhere [e.g. *Lindinger et al.*, 1998; *de Gouw et al.*, 2003; *Blake et al.*, 2009].

4.1.2.2 Discussion

Time series of NO, NO_2, and O_3 data for the first OP3 intensive observation period are shown in Figure 4.1. Although the frequency of data collection is 1 minute (section 4.1.2.1), it is shown here with a running average of 10 minutes for smoothing purposes. NO levels were typically below 0.1 ppbv, although there were regular spikes above this level which reached up to 0.4 ppbv. NO_2 levels were higher, generally below 0.4 ppbv but reaching 0.8 ppbv. Ozone concentrations ranged from near zero up to 30 ppbv, but were only consistently above 20 ppbv on three days

[2] Aircraft measurements were carried out by Dave Stewart and Claire Reeves of the University of East Anglia.

[3] Isoprene flux measurements were carried out by Ban Langford from Lancaster University and Pawel Misztal from the Centre for Ecology and Hydrology and the University of Edinburgh.

(11-13th April).

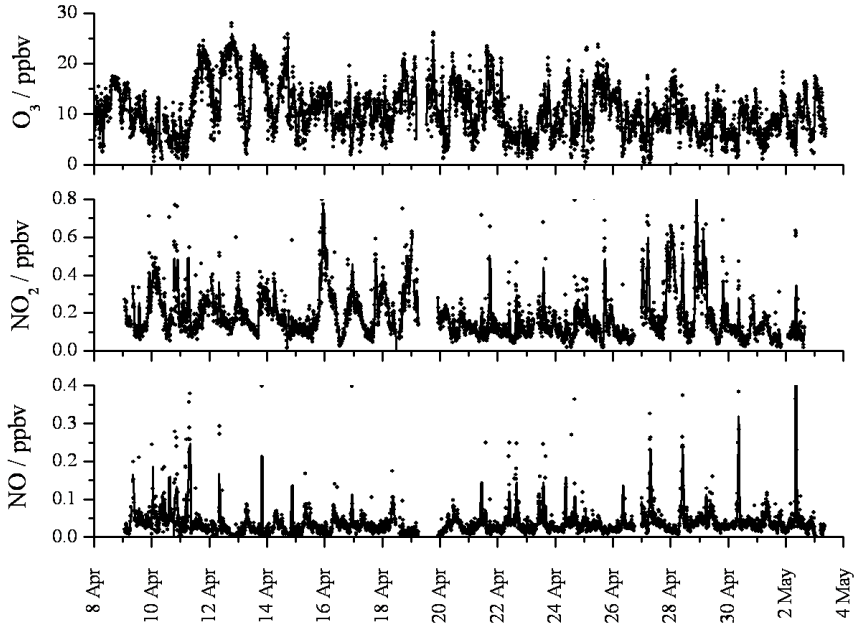

Figure 4.1. Time series of measured NO, NO_2, and O_3 at the Bukit Atur GAW ground site, plotted versus local time (GMT+8) during the first intensive observation period of OP3.

Figure 4.2 shows the median diurnal profiles for the entire April measurement period for all three species. The 25-75 quartile limit is shown in shaded regions around each of the profiles. The ozone diurnal cycle shows a minimum of approximately 6 ppbv around 7:00 h followed by a rise through the morning. Ozone concentrations of approximately 11 ppbv remain until the evening, when concentrations slowly fall to their minimum in the morning. NO_2 concentrations exhibit the most marked diurnal cycle, which peaks at midnight around 240 pptv and reaches a low of 80 pptv in mid-afternoon. The slow loss of NO_2 between midnight and midday occurs less rapidly than the buildup between late afternoon and evening. An NO peak of around 70 pptv is observed at 8:00 h and quickly recovers to a fairly constant level between 30 and 40 pptv. This persists until 18:00 h when a

further drop to 20 pptv occurs. Non-zero NO concentrations between 15-20 pptv persist throughout the night.

In July, an aircraft joined the campaign in order to make dedicated measurements above the site and over the surrounding areas. In the lower panel of Figure 4.2, the diurnal cycles of NO, NO_2, and O_3 are shown for this second observation period. These diurnal cycles are sampled only for the four days for which equivalent aircraft data is also available. The average measurements made in profile flight patterns directly over the site are plotted as whiskered points and show values for both boundary layer and free troposphere.

O_3 shows little vertical structure compared to ground measurements. The ground based measurements vary little in this time period, remaining around 9 ppbv. Morning aircraft measurements are slightly higher (10-12 ppbv) than the ground based. Aircraft measurements of ozone levels rise slightly to approximately 13 ppbv in the late afternoon, though boundary layer and free troposphere values remain identical (within uncertainty) to each other. A diurnal pattern in the ground based O_3 observations is not clear.

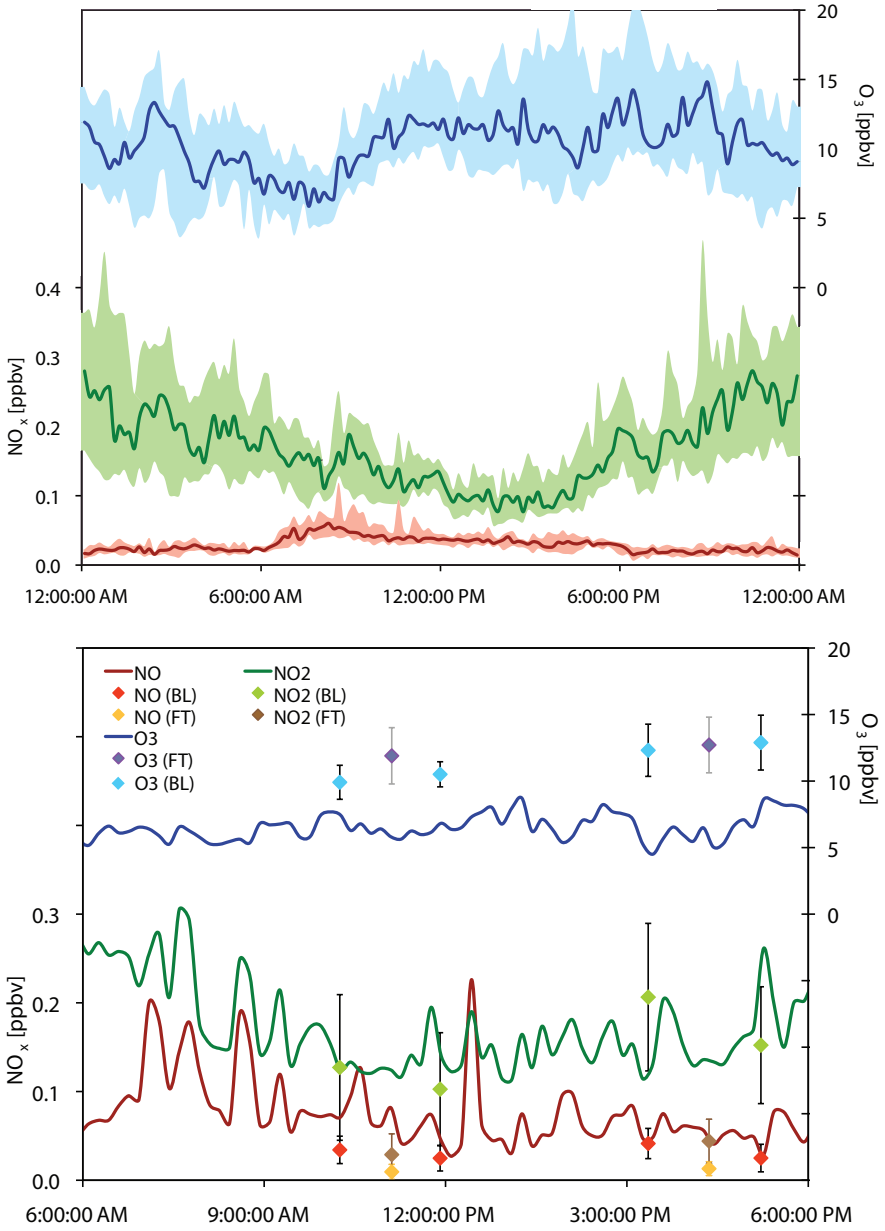

Figure 4.2. Top: Median diurnal cycle of ground-based measured NO (dark red), NO_2 (dark green), and O_3 (dark blue) in April. The corresponding 25-75 quartile interval is shown with each measurement: NO in pink, NO_2 in light green, and O_3 in light blue. Bottom: median diurnal measurements in July, shown only for the days when corresponding flight data is available between 6:00 and 18:00 h; diurnal profiles are the same color as above. Average flight data for morning and afternoon profiles above the site are shown as whiskered points and are separated by height. NO measurements are show in red (boundary layer) and yellow (free troposphere). NO_2 is shown in light green (boundary layer) and brown (free troposphere). O_3 is shown in light blue (boundary layer) and purple (free troposphere)

Boundary layer NO_2 matches the ground based measurements very closely, which remain in the range of 100-200 pptv for most of the day. NO_2 measurements show a similar structure (rise until midnight and subsequent decrease afterwards) to the first campaign, but because only four days are sampled here the full diurnal cycle is not shown. NO_2 measurements of around 20 pptv in the free troposphere are much lower than those in the boundary layer and at the surface, demonstrating that NO_2 has a strong vertical structure. NO displays a similar pattern to NO_2 with boundary layer values of 80-200 pptv, which resemble ground-based measurements well, and free tropospheric values that are much lower (less than 10 pptv). The diurnal cycle of NO also bears strong resemblance to that of the first campaign, (i.e. a rise in early morning followed by a slow tapering into the afternoon).

For comparison, the NO concentrations at the ground site in both measurement periods are in between measurements made in the Amazon Rainforest of 20 pptv [*Lelieveld et al.*, 2008] and 100 pptv [*Karl et al.*, 2009]. Ozone, on the other hand, is lower at the Borneo site than in reported values for the Amazon for both the boundary layer (19 ppbv) and the free troposphere (37 ppbv) [*Lelieveld et al.*, 2008].

4.1.3 Modelling

4.1.3.1 Model description

I use a zero-dimensional, stationary box model to simulate the diurnal cycles of NO, NO_2, and O_3 observed during the first intensive observation period. The model uses the same chemical mechanism (the ASAD chemistry package [*Carver et al.*, 1997]) which is implemented in UKCA and was run at 10 minute chemical timesteps. In the box model, six species are deposited: NO, NO_2, O_3, peroxy acetyl nitrate (PAN), peroxy-methacrylic nitric anhydride (MPAN), and a lumped nitrate species representing the products from isoprene + NO_3 and isoprene nitrates (ISON, [see *Pöschl et al.*, 2000, and section 3.2.2]), with deposition velocities from the literature [*Zhang et al.*, 2003b; *Ganzeveld and Lelieveld*, 1995] which are set

to either an average daytime or an average nighttime value depending on the model timestep. The photolysis follows the scheme of the Master Chemical Mechanism [MCM, *Saunders et al.*, 2003]. As those photolysis rate constants are originally for July, at 45°N for clear sky conditions, the rate constant for J_{NO2} was reduced by 50% to account for clouds and aerosol.

Only NO and isoprene are emitted into the box. NO emissions were 600 pptv day^{-1} (the flux is constant) unless otherwise mentioned. Isoprene emissions into the model are taken from ground based flux measurements. Occasionally, flux measurements were not available; in these instances, we used linear interpolation to connect the fluxes. In the absence of NO flux measurements at the site, we were not able to constrain NO emissions to a diurnal pattern. NO flux measurements were made in a nearby site underneath the canopy layer [*Hewitt et al.*, 2009a]. The Bukit Atur GAW station was in a clearing, and therefore canopy flux measurements are not representative of this site, as there can be a strong difference between below- and above-canopy fluxes of NO_x [e.g. *Duyzer et al.*, 2004]. For these reasons, we assume that NO is emitted constantly into the model; this is also consistent with how emissions are done in the global version of UKCA.

The box model boundary layer height is fixed to a set value during the day (6:00 to 18:00 h) and fixed to a different value at night. For the first set of sensitivities, the daytime boundary layer height was set to 1000 m, and the nighttime height was set to 200 m. The boundary layer height is effectively a mixing depth, and therefore controls the range over which emissions are mixed into the model, and the rate of sinks via deposition.

Temperature is set to 25°C and pressure to a surface value of 1013 mb in the box, appropriate to the conditions of the rainforest site. A 5°C variation in temperature showed negligible impact on box model output (not shown), so a constant temperature was used. Latitude was set to 5°N. Initial concentrations of chemical species in the box model are set to the values shown in Table 4.1. NO, NO_2, and O_3 are initialized to their midnight values from the diurnal cycle in the measure-

Table 4.1. Initial concentrations of six species used in the box model.

Species	Concentration
CO	130 ppbv
HOOH	3 ppbv
C_2H_6	500 pptv
C_3H_8	50 pptv
HCHO	1 ppbv
CH_3COCH_3	50 pptv

ments. All other species are initialized to zero.

For the following model-measurement comparisons, both the model and the data are sampled for 15 days to account for day to day variability in isoprene flux measurements.

4.1.3.2 The base case

Figure 4.3 shows the initial results from the box model (dark blue line). The box model overestimates NO concentrations (80 pptv instead of 60 pptv), though the structure is decently captured. The shape of the NO_2 curve is very different from the measurements, with NO_2 building up throughout the night. This occurs because any NO emitted into the model reacts with ozone to form NO_2. Ozone is also overestimated in the box model. The box model calculates values of approximately 30 ppbv, with an 8 ppbv diurnal cycle; measurements of 6-11 ppbv are far below this level.

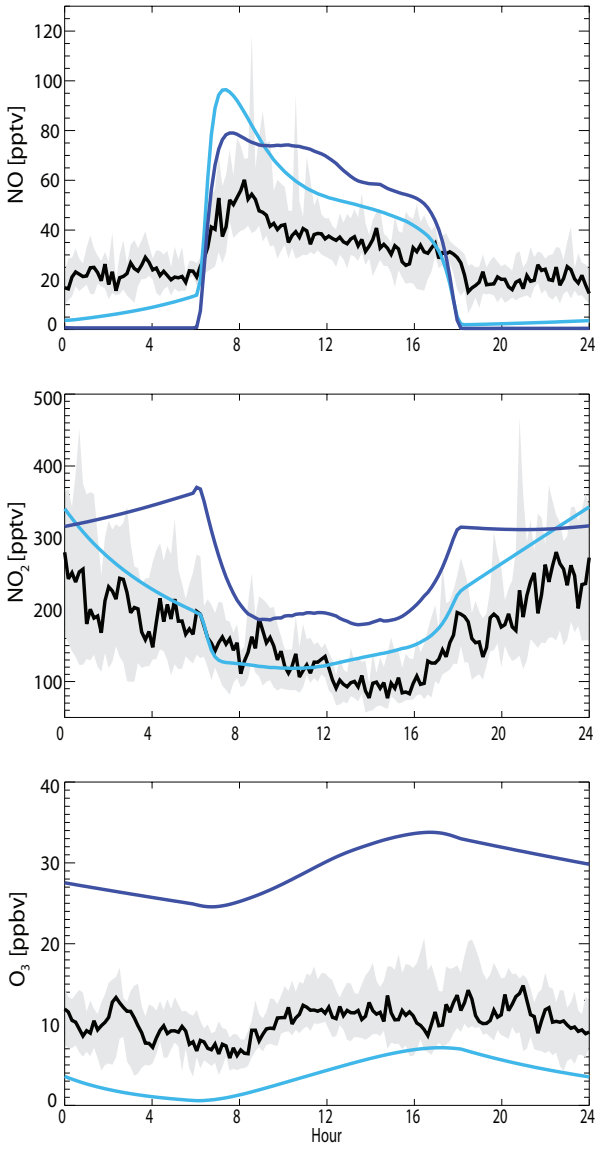

Figure 4.3. Box model comparison to measured diurnal cycle of NO, NO_2, and O_3 (black line with shading) shown dark blue (without venting) and light blue (the 'base case').

To obtain the 'base case' box model run (Figure 4.3, light blue line), one key adjustment was made to the original box model output. A dilution parameter was introduced to simulate mixing with the free troposphere resulting from a collapse of the boundary layer at night. This 'venting parameter' removes a small fraction—between 0 and 4 percent—of chemical tracers at each 10 minute timestep between 24:00 h and 6:00 h. Doppler lidar measurements of the backscatter from aerosol [*Pearson et al.*, 2009] provide strong evidence for dilution of aerosol in the Danum Valley boundary layer during this period. These measurements were made slightly afield from the Bukit Atur GAW site used for NO_x and ozone measurements in an area of complex topography; the elevation of the lidar measurement site was 198 m compared with 426 m for the Bukit Atur site. The median boundary layer height dropped to approximately 200 m according to these measurements, suggesting that on some nights the Bukit Atur site may have effectively been in the free troposphere. The venting parameter is a simple way to simulate the mixing between the boundary layer box and the free troposphere by parameterizing dilution of species which are concentrated in the boundary layer. As is evident in Figure 4.3, the box model was not able to capture the diurnal structure of NO_2 before the introduction of the venting parameter.

The base case (shown in Figures 4.3 and 4.4) shows both the strengths and weaknesses of the box model with venting. A good fit to the data for NO is obtained, simulating the morning rise in concentration due in part to the onset of photolysis of NO_2. During the day modelled NO follows a similar decay pattern to the measured data, an improvement over the model without venting.

NO_2 measurements and model simulations are in good agreement following the addition of the venting parameter (the base case) and the buildup of NO_2 until midnight and subsequent reduction in concentrations is well captured. At sunrise, when the boundary layer begins to grow, a steep drop in NO_2 concentrations appears around 6:00 h in the box model due to the onset of photolysis. The largest divergence between modelled and measured values occurs in the afternoon, be-

tween 12:00 and 16:00 h, though this is still relatively small. Base case modelled and measured ozone display similar diurnal cycles. Both show minima between 7:00 and 8:00 h and maxima in the late afternoon, though the measurements have more structure in the afternoon than the modelled ozone. However, the box model underestimates the total concentration of ozone, simulating values of 0-8 ppbv instead of 6-11 ppbv.

In summary, the 'base case' box model run performs reasonably well, although ozone is too low. The inclusion of the venting parameter, which parameterizes dilution of boundary layer air between 24:00 and 6:00 h, seems necessary in order to simulate the structure of NO_2 measurements at night.

4.1.3.3 Chemical sensitivities

I have performed a range of sensitivity experiments to explore the model performance. First, a series of emissions sensitivities were carried out (not shown.) In order to determine if the nighttime NO concentration could be captured if emissions were altered, a sensitivity study was performed in which emissions of NO were tripled to 1.8 ppbv day^{-1}. This did not improve the agreement between the modelled and measured values at night. Nonzero nighttime NO could arise from emission taking place very near to the measurement inlet, which is not reproduced by the box model as NO quickly reacts with O_3 to form NO_2 in a zero dimensional model.

I also examined the sensitivity of the model to changing isoprene emissions. Doubling the emission fluxes into the model reduced NO during the day by 12 pptv, and NO_2 was reduced by a similar amount; ozone hardly changed. Overall, the diurnal patterns were very similar between the two runs, and between these two studies I determined that the regime was likely not emissions controlled. Although it has been proposed that some chemistry in high-VOC environments might be explained by the presence of unknown reactive hydrocarbons [see *Di Carlo et al.*, 2004, and references therein], any VOC with similar reactivity to that of isoprene

Table 4.2. Summary of chemical sensitivity tests

Short name	Figure Colour	Description
Base	Light Blue	The base case
O3 phot	Aqua	J_{O_3} divided by 3
Vd O3	Orange	Ozone dep. velocities reduced by 75%
Horowitz	Green	NO_x recycling rates as in *Horowitz et al.* [2007]
ISON dep	Yellow	ISON tracer dep. velocities set equal to those of PAN
Reinit	Red	Reinitialized the model each day at midnight
Init O3=9	Purple	Reinitialise at midnight with 9 ppbv O_3

seems to be unable to explain any divergence in the model-measurement comparison.

A summary of the various chemical sensitivity runs is shown in Table 4.2, with corresponding results plotted in Figure 4.4. Generally, the diurnal cycle was modelled reasonably well for all the chemical parameters tested and was relatively insensitive to chemical changes. The overall diurnal structure for NO is well captured, with the maxima at 8:00 h. With the inclusion of the venting parameter, the NO_2 diurnal structure is also always well simulated. All the chemical sensitivities capture the cycle of ozone but not the magnitude.

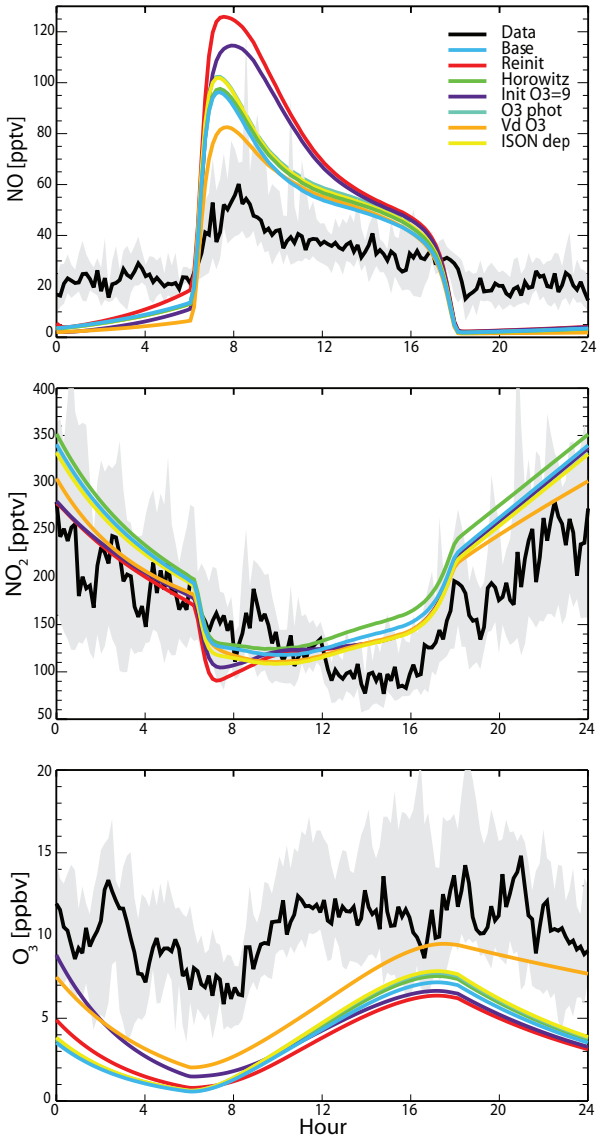

Figure 4.4. 15 day average diurnal NO [pptv], NO_2 [pptv], and O_3 [ppbv] from measurements (black) with 25-75 quartile limits shown in the shaded grey. Seven model experiments are overlaid in various colours: the base run is shown in light blue, reduction of ozone photolysis rate is shown in dark blue, reduction of ozone deposition velocities is shown in orange, adjustment of NO_x recycling rates is shown in green, ISON deposition change is shown in yellow, reinitialization at midnight is shown in red, and reinitialization with high ozone is shown in purple.

In the first chemical sensitivity test (Figure 4.4, aqua line), the photolysis rate of O_3 was reduced by a factor of three. The chemical mechanism shows very little sensitivity to J_{O_3}, barely changing from the base case run. In the second test, ozone deposition velocities (both daytime and nighttime values) were reduced by 75% (Figure 4.4, orange line). For ozone, this simulation has the most impact of any of the chemical sensitivity studies, but still does not increase the concentration enough to match measured values. The change in deposition velocities also alters the shape of the diurnal cycle, as nighttime deposition velocities approach a limit of zero.

In an attempt to keep ozone production values high by increasing the concentration of NO_x in the system, an additional simulation was carried out. Recycling of NO_x from the reaction of ISON with OH was modified by increasing the ISON + OH rate constant from 1.3 x 10^{-11} cm^3 s^{-1} [*Chen et al.*, 1998; *Pöschl et al.*, 2000] to 4.5 x 10^{-11} cm^3 s^{-1} [*Horowitz et al.*, 2007] (Figure 4.4, green line). I also performed an experiment in which NO_x concentrations would decrease; in this sensitivity study, ISON deposition velocity was increased to match nitric acid (Figure 4.4, yellow line). Neither experiment has an impact on the modelled values of O_3.

Two computational tests were also performed. In the first, the model species concentrations are reinitialized each day at midnight, rather than using the values calculated by the model the previous day (Figure 4.4, red line). This introduced a stronger bias in NO and NO_2 around 6:00 h, the first time photochemistry turns on after reinitialization. A second study reinitialized the model at an artificially high value of ozone, and this too displays a similar model bias at sunrise (Figure 4.4, purple line). These two experiments give confidence that the model sensitivity to initial conditions is eliminated by reusing the concentrations calculated from the previous day.

The six studies discussed emphasize that the results from the UKCA chemical mechanism are relatively robust to chemical, photolytic, and deposition rate

changes. As models with this level of complexity, particularly for isoprene oxidation, seem to perform relatively similarly [e.g. *Emmerson and Evans*, 2009; *Archibald et al.*, in press], it seems plausible that this is not an artefact of the model mechanism itself. From my analysis, it appears likely that the regime is more sensitive to physical processes and parameterizations than chemical ones. In order to assess the impact of these chemistry factors in relation to physical parameters controlling the processes of emission, mixing and deposition, I conducted a further series of experiments based on physical variables.

4.1.3.4 Physical sensitivities

As shown in Figure 4.2, the measured data show vertical structure in both NO and NO_2 with much lower concentrations in the free troposphere compared with the boundary layer. The venting parameter simulates exchange with free tropospheric air at night and assumes that this incoming air has lower concentrations of NO, NO_2, and ozone. However, O_3 displays little to no vertical structure in the measurements (Figure 4.2). For this reason, a simulation was run in which venting of ozone was turned off while all other species continued to be diluted. Not venting O_3 is the numerical equivalent of removing O_3 and introducing an equal amount during the same amount of time, such that a collapse of the boundary layer and influence of the free troposphere may well bring in 'new' ozone, but the concentrations will be similar to the boundary layer air it is replacing. This hypothesis is reinforced by the difference between the species in their distribution of sources and sinks; NO_x has a source which is largely surface dominated at a remote rainforest location (higher in the troposphere, lightning can contribute as well), while ozone has a strong surface sink due to deposition.

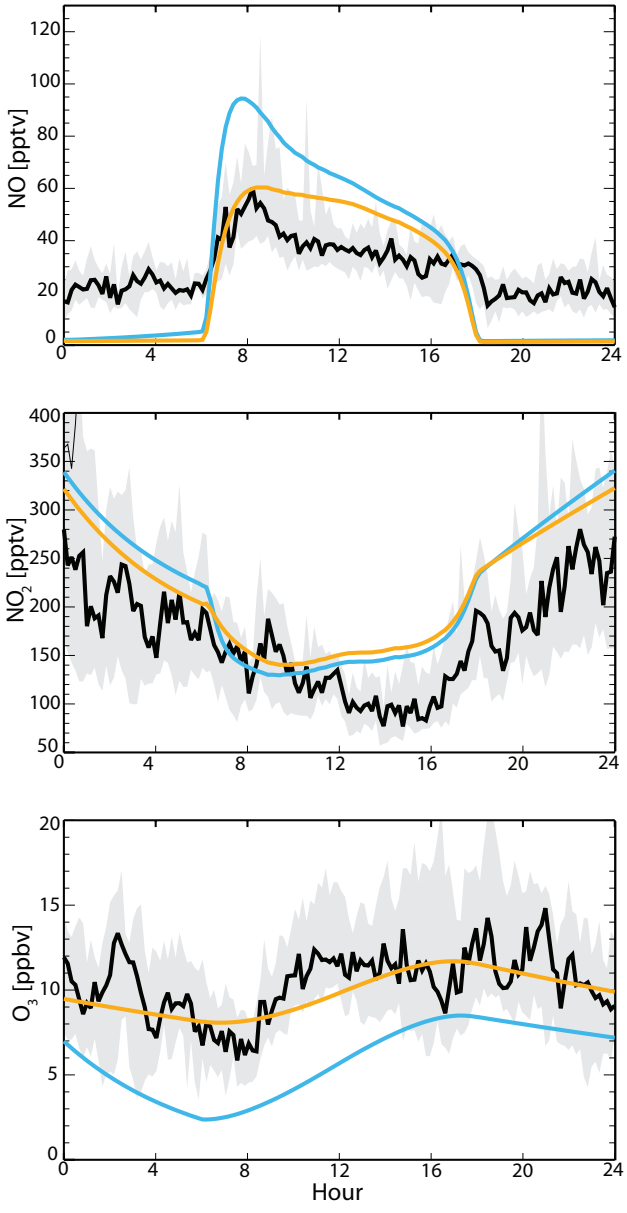

Figure 4.5. Model comparison to diurnal cycle of NO, NO_2, and O_3 (black with shading) without (orange) and with (the base case, blue) venting ozone.

Figure 4.5 shows the results of the box model when ozone is not vented, which displays much better agreement with the measurements. The amplitude of the diurnal cycle of ozone is reduced when O_3 is no longer vented, as the nighttime sinks are reduced. This dampened cycle more closely matches the measured diurnal profile. NO_2 changes little when ozone is not vented, but NO is greatly improved, particularly in the early daytime hours. By keeping O_3 in the box during the night, the chemical sink for NO remains higher, and the elevated values of NO in the morning are correspondingly reduced.

Three variables are used to further test the physical boundaries of the box model: the exact quantity of material lost at night (the venting parameter), the height of the boundary layer during the day, and the height of the boundary layer at night. In order to obtain the best value for these three parameters, a cost function analysis was used:

$$\mathrm{CF_x} = \frac{1}{\mathrm{t}} \sum_{\mathrm{t}} \frac{(|\mathrm{model_x} - \mathrm{measured_x}|)}{\mathrm{measured_x}} \tag{4.1}$$

where for each species (denoted by x) and at each timestep (t), the difference between modelled and measured values of NO, NO_2, O_3 are evaluated and averaged over a 24 hour day and 15 experiment days. The cost function gives the average deviation of the model from the measurements expressed as a fraction, where zero is a perfect match. The NO cost function is only evaluated between 6:00 and 18:00 h due to the mechanism's inability to capture nighttime NO concentrations, so that results are not skewed because of nighttime values. The results of the three cost functions are shown in Figures 4.6 and 4.7, where a lower value of the cost function represents better agreement between measurements and modelled concentrations.

The NO cost function shows a dependence on the venting fraction until the value of 2% per timestep, at which point model and measured data converge to a reasonable agreement of less than 30% difference in value. At the zero value for venting, NO shows almost no dependence on the nighttime boundary layer

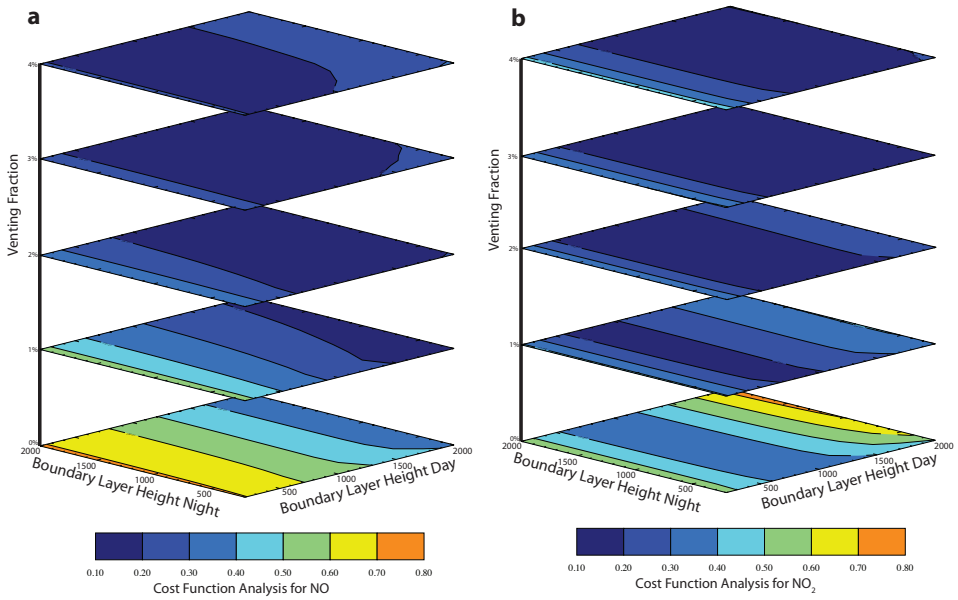

Figure 4.6. Cost function analysis of model comparison to diurnal average NO (a), and NO_2 (b). A lower value represents closer agreement between the box model and the measurements.

height, which reflects the fact that the cost function is only evaluated during daytime hours. NO matches the measurements best (with a cost function value below 0.20) for high values of the daytime boundary layer height, though the gradient of dependence on daytime boundary layer height decreases with increasing venting fraction.

At a 0% value for the venting parameter, the NO_2 cost function shows values of 0.30 to 0.80. With venting, the levels are lower (up to 0.30), which suggests that the best fit requires at least some material to be removed at night. Between 1% and 4%, however, NO_2 displays little variation in the cost function, and the entire cost function 'space' is valued under 0.40. NO_2 also shows very little dependence on the nighttime boundary layer height, demonstrating that venting is a more important loss process than deposition. The height of the boundary layer during the day is important only at heights less then approximately 500 m and above 1800 m.

Ozone was not vented in these experiments, so the cost function for ozone is

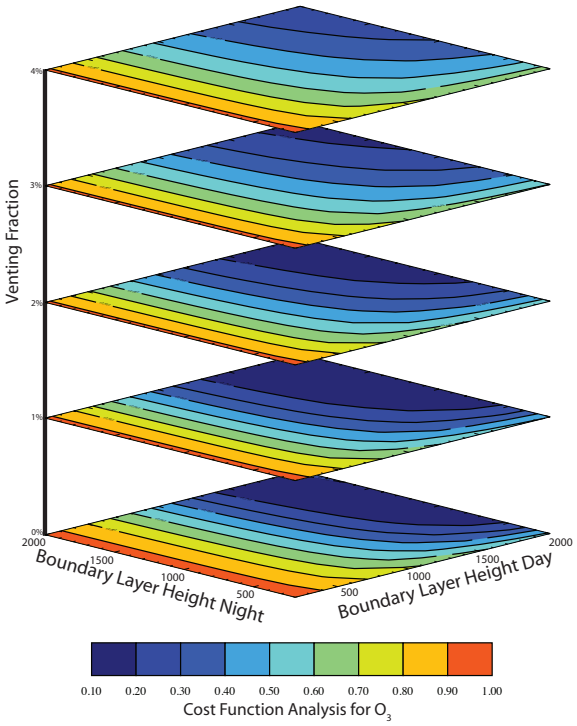

Figure 4.7. Cost function analysis of model comparison to diurnal average O_3.

relatively stable in relation to venting parameter. Ozone shows a very high sensitivity to the boundary layer height during the day (with values ranging between 0.10 and 1.0), presumably due to deposition, and little dependence at night except below 500 m.

4.1.3.5 Best fit to measurements

Figure 4.8 shows the best fit to the measurements obtained using the box model. The values for the venting parameter (2%), boundary layer height during the day (1200 m) and night (750 m) were taken from the cost function analysis minima. The results show good agreement between measured and modelled values, capturing the majority of structure and diurnal variation for all three measured species. NO matches particularly well, though the model is still not able to simulate the residual concentrations at night. As described before, these could arise from a

highly stratified boundary layer, or rapid mixing times up from the soil to the measurement inlet before chemical reaction. In either case, these processes are very small scale, and beyond the capability of a global model (with a resolution of hundreds of kilometres) to capture physically.

Modelled NO_2 is slightly higher than the measured values but captures the structure of the measurements effectively. In particular, the nighttime structure of NO_2 is well simulated once venting was included in the box model. Afternoon NO_2 concentrations are also slightly higher in the model than measurements. Since my analysis shows that transport and physical processes dominate the diurnal structure, perhaps this afternoon discrepancy arises from afternoon convection. Ozone looks very similar to measurements, though the rapid rise in the morning is not entirely captured. Nevertheless, the magnitude and basic form of the diurnal cycle are simulated well.

With the success of the chemical mechanism in this region in mind, I ran a regional sensitivity study in which phase I of the biofuel lifecycle was represented in a simple, idealized manner.

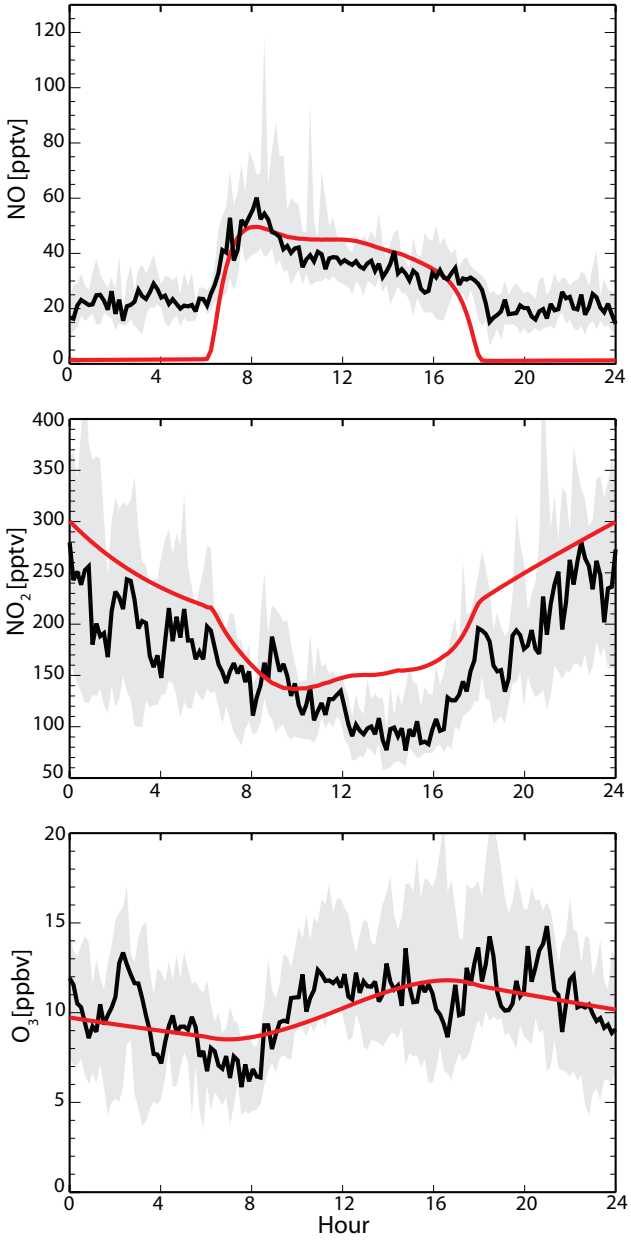

Figure 4.8. 'Best fit' model (red) compared to diurnal average NO, NO_2, and O_3 (black with shading) after optimized adjustments to the venting parameter and boundary layer heights.

4.2 Regional sensitivity study

The expansion of oil palm production in Southeast Asia has been identified as a major threat to the carbon balance [*Danielsen et al.*, 2008], bird [*Peh et al.*, 2006] and insect [*Turner and Foster*, 2009] populations, and to biodiversity in general [*Pin Koh and Wilcove*, 2007]. Oil palm is also an extremely high emitter of isoprene [*Kesselmeier and Staudt*, 1999, also shown in Table 2.2], and could therefore influence air quality significantly. In this section, my aim is to test the hypothesis that phase I of the biofuel life cycle can impact tropospheric chemistry through isoprene emissions. The first experimental sensitivity study, in which isoprene emissions are doubled, could represent a transformation of forested areas to managed oil palm plantations; the second study could represent a transition to a non-emitting crop, such as sugar cane from oil palm or rainforest. Both types of crops can be used in biofuel production (see section 1.3).

4.2.1 Experimental setup

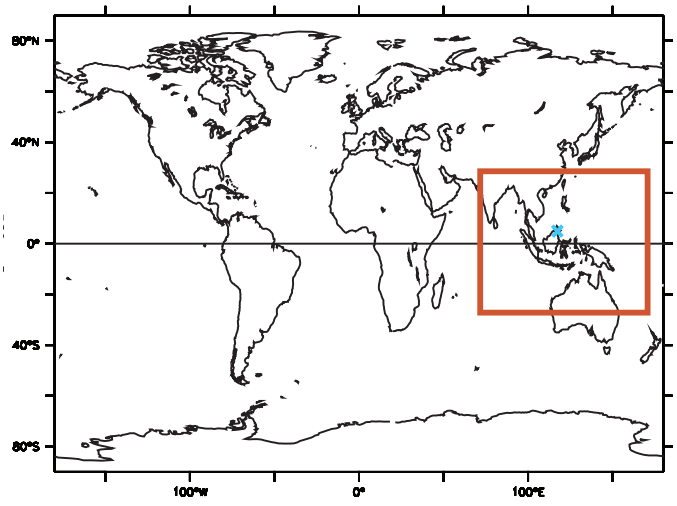

Figure 4.9. The area of emission perturbation in two sensitivity studies (outlined in red). The location of the OP3 field campaign is denoted by the blue cross.

Using UKCA, I ran two simple studies in which the emissions of isoprene

were altered. In the first, isoprene emissions were doubled (the OILPALM run) in the region between -25°S, 25°N, 70°E, and 160°E. In the second study, isoprene emissions were reduced by 25% (the SUGARCANE run) in the same region. The area of perturbation is shown in Figure 4.9. The model was run for 16 months with the first four months taken as spin up. The model year is 2001, and the sea surface temperatures are the same as in chapter 3 [*Rayner et al.*, 2003].

4.2.2 Impact on ozone

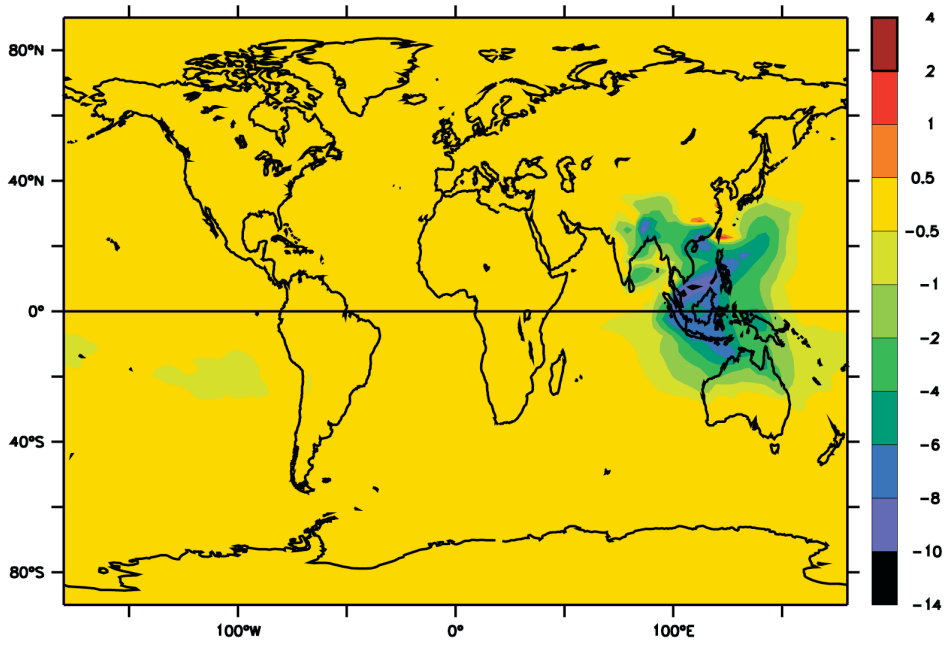

Figure 4.10. Difference in monthly mean July surface ozone [ppbv] between the OILPALM and BASE simulations.

Changes in surface ozone resulting from the OIL PALM simulation in South-east Asia are depicted in Figure 4.10. July values are shown, as isoprene emissions in the region peak in July (see Figure 3.1) and thus the impact on the local envi-

ronment regime will be largest at that time. Over the area of perturbation, ozone concentrations drop when isoprene emissions are doubled. The strongest changes modelled are up to -10 ppbv, though over the oceans the difference is generally restricted to values above -6 ppbv. The outflow area from Southeast Asia through to the South Pacific is evident from an area of small change in ozone concentrations off the western coast of South America.

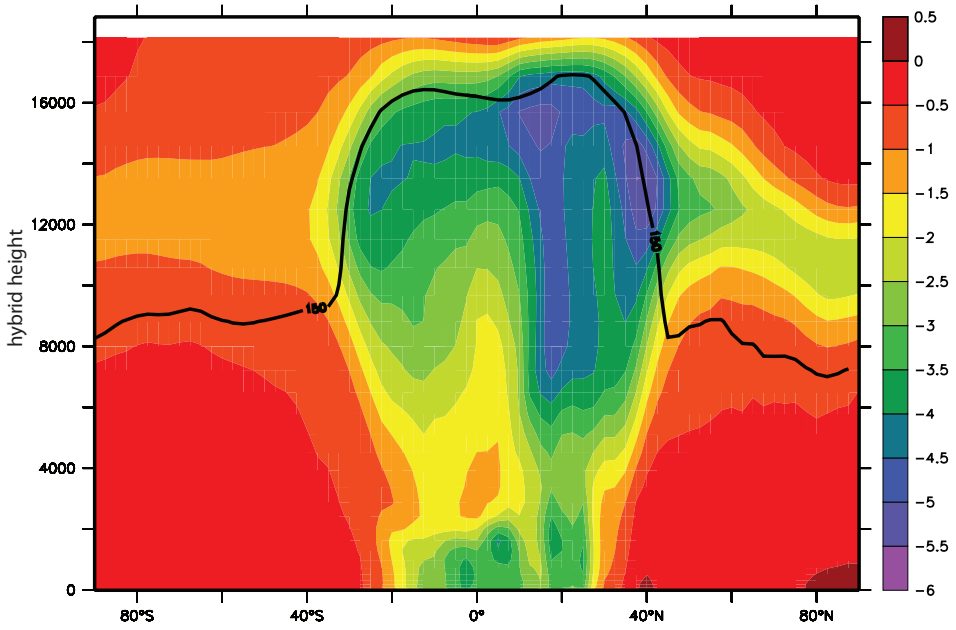

Figure 4.11. Difference in monthly mean July ozone [ppbv] averaged between 70E and 160E (the area of perturbation) between the OILPALM and BASE simluations. The chemical tropopause of 150 ppbv of ozone, as defined by *Stevenson et al.* [2006], is shown as a black line.

The effect of the OILPALM run is evident higher in the troposphere as well, as shown in Figure 4.11. The magnitude of the impact in the free troposphere is lower (6 pbbv maximum) than near the surface, though the distribution is more widespread. The largest differences are concentrated in the colder regions of the tropical upper troposphere: at 8000 m, changes in ozone of -1 to -4 ppbv are evident across much of southern Asia and the maritime continent, as well as most of the Pacific (not shown). The lower temperature is important for the lifetime

of PAN [*Moxim et al.*, 1996], where concentrations increase more (5-10%) in this region than elsewhere in the free troposphere. To show the spatial distribution in relation to ozone, the change in surface PAN concentrations resulting from the OILPALM simulation is shown in Figure 4.12. The formation of PAN increases in this study, removing NO_x from the local chemical environment and impeding ozone formation. The simultaneous reductions in ozone can therefore be explained by this 'locking up' of NO_x, preventing the conversion of NO radicals to NO_2.

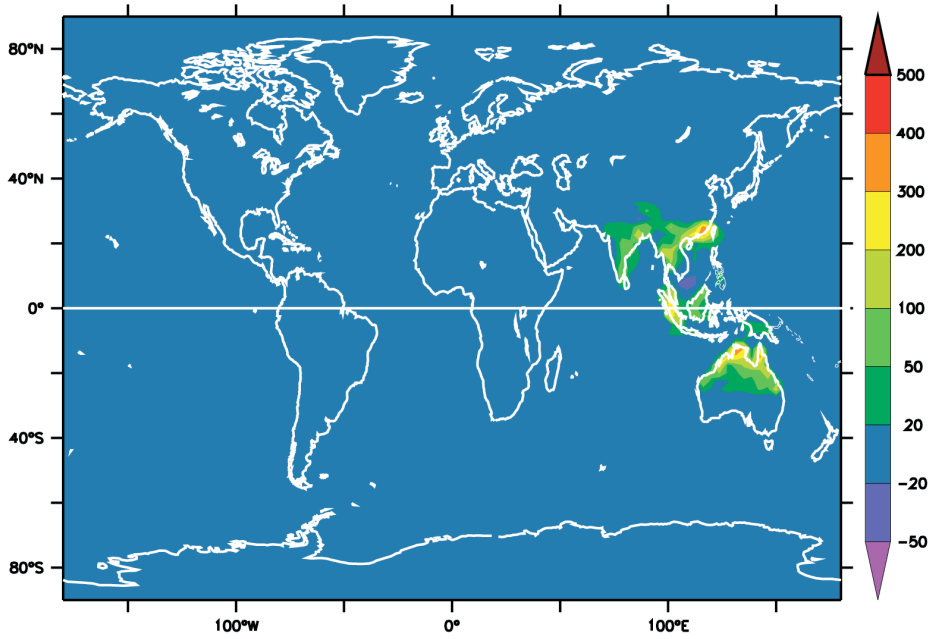

Figure 4.12. Difference in monthly mean July surface PAN [pptv] between OILPALM and BASE.

To investigate the linearity of the relationship between isoprene emissions and ozone production, a second sensitivity test was performed in which isoprene emissions were reduced by 25% (the SUGARCANE run). The change in surface ozone in July resulting from this second experiment is shown in Figure 4.13. Ozone con-

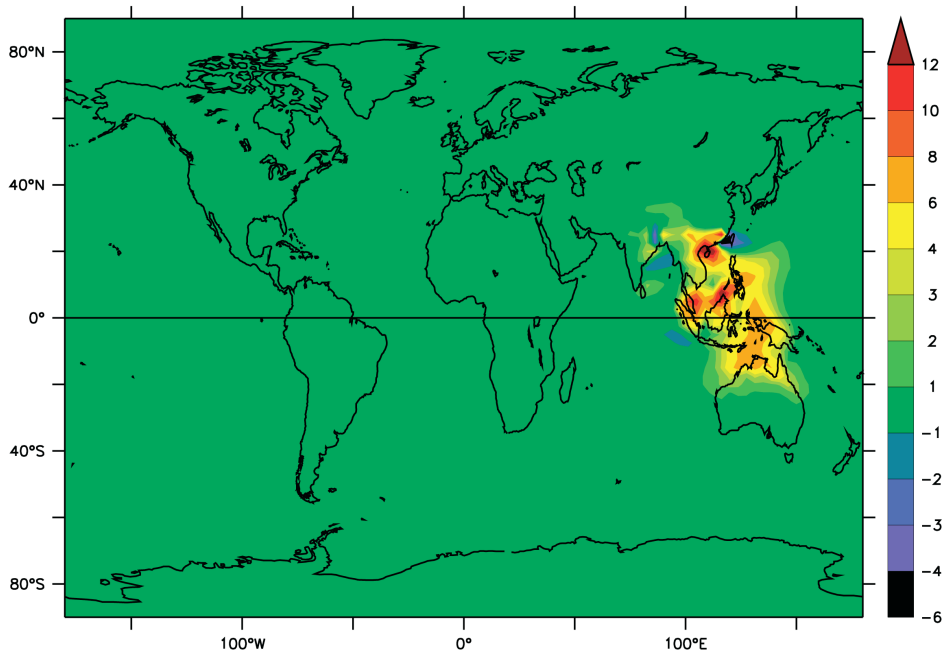

Figure 4.13. Difference in monthly mean July surface ozone [ppbv] between SUGARCANE and BASE

centrations increase in the SUGARCANE run; in fact, the values shift by a greater amount than when emissions are doubled. The perturbation to emissions does not yield a direct change in ozone; rather, a small reduction (-25%) changes ozone by a larger amount than a large increase (200%). The linearity of the maximum change in ozone as a response to these simple perturbations to isoprene emissions is shown in Figure 4.14. The response curve shown here is just one transect from a more complete ozone production isopleth plot such as the one shown in section 2.1.3.

Young [2007] performed a similar isoprene emission reduction sensitivity study to my SUGARCANE run using the UM_CAM model in a future atmosphere with A2 emissions. In January, when emissions shift South, an increase in ozone of up

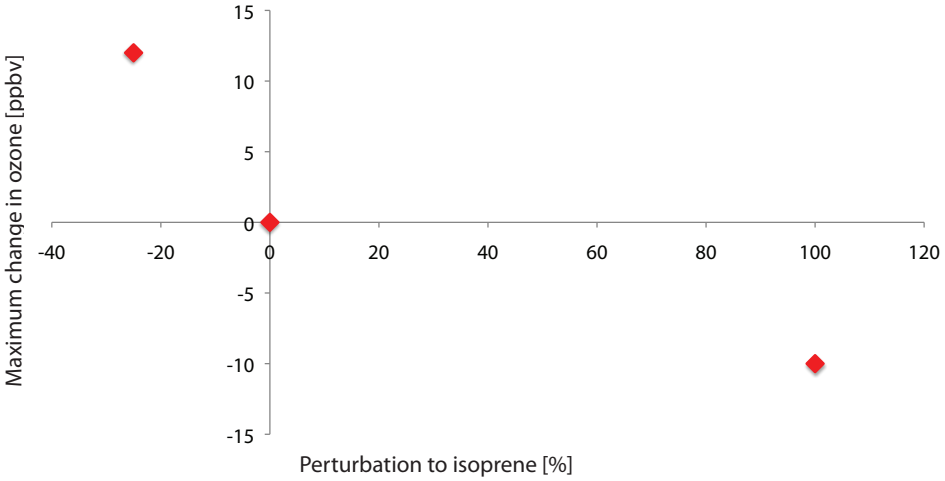

Figure 4.14. Linearity in maximum ozone response between OILPALM, SUGARCANE, and BASE. The x axis shows the amount of perturbation to isoprene emissions (%), and the y axis shows the maximum response in July surface ozone [ppbv] resulting from the perturbation.

to 5 ppbv over Australia was found, similar to the results from UKCA. Interestingly, a decrease in ozone in southeast Asia and India was also reported, colocated with strong NO_x emissions in the A2 scenario which effectively convert the region to a VOC-sensitive environment. *Wiedinmyer et al.* [2006] also did a simple sensitivity test assuming a 50% reduction of isoprene emissions in the Amazon and the southeastern United States. In the VOC-rich environment of the Amazon, ozone increased by 3-5 ppbv in July, lower in value than the response given by UKCA in the southeast Asia. In contrast, the more polluted environment of the southeastern United States displayed a decrease in monthly mean ozone of 2-4 ppbv [*Wiedinmyer et al.*, 2006].

4.2.3 Uncertainties

The uncertainties associated with this type of simple sensitivity study are large. With a large-scale shift towards oil palm production, other, non-isoprene emissions could change simultaneously. Carbon [*Houghton*, 2003] and nitrogen [*Williams*

et al., 1992; *Bouwman et al.*, 2002] emissions associated with land use change, fertilizer emissions, and post-processing power plant emissions could increase. Some terpenoid emissions from the forest or reclaimed land could decrease, depending on the speciation of the forest; simultaneously, others could increase. Furthermore, changes in biogenic isoprene and terpenoid emissions could also influence SOA production (section 2.2.1.2), which could have consequences for local climate and meteorology.

4.3 Summary

In this chapter, I began with a description of measurements of NO, NO_2, and O_3 taken during the OP3 field campaign. The box model was then presented, and a number of chemical sensitivity studies were reported on; their success in matching measured ozone levels was limited. A series of physical sensitivity studies proved to have greater success in matching the model output to measured data. I optimized a cost function based on daytime boundary layer height, nighttime boundary layer height, and venting parameter. This yielded a 'best fit' box model simulation which was quite successful at reproducing the data. My work demonstrates that the chemical mechanism in UKCA can indeed reproduce measurement data in a remote tropical rainforest site, but that it is sensitive to parameterizations of physical processes.

In the second section, I performed two simple sensitivities in which isoprene emissions were altered. Although simple, these changes could be associated with the growth of biofuel feedstocks (either oil palm for biodiesel, or sugarcane for ethanol) in the region. I then described the summertime ozone reductions resulting from the OILPALM perturbation and the associated increase in PAN. Looking at the linearity in the response, the change in ozone was stronger for the decrease in VOC emission (SUGARCANE) than for the increase (OILPALM). Since the response in ozone is non-negligible, it appears that phase I of the biofuel life cycle

can indeed influence air quality and tropospheric chemistry.

In the next chapter, I attempt to simulate a more realistic representation of future crop changes and to characterize componenents of a potential future atmosphere.

Chapter 5

Future Ozone Attribution and Phase I: Cultivation

In this chapter, I examine a global representation of phase I of the biofuel life cycle. In section 5.2 I describe the experimental setup and methodology, and in section 5.3 I look at how isoprene emissions could evolve in the future. Section 5.4 is concerned with a characterization of a potential future atmosphere using the concept of ozone attribution, with particular focus on emissions and physical climate change. In section 5.5, I examine the impact of land use change (expansion of land dedicated to growing crops) related to phase I of the biofuel life cycle. I then compare the impact of land use change to another potential isoprene emission perturbation, CO_2 suppression (previously described in section 2.2.2.2) in section 5.6.

5.1 Introduction

5.1.1 How will ozone change in the future?

The relationship between ozone and climate is complex. On a theoretical level, it starts with the direct relationship between temperature and chemistry. Higher tem-

peratures drive faster rates of chemistry [e.g. *Wild*, 2007], which can increase or decrease ozone production depending on the local chemical environment (section 2.1.2). High ozone concentrations and temperature are also correlated on the basis of the decrease in PAN lifetime (which has a thermal dependence, see section 2.1.4) and the associated increase in HO_x and NO_x released from PAN degradation [*Sillman and Samson*, 1995]. An increase in isoprene emission driven by higher temperatures could increase ozone in a high-NO_x environment, while decreasing ozone in a low-NO_x environment [*Roelofs and Lelieveld*, 2000; *Fiore et al.*, 2005].

Climate and chemistry are linked on an indirect level as well. Increasing atmospheric humidity, a result of higher temperatures [*Solomon et al.*, 2007b], will increase the destruction of ozone through the reaction of $O(^1D)$ with water vapour [*Thompson*, 1992; *Johnson et al.*, 1999]. In high-NO_x environments, this could increase ozone by stimulating oxidation processes through higher concentrations of OH, while in low-NO_x environments, the scavenging could reduce ozone levels [*Liu et al.*, 1987; *Sillman and Samson*, 1995]. Other competing climate variables are also at play, including an increase in lightning NO_x resulting from increased convection [*Zeng et al.*, 2008], an increase in stratosphere-troposphere exchange [*Zeng and Pyle*, 2003; *Hegglin and Shepherd*, 2009], and changes in both wet and dry deposition [*Zhang et al.*, 2008]. Finally, elevated temperatures could potentially alter the meteorology of the atmospheric system in ways that generally encourage ozone formation, such as increasing stagnation events, heat waves, and frequency of droughts [e.g. *Mickley et al.*, 2004].

The relationship between ozone episodes and temperature has been empirically established through observation [*Cox and Chu*, 1996; *Lin et al.*, 2001], and has led to a number of modelling studies investigating the relationship between future climate change and air quality. Some studies have examined this relationship on relatively short time horizons (between 2020 and 2030) [e.g. *Johnson et al.*, 1999; *Stevenson et al.*, 2000, 2005; *Racherla and Adams*, 2006; *Stevenson et al.*, 2006; *Unger et al.*, 2006; *Wu et al.*, 2008a]. Several studies have examined the impact

of climate change on ozone using the same time horizon (2100) used here [e.g. *Stevenson et al.*, 2000; *Hauglustaine et al.*, 2005; *Brasseur et al.*, 2006; *Liao et al.*, 2006; *Zeng et al.*, 2008]. The complexity of the relationship between ozone and climate is such that there is not a consensus prediction for how ozone will change in the future; for example, *Hauglustaine et al.* [2005] and *Liao et al.* [2006] found positive changes in surface ozone over land areas, while *Zeng et al.* [2008] reported a more geographically heterogeneous effect.

5.1.2 The impacts of future land use change

Another potential future perturbation to the Earth system is land use change. The human species relies on the earth system for water, fuel, food, and other natural resources to sustain itself. The result is that human influence over the biosphere has been in effect for centuries [*Vitousek et al.*, 1997a], and will continue to grow as global population augments.

Ramankutty and Foley [1999] were the first to quantify the total historical influence of humans on global land, and they found that 1140 million ha of woodland and 670 million ha of savannas/grasslands have been lost to cropland expansion since the year 1700. A second attempt was undertaken by *Klein Goldewijk* [2001], whose showed 1206 million ha of land has been cleared between 1700 and 1990, while pastureland has grown by 2927 million ha. *Hurtt et al.* [2006] used an accounting model to estimate that 42-68% of global land has been influenced by anthropogenic forces in the last three hundred years. *Pongratz et al.* [2008] compiled a land use change dataset for the last millenium; they were able to extend their analysis into longer timescales by using population data as a proxy for land use change. The authors reported that 500 million ha of natural vegetation was transformed to agricultural and pastoral land between 800 and 1700.

Anthropogenic land use change has been found to influence the climate system. As a result of changes in surface albedo and evapotranspiration, *Davin et al.* [2007] reported a -0.29 W m^{-2} radiative forcing due to anthropogenic land cover change

between 1860 and 1992. *Pongratz et al.* [2009] examined a longer timescale of 800 years in order to assess the impact of human-driven land use and land cover change on radiative forcing between 1100 and 1900 and found a value of -0.21 W m^{-2}. Besides radiative forcing, land use has also been found to impact temperature and wind estimates [*Civerolo et al.*, 2000; *Feddema et al.*, 2005; *Lamptey et al.*, 2005; *Voldoire et al.*, 2007], soil suitability for growing crops [*Ramankutty et al.*, 2006], and precipitation [*Lamptey et al.*, 2005; *Junkermann et al.*, 2009]. These impacts on the climate system will carry into the future; for example, *Davin et al.* [2007] projected a -0.7 W m^{-2} radiative forcing between 1992 and 2100 on account of land use change.

A number of gas fluxes into the atmosphere have also been influenced by land use change. The fluxes of NO, N_2O, and NH_3 have been increased by approximately 80%, 37%, and 70% respectively as a result of agricultural control of the nitrogen cycle [*Vitousek et al.*, 1997b]. The flux of carbon to the atmosphere as a result of anthropogenic land use change has been estimated to be between 1.6 and 2.1 Gt C yr^{-1} in the 1980's [*Jain and Yang*, 2005] and 1.1 to 1.3 Gt C yr^{-1} in the 1990's [*Shevliakova et al.*, 2009]. As for the total flux, *Houghton* [2003] estimated a carbon flux of 156 Pg C between 1850 and 2000 as a result of human driven land use change. These types of calculations have associated uncertainties due to the use of proxy data to create records about the past; *Quaife et al.* [2008] quantified this uncertainty to be approximately -15% to 8% using the UK as a case study. Carbon fluxes into the atmosphere due to land use change will continue into the future, though the extent seems to be temperature, scenario, and model dependent [*Cramer et al.*, 2004; *Gitz and Ciais*, 2004; *Sitch et al.*, 2005; *Friedlingstein et al.*, 2006; *Müller et al.*, 2007]

Besides the biogeophysical and biogeochemical variables mentioned above, land use can impact biogenic emissions such as isoprene. *Tao and Jain* [2005] modelled changes in global isoprene emissions between 1981 and 2000, and found that 2% of isoprene variability between 1981 and 2000 arose from variations in

land use (climate change and CO_2 fertilization had larger effects). *Guenther et al.* [2006] noted that present day global isoprene emissions change by -0.2 to 3% depending on the land use dataset used as input to their model. *Lathière et al.* [2006] ran two sensitivity studies: in the first case, representing tropical deforestation, isoprene emissions were reduced by -29% globally and -35% in the tropics; in the second, representing European afforestation, emissions changed by +4% globally and +126% in Europe. The impact of land cover on isoprene emissions has also been studied at smaller scales, notably for European forests [*Arneth et al.*, 2008b], though replacement of natural forests by woody biomass plantations did not alter isoprene emissions significantly in their model study.

These changes in isoprene emissions have the potential to transform local tropospheric chemistry. *Wiedinmyer et al.* [2006] found altered ozone concentrations of -5 ppbv (over the United States) to 5 ppbv (over the Amazon) from a sensitivity study in which isoprene emissions were lowered to represent urbanization. In a second sensitivity, isoprene emissions were increased to represent a transition to high-emitting tree plantations; this resulted in a decrease of ozone concentrations over the Amazon of up to 9 ppbv and a mixed signal in the north and western United States between -5 and 20 ppbv [*Wiedinmyer et al.*, 2006]. *Chen et al.* [2009a] found that future land use change decreased surface ozone over the United States under an A2 scenario by up to 5 ppbv due to changing isoprene. *Avise et al.* [2009] reported that the impact of future land use change on biogenic isoprene emissions in the United States increased ozone by 1.3 ppbv in July. Using a single column model, *Ganzeveld and Lelieveld* [2004] found that for two deforestation scenarios in the Amazon, isoprene concentrations decreased, ozone rose by under 2 ppbv at the surface, and surface OH increased by 50%. A 100% increase in biogenic VOC emissions resulted in an increase in maximum 1-hour June ozone concentrations of 30% in the Mid-Atlantic region of the United States in the work of [*Bell and Ellis*, 2004]. Finally, a 1-6 ppbv change in daily 8-hour ozone maximum (DM8H) under the A1B scenario in 2050 was attributed to future land use change in the Houston

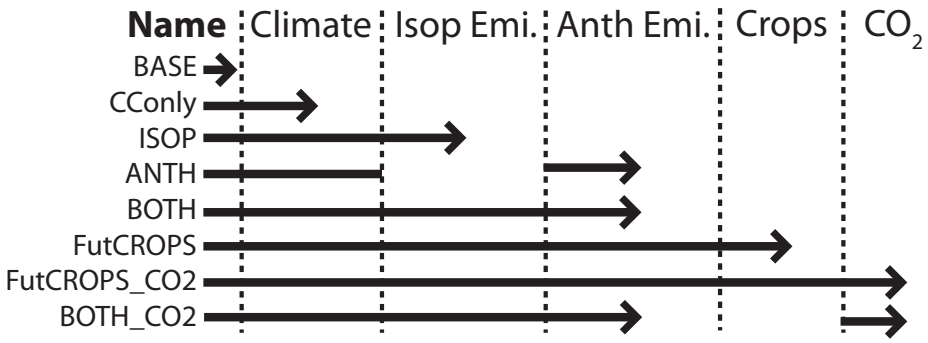

Figure 5.1. A summary of emissions and climate sensitivity experiments.

area [*Jiang et al.*, 2008].

In this chapter, my goal is to test the model sensitivity to land use change and CO_2 suppression of isoprene emission within the context of a potential future atmosphere.

5.2 Experimental setup

In order to understand how and why ozone changes in a potential future atmosphere, I ran a number of experiments to test the sensitivity of UKCA to climate change, future anthropogenic emissions, and future biogenic emissions. I used a sequential or serial methodology, such that each experiment added one more of each of these variables; the difference between each sequential experiment yielded the change from a single variable. Figure 5.1 shows the simulation names and a summary of the experimental design.

The BASE run (1999-2005) has been described in detail in section 3.2, and so will not be described here. In addition to the chemistry and emissions used in the BASE simulation, the CConly integration included long wave radiative forcing from CO_2 and CH_4 of 621 ppbv and 2973 ppbv, respectively. In addition, the radiation code includes long wave absorption of three more species, whose concentrations were set as follows: N_2O was set to 362 ppbv, CFC-11 was set to 45 pptv,

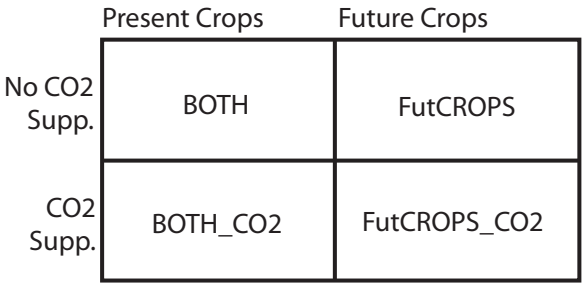

Figure 5.2. Matrix of land use change and CO_2 suppression experiments.

and CFC-12 was set to 222 pptv. Future sea surface temperatures (SSTs) were generated using the Met Office Hadley Centre Earth System Model (HadGEM) [*Stott et al.*, 2006], in which the runs of a coupled ocean-atmosphere model followed the A1B IPCC SRES scenario [*Nakicenovic et al.*, 2000] with 150 years spin up period, 30 years of which included anthropogenic forcing. SSTs are a boundary condition in UKCA (there is no slab ocean) and vary monthly and interannually throughout the course of each integration. Each of the UKCA integrations set in the future were allowed 16 months to spin up and were run for a further four years corresponding approximately to the end of the century (2096-2099).

The ISOP integration included the physical climate forcing from the additional long wave radiation and SSTs as well as future isoprene emissions. The ISOP run was designed to test the changes resulting from future biogenic isoprene emissions. The ANTH simulation also included future climate forcings, but future emissions were limited to anthropogenic emissions (isoprene emissions remained at present day values.) The BOTH simulation included both climate and emission (anthropogenic and biogenic) future forcings as a sort of 'best guess' future run. The difference between ANTH and CConly, and the difference between BOTH and ISOP, test the response resulting from change anthropogenic emissions with both present day and future isoprene emissions.

In addition to these, the FutCROPS run included the change in isoprene emissions associated with projected future cropland expansion, which could be asso-

ciated with growth of biofuel feedstocks. The impact of CO_2 suppression of isoprene emission was included in the experiment called FutCROPS_CO2. Finally, to compare the relative impacts of cropland expansion and CO_2 suppression, the BOTH_CO2 run included all future forcings and CO_2 suppression without a change in cropland expansion. The last four experiments represent a matrix, shown in Figure 5.2, designed to test CO_2 suppression with present and future crops, and land use with and without CO_2 suppression all in a potential future atmosphere.

Future anthropogenic emissions were taken from a B2+CLE scenario developed for use in *Fowler et al.* [2008] and are summarized in Table 5.1. The scenario was based on an updated IPCC B2 storyline [*Riahi et al.*, 2007], and was further revised to include legislation (Current LEgislation = CLE) and regulation passed between 2002 and 2006 as described in *Dentener et al.* [2005] and *Cofala et al.* [2007]. The B2+CLE scenario is an optimistic scenario that involves 'local solutions to economic, social and environmental sustainability', and in which global population increases at a moderate rate [*Fowler et al.*, 2008]. I chose this moderate scenario because my intention is to study phase I of the biofuel life cycle, and it seems unlikely that large scale implementation of biofuels will occur contemporaneously with a very pessimistic storyline (such as the A2). Biofuel regulation and emissions reductions are almost always colegislated (see section 1.1).

The B2+CLE emissions used here were for the year 2050, but CO and NO_2 emissions were projected to change less than five and ten percent, respectively, between 2050 and 2095. This is well within the range of uncertainties between and within the economic scenarios; for example, carbon dioxide emissions in the original B2 scenario vary between 7 and 24 Gt C $^{-1}$ (240%) within the sub-family scenarios [*Nakicenovic et al.*, 2000]. When compared with present day, NO_x emissions are reduced by 9.6 Tg N yr^{-1} (-17%) and CO by 38.6 Tg yr^{-1} (-3.6%). NMVOC increases slightly by 16.1 Tg yr^{-1} (2.4%). The emissions listed in Table 5.1 are due to anthropogenic sources only. Soil, biomass burning, oceanic, and natural (acetone) emissions were all kept constant with respect to the present day

Table 5.1. Future B2+CLE emissions of NO_x, CO, and non-methane non-isoprene VOCs.

Emitted species	Amount [Tg yr^{-1}]
NO_2, Tg N yr^{-1}	
Anthropogenic	20.2
Soil	7.0
Biomass Burning	10.2
Total	*37.4*
CO, Tg CO yr^{-1}	
Anthropogenic	432.0
Biogenic	89.0
Ocean	11.0
Biomass Burning	507.5
Total	*1039.5*
VOC, Tg VOC yr^{-1}	
Anthropogenic	99.7
Natural (acetone)	48.3
Biomass Burning	31.3
Total	*179.3*

(Table 3.2, section 3.2.3). The increase in NMVOC between present and future appears quite small, but is larger when isoprene is taken into account.

5.3 Future isoprene emissions

Three models were used to generate isoprene emission fields[1]. The Sheffield dynamic global vegetation model (SDGVM) [*Woodward et al.*, 1995; *Beerling et al.*, 1997] was forced with mean monthly temperature, humidity, and precipitation derived from the Unified Model [*Johns et al.*, 1997] run without chemistry. Using this data, the SDGVM was run to vegetative equilibrium around a fixed (no seasonal variation) map of global crop distribution, as in section 3.2.3. Future (2100) crop distribution was modelled by the Integrated Model to Assess the Global Environment [IMAGE, *Alcamo*, 1999] economic and policy model and compiled for input

[1]Isoprene emissions fields were generated by Juliette Lathière, as in Chapter 3.

into a dynamic global vegetation model. To explore the land use changes in their most extreme and in the context of large scale biofuel implementation, the crop map was forced with the SRES A2 scenario [*Nakicenovic et al.*, 2000]. The output from the SDGVM was then used in a BVOC emission model (also described in section 3.2.3) based on the parameterizations of *Guenther et al.* [2006] to calculate global isoprene emissions. Table 5.2 summmarizes the emissions estimates.

Table 5.2. Total global isoprene flux [Tg C yr^{-1}] for eight studies, calculated by the Sheffield Dynamic Global Vegetation Model.

Experiment Names	Climate	Crops	CO2 Supp.	Isop. [Tg C yr^{-1}]
BASE, CConly, ANTH	Pres.	Pres.	No	413
ISOP, BOTH	Fut.	Pres.	No	482
BOTH_CO2	Fut.	Pres.	Yes	283
FutCROPS	Fut.	Fut.	No	314
FutCROPS_CO2	Fut.	Fut.	Yes	184

The present day estimate for isoprene emissions of 413 Tg C yr^{-1} compares well with recent literature estimates between 402 and 601 Tg C yr^{-1} [see section 2.2.3.4, and *Lathière et al.*, 2009]. The present day calculation includes some land use change forcing from the existing distribution of agricultural land (see section 3.2.4). Without any crops at all, the model estimated present day isoprene emission to be 471 Tg C yr^{-1}, even closer to the median literature estimate for global isoprene flux [*Lathière et al.*, 2009].

In the future, a number of factors could influence biogenic isoprene emissions. Figure 5.3 shows the relative percentage impact of climate change, CO_2 suppression, and cropland expansion on isoprene emissions (each discussed below.)

5.3.0.1 Future isoprene

In the future calculation with present day crops (i.e. crops do not vary; this emission field was used in the ISOP and BOTH integrations), isoprene emissions increased by 17% to 482 Tg C yr^{-1} compared to the present day. This estimate is

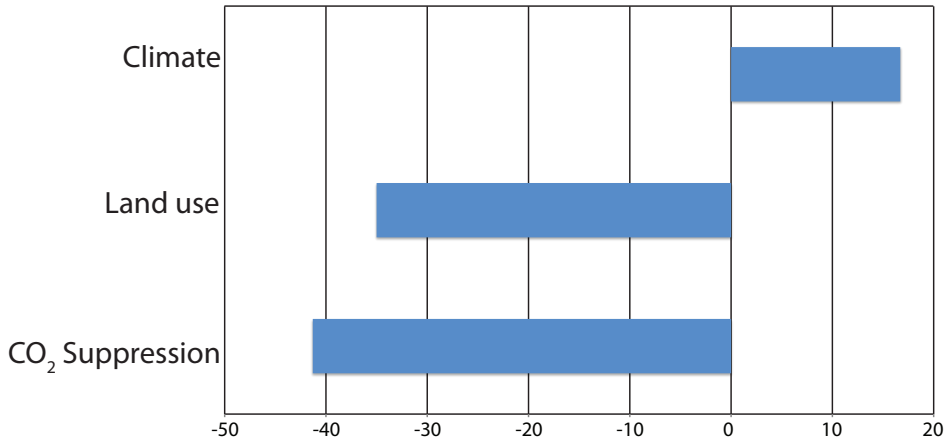

Figure 5.3. Change in isoprene emissions [%] resulting from climate change, CO_2 suppression, and cropland expansion. For the latter two, relative percentages are average for the two sets of model runs; for example, the CO_2 suppression bar is an average of the relative difference between emissions in the BOTH and BOTH_CO2 and FutCROPS and FutCROPS_CO2.

slightly lower than some other estimations of the future global isoprene flux [e.g. *Heald et al.*, 2009; *Young et al.*, 2009] because crops are included in these calculations.

Figure 5.4 shows the difference in isoprene emissions between the present and future runs. As the vegetation responds dynamically to future climate forcings, the increases in future isoprene emission are due to increases in temperature (direct effect) and to CO_2 fertilisation of the biosphere (indirect effect). Directly, higher temperatures drive higher isoprene emissions, as described in section 2.2.2.1. Indirectly, because CO_2 is the main source of carbon for photosynthesis and therefore plant growth, elevated CO_2 levels stimulate the growth of the biosphere; expansion of the high growth, high-emitting ecosystems (PFTs) such as tropical rainforests tends to increase global isoprene emissions in tropical regions such as the Amazon and central Africa. The few areas which show a decrease in isoprene emission (e.g. the northwest Amazon) are most closely linked to a decrease in soil moisture, one of the driving variables for the BVOC emission model[2].

[2]Juliette Lathière, personal communication, 10 November 2009.

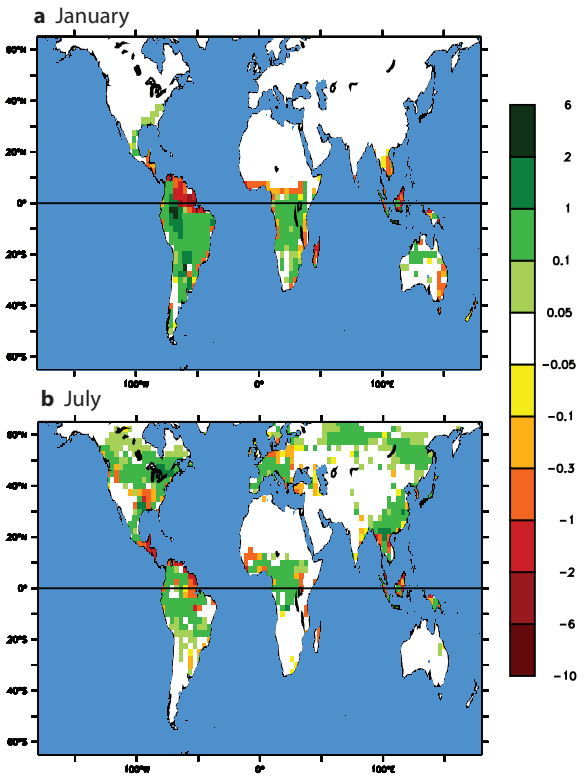

Figure 5.4. Change in isoprene emissions [g isoprene m^{-2} $month^{-1}$] between ISOP/BOTH and BASE simulations.

5.3.0.2 Land use change

Figure 5.5 shows the future change in crop fraction projected by the A2 scenario according to the IMAGE model, illustrating large scale conversion of other land types to managed agricultural and pastoral systems. The gridbox fraction of land dedicated to growing crops increases dramatically in South America (425%), the western United States (123%), central Africa (209%), and southeast Asia (141%). In the central North America, Europe, and eastern China, crop fraction decreases slightly (by less than 10%). Globally, the land area used for crops increases by 97%.

When forests (high emitter) were replaced by agricultural land (very low emitter) in the FutCROPS simulation, reduced global isoprene emissions of 314 Tg C

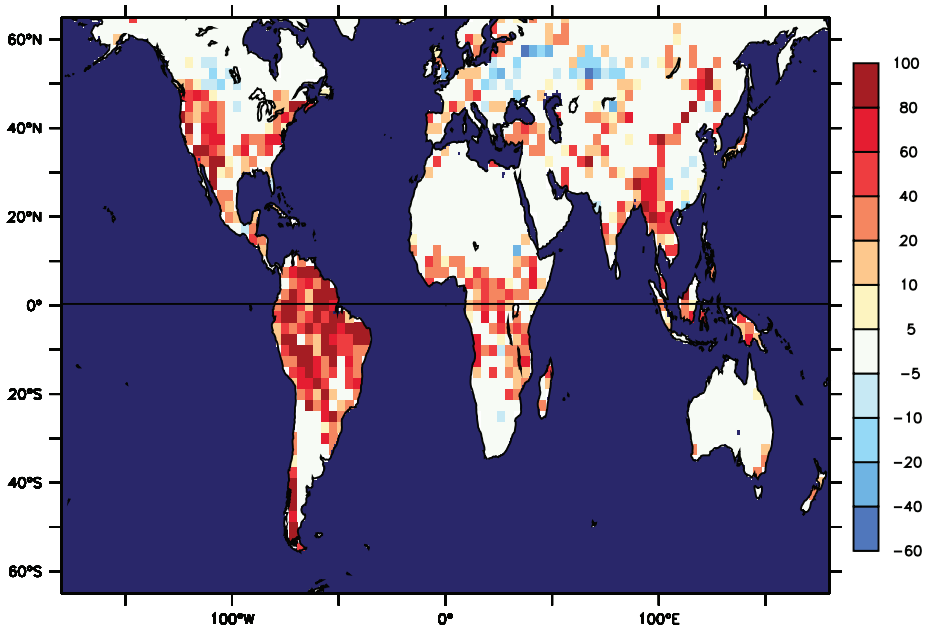

Figure 5.5. Crop mask derived from the IMAGE model and applied to the Sheffield Dynamic Global Vegetation Model for estimates of isoprene emissions used in the FutCROPS and FutCROPS_CO2 simulation. Units are in percent of gridbox assigned to crops.

yr^{-1} were calculated, as shown in Figure 5.6. In the emission model, the crop plant functional type (PFT) was assigned an emission factor of 0.09 mg isoprene m^{-2} h^{-1} after *Guenther et al.* [2006]. For reference, a high emitting PFT such as broadleaf rainforest had an emission factor of 12.6 mg isoprene m^{-2} h^{-1} [*Lathière et al.*, 2009]. The low isoprene emission of the crop PFT could be representative of a number of biofuel feedstocks, notably corn and sugarcane, which are commonly used to produce ethanol (see section 1.3.2.2). Globally isoprene emissions are reduced by 35% on account of land use change (both with and without CO_2 suppression, Figure 5.3). Emissions from current isoprene 'hotspots' are dramatically reduced, notably over the Amazon (-57%), and central Africa (-26%), and summertime emissions from south eastern United States (-27%), and Southeast

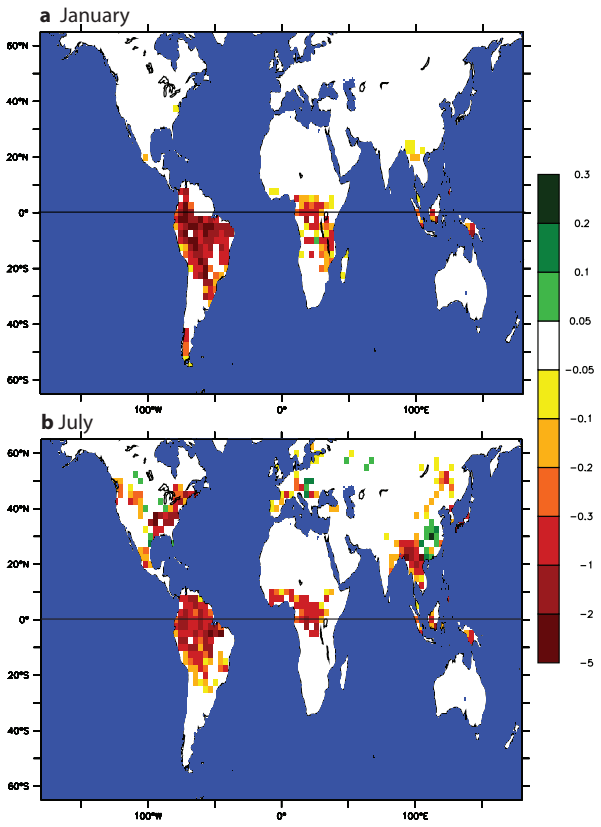

Figure 5.6. Change in isoprene emissions [g isoprene m^{-2} $month^{-1}$] between BOTH and FutCROPS simulations.

Asia (-16%). Where the crop fraction increases (Figure 5.5) and isoprene emissions remain constant (Figure 5.6), this is because the previous plant functional type (PFT) in that region was a low emitter (e.g. the southwest United States).

5.3.0.3 CO_2 suppression

The inhibition of isoprene emission at high ambient atmospheric CO_2 concentrations was introduced in section 2.2.2.2. Both *Possell et al.* [2005] and *Wilkinson et al.* [2009] have empirically parameterized the isoprene emission-CO_2 relationship, and *Wilkinson et al.* [2009] supplied a plant physiological rationale behind the reduction in emissions based on competition within the plant for pyruvate. At the

time this work started, the study of *Wilkinson et al.* [2009] was not yet available, so the relationship of *Possell et al.* [2005] was employed. Within the range studied here (345-621 ppmv CO_2), however, there is hardly any difference between the two. When CO_2 suppression was included and crops were left at present day levels, isoprene emissions were reduced by 199 Tg C yr^{-1}, or 41% (the difference between BOTH and BOTH_CO2). When crops were held at the future distribution instead, CO_2 suppression accounted for a 130 Tg C yr^{-1} decrease, again a reduction of 41% (the difference between the FutCROPS and FutCROPS_CO2 runs.) CO_2 suppression is thus the largest relative factor in controlling global isoprene emissions within the four matrix experiments (Figure 5.3). The relative reduction in isoprene emissions resulting from CO_2 suppression is similar to the values previously reported in *Heald et al.* [2009] of -31% and *Young et al.* [2009] of -55%.

5.4 Characterizing a potential future atmosphere through ozone attribution

5.4.1 Introduction

Attribution is commonly used as a method to deconvolve the various causes of changes in air pollutants or climate change. In the United States, this is closely tied to modelling of specific air quality targets or 'policy-relevant' background ozone levels (the level of ozone that would be present without anthropogenic emissions from North America) [*Wu et al.*, 2008a]. Depending on the model and emissions, the greatest positive contributing factor to future ozone has been attributed to biogenic emissions [*Hogrefe et al.*, 2004], anthropogenic emissions and scenario [*Tao et al.*, 2007], climate [*Steiner et al.*, 2006; *Tagaris et al.*, 2007], and long range transport [also chemical boundary conditions, see *Avise et al.*, 2009]. In this section, my aim is to find out what the largest contributors are to future ozone changes in UKCA.

5.4.2 The impact of climate change

The upper left of Figure 5.7 shows the effect of climate change only on future average near surface ozone in UKCA. The northeast of the United States, California, the extended region around the Mediterranean, parts of Eurasia, and east Africa all exhibit increases in ozone concentrations between 6 and 12 ppbv. Over the continents, there are colocated increases in OH of up to 70%. A very widespread but lower (2-6 ppbv) increase in ozone is also modelled throughout much of the model domain. Small decreases are modelled throughout the tropics over the oceans, with an area near Greenland and the ITCZ region east of the maritime continent both showing stronger negative signals. The area near Greenland may be linked to colocated decreases in temperature of -2 °C, a response that was also found in *Solomon et al.* [2007b].

The change in ozone resulting from climate change is slightly larger than values reported by *Zeng et al.* [2008] ($\pm$ 10 ppbv) using a similar chemical mechanism, though their results were more heterogeneous spatially. Decreases in ozone throughout the tropics are evident in the work of *Young* [2007] and *Zeng et al.* [2008]. The results in UKCA are closer to those reported in *Hauglustaine et al.* [2005] for 2100, though in UKCA decreases in ozone over the oceans are limited to the tropics rather than the more widespread phenomenon reported in that study. It is worth clarifying that both *Zeng et al.* [2008] and *Hauglustaine et al.* [2005] used future emissions in both the runs with and without climate change, so the photochemical response may not be exactly comparable (the CConly and BASE runs both use present day emissions). In addition, the general increase in global ozone modelled by UKCA is in contrast to the general background decrease in ozone noted by *Liao et al.* [2006] using the GISS model.

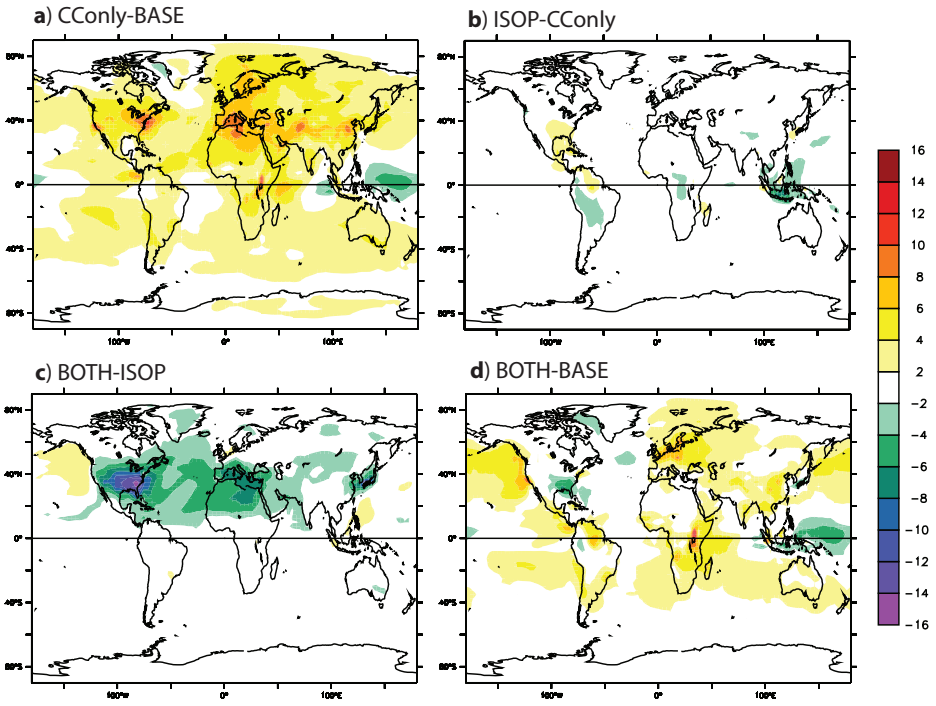

Figure 5.7. Difference in annual average near surface (600 m and below) ozone [ppbv] for the four year model period (2096-2099). a) the difference between CConly and BASE runs, or the impact of climate change; b) the difference between ISOP and CConly runs, or the impact of future biogenic isoprene emissions; c) the difference between the BOTH and ISOP runs, or the impact of future anthropogenic emissions; and d) the difference between BOTH and BASE runs, or the sum of the total impact of emissions and climate.

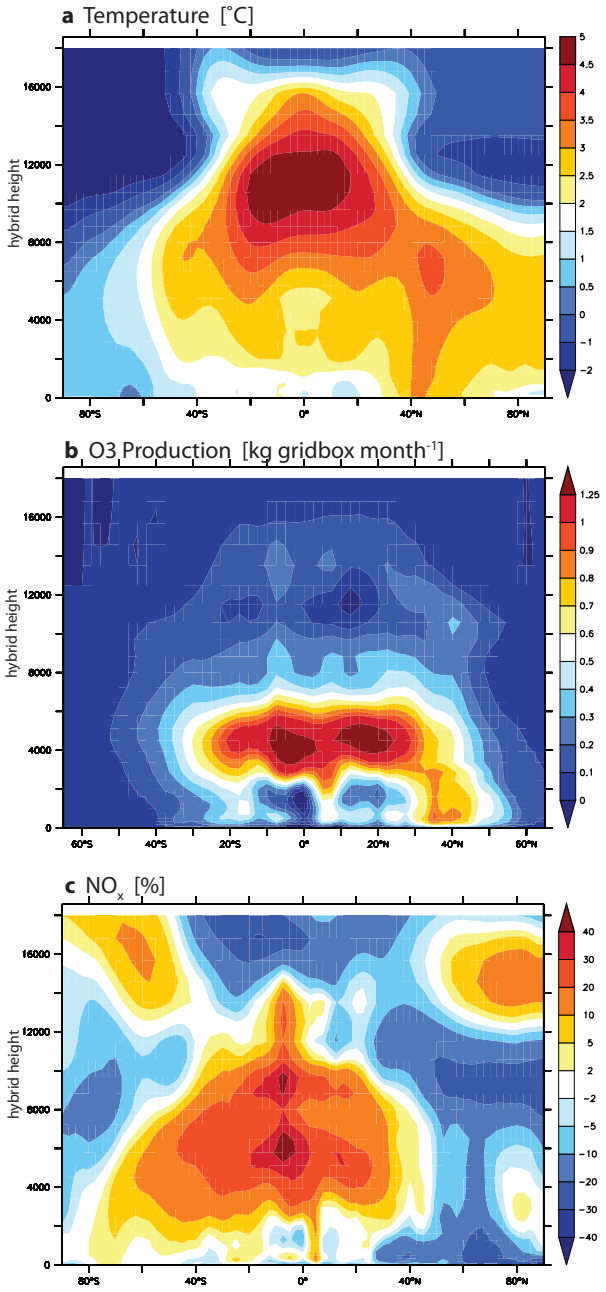

Figure 5.8. Difference in annual average zonal mean a) temperature [°C], b) ozone production [kg O_3 gridbox month^{-1}], and c) NO_x [%] between CConly and BASE runs.

Figure 5.8 shows an example of the type of chemistry-climate interactions described in section 5.1.1. The change in annual average zonal mean temperature is shown in the top panel, showing increases of 2-3.5 °C throughout much of the troposphere, and even higher changes in the upper troposphere (4-5 °C), where greenhouse gases are most effective. The distribution of the change is similar to that reported in *Solomon et al.* [2007b] and *Young* [2007]. At the surface, much of the increases occur over the Artic and over continental regions, the latter due to higher heat capacities and changes in boundary layer humidity and soil moisture [*Joshi et al.*, 2008]. One of the key changes that happens in the free troposphere due to climate change is the increase in ozone production (middle panel of Figure 5.8), which rises by over 1 kg O_3 gridbox month^{-1} around 4000 m. Colocated ozone concentrations increase by 8-14 ppbv, even higher than changes at the surface. One of the contributing factors to increased ozone production in the region is the thermal dissociation of PAN, which releases NO_x into the chemical system (Figure 5.8, bottom panel). NO_x concentrations in much of the free troposphere increase by 5-40 %. PAN concentrations throughout the troposphere decrease between 10% and 50%, and the tropospheric burden drops by 17% on account of climate change.

The impact of climate change on ozone at a regional level has been well studied for both the United States and Europe [e.g. *Liao et al.*, 2006; *Dawson et al.*, 2007; *Meleux et al.*, 2007; *Tagaris et al.*, 2007; *Racherla and Adams*, 2008]. In Figure 5.9, the impact of climate change on four-year average July ozone is shown. The 'ozone season' is defined as a period in which ozone (usually DM8H) can exceed a threshold value such as 75 ppbv [*Chen et al.*, 2009b], and usually occurs between April and September for polluted northern hemisphere sites. July is often taken as a case study month for this period [e.g. *Cox and Chu*, 1996; *Nolte et al.*, 2008]. In UKCA, increases of 2-16 ppbv are modelled over much of this domain; the Mediterranean and Sahara show particularly strong increases, as does the western United States. A decrease of 4-8 ppbv is modelled over the Pacific ocean near

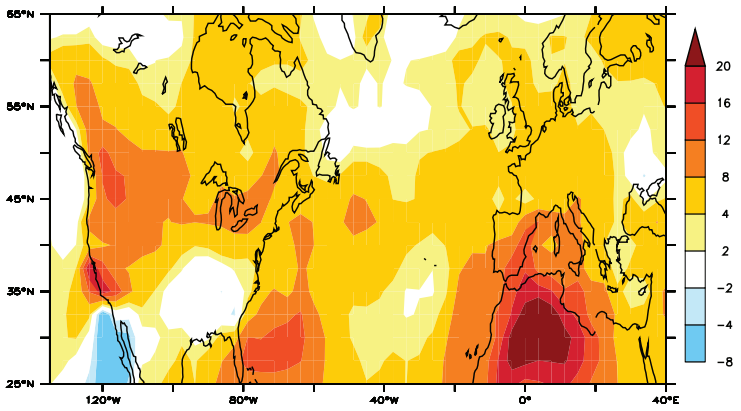

Figure 5.9. Difference in four-year average July ozone [ppbv] between CConly and BASE runs for the United States and Europe (the difference due to climate change).

the Baja peninsula of Mexico. These results compare favorably with the literature. *Lin et al.* [2008] and *Liao et al.* [2006] reported increases in surface ozone over the United States of +3-12 ppbv, and *Hogrefe et al.* [2004] found values of up to 14 ppbv. *Hogrefe et al.* [2004] also reported small decreases in ozone over the southeast US. Over Europe, *Liao et al.* [2006] reported increases of 2-8 ppbv, while *Meleux et al.* [2007] reported values of +8-20 ppbv.

5.4.3 The impact of biogenic isoprene emissions

The upper right panel of Figure 5.7 shows the change in ozone concentrations when future biogenic isoprene emissions are included in calculations. In the southern Amazon, central Africa, and maritime continent regions, future isoprene emissions decrease ozone by 2-4 ppbv. This is due to an increase in ozonolysis and the removal of ozone precursor gases; these regions display similar behaviour when isoprene was incorporated into UKCA (section 3.5.1.2). Two regions show an increase in ozone as a result of increased future isoprene emissions, which are the eastern United States and the northern part of South America. The differences between regions are due to the variation in chemical regime into which isoprene is emitted (see section 3.5.1.3) and the season. Globally, the impact is relatively

small: the PAN burden increases by only 6%, compared with -17% due to climate change, and the CO burden increases by 5%.

The decreases in ozone in the Amazon, central Africa, and the maritime continent are similar to those reported in *Zeng et al.* [2008] of more than 3 ppbv. In their study, ozone concentrations increased throughout much of the northern hemisphere, which was not reproduced by UKCA. Two possible explanations for this divergence are the much higher NO_x emissions used in that study (A2), and perhaps more importantly, the geographically constant scaling factor of 50% applied to all isoprene emissions. Here, vegetation is allowed to vary with climate and thus global isoprene emissions only increase by 17% and have more geographical variability (Figure 5.4).

5.4.4 The impact of anthropogenic emissions

In this scenario, the major polluting regions in North America, Europe, Japan, and the Antipodes are all projected to reduce NO_x emissions dramatically—between 100 and 500 Gg N yr^{-1}. Figure 5.10 shows future NO_x emissions compared to those for the present day. Emissions in developing countries are projected to increase, particularly in Nigeria, Kenya, South Africa, southern Brazil, India, and China.

The influence of anthropogenic emissions on ozone is evaluated from the difference between the BOTH and ISOP simulations (lower left panel of Figure 5.7). The overwhelming impact is the reduction in ozone due to the reduction in precursor emissions in the B2+CLE scenario. The greatest changes are modelled over the southeastern United States, where ozone is reduced by up to 16 ppbv. Relatively large changes (4-8 pbbv) are also modelled over the Mediterranean and east Asia. Slight (2-4 ppbv) increases are modelled in the Pacific in the midlatitudes. This response was relatively robust to the level of isoprene emissions. Using present day isoprene emissions (ANTH-CConly, not shown), the distribution of ozone reductions was very similar, although the absolute value of the change

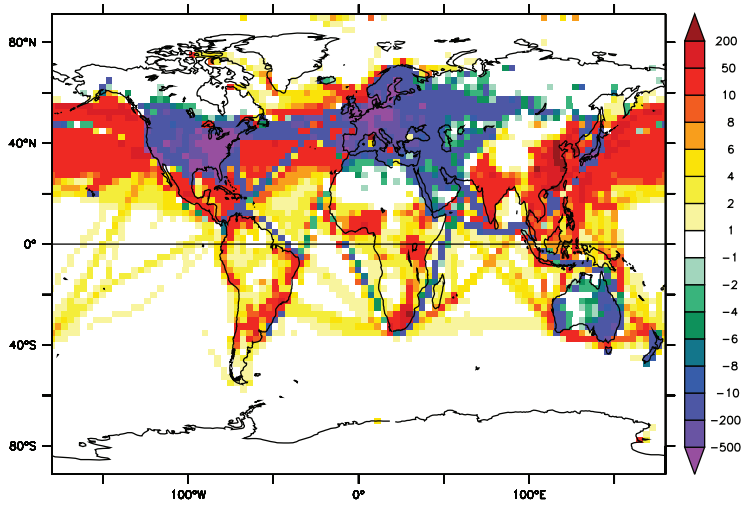

Figure 5.10. Change in annual average surface NO_2 emissions [Gg N yr^{-1}] between future (B2+CLE) and present day emissions.

was approximately 4 ppbv lower throughout the domain. This result demonstrates that reductions of anthropogenic emissions, as projected by the B2+CLE scenario, are an effective way to reduce future surface ozone, and that reductions are not dependent on the isoprene emission scenario. In fact, future isoprene emissions only increase the importance of NO_x reductions.

Precursor emissions have been previously shown to be an important factor in controlling future ozone concentrations. Simulations with low emissions, particularly for NO_x, have generally shown decreases in ozone [e.g. *Szopa et al.*, 2006]. In contrast, high levels of emissions generally lead to higher future ozone concentrations [e.g. *Wu et al.*, 2008b; *Zeng et al.*, 2008]. The reduction in surface ozone due to the B2+CLE emissions was also shown in the results of *Fowler et al.* [2008], which used a mean of five model simulations. The results were presented for each season, and the greatest reductions were modelled in spring (MAM) and summer (JJA). Smaller reductions (2-4 ppbv) were apparent in fall (SON) and winter (DJF). In winter, however, *Fowler et al.* [2008] reported slight increases over the United States and Europe (between 2-8 ppbv). Similar (2-10 ppbv) increases were mod-

elled by UKCA. In summary, the results of UCKA match well with the reported multi-model means in *Fowler et al.* [2008].

5.4.5 The combined impacts

In the lower right panel of Figure 5.7, the combined effect of anthropogenic emissions, biogenic emissions, and climate change is shown. The total change in ozone is quasi-linear when considered in comparison to the impact of each of the individual variables. Much of the globe retains low to mid level increases (2-6 ppbv) in ozone due to the physical climate change forcings, and the low levels and reductions of ozone across the tropical oceans are also present. Over western South America, the impact of biogenic emissions cancels out the increase due to climate change, so no change is modelled. Even more dramatically, the reductions in ozone due to anthropogenic emissions across North America, the Mediterranean, and parts of Eurasia negate the impact of climate change. In the southeastern United States this even leads to a decrease in ozone in the BOTH simulation compared with the BASE case (-2 to -6 ppbv).

For simplicity, and to eliminate differences due to seasonal variability of emissions and climate change, changes in ozone presented thus far have been temporally averaged over the study period. Figure 5.11 shows the seasonal variation for the total future impact (all emissions and climate) compared with the BASE run. In January, UKCA models an increase in ozone throughout much of the northern hemisphere. The decrease in ozone east of the maritime continent is strong in this season. The signal throughout the rest of tropics is heterogenous, and little change is modelled through the southern hemisphere. It seems that climate change forcings are the dominant cause of changes in ozone concentrations in this season. In July, the polluted regions of North America, Europe, southeast Asia, and east Asia show a decrease in surface ozone between the BASE and BOTH simulations. Reductions in anthropogenic precursor emissions appear to be the strongest cause for changes in ozone in the summer. In both seasons, ozone reductions over the

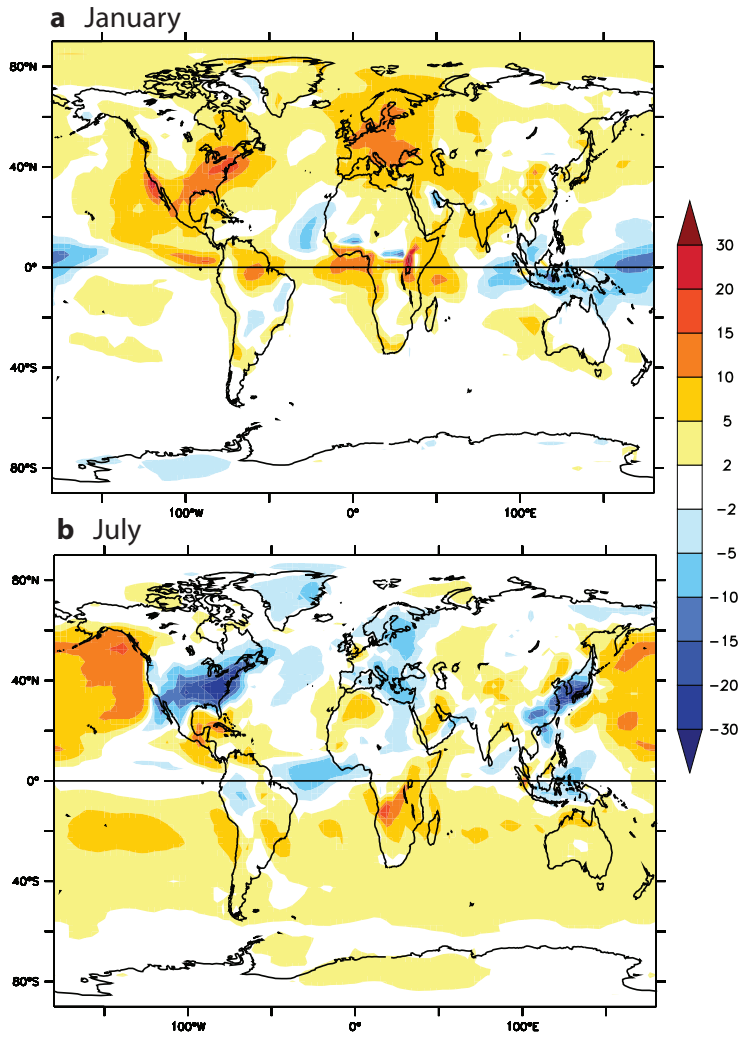

Figure 5.11. Change in near-surface (up to 600 m) ozone concentrations [ppbv] between BOTH (2096-2099) and BASE (2001-2005) simulations for a) January, and b) July.

tropical oceans are evident, presumably due to climate change.

As modelled by UKCA, climate change has the most widespread impact, while anthropogenic emissions have the largest and most acute impact on future surface ozone. Biogenic emissions, on the other hand, play a much smaller role. In terms of policy relevance, the results from UKCA support reductions in anthropogenic ozone precursor emissions as a way to improve future air quality. In fact, the

reductions are concentrated in the summer months (the ozone season), when they are most warranted.

5.4.6 The future tropospheric ozone budget

Table 5.3 shows the ozone budgets for the attribution experiments. The budget of the BASE integration has been discussed in section 3.5.1.1. The budget changes markedly in the CConly simulation, such that production increases by 16%, loss increases by 20%, and deposition rises by 9%. These are very similar to the numbers reported by *Zeng and Pyle* [2003] of 11%, 21%, and 10% respectively, in which a predecessor mechanism (albeit without isoprene chemistry) was employed. Similar values have also been reported by a number of other studies [*Stevenson et al.*, 2000; *Hauglustaine et al.*, 2005; *Liao et al.*, 2006, as summarized in *Wu et al.* [2008a]].

Table 5.3. Ozone budgets from emissions and climate change attribution experiments. Production, loss, and are in [Tg O_3 yr^{-1}], ozone lifetime is in days, and ozone burden is given in Tg. All values are for the troposphere below the chemical tropopause (150 ppbv) defined in *Stevenson et al.* [2006].

Experiment	Prod.	Loss	Dep.	O_3 τ	O_3 Burden
BASE	3215	2813	795	31.6	317
CConly	3728	3367	868	29.1	343
ISOP	3717	3350	865	28.8	338
ANTH	3607	3287	842	29.4	337
BOTH	3572	3255	837	29.1	331

In UKCA, the ozone lifetime decreased by 8% while the global burden increased by 8% as a result of climate change. In the survey of *Wu et al.* [2008a], ozone lifetime decreased by 10-18% (summarized from four studies), similar to my results. The direction of change in the ozone burden was not consistent between the same four model studies, with values of between -12 and +5% reported, indicating that the complex relationship between ozone and climate can lead to changes in both directions depending on model parameterizations [*Wu et al.*, 2008a]. The

ozone burden remained relatively constant throughout the future model studies. Future isoprene emissions negligibly reduced both ozone production (11 Tg, 0.3%) and loss (17 Tg, 0.5%) compared to the run with only climate change, similar to the low change in surface ozone. In contrast, future anthropogenic emissions reduced ozone production and loss (121 Tg, 3.2% and 80 Tg and 2.4%, respectively). The BOTH run had the lowest levels of ozone production and loss of any of the model simulations set in the future.

5.5 Future land use change: Phase I of the biofuel life cycle

It has been shown that cropland expansion, which could be associated with an increased growth of biofuel feedstocks, could reduce future isoprene emissions (section 5.3.0.2). It has also been shown in sections 3.5 and 5.4.3 that isoprene emissions can influence tropospheric chemistry. In this section, I examine how reduced isoprene emissions from land use change could impact atmospheric chemistry in the future.

5.5.1 Ozone

To the best of my knowledge, the impact of anthropogenic land use change on atmospheric chemistry at a global scale has not previously been studied.

Figure 5.12 shows that future cropland expansion (Figures 5.5 and 5.6) leads to an increase in regional ozone of up to 50% (over 10 ppbv in hotspot regions) in the FutCROPS simulation compared with the BOTH simulation. In January, the largest changes are modelled over the Amazon, the tropical Atlantic, and the tropical Pacific. Over the Amazon, dramatic reductions in isoprene flux due to cropland expansion generate elevated ozone concentrations by both reducing isoprene ozonolysis and reducing NO_x sequestration which forms organic nitrate species. As a result of the latter, NO_x concentrations rise by 150% over the Amazon. The strong

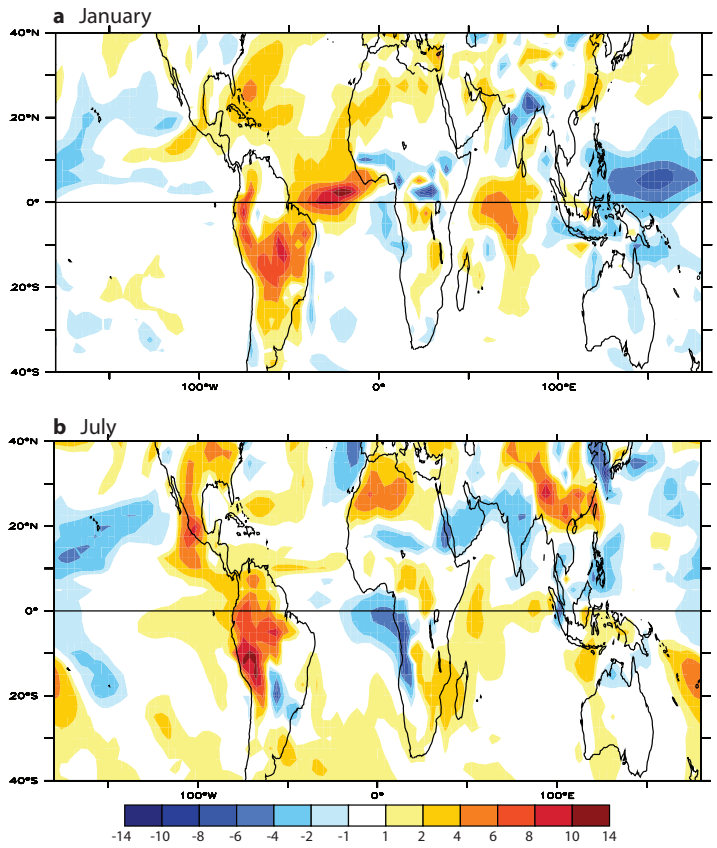

Figure 5.12. Change in near-surface (averaged up to 600 m) ozone concentrations [ppbv] between BOTH and FutCROPS (2096-2099) for a) January, and b) July.

link between isoprene chemistry and nitrate species is demonstrated by the signal over the tropical oceans, where changes in PAN concentrations lead to changes in NO_x concentrations of -30% over the Pacific and +50% over the Atlantic.

In July, with the peak growing and emitting season in the northern hemisphere, the terrestrial ozone signal shifts northwards. Large ozone changes (over 8 ppbv) are modelled over North America, the Mediterranean, China, and the Amazon. The shape of the impact in ozone over the Amazon correlates spatially with changes in emission of isoprene due to crops. Over North America and China, where isoprene emissions decrease with anthropogenic land use change, regional NO_x concentrations increase by 40% and 90%, respectively, leading to higher ozone concentra-

tions. The signal over Northern Africa is linked to elevated ozone concentrations in the Mediterranean, again via the formation and transport of nitrate species such as PAN.

Both *Wiedinmyer et al.* [2006] and *Chen et al.* [2009a] reported decreases in ozone over the United States as a result of allowing land use change to reduce biogenic isoprene emissions. The present day emissions in *Wiedinmyer et al.* [2006] and the A2 emissions in *Chen et al.* [2009a] both have higher NO_x emissions than the B2+CLE scenario, perhaps explaining the divergence in our results. High NO_x emissions would lead to a VOC-sensitive chemical regime, and thus a reduction in VOC would lead to a reduction in ozone. *Wiedinmyer et al.* [2006] reported increases in ozone over the Amazon (+3-5 ppbv) on account of land use, which are also modelled by UKCA. *Avise et al.* [2009] found very small increases in ozone resulting from land use change. From these studies, it seems that the change in ozone resulting from land use change is both model and scenario specific for polluted regions such as the United States, but that the response in VOC-rich regions may be more robust. Keeping in mind that these studies are just sensitivities, it seems most appropriate to propose that large scale land use change throughout the high isoprene emitting regions of the tropics will be detrimental to air quality, but that the effect on the northern hemisphere is more likely to be scenario dependent.

The change in chemical ozone production between the FutCROPS and BOTH runs is shown in Figure 5.13. In this image it becomes apparent that ozone production increases directly over the regions of perturbation to isoprene. Part of this increase in ozone can be explained by a reduction in NO_z which occurs in the same regions (NO_z = all nitrogen containing compounds - NO_x), which is also shown in Figure 5.13. The decrease in isoprene due to cropland expansion decreases the formation of NO_z, and ozone production rises in these areas (most of which are NO_x-sensitive).

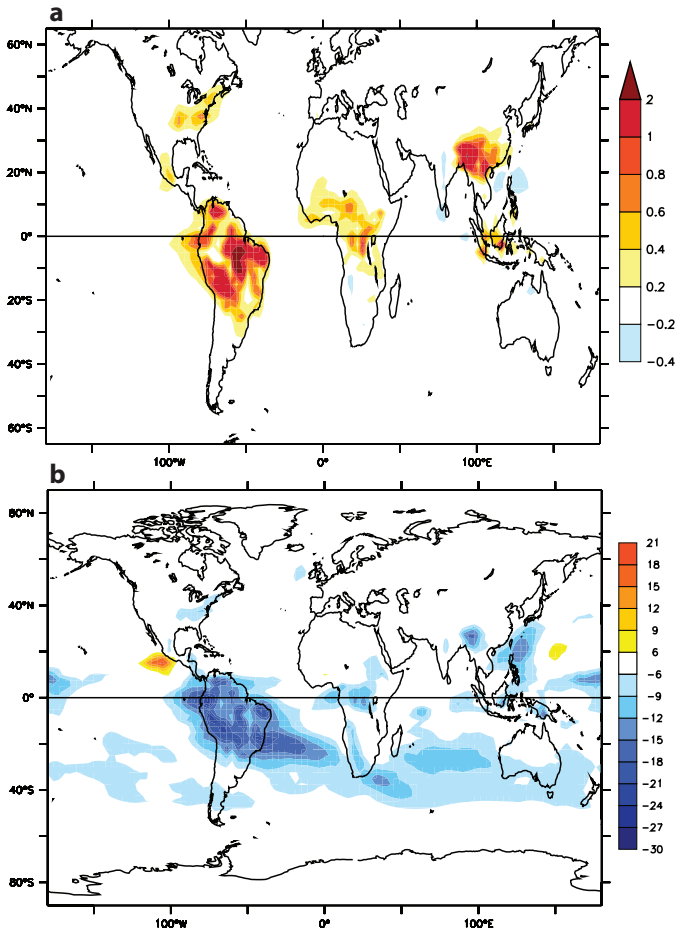

Figure 5.13. Difference in annual average a) chemical ozone production [kg O_3 gridbox month^{-1}] and b) column NO_z [%] between the FutCROPS and BOTH simulations.

5.5.2 Crops: exposure to ozone

In these simulations, the inclusion of anthropogenic land use change leads to increases in ozone over the very areas where cropland is projected to expand in the future. Ozone has been found to be damaging to crops [*Hayes et al.*, 2007; *Mills et al.*, 2007; *van Dingenen et al.*, 2009], whose productivity has been shown to decline after prolonged exposure to ozone concentrations above 35 ppbv [*Long et al.*, 2005], and the geographical area exposed to this concentration increases in the model when land use change is included. Figure 5.14 shows the change in the

number of months that a gridbox is exposed to monthly mean ozone concentrations above 35 ppbv for an average model year between the FutCrops and BOTH runs. Zero values indicate gridboxes that were either exposed to mixing ratios of ozone greater than 35 ppbv for the same number of months, or which never attain ozone values of that level. Three regions show a marked increase in the duration of exposure: the southern and eastern United States, Southeast Asia, and the Amazon. These are precisely the three regions in which cropland is predicted to expand and where exposure to ozone has the greatest potential to reduce the productivity of crops. It should be noted that the monthly mean output of a global model is not equal to the maximum ozone or to the DM8H values; still, these results suggest a positive ozone feedback loop.

This potential feedback loop between crop expansion, ozone elevation, and crop health and productivity is robust to the inclusion of CO_2 suppression, as shown in the bottom panel of Figure 5.14. Even with the inclusion of CO_2 suppression in the model, in which the total global isoprene flux is 41% lower, the three regions in which land use markedly reduces isoprene emissions (southeastern United States, southeast Asia, and the Amazon) show up to 3 months increase in exposure to ozone above 35 ppbv. With CO_2 suppression included, over the United States and southeast Asia the maxima of the responses are elevated, though in the United States the spatial extent is slightly smaller. In the Amazon, though the change is still evident, the total change in exposure is lower. Africa shows a more widely distributed response to land use change when CO_2 suppression is accounted for versus when it is not.

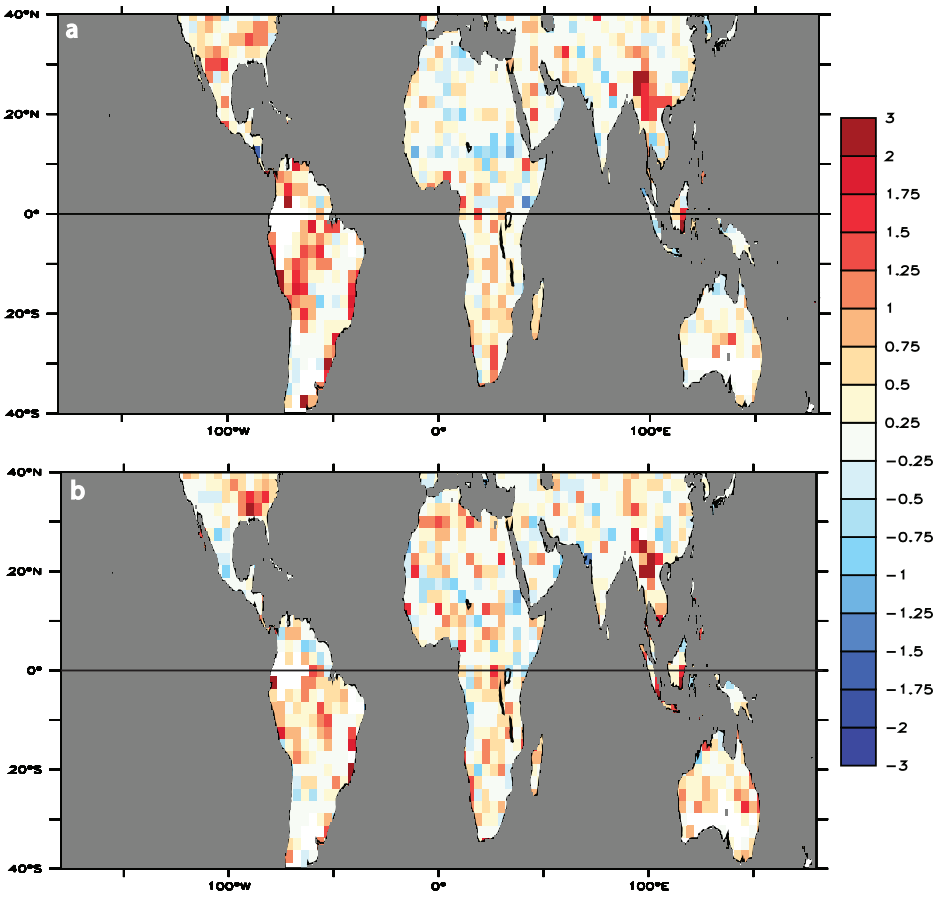

Figure 5.14. Increase in the number of months a gridbox experiences surface ozone above 35 ppbv in an average model year as a result of land use change. a) difference between FutCROPS and BOTH simulations (without CO_2 suppression) and (b) difference between FutCROPS_CO2 and BOTH_CO2 (with CO_2 suppression).

5.6 How does land use change compare to CO_2 suppression of isoprene emission?

As CO_2 rises in a potential future atmosphere, another possible impact on isoprene is CO_2 suppression of its emission. *Arneth et al.* [2007a] and *Heald et al.* [2009] both found that the suppression was enough to offset CO_2 fertilization and temperature induced increases in emission that have been predicted elsewhere (see e.g. *Lathière et al.* [2005]; *Tao and Jain* [2005]; *Guenther et al.* [2006]). *Heald et al.* [2009] found that CO_2 suppression reduced isoprene emissions by 217 Tg yr^{-1} when vegetation was kept fixed, while emissions dropped by 610 Tg yr^{-1} when vegetation was dynamic. Using the parameterizations described in *Arneth et al.* [2007a], *Arneth et al.* [2007b] reported reductions in future (2081-2100) isoprene emission estimates of 930-990 Tg C yr^{-1} for the A2 scenario and 450-480 Tg C yr^{-1} for the B1 scenario for European forests. *Young et al.* [2009] assessed the potential that CO_2 suppression of isoprene emission could have on the oxidizing capacity of the troposphere by using the UM_CAM model, a predecessor to UKCA. They found that CO_2 suppression of isoprene emission impacted surface ozone concentrations by up to 10 ppbv over terrestrial emission regions, though it reduced ozone in Europe, east Asia, and the Indian ocean.

The response of the Sheffield Dynamic Global Vegetation model showed a slightly larger decrease in isoprene resulting from CO_2 suppression than for land use change (Figure 5.3). In this section I compare the two effects on atmospheric chemistry.

5.6.1 Land use and CO_2 suppression: ozone

In order to compare the impact on the oxidizing capacity of the atmosphere from CO_2 suppression and future land use change, the differences in average near-surface ozone from the four matrix experiments are shown in Figure 5.15. The top two panels display the difference in ozone as caused by land use change both

with and without CO_2 suppression. Without CO_2 suppression (top panel), the change in ozone concentrations is the most marked of any of the experiments, with particularly strong increases appearing over the Amazon of over 6 ppbv. Smaller terrestrial differences come through over southeast Asia and central and northern Africa, though these are on a similar level (less than 2 ppbv) to the change modelled over parts of the Pacific and Atlantic oceans. The change over the maritime continent is mixed, ranging between -2 and 4 ppbv. A similar profile occurs when land use change is studied with CO_2 suppression included (second panel of Figure 5.15). Again, the Amazon shows the highest levels of change in ozone concentrations (up to 6 ppbv). The differences in equatorial Africa and the southeastern United States are slightly lower than without CO_2 suppression. The change in southeast Asia remains on a similar scale as it was before.

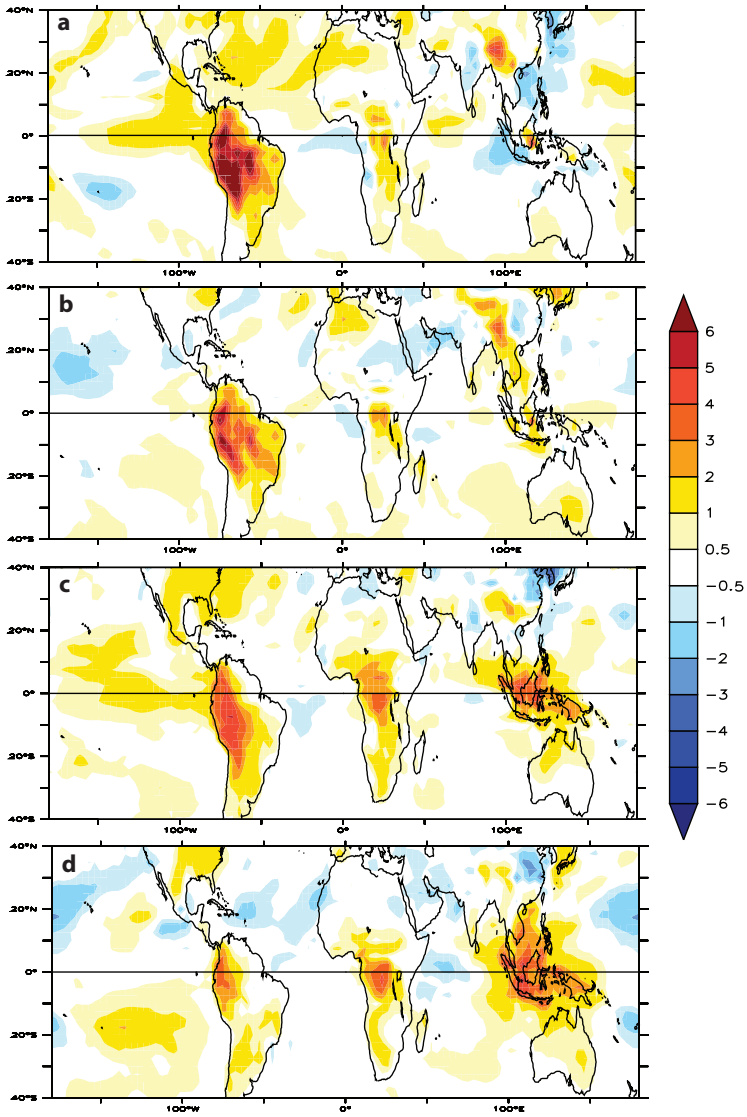

Figure 5.15. Annual average change in near surface (0-600 m average) ozone [ppbv] over the four year model period 2096-2099 for a) the difference from crops without CO_2 suppression (FutCROPS-BOTH), b) the difference from crops with CO_2 suppression (FutCrops_CO2-BOTH_CO2), c) the difference from CO_2 suppression with present day crops (BOTH_CO2-BOTH), and d) the difference from CO_2 suppression with future crops (FutCrops_CO2-FutCROPS).

In contrast, the impact of CO_2 suppression when crops are kept to their present day geographic area (Figure 5.15, third panel) shows less drastic changes in ozone with a wider spatial extent than changes from land use. All four hot-spot emitting regions (southeastern United States, the Amazon, central Africa, and southeast Asia) display ozone change on the order of 1-4 ppbv as a result of CO_2 suppression. In many ways, this is to be expected: the changes occurring from land use change are spatially heterogeneous and will effect different areas with variable levels of intensity. CO_2 suppression, on the other hand, is applied to all emissions with a simple empirical relationship (described in section 2.2.2.2). Finally, the change in ozone from CO_2 suppression when crops are held at future values is shown in the bottom panel. Again, the four hot-spot regions appear with increases in average ozone concentrations. The maritime continent reveals the strongest signal, while the signal from the Amazon is almost negligible compared to land use change. Since the future land use scenario predicts notable increases in cropland in the Amazon, the number of gridboxes which emit isoprene in the region has already been reduced significantly. Thus the potential reduction in emissions due to CO_2 suppression is fractionally much smaller.

For all the studies, the change in annual average ozone is higher than the ozone attibuted to biogenic isoprene emissions in Figure 5.7. The change in isoprene resulting from land use change and CO_2 suppression is also higher (section 5.3), explaining some degree of the difference in magnitude. An additional contributing factor to the acute increase in ozone modelled due to land use change would be deposition. One weakness of my experiments is that the land surface type in UKCA remains constant throughout the model study, so deposition is not altered while isoprene emissions are. Cropland expansion would likely *decrease* deposition, as the UKCA deposition velocity for shrubs is 23% lower than for forests, which would further exacerbate the acute response of surface ozone. This feedback would not exist for CO_2 suppression, for which the surface characteristics would not change.

5.6.2 Land use and CO_2 suppression: HO_x

The impact of both CO_2 suppression and land use change on the oxidizing capacity of the atmosphere is also significant for the concentration of OH and its role in the HO_x cycle. Figure 5.16 shows the change in the HO_2:OH ratio, which has been shown to be a good indicator for HO_x cycling [e.g. *Ren et al.*, 2008]. Here, as with ozone, the difference in OH between land use change (upper panel) and CO_2 suppression (lower panel) does not change much with the variation in the other variable. Because the change in the ratio of HO_2 to OH is very similar for both the land use experiments (with and without CO_2 suppression) and the CO_2 suppression experiments (with present and future crops), only one example for each variable is shown in Figure 5.16.

The maximum impact of land use change on the ratio of HO_2 to OH in modelled over the Amazon, where the change is greater than -90%. This arises largely because the sink of OH via reaction with isoprene is lower with lower isoprene emissions. Lower isoprene emissions will also decrease the amount of HO_2 in the system, as the recycling of HO_2 is more effective with NO than O_3 (see section 3.5.2.1). Isoprene is therefore altering both the numerator and denominator of this ratio through direct (reaction with OH) and indirect (altering the O_3 and NO concentrations in the region) means. Three other regions show decreases in the percentage HO_2 to OH ratio: the southeastern United States, southeast Asia, and central Africa. None are as large as the impact over the Amazon. In contrast, CO_2 suppression has a much more widespread impact on the HO_x family and the decreases are lower in magnitude. In general, the ratio decreases by less than 60%, but it does so across all the four key emitting regions. The increase in OH concentrations as a result of CO_2 suppression has been reported elsewhere [*Young et al.*, 2009].

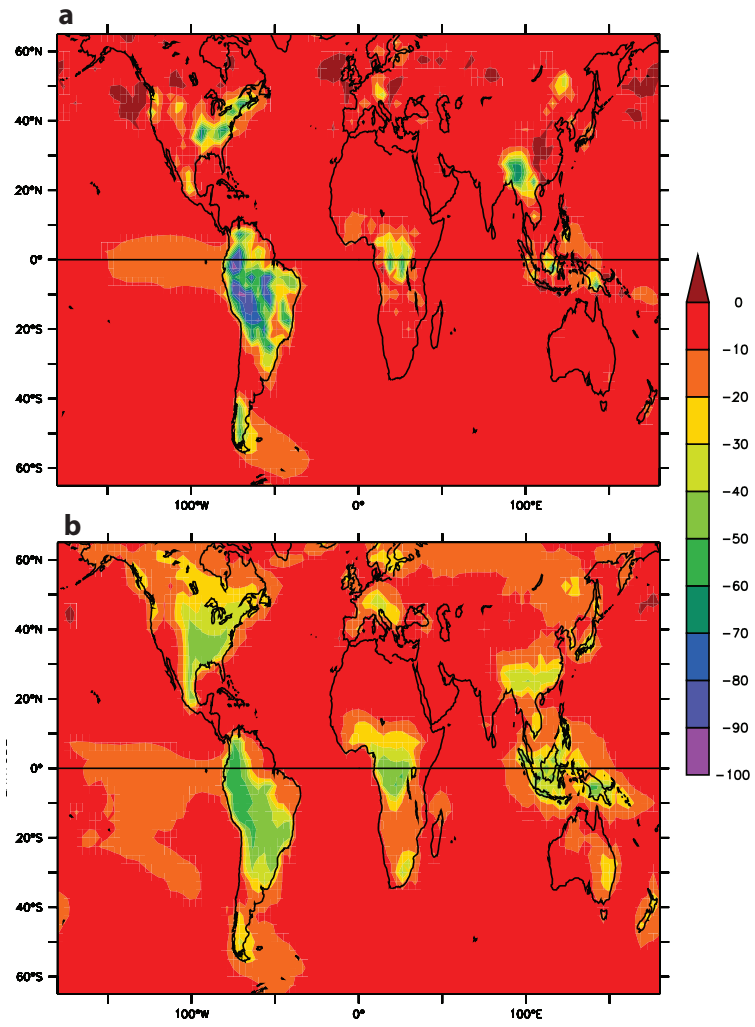

Figure 5.16. Average monthly change [%] in the HO_2:OH ratio over the four year model period 2096-2099 in the troposphere up to 5000 m for (a) FutCROPS-BOTH, or the difference from crops without CO_2 suppresion, and (b) BOTH_CO2-BOTH the difference from CO_2 suppression with present day crops.

5.6.3 Land use and CO_2 suppression: budgets

Although the changes in regional ozone concentrations resulting from land use change and CO_2 suppression can be marked, the global impact on the budget seems to have a rather smaller effect. The production of ozone increases by a maximum of 54 Tg yr^{-1} (1.5%) when both crops and CO_2 suppression and included

Table 5.4. Ozone budgets as a result of CO_2 suppression and land use change. All values are averaged from four model years (2096-2099) and averaged for the troposphere using the chemical tropopause defined in *Stevenson et al.* [2006]. Production, loss, and deposition are in [Tg O_3 yr^{-1}], ozone lifetime is in days, and the burden is given in Tg.

Experiment	Prod.	Loss	Dep.	O_3 τ	O_3 Burden
BOTH	3572	3255	837	29.1	331
FutCROPS	3586	3255	850	30.0	338
FutCROPS_CO2	3626	3281	854	30.0	344
BOTH_CO2	3587	3261	845	29.7	339

(FutCROPS_CO2 minus BOTH). The ozone burden is nearly identical for all four of the runs that include either land use change or CO_2 suppression. For the BOTH (with the highest isoprene) integration the ozone lifetime is the shortest of the matrix, at 29.1 days. The ozone lifetime and burden are largest for the run with the lowest amount of isoprene emission (FutCROPS_CO2), indicating that the global impact of isoprene in these experiments is to reduce total tropospheric ozone. This is supported by both the surface ozone distributions (Figure 5.15) and the exposure values (Figure 5.14); in both cases, reducing isoprene emission increased ozone.

Young et al. [2009] reported that CO_2 suppression accounted for a reduction in ozone production, while here we show an increase. A likely reasons for this divergence is the difference in anthropogenic emissions used; their study employed the SRES A2 scenario, a pessimistic scenario with large increases in NO_x emission compared to present day. With over three times (331% more, 124.1 Tg N yr^{-1}) more NO_x in the system, it is likely that ozone production is limited instead by VOC, such that a reduction in VOC due to CO_2 suppression will reduce ozone production. In this work, much lower NO_x emissions are employed, and the production of ozone is more likely NO_x-sensitive.

5.6.4 Land use and CO_2 suppression: reaction fluxes

The inverse relationship between isoprene emission and ozone concentrations in UKCA is driven by both direct and indirect means. The relative significance of the two can be described by the annual flux through key reactions, as shown in Table 5.5, which demonstrates that changes in ozonolysis (direct) are nearly equal to changes in the formation of NO_2 (indirect) from VOC oxidation. The average impact of land use is to reduce the ozonolysis flux by 42% per year, while CO_2 suppression leads to an average -53% change in the flux. The impact on NO_2 regeneration is lower; land use change changes the flux by -11% per year, while CO_2 suppression accounts for a 13% reduction.

Table 5.5. Annual average fluxes for four experiments involving CO_2 suppression and land change given in [Tg O_3 yr^{-1}].

Flux	BOTH	FutCROPS	FutCROPS_CO2	BOTH_CO2
RO_2 + NO	342	305	264	295
Ozonolysis	93	53	25	43

The correlation of the total flux through these reactions with the change in isoprene emission also gives some indication of the strength of their chemical relationship. Using all four experiments, the slope of the correlation between total ozonolysis flux and global isoprene emission is 0.23 (with an R^2 value of .997), while the relationship is 0.26 (R^2 of .989) for the recycling of NO. These slopes are remarkably similar. From the basis of these two reactions only, it would be difficult to predict a positive or negative change in ozone. However, besides ozonolysis, another loss process for NO_x (which reduces ozone production) is the formation of reservoir species such as PAN or isoprene nitrates. When this is considered in conjunction with the the fluxes above, it becomes evident that the globally averaged effect of increasing isoprene emissions in UKCA is to increase ozone loss, for which chemical recycling of NO_2 does not compensate. This result is in agreement with the budgets, and with the surface ozone concentrations.

5.6.5 Uncertainties

There is a range of uncertainty associated with this type of study. The extent of future land use change depends on the model and scenario [*Alo and Wang*, 2008]. Auxiliary changes would inevitably accompany a large scale change in land use, including biogenic [*Yienger and Levy II*, 1995] and fertilizer [*Bouwman et al.*, 2002] nitrogen emissions [*Vitousek et al.*, 1997b] and surface climate and radiation impacts [*Georgescu et al.*, 2009; *Pongratz et al.*, 2009]. The scientific understanding of the impact of land use change on climate is not robust, as past land cover change has not been shown to have a common or singular effect in models, but rather that the response depends on the parameterizations and assumptions in the a model physics [*Pitman et al.*, 2009]. Future climate change will also have impact on the terrestrial carbon cycle, though the extent and direction of the flux is also still uncertain [*Arora and Matthews*, 2009]. In addition, there are multiple scenarios which describe different levels of population growth, economic decisions [*Nakicenovic et al.*, 2000; *Fowler et al.*, 2008], and climate forcing, which impacts the anthropogenic influence on the landscape [*Alo and Wang*, 2008; *Lapola et al.*, 2009].

5.7 Summary

In this chapter I have described a series of eight experiments designed to both attribute ozone in the future as well as test the sensitivity of the model to CO_2 suppression and land use change as they impact isoprene emissions. In the first set of experiments, I used a serial methodology to attribute certain changes in future ozone, as calculated by UKCA, to climate change, anthropogenic (B2+CLE), or future biogenic emissions. The future run which included all variables was quasi-linear in response to the sum of the variables versus the integrations in which each perturbation was tested individually. I found that the largest and most widespread positive changes in future surface ozone arose from physical climate change forc-

ings, and that the largest negative changes were linked to reductions in anthropogenic emissions. Biogenic isoprene emissions did not have that much of an impact.

In the second set of experiments, I focused on the impact of land use change and CO_2 suppression on isoprene emissions and the resulting change in tropospheric chemistry. Land use change, which could be associated with large scale growth of biofuel feedstocks, increased ozone production over key hot-spot emitting regions. I found that there could be a feedback loop between land use change, reduced isoprene emissions, and increased ozone; in these areas exposure to high levels of ozone could reduce crop productivity, a potentially significant impact on the agricultural cycle and the production of biofuel feedstocks. In the comparison between land use change and CO_2 suppression, I found that land use change had a more acute effect on ozone and HO_x, and that the impact from CO_2 suppression was more widespread. Despite these regional differences, the change in global budget numbers was relatively small between the experiments.

In the next chapter, I examine the final phase of the biofuel life cycle.

Chapter 6

Phase III: Combustion

In this chapter, I turn to the final phase of the biofuel life cycle: combustion. I present a set of four experiments which focus on tailpipe emissions from biofuels and their potential impact on tropospheric chemistry. In section 6.2 I describe the experimental methodology, and then I examine the BASE scenario using a chemical sensitivity indicator in section 6.3. I look at the change in ozone resulting from a shift to biofuels in section 6.4, and break the response down into both a linear and nonlinear component.

6.1 Introduction

Emissions from transportation comprise a large fraction of total anthropogenic emissions worldwide. Because transportation emissions are emitted from mobile sources, the spatial distribution is wider than that of other sectors, such as power generation or industry. It is also the largest growing sector for end use of oil, growing by 1146.47 Mtoe [Million tonnes of oil equivalent] (106%) in OECD countries and 584.4 Mtoe (82%) globally between 1973 and 2006 [*International Energy Agency*, 2008]. This growth is expected to continue at a significant rate [*International Energy Agency*, 2007]. Because of its wide spatial distribution, complex emissions, and projected growth, transportation is particularly important to study

in order to understand future changes in the troposphere.

6.1.1 Impact on the atmosphere

The transport sector has been shown to impact the radiative balance of Earth's atmosphere. *Fuglestvedt et al.* [2008] found that the transport sector has contributed 15% of CO_2 radiative forcing and 31% of tropospheric ozone forcing since preindustrial times. For the present day, *Niemeier et al.* [2006] reported that 30 mW m^{-2} in January and 50 mW m^{-2} in July of radiative forcing could be attributed to ozone caused by emissions from road transport. In the future, the radiative forcing impact due transport could change due to changing emissions. *Shindell et al.* [2008] found a 30% reduction in road transport emissions resulted in a change of -21 mW m^{-2} in RF resulting from CO_2 and -5 mW m^{-2} due to O_3. *Unger et al.* [2009] reported that a 50% reduction of road transport emissions resulted in a -19 mW m^{-2} shift in radiative forcing, but when the reduction was applied in the United States only, it resulted in a change of only -5 mW m^{-2}.

In addition to impacting the climate system, road transport has a profound impact on air quality and tropospheric chemistry. *Niemeier et al.* [2006] found that road transport accounted for up to 10-50 ppbv ozone in polluted regions in July. For the same month, *Matthes et al.* [2007] reported that road traffic accounted for over 15% of surface ozone, particularly over North America and Europe. *Castellanos et al.* [2009] found that instead of diurnal variation, temporally uniform emissions from mobile sources led to a reduction in the number of days with DM8H ozone exceeding 80 ppbv.

Changes in the emissions from transportation can also lead to changes in air quality and atmospheric chemistry. *Hoor et al.* [2009] found that for a 5% reduction in all transport emissions, ozone increased in an average of five models. Individual sector reductions showed that reducing emissions from road transport (instead of from shipping or aviation) had the largest acute effect on ozone. Shipping had a more widespread impact, as the global average change in ozone re-

sulting from a 5% decrease in ship emissions was 0.06 ppbv, while for road it was 0.0435 ppbv, and for aircraft was 0.015 ppbv. When *Niemeier et al.* [2006] scaled global road transport emissions to European levels (representing a growth in transport in the developing world), ozone increased by 5-40 ppbv, with particularly strong changes in southern and eastern Asia. When the scale was adopted for North American road transport emissions (representing even higher growth) ozone increased by 10-100 ppbv, again with the strongest response in southern and eastern Asia. Finally, *Bell and Ellis* [2004] found that when road transport emissions were increased, the average increase in summertime hourly max ozone went up by 9 ppbv in urban locations and 6 ppbv in rural locations in the eastern United States.

6.1.2 Biofuel emissions from the tailpipe

The impact of the transportation sector on climate and air quality would be modified by the use of non-conventional fuels, which have a different emissions profile than their conventional analogues. One potential alternative liquid fuel for transport, biodiesel, emits higher NO_x and lower CO and hydrocarbons than conventional diesel. Elevated NO_x emissions have been linked to both the level of unsaturation of biodiesel fuel molecules [*McCormick et al.*, 2001; *Fernando et al.*, 2006; *Knothe et al.*, 2006; *Ban-Weiss et al.*, 2007] and to the advance timing of fuel injection [*Monyem and H. Van Gerpen*, 2001; *Szybist et al.*, 2005, 2007]. Unsaturated molecules have a slightly higher flame temperature, encouraging NO_x formation in the piston [*Ban-Weiss et al.*, 2007]. The change in injection timing in a compression-ignition engine leads to a longer time period in which the temperatures are high enough to form thermal NO_x (section 1.4.3) before the reactions are quenched by expansion of the piston [*Szybist et al.*, 2007]. The advance in timing has been attributed to lower compressibility of biodiesel in comparison to diesel [*Lapuerta et al.*, 2008]. Biodiesel is also an oxygenated fuel, and therefore combustion in a compression-ignition engine will be more complete, reducing both the unburnt hydrocarbon and CO emissions [*Agarwal*, 2007]. This level of comple-

tion in the combustion chamber is a contributing factor to the higher temperatures which are conducive to NO_x formation [*Agarwal*, 2007].

For ethanol, the comparison to conventional gasoline emissions profile is different. VOC emissions are much higher for ethanol, a fuel with a higher vapour pressure than conventional fuel [*Koc et al.*, 2009]. Evaporative emissions therefore rise [*Huo et al.*, 2009]. Cracking of ethanol leads to the production of acetaldehyde [*Gaffney and Marley*, 2009], the emissions of which have been shown to be much higher for vehicles run with higher percentages of ethanol [*Graham et al.*, 2008]. CO emissions are slightly elevated for ethanol, and are controlled by the flammability and oxygenation of the fuel [*Koc et al.*, 2009]. NO_x emissions depend on peak temperatures achieved in the spark-ignition engine during combustion. Because the latent heat of vaporization is higher for ethanol than conventional gasoline, the flame temperature is lowered, which in turn leads to reduced NO_x emissions [*Koc et al.*, 2009]. In general, ethanol is mixed with a small fraction of gasoline (commonly 15%) to allow for fuel ignition in the engine on cold days [*Sustainable biofuels: prospects and challenges*, 2008].

These changes in tailpipe emissions resulting from the combustion of biofuels (either for ethanol or biodiesel) have the potential to alter emissions from the transport sector. As described above, surface transport has already been shown to influence both tropospheric chemistry and climate. It follows that any change in emissions resulting from a shift in fuel mix could alter air quality. In this chapter, my aim is to understand how surface transport emissions from biofuels could affect tropospheric chemistry.

6.2 Experimental setup

I ran four sensitivity experiments—BASE, E85, BD20, and BD100—in order to test the sensitivity of the model chemistry to surface transport emissions. Each was run between 1999 and 2005 with 16 months removed for spin-up. Physical

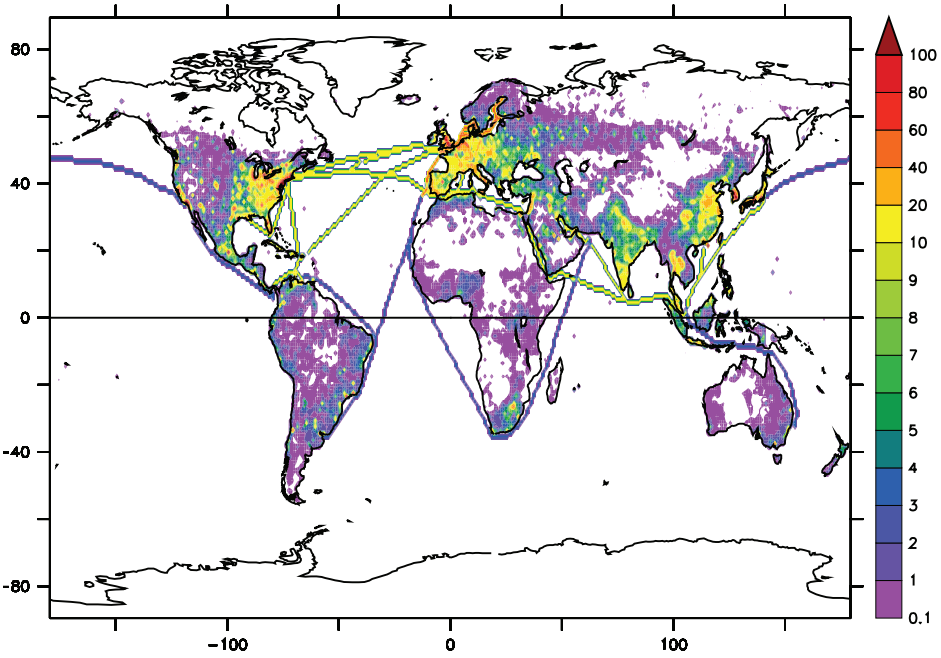

Figure 6.1. High resolution (1x1°) NO_2 emissions from surface transport for the BASE case, in 10^6 kg NO_2 $year^{-1}$.

forcing factors (radiation and SSTs) were the same as the BASE run in Chapters 3 (section 3.2) and 5 (section 5.2). Present day emissions [*Dentener et al.*, 2005] are also the same for the BASE case and are described in section 3.2.3. The emissions were put together using the Regional Air Pollution Information and Simulation (RAINS) model [*Dentener et al.*, 2005]. For transportation emissions, NO_x emissions factors for Europe, North America, Russia, and Southeast Asia were specific to national characteristics such as fleet composition, fuel quality, and maintenance levels. In other places, default emission factors were applied. Emissions from surface transport do not have seasonal or monthly variation.

High resolution NO_2 emissions from the surface transport sector are depicted in Figure 6.1. These emissions are degraded to the resolution of UKCA (3.75° by 2.5°) when used in the model, but are shown here at higher resolution to illustrate the heterogeneity and complexity of surface transport emissions. NO_2 emissions

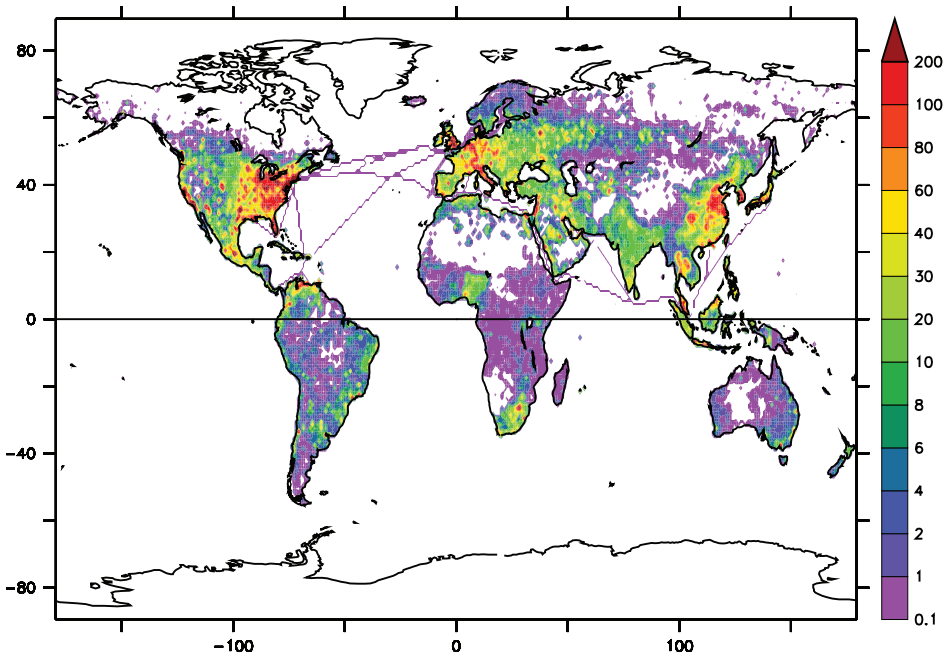

Figure 6.2. High resolution (1x1°) CO emissions from surface transport for the BASE case, in 10^6 kg CO year^{-1}.

from road transport cover most of the exposed (i.e. without seasonal or permanent ice) land surface of the earth, with the except of the Sahara, parts of southern Africa, central Eurasia, and central Australia. Key shipping routes are also visible, especially the Atlantic corridor between Europe and North America. There are a few areas of particularly high density in the NO_2 emissions field: the eastern United States, Europe, India, Thailand, and China. In contrast, emissions of CO (shown in Figure 6.2), which are elevated in the same key regions, are also elevated in South Africa, Nigeria, central America, and a larger extent of eastern Europe. This could be related to the increased average age of vehicles in these countries, which has been shown to be linked to emissions [*Pandian et al.*, 2009]. Surface transport emissions comprise 36% of the total NO_2 emitted in the BASE run, and 18% of CO.

These surface transport emissions fields were altered for the sensitivity studies

Table 6.1. Emission scaling factors used to modify existing traffic emission fields. Scaling factors for biodiesel were reported in *United States Environmental Protection Agency* [2002], and scaling factors for E85 are from *Jacobson* [2007].

Fuel Type	NO_x	CO	VOCs
E85	.70	1.05	See Table 6.2
BD20	1.024	.869	.821
BD100	1.134	.573	.368

Table 6.2. Emission scaling factors for E85 VOCs as reported in *Jacobson* [2007].

Species	Scaling Factor
Ethane	1
Propane	.35
Formaldehyde	1.6
Acetaldehyde	20.0
Acetone	1

by scaling factors appropriate to three fuel types: 20% biodiesel mixed with 80% conventional diesel (BD20), 100% biodiesel (BD100), and 85% ethanol mixed with 15% conventional gasoline (E85). The scaling factors for each study are listed in Table 6.1. The scaling factors for biodiesel (both BD20 and BD100) were reported in *United States Environmental Protection Agency* [2002]. The authors used 39 emission datasets for heavy duty diesel vehicle (HDDV) engines tested with soybean derived biodiesel. The data was analyzed using statistical curve fitting in order to obtain a relationship between the percentage of fuel comprised of biodiesel and the measured emissions of criteria air pollutants. According to *United States Environmental Protection Agency* [2002], the impact of biodiesel on HDDV emissions was to increase NO_x by 13.4% for 100% biodiesel, and to decrease both CO and VOCs by 42.7% and 63.2%, respectively. BD20 scaled almost linearly with the 100% biodiesel results, in other words, the change in emissions for 20% biodiesel is approximately equal to 20% of the change for 100% biodiesel.

The scaling factors for E85 were reported in *Jacobson* [2007] and are the aver-

age of 10 studies which examined the relative impacts of E85 versus conventional gasoline or petrol. NO_x emissions are reduced by 30% for E85 compared to conventional fuel, and CO rises by 5%. Importantly, the work of *Jacobson* [2007] included a speciation of emission scaling factors for individual organic species. To capture the most variability possible (and the best information in the literature), these individual scaling factors were used in the E85 run. The values for these speciated VOC scaling factors are listed in Table 6.2. The largest change in VOC emissions for E85 is the 2000% jump in acetaldehyde emissions, which is a conservative estimate from the observed data in the 10 studies used by *Jacobson* [2007]. Propane emissions were reduced by 65%, and formaldehyde emissions jumped by 60%. Ethane and acetone emissions were left unchanged.

6.3 The BASE case

One of the major difficulties in modelling tropospheric chemistry is understanding and identifying when a chemical regime is NO_x-sensitive or VOC-sensitive with respect to ozone production. *Sillman* [1995] addressed this issue by examining possible indicator species for VOC- versus NO_x-sensitivity; defined as which species (NO_x or VOC) will promote an increase in ozone production. In a NO_x-sensitive environment, where many peroxy radicals are present, a significant radical termination process is the formation of hydroperoxides,

$$HO_2 + HO_2 \rightarrow H_2O_2. \tag{2.21}$$

In contrast, in a VOC-sensitive environment, where large amounts of NO_2 are present, a stronger loss process is the formation of nitric acid,

$$OH + NO_2 + M \rightarrow HNO_3 + M \tag{2.23}$$

both of these radical-radical reactions have been described in section 2.1.3. The dominant loss process of HO_x radicals (which initiate the majority of tropospheric oxidation cycles, see section 2.1.1) therefore can be indicative of the type of chemical regime.

Sillman [1995] established that the ratio of concentrations of H_2O_2/HNO_3 was indeed a strong indicator of the sensitivity of a chemical regime with respect to ozone production. Using measurements from eight sites, the authors found that this flux ratio was able to distinguish between the NO_x-sensitivity and VOC-sensitivity across the widest range of emissions and meteorological conditions. *Sillman* [1999] reviewed VOC-NO_x-ozone chemistry, revisiting the H_2O_2/HNO_3 ratio as an appropriate and useful indicator for the sensitivity of a chemical regime to VOC versus NO_x. More recently, *Sillman and West* [2009] tested this sensitivity parameter against measurements in Mexico City and found that the formation flux ratio of H_2O_2/HNO_3 was one of the only useful parameters in that polluted environment.

Both *Sillman* [1995] and *Sillman and West* [2009] used instantaneous tracer concentrations in their studies. Equivalent concentrations are not available as output of a global model (I have monthly mean data instead); however, the flux of formation of the two molecules can be a diagnostic output. In theory, the flux of formation is even more closely linked to the sensitivity of the chemistry because it eliminates differences in chemical (e.g. via reaction with OH) and physical (e.g. via wet deposition) sinks between the two species. This approach was used in a model by *Steiner et al.* [2006] to identify chemical regimes in California. The authors successfully differentiated between a NO_x-rich region (the Bay area) and a NO_x-sensitive regime (the southern Sierra Nevada mountains) using afternoon production fluxes for hydrogen peroxide and nitric acid. *Zhang et al.* [2009] also successfully used the production fluxes to verify the sensitivity of chemical regimes in the United States to VOC or NO_x.

In Figure 6.3, the seasonality of the indicator flux ratio H_2O_2/HNO_3 is shown

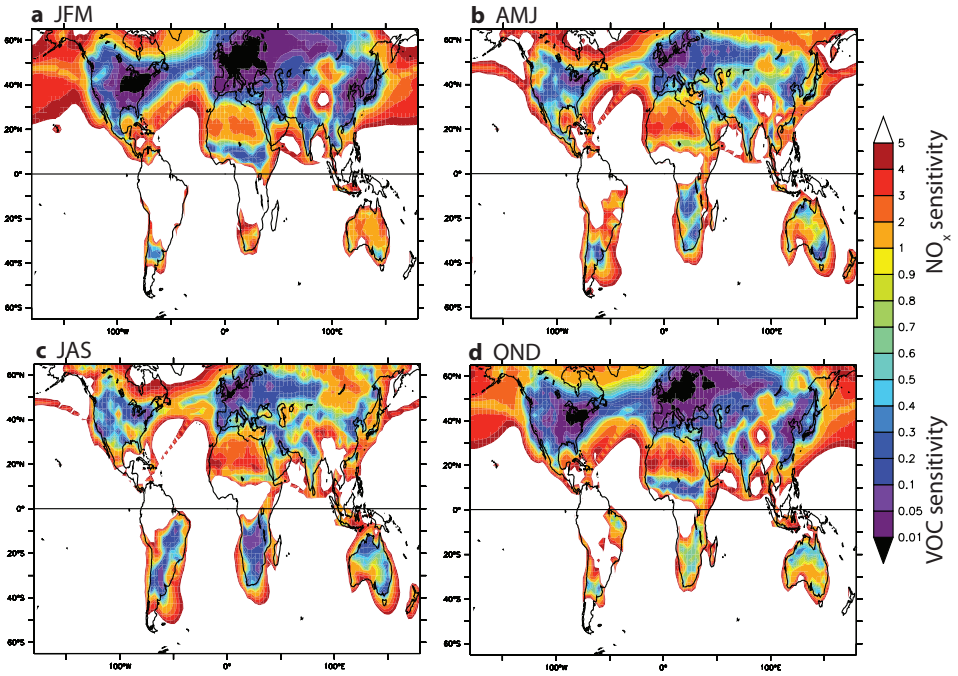

Figure 6.3. Seasonal variation in the ratio of the flux of formation of H_2O_2 over HNO_3 for averaged a) January, February, and March; b) April, May, and June; c) July, August, and September; and d) October, November, and December.

for the BASE integration. *Sillman* [1995] found that the VOC sensitive regime was generally indicated by values less than 0.3, the NO_x sensitive regime was indicated by values above 0.5, and that values in between indicated a transition regime. For their work in Mexico city, *Sillman and West* [2009] reported that VOC sensitive air masses were marked by ratio values below 0.1, while NO_x sensitive air was marked by ratio values above 0.2. The H_2O_2/HNO_3 indicator flux ratio is therefore not an absolute measure of the chemical sensitivity, but rather an indicative one which needs to be calibrated for a particular location. Generally, a low value of the flux ratio will be suggestive of a VOC-sensitive regime (there is little peroxide production in comparison with nitric acid), while high values of the ratio suggest NO_x-sensitivity (much more peroxide is produced compared with nitric acid.)

In the winter months for the northern hemisphere, a strong VOC-sensitivity covers much of North America and Europe. Most of South America, Australia,

and Africa are NO_x-sensitive, with the exception of a strip across the Sahel where biomass burning NO_x emissions are present in the months between November and March. The northern parts of the Pacific and Atlantic are also NO_x-sensitive during this time period. In the northern hemisphere summer months, parts of North America switch to NO_x-sensitive regimes, concurrent and colocated with seasonal biogenic emissions of isoprene, a result that is consistent with *Zhang et al.* [2009]. A ridge through South America and a swath of southern Africa display areas of VOC-sensitivity which were not present during the winter months, both are areas where biomass burning emissions are elevated during this period. The northern section of Australia also transitions to VOC-sensitivity due to seasonal isoprene emissions; a change from the strongly NO_x-sensitivity of the boreal winter (Austral summer). Southeast Asia also transitions strongly between the two halves of the year, albeit with opposite seasonality to Australia.

6.4 What is the impact of biofuels?

6.4.1 Ozone

Figure 6.4 shows the annual average change in surface ozone due to a shift to 100% biodiesel (BD100) or 85% ethanol (E85). The strongest impact of BD100 is to reduce ozone throughout the northern hemisphere. The response is on the order of 1-4 ppbv, with greater reductions in southern California (-8 ppbv) and in Japan and Korea (-6 ppbv). Slight increases up to 2 ppbv are modelled over parts of central Eurasia and a few scattered areas throughout the tropics. Biodiesel increases NO_x emissions and decreases VOC emissions, and as shown in Figure 6.3, the northern hemisphere is strongly VOC-sensitive throughout most of the year.

In contrast, the effect of E85 fuel (Figure 6.4, bottom panel) is to increase ozone strongly in UKCA. Increases are modelled over most of the northern hemisphere on the order of 1-10 ppbv. Increases over Europe reach up to 15 ppbv, while increases over Asia and North America are even higher: over Asia, values reach 20

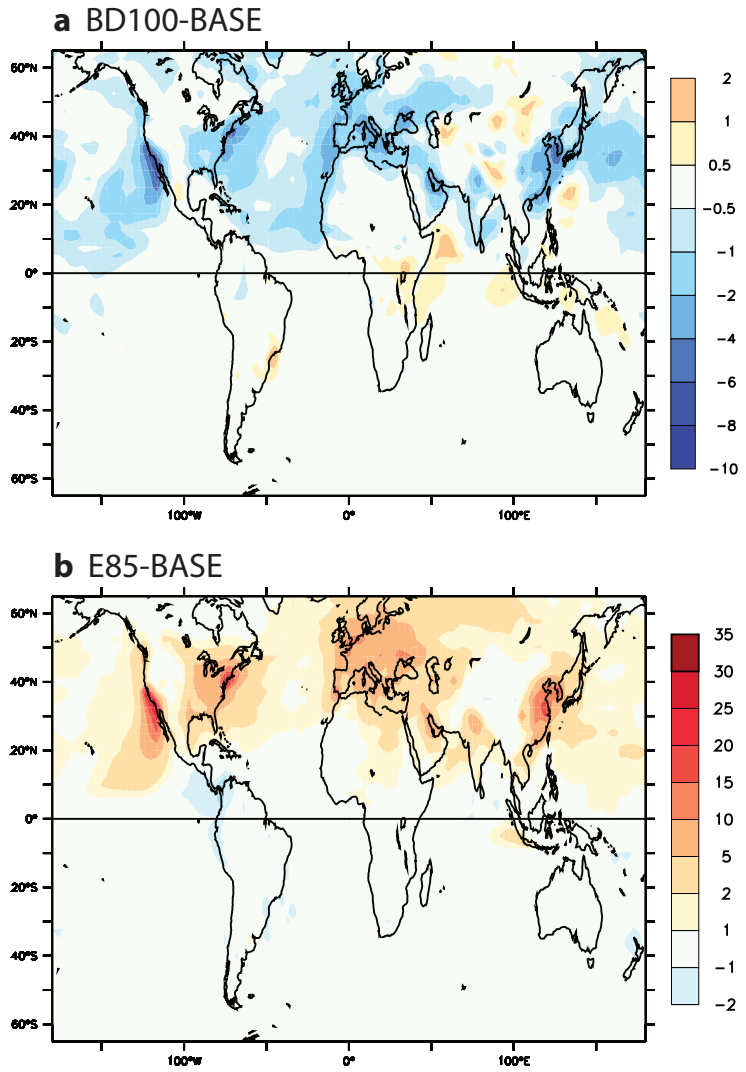

Figure 6.4. Average change in monthly mean surface ozone [ppbv] between a) BD100 and b) E85 and BASE. Note the different scales.

ppbv, while over the northeastern United States values reach 25 ppbv. The largest increases are modelled over southern California and climb to 35 ppbv. Similar to the BD100 sensitivity study, the opposite signal is modelled throughout central Eurasia (up to -1 ppbv) and scattered areas in the tropics (up to -2 ppbv.) Most of the affected domain throughout the northern hemisphere was VOC-sensitive (Figure 6.3), and thus increasing VOC emissions and reducing NO_x is a powerful way

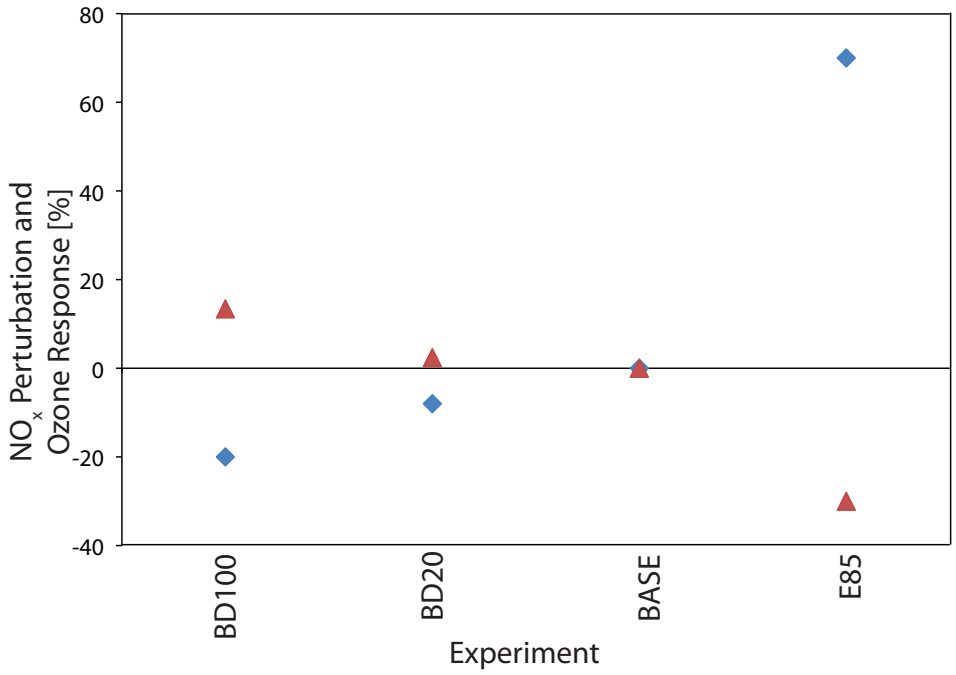

Figure 6.5. Maximum change in relative surface ozone [%] between BD100, BD20, and E85 and BASE (blue), and the change in NO_x emissions for the same runs (red).

to increase ozone production. *Jacobson* [2007] performed a very similar experiment in which the scaling factors for E85 were applied to the present day fleet in the United States and California (they used two model domains). They found that ozone increased in the Los Angeles area by up to 15 ppbv in August. They also found that in the polluted environment of Los Angeles, the change in ozone was directly related to the relative reduction in NO_x. The NO_x-VOC sensitivity indicator results above indicate that this region is VOC sensitive, consistent with their results. An increase in acetaldehyde emissions in a 2012 future scenario with E10 fuel (10% ethanol mixed with 90% conventional fuel) also showed high ozone increases in Bangkok in the work of *Milt et al.* [2009].

In order to investigate the relative relationships between all the sensitivity studies, Figure 6.5 shows the linearity of the maximum relative response in ozone and the change in NO_x for each set of model experiments. The largest relative change

in ozone is modelled for the E85 sensitivity, with a value of 70%; the change in NO_x is 30% for this study. The maximum response for BD100 is -10 ppbv (with an increase in NO_x of 13.4%), while the smaller perturbation from the BD20 experiment changes ozone by a maximum of only 3 ppbv (for a +2.4% change in NO_x). *Matthes et al.* [2007] examined the relative contribution of NO_x and VOC emissions from traffic, found that NO_x was the largest contributor, a result which is in agreement with the high correlation of between ozone and NO_x emissions shown in Figure 6.5. These numbers show both linear and nonlinear components. For ethanol, as an example, the perturbation of 30% in NO_x emissions leads to a relative change in ozone of 70%. In contrast, BD100 leads to a 20% change in ozone through a 13.4% change in NO_x emissions. The linearity of the response seems to be dependent on the direction of the perturbation and the chemical regime.

6.4.2 NO_x-VOC sensitivity

With the diagnostic flux indicator, it is possible to understand the nonlinear component of the change in ozone described above. The flux ratio of H_2O_2 to HNO_3 formation changes with the emissions depending on fuel type used in the model, as shown in Figure 6.6. When 100% biodiesel is used, a fuel that emits more NO_x and less VOC, the sensitivity flux parameter is reduced, indicating a transition to a more VOC-sensitive regime (in which more nitric acid and less hydroperoxide is produced). The largest changes are modelled over the UK and northern France, southern California, and the eastern seaboard of North America. These are all areas of very high emissions from surface transport (Figures 6.1 and 6.2). The BD20 simulation also showed decreases in the flux parameter, although to a lower extent (not shown.)

In contrast, the choice to move to E85 fuel moves the chemical system towards NO_x-sensitivity. E85 emits more VOC (+22%) and CO (+5%) (see Table 6.1) than conventional fuel while emitting much less NO_x (-30%). The largest response is found above polluted continental regions; every region with high surface transport

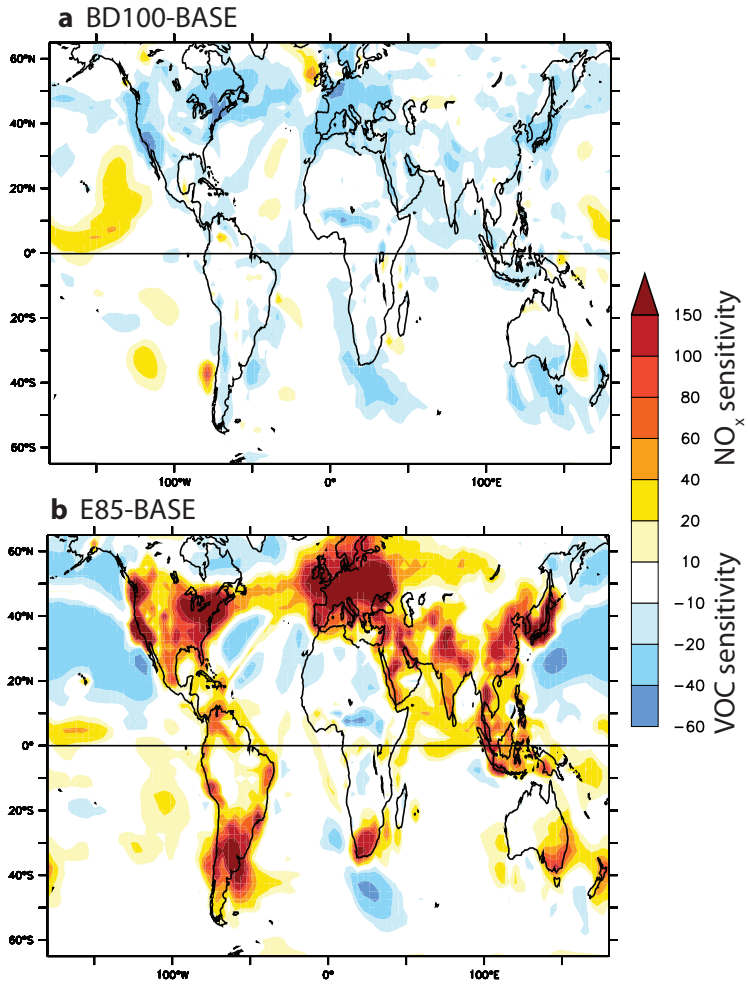

Figure 6.6. Percentage change in ratio of formation of H_2O_2 and HNO_3 between BD100 and E85 runs relative to the BASE case.

emissions shows a move towards NO_x sensitivity. The northern oceans show a less extreme shift in the opposite direction—towards VOC sensitivity. For both sensitivity studies, the largest changes in the indicator flux parameter occur in the northern hemisphere. This is colocated with the areas of highest surface transport emissions (Figures 6.1 and 6.2), and with highest VOC-sensitivity (Figure 6.3).

6.4.3 Seasonality

The nonlinear component of the ozone response, because it is dependent on local chemical conditions, is likely to be seasonally dependent. Despite the fact that in these experiments surface transport emissions do not vary with time, other emissions in the model do change. There is also some suggestion from the literature that the response does vary with season; *Niemeier et al.* [2006] performed an experiment in which road traffic emissions were shut off entirely, and found that ozone decreased in Europe in January by over 25 ppbv while increasing over much of the continental tropics. In July, however, the signal was more uniform, and ozone increased by up to 25 ppbv over most of the industrialized areas of northern hemisphere.

In Figure 6.7, the change in ozone for average January and July are shown for the E85 simulation compared to the BASE simulation. Because the E85 perturbation involves an increase in VOC emissions and a decrease in NO_x, the strongest response occurs in January. The eastern United States, where some of the the highest increases occur, has been shown to be VOC-sensitive during this period [*Jacob et al.*, 1995; *Zhang et al.*, 2009, and Figure 6.3]. If we take this to be representative of the northern hemisphere, then this would explain the large ozone changes that occur in winter that are not present in summer. In July, the response is markedly smaller in both magnitude and geographic extent, coinciding with the period when biogenic VOC emissions are higher in the northern hemisphere and ozone production is NO_x-sensitive in some regions. The southeastern United States, a particularly strong emission hot-spot, even shows a decrease (over -5 ppbv) in ozone during this time period due to extreme VOC saturation of the chemical system. Smaller decreases (between 2 and 5 ppbv) are scattered across the northern hemisphere during this season. Similar decreases are modelled throughout the southern hemisphere during January. These small decreases (between 2 and 5 ppbv of ozone) follow the seasonality of isoprene emissions.

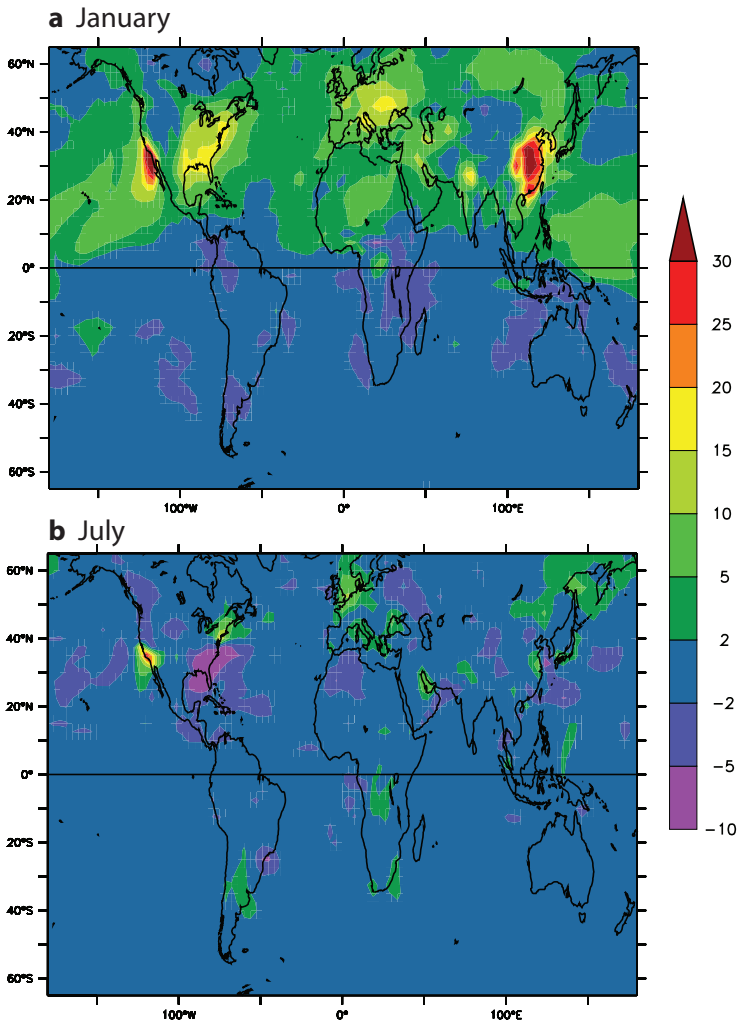

Figure 6.7. Change in near surface (up to 600 m) average ozone [ppbv] between the E85 and BASE runs for a) January and b) July.

6.5 Uncertainties

A sensitivity study of this nature could not possibly capture the complexity of the vehicle fleet in a single country, let alone worldwide. It is intended to probe the possible limits or boundaries in the potential atmospheric perturbation that a switch to biofuels would entail. Notably, the whole world does not operate one type of fuel, for which there could possibly be one type of fuel replacement. Instead, the fuel market is split largely down country lines [*International Energy Agency*, 2007]. For example, the United States light duty vehicle market veers heavily towards gasoline/petrol (76% in 2006) [*Energy Information Administration*, 2007]. In contrast, the Germany light duty market operates 54% (in 2005) on diesel [*Mineralwirtschaftsverband*, 2006]. A switch to biofuels in the United States would therefore likely veer towards ethanol (a gasoline replacement), while a similar shift in Germany would likely head to biodiesel (a diesel replacement). A single change applied across the globe is therefore not an accurate portrayal of what is most likely to occur in the future, as changes are more likely to be regional.

In addition, the scaling factors used for E85 were based on mostly light duty vehicle (LDV) testing, while the scaling factors for biodiesel were based on emissions testing from heavy duty vehicles (HDVs). Perhaps the response in emissions testing would change for testing of different vehicles. Finally, the exact changes in emissions are scaled up from small laboratory experiments, and may not be representative of the entire fleet. For example, the NO_x emissions from biodiesel reported in *United States Environmental Protection Agency* [2002] are still under discussion. The exact increase in NO_x emissions (13%) was replicated by *Monyem and H. Van Gerpen* [2001], but smaller changes were observed in *Szybist et al.* [2005] (10%) and *Karavalakis et al.* [2009] (11%).

6.6 Summary

In this chapter, I used a set of four sensitivity studies to estimate the upper bounds of the impact that combustion of biofuels could have on air quality. I characterized the BASE simulation through the use of flux ratio indicators, which showed the strongest seasonality in the northern hemisphere, where VOC-sensitive conditions dominate in the winter, but where the sensitivity is more heterogeneous in the summer. I then described the impact of phase III of the life cycle (combustion) on tropospheric chemistry. I found that biodiesel decreased surface ozone by up to 10 ppbv, and that ethanol had a much more stark effect as ozone increased by 35 ppbv; a strongly nonlinear response. I also found that seasonality was important, especially for ethanol, and that the positive response in surface ozone was dominant in winter.

Although there are uncertainties associated with this type of large scale study, my results point out that our choice of future fuel will have different and profound effects on air quality. Increases in ozone of such a scale due to ethanol could be disastrous for human and crop health, and for positive radiative forcing of the climate system. Although these results cannot be taken as a projection, they do call for more research and perhaps raise a red flag for the future ethanol industry. In contrast, the move to biodiesel seems to be a safe choice for air quality; in the best case scenario, high NO_x emissions from biodiesel decrease ozone, while in the worst case, ozone will remain the same.

In the next chapter, I summarize the novel work performed in my thesis and describe some of the summed impacts of phase I and phase III of the biofuel life cycle.

Chapter 7

Conclusions

In this final chapter, I review the novel work that was presented throughout this thesis (section 7.1). I then discuss the aggregated impact of the two phases of the biofuel life cycle on air quality in section 7.2, followed by some ideas for further studies that could build directly from my work (section 7.3). In section 7.4, I conclude with a brief longer term outlook on the future of this type of life cycle-atmosphere research.

7.1 Summary of novel work

1. Implemented isoprene chemistry in UKCA

I included a representation of isoprene oxidation chemistry in the tropospheric configuration of UKCA. My analysis showed that isoprene had a particularly strong positive impact on ozone in the northern hemisphere during summer, and that generally over hot-spot emission regions with low NO_x emissions, ozone was reduced. I was able to distinguish between both VOC-rich and VOC-sensitive regimes and NO_x-rich and NO_x-sensitive regimes through examining scatter relationships. I also found that isoprene increased the methane lifetime by 22.5% in UKCA, and that OH was substantially reduced over hot-spot emission regions. I characterized the impact of isoprene oxidation on key tropospheric trace gases, setting up that

changes in isoprene emissions resulting from the growth of energy crops could have strong influences on air quality in regions where land use could change in the future.

2. Used a box model to compare the chemical mechanism with measurements from a field campaign

Using a box model, I examined the ability of UKCA's chemical mechanism against NO, NO_2, and O_3 data from the OP3 field campaign in Malaysian Borneo. I found that the mechanism was relatively insensitive to a series of chemical, photolytic, and deposition parameters, but that representations of physical processes were more important. In particular, the implementation of a nighttime 'venting parameter' was necessary in order to capture the diurnal cycle of NO_2. Using a cost function analysis of three physical variables, I produced a best fit simulation which matched the measurements closely and demonstrated that the UKCA mechanism could capture the chemistry of NO_x and ozone during the campaign. My work demonstrated that a global model chemical mechanism can capture the chemistry at an individual field site, but that parameterizations of physical processes are important in order to do so successfully.

3. Performed two global sensitivity studies for Southeast Asia

Considering the region of Southeast Asia in a global model, I performed two sensitivity studies, OILPALM and SUGARCANE, which were simple representations of how changes in isoprene could result from cultivation of biofuel feedstocks. When isoprene emissions were increased in the OILPALM study, surface ozone concentrations dropped, while when isoprene emissions were decreased (for the SUGARCANE study) ozone strongly increased. This simple study substantiated the hypothesis that phase I of the biofuel life cycle could indeed impact tropospheric chemistry through changes in isoprene emissions. The magnitude of the response depended on the direction of the isoprene perturbation, and therefore on the type of feedstock crop.

4. Characterized a potential future atmosphere through ozone attribution

Using the concept of attribution and a serial methodology, I found that future surface ozone increased due to climate change and decreased due to changes in anthropogenic emissions. Biogenic isoprene emissions had a smaller effect, and the total surface ozone in the 'best guess' future run was quasi-linear with respect to each individual variable. My results suggest that reducing anthropogenic precursor emissions is an effective way to reduce future ozone. I also found that these ozone reductions were largest in the summer months, coinciding with the 'ozone season'.

5. Examined changes due to land use change and CO_2 suppression of isoprene emission at the global scale

I performed the first global study which examined isoprene emissions, land use change, and the resulting change in tropospheric chemistry. I found that ozone increased as a result of land use change, and that this increase occured directly over the regions of perturbation and was robust to the inclusion of CO_2 suppression. This could be significant for crop health and productivity, and in the worst case scenario, may encourage more cropland expansion (as existing crops produce less than expected). I also compared the impact of land use change with another perturbation to isoprene emission, CO_2 suppression, and found that the spatial variation was different but that both increased ozone. Overall, land use had a more acute effect than CO_2 suppression on both ozone and HO_x, but the global budget numbers were relatively unchanged.

6. Explored the sensitivity to biofuel emissions from surface transport

I performed the first study of changes in tropospheric chemistry resulting from biofuel use at the global level. I found that ethanol increased ozone markedly (+35 ppbv) and biodiesel decreased ozone, but to a smaller extent (-10 ppbv). I used chemical reaction fluxes to identify NO_x- and VOC-sensitive regimes. I reported that most extreme ozone increases due to ethanol occured in the northern hemi-

spheric winter, when the regime is strongest in its VOC-sensitivity. My results indicate that biofuels could have a strong impact on tropospheric chemistry for phase III (combustion), and that ethanol seems to be a worse choice for air quality than biodiesel.

7.2 The impact of the full life cycle

Although I examined them separately, the aggregate impacts of phase I and phase III of the biofuel life cycle on air quality and tropospheric chemistry are worth considering. The response will not necessarily be linear, but from both the ozone attribution study (section 5.4) and the surface transport experiments (section 6.4), it seems probable that there will be a large linear component in the ozone response. I found that the changes in ozone resulting from the oil palm biodiesel fuel-feedstock system were consistently negative across both phases of the life cycle. In the simple phase I sensitivity study (OILPALM, chapter 3) the increase in isoprene led to reduced ozone (-10 ppbv) in the VOC-rich region of Southeast Asia. In the phase III studies (BD20 and BD100, chapter 6), the change in ozone was again negative (-10 ppbv). Phase I would reduce ozone in tropical regions (where oil palm can be cultivated), while phase III would be more influential in the northern midlatitudes, where more surface transport emissions are present. These are big changes; it seems plausible that these reductions in ozone should be considered in the discourse surrounding biodiesel policy.

In contrast, the sugarcane ethanol fuel-feedstock system led to increases in ozone. This occured in the simple sensitivity (SUGARCANE, chapter 3 and in the more realistic representation of cropland expansion (FutCrops and FutCROPS_CO2, chapter 5). When I considered the final phase of the life cycle, ozone again increased; in some regions ozone was elevated by over 30 ppbv. These positive increases in ozone concentrations resulting from two phases of the ethanol life cycle are clearly an important consideration in the decision to produce and use ethanol

as a liquid fuel for transport.

While many other factors, including the carbon balance, need to be considered, my work shows that the impact on air quality can also be very significant.

7.3 Potential further studies

A number of further studies could be carried on directly from this work. In chapter 5, I examined phase I of the life cycle by looking at cropland expansion. The crops in my experiments were low emitting crops (representing sugarcane or corn, for example). The experiment in chapter 4 in which I increased isoprene emissions, however, also displayed changes in ozone resulting from emissions perturbation; from this it follows that the cropland expansion work could be made more robust by also studying a high isoprene emitting crop. It would be interesting to see if the surface ozone response from the simple sensitivity remain as consistent for a high emitting crop (negative) as they did for a low emitting crop (positive).

In chapter 6, I performed three sensitivity studies in which surface transport emissions were scaled to biofuel tailpipe emissions. A more accurate representation of the change in transport emissions from biofuels would entail an additional scaling factor which accounts for the portion of a vehicle fleet which uses a particular type of fuel. A set of regional sensitivity studies could also be run, in which ethanol is used in one part of the domain and biodiesel another. These types of studies might mitigate the response of surface ozone to a particular biofuel mix, and could give a more realistic quantification of potential future changes in ozone and oxidizing capacity.

Perhaps most importantly, the sensitivity of air quality and atmospheric chemistry to phase I and phase III of the biofuel life cycle should be tested together as well as separately. An experiment in which both cropland expansion (chapter 5) and changes in surface transport emissions (chapter 6) are included would be a good first step. As I described above, my hypothesis is that a large part of the

summed response would be linear, and thus the positive ozone responses to the sugarcane ethanol system would compound each other, while the negative responses to the oil palm biodiesel system would also add up. Some portion of the change would likely be nonlinear, however, and would be interesting to investigate.

7.4 Outlook

Although there are multiple experiments which follow directly from my simulations, some more general additions to the methodology could also be made. Most importantly, I have neglected the second phase of the biofuel lifecycle, transformation, in examining the impact of biofuel production on tropospheric chemistry. The transformation stage, particularly the processing to form crude biofuel on feedstock cultivation sites, could change the impact of changing VOC emissions in these areas; for example, if NO_x emissions from on site crude processing plants increase, perhaps the ozone response to increased isoprene would shift. I can imagine a series of experiments using the box model and oil palm isoprene flux data that could probe these questions; a global study in which point source NO_x emissions are added to feedstock growing areas would also be interesting. Phase II of the life cycle should be examined on its own to begin with, and then could be added to both phase I and phase III in order to test the total response to a particular feedstock-fuel system.

The ultimate goal of this type of biofuel research is to include the entire life cycle in the emissions of a regional or global model. In this thesis, I have examined two phases of the biofuel life cycle and their influence on tropospheric chemistry. The changes in trace gas constituents and the oxidizing capacity of the atmosphere are significant, warranting more research in this area. The more we understand about the impact of the entire life cycle on air quality and atmospheric chemistry, the more informed we will be in making decisions about the implementation of biofuels at a large scale.

Bibliography

Abbe, C. (1901), The physical basis of long-range weather forecasts, *Mon. Wea. Rev.*, *29*, 551–561.

Adams, J. M., J. V. H. Constable, A. B. Guenther, and P. Zimmerman (2001), An estimate of natural volatile organic compound emissions from vegetation since the last glacial maximum, *Chemosphere*, *3*, 73–91.

Agarwal, A. K. (2007), Biofuels (alcohols and biodiesel) applications as fuels for internal combustion engines, *Prog. Energ. Combust.*, *33*, 233–271.

Aghedo, A. M., M. G. Schultz, and S. Rast (2007), The influence of African air pollution on regional and global tropospheric ozone, *Atmos. Chem. Phys.*, *7*, 1197–1212.

Alcamo, K. E. . L. R., J. (Ed.) (1999), *Global Change Scenarios of the 21st Century: Results from the IMAGE 2.1 Model*, Oxford: Pergamon/Elsevier Science.

Alo, C. A., and G. Wang (2008), Potential future changes of the terrestrial ecosystem based on climate projections by eight general circulation models, *J. Geophys. Res.*, *113*, G01,004, doi:10.1029/2007JG000528.

AltIn, R., S. Çetinkaya, and H. S. Yücesu (2001), The potential of using vegetable oil fuels as fuel for diesel engines, *Energ. Convers. Manage.*, *42*, 529–538.

Anderson, D., et al. (2004), *World Energy Assessment: Overview*, New York:

United Nations Development Programme, United Nations Department of Economic and Social Affairs, and World Energy Council.

Andreae, M. O., and P. Merlet (2001), Emission of trace gases and aerosols from biomass burning, *Global Biogeochem. Cycles*, *15*, 955–966.

Aplincourt, P., and J. M. Anglada (2003), Theoretical studies of the isoprene ozonolysis under tropospheric conditions. 2. Unimolecular and water assisted decomposition of α-hydroperoxides, *J. Phys. Chem. A*, *107*, 5812–5820.

Archibald, A., M. Jenkin, and D. Shallcross (), An isoprene mechanism intercomparison, *Atmos. Environ.*, *In Press, Accepted Manuscript*, –, doi:10.1016/j.atmosenv.2009.09.016.

Arneth, A., et al. (2007a), Process-based estimates of terrestrial ecosystem isoprene emissions: incorporating the effects of a direct CO_2-isoprene interaction, *Atmos. Chem. Phys.*, *7*, 31–53.

Arneth, A., P. M. Miller, M. Scholze, T. Hickler, G. Schurgers, B. Smith, and I. C. Prentice (2007b), CO_2 inhibition of global terrestrial isoprene production: Potential implications for atmospheric chemistry, *Geophys. Res. Lett.*, *34*, L18,813, doi:10.1029/2007GL030615.

Arneth, A., R. K. Monson, G. Schurgers, U. Niinemets, and P. I. Palmer (2008a), Why are estimates of global terrestrial isoprene emissions so similar (and why is this not so for monoterpenes)?, *Atmos. Chem. Phys.*, *8*, 4605–4620.

Arneth, A., G. Schurgers, T. Hickler, and P. A. Miller (2008b), Effects of species composition, land surface cover, CO_2 concentration and climate on isoprene emissions from European forests, *Plant Biology*, *10*, 150–162.

Arnold, S. R., M. P. Chipperfield, and M. A. Blitz (2005), A three-dimensional model study of the effect of new temperature-dependent quantum yields for acetone photolysis, *J. Geophys. Res.*, *110*, D22305, doi:10.1029/2005JD005998.

Arora, V. K., and H. D. Matthews (2009), Characterizing uncertainty in modeling primary terrestrial ecosystem processes, *Global Biogeochem. Cycles*, *23*, GB2016, doi:10.1029/2008GB003398.

Atkinson, R. (2000), Atmospheric chemistry of VOCs and NO_x, *Atmos. Environ.*, *34*, 2063–2101.

Atkinson, R., and J. Arey (2003), Gas-phase tropospheric chemistry of biogenic volatile organic compounds: A review, *Atmos. Environ.*, *37*, S197–S219.

Atkinson, R. A., S. M. Aschmann, J. Arey, and B. Shorees (1992), Formation of OH radicals in the gas-phase reactions of O_3 with a series of terpenes, *J. Geophys. Res.*, *97*, 6065–6073.

Avise, J., J. Chen, B. Lamb, C. Wiedinmyer, A. Guenther, E. Salath, and C. Mass (2009), Attribution of projected changes in summertime US ozone and $PM_{2.5}$ concentrations to global changes, *Atmos. Chem. Phys.*, *9*, 1111–1124.

Bakwin, P. S., S. C. Wofsy, S. Fan, M. Keller, S. E. Trumbore, and J. M. D. Costa (1990), Emission of nitric oxide (NO) from tropical forest soils and exchange of NO between the forest canopy and atmospheric boundary layers, *J. Geophys. Res.*, *95*, 16,755–16,764.

Ban-Weiss, G. A., J. Chen, B. A. Buchholz, and R. W. Dibble (2007), A numerical investigation into the anomalous slight nox increase when burning biodiesel; a new (old) theory, *Fuel Process.Technol.*, *88*, 659–667.

Barket Jr., D. J., et al. (2004), A study of the NO_x dependence of isoprene oxidation, *J. Geophys. Res.*, *109*, D11,310, doi:10.1029/2003JD003965.

Battjes, J. (1994), *Global options for biofuels from plantations according to IMAGE simulations*, The Netherlands: Interfacultaire Vakgoep Energie en Milieukunde, Rijksuniversiteit Groningen.

Beerling, D. J., F. I. Woodward, M. Lomas, and A. J. Jenkins (1997), Testing the responses of a dynamic global vegetation model to environmental change: A comparison of observations and predictions, *Global Eco. Biogeogr.*, *6*, 439–450.

Bell, M., and M. Ellis (2004), Sensitivity analysis of tropospheric ozone to modified biogenic emissions for the Mid-Atlantic region, *Atmos. Environ.*, *38*, 1897–1889.

Bellouin, N., O. Boucher, J. Haywood, and M. Shekar Reddy (2005), Global estimate of aerosol direct radiative forcing from satellite measurements, *Nature*, *438*, 1138–1141.

Berndes, G., M. Hoogwijk, and R. van den Broek (2003), The contribution of biomass in the future global energy supply: a review of 17 studies, *Biomass & Bioenergy*, *25*, 1–28.

Bey, I., et al. (2001), Global modeling of tropospheric chemistry with assimilated meteorology: Model description and evaluation, *J. Geophys. Res.*, *106*, 23,073–23,096.

Biesenthal, T. A., J. W. Bottenheim, P. B. Shepson, S. Li, and P. C. Brickell (1998), The chemistry of biogenic hydrocarbons at a rural site in eastern Canada, *J. Geophys. Res.*, *103*, 25,487–25,498.

Bjerknes, V. (1904), Das problem der wettervorhersage, betrachtet vom standpunkte der mechanik und der physik., *Meteor. Z.*, *21*, 1–7.

Blake, R. S., P. S. Monks, and A. M. Ellis (2009), Proton-transfer reaction mass spectrometry, *Chem. Rev.*, *109*, 861–896.

Bousquet, P., et al. (2006), Contribution of anthropogenic and natural sources to atmospheric methane variability, *Nature*, *443*, 439–443.

Bouwman, A. F., L. J. M. Boumans, and N. H. Batjes (2002), Emissions of N_2O

and NO from fertilized fields: Summary of available measurement data, *Global Biogeochem. Cycles*, *16*, 1058.

Brasseur, G. P., D. A. Hauglustaine, S. Walters, P. J. Rasch, J. F. Müller, C. Grainer, and X. X. Tie (1998), MOZART, a global chemical transport model for ozone and related chemical tracers: 1. Model description, *J. Geophys. Res.*, *103*, 28,265–28,291.

Brasseur, G. P., M. Schultz, C. Granier, M. Saunois, T. Diehl, M. Botzet, E. Roeckner, and S. Walters (2006), Impact of climate change on the future chemical composition of the global troposphere, *J. Climate*, *19*, 3932–3951.

Brewer, A. W. (1949), Evidence for a world circulation provided by the measurements of helium and water vapour distribution in the stratosphere, *Q. J. Roy. Meteor. Soc.*, *75*, 351–363.

Brough, N., et al. (2003), Intercomparison of aircraft instruments on board the C-130 and Falcon 20 over southern Germany during export 2000, *Atmos. Chem. Phys.*, *3*, 2127–2138.

Butkovskaya, N., A. Kukui, and G. Le Bras (2007), HNO_3 forming channel of the HO_2 + NO reaction as a function of pressure and temperature in the ranges of 72–600 Torr and 223–323 K, *J. Phys. Chem. A*, *111*, 9047–9053.

Butkovskaya, N. I., A. Kukui, N. Pouvesle, and G. Le Bras (2005), Formation of nitric acid in the gas-phase HO_2 + NO reaction: Effects of temperature and water vapor, *J. Phys. Chem. A*, *109*, 6509–6520.

Butler, T. M., D. Taraborrelli, C. Brühl, H. Fischer, H. Harder, M. Martinez, J. Williams, M. G. Lawrence, and J. Lelieveld (2008), Improved simulation of isoprene oxidation chemistry with the ECHAM5/MESSy chemistry-climate model: lessons from the GABRIEL airborne field campaign, *Atmos. Chem. Phys.*, *8*, 4529–4546.

California Congress (2005-2006 Session), *Global Warming Solutions Act, Resolution AB32*.

California Environmental Protection Agency: Air Resources Board (Accessed 15 September 2009), Low carbon fuel standard program, Online: http://www.arb.ca.gov/fuels/lcfs/lcfs.htm#wg.

Campbell, J. E., D. B. Lobell, and C. B. Field (2009), Greater transportation energy and GHG offsets from bioelectricity than ethanol, *Science*, *324*, 1055–1057.

Carbajo, P. G., S. C. Smith, A.-L. Holloway, C. A. Smith, F. D. Pope, D. E. Shallcross, and A. J. Orr-Ewing (2008), Ultraviolet photolysis of HCHO: Absolute HCO quantum yields by direct detection of the HCO radical photoproduct, *J. Phys. Chem. A*, *112*, 12,437–12,448.

Cariolle, D., M. J. Evans, M. P. Chipperfield, N. Butkovskaya, A. Kukui, and G. Le Bras (2008), Impact of the new hno_3-forming channel of the ho_2+no reaction on tropospheric hno_3, no_x, ho_x and ozone, *Atmos. Chem. Phys.*, *8*, 4061–4068.

Carlier, P., H. Hannachi, and G. Mouvier (1986), The chemistry of carbonyl compounds in the atmosphere: A review, *Atmos. Environ.*, *20*, 2079–2099.

Carlton, A. G., C. Wiedinmyer, and J. H. Kroll (2009), A review of Secondary Organic Aerosol (SOA) formation from isoprene, *Atmos. Chem. Phys.*, *9*, 4987–5005.

Carslaw, N., et al. (2001), OH and HO_2 radical chemistry in a forested region of north-western Greece, *Atmos. Environ.*, *35*, 4725–4737.

Carter, W. P. L., and R. Atkinson (1996), Development and evaluation of a detailed mechanism for the atmospheric reactions of isoprene and NO_x, *Int. J. Chem. Kinet.*, *28*, 497–530.

Carver, G. D., P. D. Brown, and O. Wild (1997), The ASAD atmospheric chemistry integration package and chemical reaction database, *Comput. Phys. Commun.*, *105*, 197–215.

Castellanos, P., J. W. Stehr, R. R. Dickerson, and S. H. Ehrman (2009), The sensitivity of modeled ozone to the temporal distribution of point, area, and mobile source emissions in the eastern united states, *Atmos. Environ.*, *43*, 4603–4611.

Chameides, W. L., et al. (1992), Ozone precursor relationships in the ambient atmosphere, *J. Geophys. Res.*, *97*, 6037–6055.

Chen, J., J. Avise, A. Guenther, C. Wiedinmyer, E. Salathe, R. B. Jackson, and B. Lamb (2009a), Future land use and land cover influences on regional biogenic emissions and air quality in the united states, *Atmos. Environ.*, *43*, 5771–5780.

Chen, J., et al. (2009b), The effects of global changes upon regional ozone pollution in the united states, *Atmos. Chem. Phys.*, *9*, 1125–1141.

Chen, X., D. Hulbert, and P. B. Shepson (1998), Measurement of the organic nitrate yield from OH reaction with isoprene, *J. Geophys. Res.*, *103*, 25,563–25,568.

Civerolo, K. L., G. Sistla, S. T. Rao, and D. J. Nowak (2000), The effects of land use in meteorological modeling: Implications for assessment of future air quality scenarios, *Atmos. Environ.*, *34*, 1615–1621.

Cofala, J., M. Amann, Z. Klimont, K. Kupiainen, and L. Höglund-Isaksson (2007), Scenarios of global anthropogenic emissions of air pollutants and methane until 2030, *Atmos. Environ.*, *41*, 8486–8499.

Communication from the commission to the European Parliamant (23 January 2008), 20 20 by 2020, Europe's Climate Change Opportunity, Brussels.

Cook, P. A., et al. (2007), Forest fire plumes over the North Atlantic: p-TOMCAT model simulations with aircraft and satellite measurements from

the ITOP/ICARTT campaign, *J. Geophys. Res.*, *112*, D10S43, doi:0.1029/2006JD007563.

Cox, W. M., and S.-H. Chu (1996), Assessment of interannual ozone variation in urban areas from a climatological perspective, *Atmos. Environ.*, *30*, 2615–2625.

Cramer, W., A. Bondeau, S. Schaphoff, W. Lucht, B. Smith, and S. Sitch (2004), Tropical forests and the global carbon cycle: impacts of atmospheric carbon dioxide, climate change and rate of deforestation, *Phil. Trans. R. Soc. B*, *359*, 331–343.

Crutzen, P. J. (1970), The influence of nitrogen oxides on the atmospheric ozone content, *Q. J. Roy. Meteor. Soc.*, *96*, 320–325.

Crutzen, P. J. (1973), A discussion of the chemistry of some minor constituents in the stratosphere and troposphere, *Pure Appl. Geophys.*, *106*, 1385–1399.

Crutzen, P. J. (1979), The role of NO and NO_2 in the chemistry of the troposphere and stratosphere, *Annu. Rev. Earth Pl. Sci.*, *7*, 443–472.

Crutzen, P. J., and M. O. Andreae (1990), Biomass burning in the tropics: Impact on atmospheric chemistry and biogeochemical cycles, *Science*, *250*, 1669–1678.

Crutzen, P. J., A. R. Mosier, K. A. Smith, and W. Winiwarter (2008), N_2O release from agro-biofuel production negates global warming reduction by replacing fossil fuels, *Atmos. Chem. Phys.*, *8*, 389–395.

Danielsen, F., et al. (2008), Biofuel plantations on forested lands: double jeopardy for biodiversity and climates, *Conservation Biology*, *23*, 348 – 358.

Davies, T., M. J. P. Cullen, A. J. Malcolm, M. H. Mawson, A. Staniforth, A. A. White, and N. Wood (2005), A new dynamical core for the met office's global and regional modelling of the atmosphere, *Q. J. Roy. Meteor. Soc.*, *131*, 1759–1782.

Davin, E. L., N. de Noblet-Ducondré, and P. Friedlingstein (2007), Impact of land cover change on surface climate: Relevance of the radiative forcing concept, *Geophys. Res. Lett.*, *34*, L13,702, doi:10.1029/2007GL029678.

Dawson, J. P., P. J. Adams, and S. N. Pandis (2007), Sensitivity of ozone to summertime climate in the eastern USA: A modeling case study, *Atmos. Environ.*, *41*, 1494–1511.

de Gouw, J., C. Warneke, T. Karl, G. Eerdekens, C. van der Veen, and R. Fall (2003), Sensitivity and specificity of atmospheric trace gas detection by proton-transfer-reaction mass spectrometry, *Int. J. Mass Spectrom.*, *223-224*, 365–382.

Delon, C., C. E. Reeves, D. J. Stewart, D. Serça, R. Dupont, C. Mari, J.-P. Chaboureau, and P. Tulet (2008), Biogenic nitrogen oxide emissions from soils impact on NO_x and ozone over West Africa during AMMA (African Monsoon Multidisciplinary Experiment): modelling study, *Atmos. Chem. Phys.*, *8*, 2351–2363.

Demirbas, A. (2007a), Progress and recent trends in biofuels, *Prog. Energ. Combust.*, *33*, 1–18.

Demirbas, A. (2007b), Importance of biodiesel as transportation fuel, *Energy Policy*, *35*, 4661–4670.

Dentener, F., D. Stevenson, J. Cofala, R. Mechler, M. Amann, P. Bergamaschi, F. Raes, and R. Derwent (2005), The impact of air pollutant and methane emission controls on tropospheric ozone and radiative forcing: CTM calculations for the period 1990–2030, *Atmos. Chem. Phys.*, *5*, 1731–1755.

Di Carlo, P., et al. (2004), Missing OH reactivity in a forest: Evidence for unknown reactive biogenic VOCs, *Science*, *304*, 722–724.

Dobson, G. M. B., A. W. Brewer, and B. M. Cwilong (1946), Bakerian lecture. meteorology of the lower stratosphere, *Phil. Trans. R. Soc. A*, *185*, 144–175.

Duyzer, J. H., J. R. Dorsey, M. W. Gallagher, K. Pilegaard, and S. Walton (2004), Oxidized nitrogen and ozone interaction with forests. ii: Multi-layer process-oriented modelling results and a sensitivity study for douglas fir, *Q. J. Roy. Meteor. Soc.*, *130*, 1957–1971.

Edwards, J. M., and A. Slingo (1996), Studies with a flexible new radiation code. I: Choosing a configuration for a large-scale model, *Q. J. Roy. Meteor. Soc.*, *122*, 689–719.

Emmerson, K. M., and M. J. Evans (2009), Comparison of tropospheric chemistry schemes for use within global models, *Atmos. Chem. Phys.*, *9*, 1831–1845.

Energy Information Administration (2007), Alternatives to traditional transportation fuels 2007, *Tech. rep.*, Department of Energy, United States Government.

Englert, N. (2004), Fine particles and human health–a review of epidemiological studies, *Toxicology Letters*, *149*, 235–242.

European Commission (23 April 2009), Directive 2009/28/EC of the European Parliament and of the Council on the promotion of the use of energy from renewable sources and amending and subsequently repealing Directives 2001/77/EC and2003/30/EC, *Official Journal of the European Union*, p. L140/16.

European Commission (23April 2009), Directive 2009/29/EC of the European Parliament and of the Council of amending Directive 2003/87/EC so as to improve and extend the greenhouse gas emission allowance trading scheme of the Community, *Official Journal of the European Union*, p. L140/63.

European Commission (8 May 2003), Directive 2003/30/EC of the European Parliament and of the Council on the promotion of the use of biofuels or other renewable fuels for transport, *Official Journal of the European Union*, p. L 123/42.

Eyers, C., et al. (2004), AERO2K global aviation emissions inventories for 2002 and 2025, *Tech. Rep. QinetiQ/04/01113*, QinetiQ, Farnborough.

Fall, R., and S. D. Copley (2000), Bacterial sources and sinks of isoprene, a reactive atmospheric hydrocarbon, *Environ. Microbiol.*, *2*, 123–130.

Fall, R., and M. C. Wildermuth (1998), Isoprene synthase: From biochemical mechanism to emission algorithm, *J. Geophys. Res.*, *103*, 25,599–25,609.

Feddema, J. J., K. W. Oleson, G. B. Bonan, L. O. Mearns, L. E. Buja, G. A. Meehl, and W. M. Washington (2005), The importance of land-cover change in future climates, *Science*, *310*, 1674–1678.

Fehsenfeld, F., et al. (1992), Emissions of volatile organic compounds from vegetation and their implications for atmospheric chemistry, *Global Biogeochem. Cycles*, *6*, 389–430.

Fernando, S., C. Hall, and S. Jha (2006), NO_x reduction from biodiesel fuels, *Energy & Fuels*, *20*, 376–382.

Fiore, A. M., L. W. Horowitz, D. W. Purves, H. Levy II, M. J. Evans, Y. Wang, Q. Li, and R. M. Yantosca (2005), Evaluating the contribution of changes in isoprene emissions to surface ozone trends over the eastern United States, *J. Geophys. Res.*, *110*, D12,303, doi:10.1029/2004JD005485.

Fischer, G., and L. Schrattenholzer (2001), Global bioenergy potentials through 2050, *Biomass Bioenerg.*, *20*, 151–159.

Folberth, G. A., D. A. Hauglustaine, J. Lathière, and F. Brocheton (2006), Interactive chemistry in the Laboratoire de Météorologie Dynamique general circulation model: Model description and impact analysis of biogenic hydrocarbons on tropospheric chemistry, *Atmos. Chem. Phys.*, *6*, 2273–2319.

Foley, J. A., et al. (2005), Global consequences of land use, *Science*, *309*, 570–574, doi:10.1126/science.1111772.

Forster, P. M. D., C. E. Johnson, K. S. Law, J. A. Pyle, and K. P. Shine (1996), Further estimates of radiative forcing due to tropospheric ozone changes, *Geophys. Res. Lett.*, *23*, 3221–3324.

Fowler, D., et al. (2008), *Ground-level ozone in the 21st century: future trends, impacts and policy implications*, London: The Royal Society.

Franzblau, E., and C. J. Popp (1989), Nitrogen oxides produced from lightning, *J. Geophys. Res.*, *94*, 11,089–11,104.

Friedlingstein, P., et al. (2006), Climate-carbon cycle feedback analysis: Results from the C4MIP model intercomparison, *J. Climate*, *19*, 3337–3353.

Fuentes, J. D., et al. (2000), Biogenic hydrocarbons in the boundary layer: A review, *Bull. Amer. Meteor. Soc.*, *81*, 1537–1575.

Fuglestvedt, J., T. Berntsen, G. Myhre, and K. Rypdal (2008), Climate forcing from the transport sectors, *Proc. Natl. Acad. Sci. USA*, *105*, 454–458.

Fuglestvedt, J. S., T. K. Berntsen, I. S. A. Isaksen, H. Mao, X.-L. Liang, and W.-C. Wang (1999), Climatic forcing of nitrogen oxides through changes in tropospheric ozone and methane; global 3D model studies, *Atmos. Environ.*, *33*, 961–977.

Fujino, J., K. Yamaji, and H. Yamamoto (1999), Biomass-balance table for evaluating bioenergy resources, *Appl. Energ.*, *63*, 75–89.

Gaffney, J. S., and N. A. Marley (2009), The impacts of combustion emissions on air quality and climate–from coal to biofuels and beyond, *Atmos. Environ.*, *43*, 23–36.

Ganzeveld, L., and J. Lelieveld (1995), Dry deposition parametisation in a chemistry general circulation model and its influence on the distribution of reactive trace gases, *J. Geophys. Res.*, *100*, 20,999–21,012.

Ganzeveld, L., and J. Lelieveld (2004), Impact of Amazonian deforestation on atmospheric chemistry, *Geophys. Res. Lett.*, *31*, L06105, doi:10.1029/2003GL01925.

Gauss, M., et al. (2003), Radiative forcing in the 21st century due to ozone changes in the troposphere and the lower stratosphere, *J. Geophys. Res.*, *108*, D94,292, doi:10.1029/2002JD002624.

Georgescu, M., D. B. Lobell, and C. B. Field (2009), Potential impact of u.s. biofuels on regional climate, *Geophys. Res. Lett.*, *36*, L21,806.

Gettelman, A., J. R. Holton, and K. H. Rosenlof (1997), Mass fluxes of O_3, CH_4, N_2O and CF_2Cl_2 in the lower stratosphere calculated from observational data, *J. Geophys. Res.*, *102*, 19,149–19,159.

Giannakopoulos, C., M. P. Chipperfield, K. S. Law, and J. A. Pyle (1999), Validation and intercomparison of wet and dry deposition schemes using Pb-210 in a global three-dimensional off-line chemical transport model, *J. Geophys. Res.*, *104*, 23,761–23,784.

Gitz, V., and P. Ciais (2004), Future expansion of agriculture and pasture acts to amplify atmospheric CO_2 levels in response to fossil-fuel and land-use change emissions, *Climatic Change*, *67*, 161–184.

Global Emissions Inventory Activity (Accessed 21 October, 2009), Online: http://www.geiacenter.org.

Goldemberg, J. (2007), Ethanol for a sustainable energy future, *Science*, *315*, 808–810.

Graham, L. A., S. L. Belisle, and C.-L. Baas (2008), Emissions from light duty gasoline vehicles operating on low blend ethanol gasoline and E85, *Atmos. Environ.*, *42*, 4498–4516.

Granier, C., G. Pétron, J.-F. Müller, and G. Brasseur (2000), The impact of natural and anthropogenic hydrocarbons on the tropospheric budget of carbon monoxide, *Atmos. Environ.*, *34*, 5255–5270.

Gregory, D., and P. R. Rowntree (1990), A mass flux convection scheme with representation of cloud ensemble characteristics and stability-dependent closure, *Mon. Wea. Rev.*, *118*, 1483–1506.

Grosjean, D., E. L. Williams II, and E. Grosjean (1993), Atmospheric chemistry of isoprene and its carbonyl products, *Environ. Sci. Technol.*, *27*, 830–840, doi: 10.1021/es00042a004.

Guenther, A., et al. (1995), A global model of natural volatile organic compound emissions, *J. Geophys. Res.*, *100*, 8873–8892.

Guenther, A., T. Karl, P. Harley, C. Wiedinmyer, P. I. Palmer, and C. Geron (2006), Estimates of global terrestrial isoprene emissions using MEGAN (Model of Emissions of Gases and Aerosols from Nature), *Atmos. Chem. Phys.*, *6*, 3181–3210.

Haagen-Smit, A. J. (1952), Chemistry and physiology of Los Angeles smog, *Ind. Eng. Chem.*, *44*, 1342–1346.

Hall, D., R.-C. F., R. Williams, and J. Woods (1993), *Renewable Energy: Sources for Fuels and Electricity*, chap. Biomass for energy: supply prospects, pp. 593–691, Washington, DC: Island Press.

Hamilton, J. F., et al. (2008), Observations of an atmospheric chemical equator and its implications for the tropical warm pool region, *J. Geophys. Res.*, *113*, D20,313, doi:10.1029/2008JD009940.

Hanson, R. K., and S. Saliman (1984), *Combustion Chemistry*, chap. Survey of Rate Constants in the N/H/O System, pp. 361–421, New York: Springer-Verlag.

Harwood, R. S., and J. A. Pyle (1975), 2-dimensional mean circulation model for the atmosphere below 80 km, *Q. J. Roy. Meteor. Soc.*, *101*, 723–747.

Hauglustaine, D. A., F. Hourdin, L. Jourdain, M.-A. Filiberti, S. Walters, J.-F. Lamarque, and E. A. Holland (2004), Interactive chemistry in the Laboratoire de Météorologie Dynamique general circulation model: Description and background tropospheric chemistry evaluation, *J. Geophys. Res.*, *109*, D04,314, doi: 10.1029/2003JD003957.

Hauglustaine, D. A., J. Lathière, S. Szopa, and G. A. Folberth (2005), Future tropospheric ozone simulated with a climate-chemistry-biosphere model, *Geophys. Res. Lett.*, *32*, L24,807, doi:10.1029/2005GL024031.

Hayes, F., M. Jones, G. Mills, and M. Ashmore (2007), Meta-analysis of the relative sensitivity of semi-natural vegetation species to ozone, *Environmental Pollution*, *146*, 754–762.

Heald, C. L., et al. (2008), Predicted change in global secondary organic aerosol concentrations in response to future climate, emissions, and land use change, *J. Geophys. Res.*, *113*, D05,211, doi:10.1029/2007JD009092.

Heald, C. L., M. J. Wilkinson, R. K. Monson, C. A. Alo, G. L. Wang, and A. Guenther (2009), Response of isoprene emission to ambient co2 changes and implications for global budgets, *Global Change Biol.*, *15*, 1127–1140.

Hegglin, M. I., and T. G. Shepherd (2009), Large climate-induced changes in ultraviolet index and stratosphere-to-troposphere ozone flux, *Nature Geosci*, *2*, 687–691.

Hewitt, C. N., et al. (2009a), Oxidant and particle photochemical processes above a south-east asian tropical rain forest (the OP3 project): introduction, rationale, location characteristics and tools, *Atmos. Chem. Phys. Disc.*, *9*, 18,899–18,963.

Hewitt, C. N., et al. (2009b), Nitrogen management is essential to prevent tropical oil palm plantations from causing ground-level ozone pollution, *Proc. Natl. Acad. Sci. USA*, *106*, 18,447–18,451, doi:10.1073/pnas.0907541106.

Hill, J., E. Nelson, D. Tilman, S. Polasky, and D. Tiffany (2006), From the Cover: Environmental, economic, and energetic costs and benefits of biodiesel and ethanol biofuels, *Proc. Natl. Acad. Sci. USA*, *103*, 11,206–11,210.

Hill, J., S. Polasky, E. Nelson, D. Tilman, H. Huo, L. Ludwig, J. Neumann, H. C. Zheng, and D. Bonta (2009), Climate change and health costs of air emissions from biofuels and gasoline, *Proc. Natl. Acad. Sci. USA*, *106*, 2077–2082.

Hofzumahaus, A., et al. (2009), Amplified trace gas removal in the troposphere, *Science*, *324*, 1702–1704.

Hogrefe, C., et al. (2004), Simulating changes in regional air pollution over the eastern united states due to changes in global and regional climate and emissions, *J. Geophys. Res.*, *109*, D22,301, doi:10.1029/2004JD004690.

Holton, J. R., P. H. Haynes, M. E. McIntyre, A. R. Douglass, R. B. Rood, and L. Pfister (1995), Stratosphere-troposphere exchange, *Rev. Geophys.*, *33*, 403–439.

Hoor, P., et al. (2009), The impact of traffic emissions on atmospheric ozone and oh: results from quantify, *Atmos. Chem. Phys.*, *9*, 3113–3136.

Hopkin, M. (30 September, 2004), Russia backs Kyoto treaty, *Nature*, p. Published Online, doi:10.1038/news040927-15.

Horowitz, L. W., J. Liang, G. M. Gardner, and D. J. Jacob (1998), Export of reactive nitrogen from North America during summertime: Sensitivity to hydrocarbon chemistry, *J. Geophys. Res.*, *103*, 13,451–13,476.

Horowitz, L. W., et al. (2003), A global simulation of tropospheric ozone and related tracers: Description and evaluation of MOZART, version 2, *J. Geophys. Res.*, *108*, D24,4784, doi:10.1029/2002JD002853.

Horowitz, L. W., A. M. Fiore, G. P. Milly, R. C. Cohen, A. Perring, P. J. Wooldridge, P. G. Hess, L. K. Emmons, and J.-F. Lamarque (2007), Observational constraints on the chemistry of isoprene nitrates over the eastern United States, *J. Geophys. Res.*, *112*, D12S08, doi:10.1029/2006JD007747.

Houghton, J., G. Jenkins, and J. Ephraums (Eds.) (1990), *Scientific Assessment of Climate Change; Contribution of Working Group I*, Cambridge: Cambridge University Press.

Houghton, J. T., Y. Ding, D. J. Griggs, M. Noguer, P. J. van der Linden, X. Dai, K. Maskell, and C. A. Johnson (Eds.) (2001), *Climate Change 2001: The Scientific Basis, Contribution of Working Group I to the Third Assessment Report of the Intergovernmental Panel on Climate Changes*, Cambridge: Cambridge University Press.

Houghton, R. A. (2003), Revised estimates of the annual net flux of carbon to the atmosphere from changes in land use and land management 1850-2000, *Tellus B*, *55*, 378–390.

Houweling, S., F. Dentener, and J. Lelieveld (1998), The impact of non-methane hydrocarbon compounds on tropospheric photochemistry, *J. Geophys. Res.*, *103*, 10,673–10,696.

Hoyle, C. R., T. Berntsen, G. Myhre, and I. S. A. Isaksen (2007), Secondary organic aerosol in the global aerosol—chemical transport model Oslo CTM2, *Atmos. Chem. Phys.*, *7*, 5675–5644.

Huo, H., M. Wang, C. Bloyd, and V. Putsche (2008), Life-cycle assessment of energy and greenhouse gas effects of soybean-derived biodiesel and renewable

fuels, *Tech. Rep. ANL/ESD/08-2*, Argonne National Laboratory, Energy Systems Division.

Huo, H., Y. Wu, and M. Wang (2009), Total versus urban: Well-to-wheels assessment of criteria pollutant emissions from various vehicle/fuel systems, *Atmos. Environ.*, *43*, 1796–1804.

Hurtt, G. C., S. Frolking, M. G. Fearon, B. Moore, E. Shevliakova, S. Malyshev, S. W. Pacala, and R. A. Houghton (2006), The underpinnings of land-use history: three centuries of global gridded land-use transitions, wood-harvest activity, and resulting secondary lands, *Global Change Biol.*, *12*, 1208–1229.

International Energy Agency (2007), *World Energy Outlook 2007*, Paris: OECD/IEA.

International Energy Agency (2008), *Key World Energy Statistics*, Paris: OECD/IEA.

Jacob, D. J., L. W. Horowitz, J. W. Munger, B. G. Heikes, R. R. Dickerson, R. S. Artz, and W. C. Keene (1995), Seasonal transition from NO_x to hydrocarbon-limited conditions for ozone production over the eastern United States in September, *J. Geophys. Res.*, *100*, 9315–9324.

Jacobson, M. (2007), Effects of ethanol (E85) versus gasoline vehicles on cancer and mortality in the united states, *Environ. Sci. Technol.*, *41*, 4150–4157.

Jaeglé, L., et al. (2004), Satellite mapping of rain-induced nitric oxide emissions from soils, *J. Geophys. Res.*, *109*, D21,310, doi:10.1029/2004JD004787.

Jain, A. K., and X. Yang (2005), Modeling the effects of two different land cover change data sets on the carbon stocks of plants and soils in concert with co2 and climate change, *Global Biogeochem. Cycles*, *19*, GB2015, doi: 10.1029/2004GB002349.

Jain, A. K., Z. Tao, X. Yang, and C. Gillespie (2006), Estimates of global biomass burning emissions for reactive greenhouse gases (CO, NMHCs, and NO_x) and CO_2, *J. Geophys. Res.*, *111*, D06,304, doi:10.1029/2005JD006237.

Jenkin, M. E., and K. C. Clemitshaw (2000), Ozone and other secondary photochemical pollutants: Chemical processes governing their formation in the planetary boundary layer, *Atmos. Environ.*, *34*, 2499–2527.

Jenkin, M. E., S. M. Saunders, and M. J. Pilling (1997), The tropospheric degradation of volatile organic compounds: A protocol for mechanism development, *Atmos. Environ.*, *31*, 81–104.

Jerrett, M., R. T. Burnett, I. Pope, C. Arden, K. Ito, G. Thurston, D. Krewski, Y. Shi, E. Calle, and M. Thun (2009), Long-term ozone exposure and mortality, *N. Engl. J. Med.*, *360*, 1085–1095.

Jiang, X., C. Wiedinmyer, F. Chen, Z. Yang, and J. C. Lo (2008), Predicted impacts of climate and land use change on surface ozone in the Houston, Texas, areas, *J. Geophys. Res.*, *113*, D20,312, doi:10.1029/2008JD009820.

Jöckel, P., et al. (2006), The atmospheric chemistry general circulation model ECHAM5/MESSy 1: consistent simulation of ozone from the surface to the mesosphere, *Atmos. Chem. Phys.*, *6*, 5067–5104.

Johansson, T., H. Kelly, A. Reddy, and R. Williams (1993), *Renewable Energy: Sources for Fuels and Electricity*, chap. A renewables-intensive global energy scenario (appendix to Chapter 1), Washington, DC: Island Press.

Johns, T. C., R. E. Carnell, J. F. Crossley, J. M. Gregory, J. F. B. Mitchell, C. A. Senior, S. F. B. Tett, and R. A. Wood (1997), The second Hadley Centre coupled ocean-atmosphere GCM: Model description, spinup and validation, *Climate Dyn.*, *13*, 103–134.

Johnson, C. E., W. J. Collins, D. S. Stevenson, and R. G. Derwent (1999), Relative roles of climate and emissions changes on future tropospheric oxidant concentrations, *J. Geophys. Res.*, *104*, 18,631–18,645.

Jones, C. A., and R. A. Rasmussen (1975), Production of isoprene by leaf tissue, *Plant Physiol.*, *55*, 982–987.

Joshi, M., J. Gregory, M. Webb, D. Sexton, and T. Johns (2008), Mechanisms for the land/sea warming contrast exhibited by simulations of climate change, *Climate Dynamics*, *30*, 455–465.

Junkermann, W., J. Hacker, T. Lyons, and U. Nair (2009), Land use change suppresses precipitation, *Atmos. Chem. Phys.*, *9*, 6531–6539.

Kanakidou, M., et al. (2005), Organic aerosol and global climate modelling: A review, *Atmos. Chem. Phys.*, *5*, 1053–1123.

Karavalakis, G., S. Stournas, and E. Bakeas (2009), Effects of diesel/biodiesel blends on regulated and unregulated pollutants from a passenger vehicle operated over the european and the athens driving cycles, *Atmos. Environ.*, *43*, 1745–1752.

Karl, T., A. Guenther, A. Turnipseed, G. Tyndall, P. Artaxo, and S. Martin (2009), Rapid formation of isoprene photo-oxidation products observed in amazonia, *Atmos. Chem. Phys.*, *9*, 7753–7767.

Kasibhatla, P. S. (1993), NO_y from sub-sonic aircraft emissions: A global three-dimensional model study, *Geophys. Res. Lett.*, *20*, 1707–1710.

Keenan, T., . Niinemets, S. Sabate, C. Gracia, and J. Peuelas (2009), Process based inventory of isoprenoid emissions from european forests: model comparisons, current knowledge and uncertainties, *Atmos. Chem. Phys.*, *9*, 4053–4076.

Kesselmeier, J., and M. Staudt (1999), Biogenic volatile organic compounds

(VOC): An overview of emission, physiology and ecology, *J. Atmos. Chem.*, *33*, 23–88.

Klein Goldewijk, K. (2001), Estimating global land use change over the past 300 years: the hyde database, *Global Biogeochem. Cycles*, *15*, 417–433.

Knothe, G., C. A. Sharp, and T. W. Ryan (2006), Exhaust emissions of biodiesel, petrodiesel, neat methyl esters, and alkanes in a new technology engine, *Energ. Fuels*, *20*, 403–408.

Koc, M., Y. Sekmen, T. Topgul, and H. S. Yucesu (2009), The effects of ethanol-unleaded gasoline blends on engine performance and exhaust emissions in a spark-ignition engine, *Renew. Energ.*, *34*, 2101–2106.

Kuhn, U., et al. (2007), Isoprene and monoterpene fluxes from Central Amazonian rainforest inferred from tower-based and airborne measurements, and implications on the atmospheric chemistry and the local carbon budget, *Atmos. Chem. Phys.*, *7*, 2855–2879.

Kuzma, J., and R. Fall (1993), Leaf isoprene emission rate is dependent on leaf development and the level of isoprene synthase, *Plant Physiol.*, *101*, 435–440.

Lamb, B., A. Guenther, D. Gay, and H. Westberg (1987), A national inventory of biogenic hydrocarbon emissions, *Atmos. Environ.*, *21*, 1695–1705.

Lamptey, B. L., E. J. Barron, and D. Pollard (2005), Simulation of the relative impact of land cover and carbon dioxide to climate change from 1700 to 2100, *J. Geophys. Res.*, *110*, D20103, doi:10.1029/2005JD005916.

Lapola, D. M., M. D. Oyama, and C. A. Nobre (2009), Exploring the range of climate biome projections for tropical south america: The role of CO_2 fertilization and seasonality, *Global Biogeochem. Cycles*, *23*, GB3003, doi: 10.1029/2008GB003357.

Lapuerta, M., O. Armas, and J. Rodrguez-Fernndez (2008), Effect of biodiesel fuels on diesel engine emissions, *Prog. Energ. Combust.*, *34*, 198–223.

Lardon, L., A. Helias, B. Sialve, J.-P. Steyer, and O. Bernard (2009), Life-cycle assessment of biodiesel production from microalgae, *Environ. Sci. Technol.*, *43*, 6475–6481.

Lathière, J., D. A. Hauglustaine, A. D. Friends, N. De Noblet-Ducoudré, N. Viovy, and G. A. Folberth (2006), Impact of climate variability and land use changes on global biogenic volatile organic compound emissions, *Atmos. Chem. Phys.*, *6*, 2129–2146.

Lathière, J., C. Hewitt, and D. Beerling (2009), Sensitivity of isoprene emissions from the terrestrial biosphere to 20th century changes in atmospheric co concentration, climate and land use, *Global Biogeochem. Cycles*, *in press.*

Lathière, J. A., D. A. Hauglustaine, N. De Noblet-Ducoudré, G. Krinner, and G. A. Folberth (2005), Past and future changes in biogenic volatile organic compound emissions simulated with a global dynamic vegetation model, *Geophys. Res. Lett.*, *32*, L20,818, doi:10.1029/2005GL024164.

Law, K. S., and J. A. Pyle (1993a), Modeling trace gas budgets in the troposphere 1. Ozone and odd nitrogen, *J. Geophys. Res.*, *98*, 18,377–18,400.

Law, K. S., and J. A. Pyle (1993b), Modeling trace gas budgets in the troposphere 2. CH_4 and CO, *J. Geophys. Res.*, *98*, 18,401–18,412.

Law, K. S., P. H. Plantevin, D. E. Shallcross, H. J. Rogers, J. A. Pyle, C. Grouhel, V. Thouret, and A. Marenco (1998), Evaluation of modeled O_3 using Measurement of Ozone by Airbus In-Service Aircraft (MOZAIC) data, *J. Geophys. Res.*, *103*, 25,721–25,737.

Lelieveld, J., P. J. Crutzen, and F. J. Dentener (1998), Changing concentration, lifetime and climate forcing of atmospheric methane, *Tellus B*, *50*, 128–150.

Lelieveld, J., et al. (2008), Atmospheric oxidation capacity sustained by a tropical forest, *Nature*, *452*, 737–740.

Lerdau, M., and D. Gray (2003), Ecology and evolution of light-dependent and light-independent phytogenic volatile organic carbon, *New Phytol.*, *157*, 199–211.

Levis, S., C. Wiedinmyer, G. B. Bonan, and A. Guenther (2003), Simulating biogenic volatile organic compound emissions in the Community Climate System Model, *J. Geophys. Res.*, *108*, D21,4659, doi:10.1029/2002JD003203.

Levy II, H. (1971), Normal atmosphere: Large radical and formaldehyde concentrations predicted, *Science*, *173*, 141–143.

Levy II, H., W. J. Moxim, A. A. Klonecki, and P. S. Kasibhatla (1999), Simulated tropospheric NO_x : Its evaluation, global distribution and individual source contributions, *J. Geophys. Res.*, *104*, 26,279–26,306.

Li, D., and K. P. Shine (1995), A 4-dimensional ozone climatology for UGAMP models, *UGAMP Internal Report No. 35*, United Kingdom University Global Atmospheric Modelling Programme, Reading, UK.

Liao, H., W.-T. Chen, and J. H. Seinfeld (2006), Role of climate change in global predictions of future tropospheric ozone and aerosols, *J. Geophys. Res.*, *111*, D12304, doi:10.1029/2005JD006852.

Lin, C. Y. C., D. J. Jacob, and A. M. Fiore (2001), Trends in exceedances of the ozone air quality standard in the continental united states, 1980-1998, *Atmos. Environ.*, *35*, 3217–3228.

Lin, J.-T., K. O. Patten, K. Hayhoe, X.-Z. Liang, and D. J. Wuebbles (2008), Effects of future climate and biogenic emissions changes on surface ozone over the United States and China, *J. Appl. Meteor. Climatol.*, *47*, 1888–1909.

Lin, Y., and S. Tanaka (2006), Ethanol fermentation from biomass resources: current state and prospects, *Appl. Microbio. Biot.*, *69*, 627–642.

Lindinger, W., A. Hansel, and A. Jordan (1998), On-line monitoring of volatile organic compounds at pptv levels by means of proton-transfer-reaction mass spectrometry (PTR-MS) medical applications, food control and environmental research, *Int. J. Mass Spectrom. Ion Processes*, *173*, 191–241.

Liu, S. C., M. Trainer, F. C. Fehsenfeld, D. D. Parrish, E. J. Williams, D. W. Fahey, G. Hübler, and P. C. Murphy (1987), Ozone production in the rural troposphere and the implications for regional and global ozone distributions, *J. Geophys. Res.*, *92*, 4191–4207.

Logan, B. A., R. K. Monson, and M. J. Potosnak (2000), Biochemistry and physiology of foliar isoprene production, *Trends Plant Sci.*, *5*, 477–481.

Logan, J. A. (1999), An analysis of ozonesonde data for the troposphere: Recommendations for testing 3-D models and development of a gridded climatology for tropospheric ozone, *J. Geophys. Res.*, *104*, 16,115–16,150.

Logan, J. A., M. J. Prather, S. C. Wolfsy, and M. B. McElroy (1981), Tropospheric chemistry: A global perspective, *J. Geophys. Res.*, *86*, 7210–7254.

Long, S. P., E. A. Ainsworth, A. D. Leakey, and P. B. Morgan (2005), Global food insecurity. treatment of major food crops with elevated carbon dioxide or ozone under large-scale fully open-air conditions suggests recent models may have overestimated future yields, *Phil. Trans. R. Soc. B*, *360*, 2011–2020.

Loreto, F., and T. D. Sharkey (1990), A gas-exchange study of photosynthesis and isoprene emission in quercus-rubra l, *Planta*, *182*, 523–531.

Loreto, F., M. Mannozzi, C. Maris, P. Nascetti, F. Ferranti, and S. Pasqualini (2001), Ozone quenching properties of isoprene and its antioxidant role in leaves, *Plant Physiol.*, *126*, 993–1000.

Loveland, T. R., B. C. Reed, J. F. Brown, D. O. Ohlen, Z. Zhu, L. Yang, and J. W. Merchant (2000), Development of a global land cover characteristics database and IGBP DISCover from 1 km AVHRR data, *Int. J. Remote Sens.*, *21*, 1303–1330.

Lynch, P. (2008), The origins of computer weather prediction and climate modeling, *Journal of Computational Physics*, *227*, 3431–3444.

Ma, F., and M. A. Hanna (1999), Biodiesel production: a review, *Bioresource Technol.*, *70*, 1–15.

MacLean, H. L., and L. B. Lave (2003), Evaluating automobile fuel/propulsion system technologies, *Prog. Energ. Combust.*, *29*, 1–69.

Martin, M. J., C. M. Stirling, S. W. Humphries, and S. P. Long (2000), A process-based model to predict the effects of climatic change on leaf isoprene emission rates, *Ecol. Model.*, *131*, 161–174.

Matthes, S., V. Grewe, R. Sausen, and G.-J. Roelofs (2007), Global impact of road traffic emissions on tropospheric ozone, *Atmos. Chem. Phys.*, *7*, 1707–1718.

McCormick, R. L., M. S. Graboski, T. L. Alleman, A. M. Herring, and K. S. Tyson (2001), Impact of biodiesel source material and chemical structure on emissions of criteria pollutants from a heavy-duty engine, *Environ. Sci. Technol.*, *35*, 1742–1747.

Meleux, F., F. Solmon, and F. Giorgi (2007), Increase in summer european ozone amounts due to climate change, *Atmos. Environ.*, *41*, 7577–7587.

Mickley, L. J., D. J. Jacob, B. D. Field, and D. Rind (2004), Effects of future climate change on regional air pollution episodes in the United States, *Geophys. Res. Lett.*, *31*, L24,103, doi:10.1029/2004GL021216.

Millet, D. B., D. J. Jacob, K. F. Boersma, T.-M. Fu, T. P. Kurosu, K. Chance, C. L. Heald, and A. Guenther (2008), Spatial distribution of isoprene emissions from

North America derived from formaldehyde column measurements by the OMI satellite sensor, *J. Geophys. Res.*, *113*, D02,307, doi:10.1029/2007JD008950.

Mills, G., A. Buse, B. Gimeno, V. Bermejo, M. Holland, L. Emberson, and H. Pleijel (2007), A synthesis of aot40-based response functions and critical levels of ozone for agricultural and horticultural crops, *Atmos. Environ.*, *41*, 2630–2643.

Milt, A., A. Milano, S. Garivait, and R. Kamens (2009), Effects of 10substitution on ground level ozone formation in bangkok, thailand, *Atmospheric Environment*, *43*, 5962–5970.

Minerallwirtschaftsverband (2006), Mwv-prognose 2025 fr die bundesrepublik deutschland, *Tech. rep.*, Minerallwirtschaftsverband.

Monks, P. S. (2000), A review of the observations and origins of the spring ozone maximum, *Atmos. Environ.*, *34*, 3545–3561.

Monson, R. K., and R. Fall (1989), Isoprene emission from aspen leaves: Influence of the environment and relation to photosynthesis and phytorespiration, *Plant Physiol.*, *90*, 267–274.

Monyem, A., and J. H. Van Gerpen (2001), The effect of biodiesel oxidation on engine performance and emissions, *Biomass and Bioenerg.*, *20*, 317–325.

Moreira, J. R. (2000), Sugarcane for energy—recent results and progress in brazil, *Energy for Sustainable Development*, *4*, 43–54.

Moreira, R. (2006), Global biomass energy potential, *Mitigation and Adaptation Strategies for Global Change*, *11*, 313–333.

Morgenstern, O., P. Braesicke, M. M. Hurwitz, F. M. O'Connor, A. C. Bushell, C. E. Johnson, and J. A. Pyle (2008), The World Avoided by the Montreal Protocol, *Geophys. Res. Lett.*, *35*, L16,811, doi:10.1029/2008GL034590.

Morgenstern, O., P. Braesicke, F. M. O'Connor, A. C. Bushell, C. E. Johnson, S. M. Osprey, and J. A. Pyle (2009), Evaluation of the new UKCA climate-composition model Part I: The stratosphere, *Geosci. Model Dev.*, *2*, 43–57.

Moxim, W. J., H. Levy II, and P. S. Kasibhatla (1996), Simulated global tropospheric PAN: Its transport and impact on NO_x, *J. Geophys. Res.*, *101*, 12,621–12,638.

Müller, C., B. Eickhout, S. Zaehle, A. Bondeau, W. Cramer, and W. Lucht (2007), Effects of changes in CO_2, climate, and land use on the carbon balance of the land biosphere during the 21st century, *J. Geophys. Res.*, *112*, G02,032, doi: 10.1029/2006JG000388.

Müller, J.-F. (1992), Geographical distribution and seasonal variation of surface emissions and deposition velocities of atmospheric trace gases, *J. Geophys. Res.*, *97*, 3787–3804.

Müller, J.-F., and G. Brasseur (1995), IMAGES: A three-dimensional chemical transport model of the global troposphere, *J. Geophys. Res.*, *100*, 16,445–16,490.

Murphy, D. M., and D. W. Fahey (1994), An estimate of the flux of stratospheric reactive nitrogen and ozone into the troposphere, *J. Geophys. Res.*, *99*, 5325–5332.

Naik, V., C. Delire, and D. J. Wuebbles (2004), Sensitivity of global biogenic isoprenoid emissions to climate variability and atmospheric CO_2, *J. Geophys. Res.*, *109*, D06301, doi:10.1029/2003JD004236.

Nakicenovic, N., et al. (2000), *IPCC Special Report on Emissions Scenarios*, Cambridge: Cambridge University Press.

Niemeier, U., C. Granier, L. Kornblueh, S. Walters, and G. Brasseur (2006), Global

impact of road traffic on atmospheric chemical composition and on ozone climate forcing, *J. Geophys. Res.*, *111*, D09301, doi:10.1029/2005JD006407.

Niinemets, U., J. D. Tenhunen, P. C. Harley, and R. Steinbrecher (1999), A model of isoprene emission based on energetic requirements for isoprene synthesis and leaf photosynthetic properties for *Liquidambar* and *Quercus*, *Plant Cell Environ.*, *22*, 1319–1335.

Nolte, C. G., A. B. Gilliland, C. Hogrefe, and L. J. Mickley (2008), Linking global to regional models to assess future climate impacts on surface ozone levels in the United States, *J. Geophys. Res.*, *113*, D14,307, doi:10.1029/2007JD008497.

O'Connor, F. M., C. E. Johnson, O. Morgenstern, and W. J. Collins (2009), Interactions between tropospheric chemistry and climate model temperature and humidity biases, *Geophys. Res. Lett.*, *36*, L16,801, doi:10.1029/2009GL039152.

Office of the Governor of California (18 January 2007), *Governor's Executive Order S-01-07*.

Ohlrogge, J., D. Allen, B. Berguson, D. DellaPenna, Y. Shachar-Hill, and S. Stymne (2009), Driving on biomass, *Science*, *324*, 1019–1020.

Olivier, J., and J. Berdowski (2001), *The Climate System*, chap. Global emissions sources and sinks, pp. 33–78, Leiden, The Netherlands: A.A. Balkema Publishers/Swets & Zeitlinger Publishers.

One Hundred Tenth Congress of the United States of America (4 January, 2007), HR6: Energy Independence and Security Act.

OP3 (Accessed 11 November, 2009), Online: http://www.es.lancs.ac.uk/op3/.

Pacala, S., and R. Socolow (2004), Stabilization Wedges: Solving the Climate Problem for the Next 50 Years with Current Technologies, *Science*, *305*, 968–972.

Palmer, P. I., D. J. Jacob, A. M. Fiore, R. V. Martin, K. Chance, and T. P. Kurosu (2003), Mapping isoprene emissions over North America using formaldehyde column observations from space, *J. Geophys. Res.*, *108*, D64,180.

Pandian, S., S. Gokhale, and A. K. Ghoshal (2009), Evaluating effects of traffic and vehicle characteristics on vehicular emissions near traffic intersections, *Transport. Res. D–Tr. E.*, *14*, 180–196.

Park, R. J., K. E. Pickering, D. J. Allen, G. L. Stenchikov, and M. S. Fox-Rabinovitz (2004), Global simulation of tropospheric ozone using the University of Maryland Chemical Transport Model (UMD-CTM): 1 Model description and evaluation, *J. Geophys. Res.*, *109*, D09301, doi:10.1029/2003JD004266.

Patterson, T., R. Dinsdale, and S. Esteves (2008), Review of energy balances and emissions associated with biomass-based transport fuels relevant to the united kingdom context, *Energy & Fuels*, *22*, 3506–3512.

Paulot, F., J. D. Crounse, H. G. Kjaergaard, A. Kurten, J. M. St. Clair, J. H. Seinfeld, and P. O. Wennberg (2009), Unexpected epoxide formation in the gas-phase photooxidation of isoprene, *Science*, *325*, 730–733.

Pearson, G., F. Davies, and C. Collier (2009), Remote sensing of the tropical rain forest boundary layer using pulsed doppler lidar, *Atmos. Chem. Phys.*, in prep.

Peh, K. S.-H., N. S. Sodhi, J. de Jong, C. H. Sekercioglu, C. A.-M. Yap, and S. L.-H. Lim (2006), Conservation value of degraded habitats for forest birds in southern peninsular Malaysia, *Divers. Distrib.*, *12*, 572–581.

Pfister, G. G., L. K. Emmons, P. G. Hess, J.-F. Lamarque, J. J. Orlando, S. Walters, A. Guenther, P. I. Palmer, and P. J. Lawrence (2008a), Contribution of isoprene to chemical budgets: A model tracer study with the NCAR CTM MOZART-4, *J. Geophys. Res.*, *113*, D05,308, doi:10.1029/2007JD008948.

Pfister, G. G., L. K. Emmons, P. G. Hess, J.-F. Lamarque, A. M. Thompson, and J. E. Yorks (2008b), Analysis of the summer 2004 ozone budget over the united states using intercontinental transport experiment ozonesonde network study (ions) observations and model of ozone and related tracers (MOZART-4) simulations, *J. Geophys. Res.*, *113*, D23,306, doi:10.1029/2008JD010190.

Pierce, T., C. Geron, L. Bender, R. Dennis, G. Tonnesen, and A. Guenther (1998), Influence of increased isoprene emissions on regional ozone modeling, *J. Geophys. Res.*, *103*, 25,611–25,630.

Pin Koh, L., and D. S. Wilcove (2007), Cashing in palm oil for conservation (commentary), *Nature*, *448*, 993–994.

Pinzi, S., I. L. Garcia, F. J. Lopez-Gimenez, M. D. Luque de Castro, G. Dorado, and M. P. Dorado (2009), The ideal vegetable oil-based biodiesel composition: A review of social, economical and technical implications, *Energy & Fuels*, *23*, 2325–2341.

Pitman, A. J., et al. (2009), Uncertainties in climate responses to past land cover change: First results from the LUCID intercomparison study, *Geophys. Res. Lett.*, *36*, L14,814, doi:10.1029/2009GL039076.

Platzman, G. W. (1979), The ENIAC computations of 1950–gateway to numerical weather prediction, *Bull. Am. Meteor. Soc.*, *60*, 302–312.

POET Inventory (Accessed 21 October, 2009), Online: http://www.aero.jussieu.fr/projet/ACCENT/POET.php.

Pongratz, J., C. Reick, T. Raddatz, , and M. Claussen (2008), A reconstruction of global agricultural areas and land cover for the last millennium, *Global Biogeochem. Cycles*, *22*, GB3018, doi:10.1029/2007GB003153,2008.

Pongratz, J., T. Raddatz, C. H. Reick, M. Esch, and M. Claussen (2009), Radiative

forcing from anthropogenic land cover change since a.d. 800, *Geophys. Res. Lett.*, *36*, L02,709, doi:10.1029/2008GL036394.

Pöschl, U., R. von Kulhmann, N. Poisson, and P. J. Crutzen (2000), Development and intercomparison of condensed isoprene oxidation mechanisms for global atmospheric modelling, *J. Atmos. Chem.*, *37*, 29–52.

Possell, M., C. N. Hewitt, and D. J. Beerling (2005), The effects of glacial atmospheric CO_2 concentrations and climate on isoprene emissions by vascular plants, *Global Change Biol.*, *11*, 60–69.

Potter, C. S., S. E. Alexander, J. C. Coughlan, and S. A. Klooster (2001), Modeling biogenic emissions of isoprene: Exploration of model drivers, climate control algorithms and use of global satellite observations, *Atmos. Environ.*, *35*, 6151–6165.

Prather, M., et al. (2001), *Climate Change 2001: The Scientific Basis, Contribution of Working Group I to the Third Assessment Report of the Intergovernmental Panel on Climate Change*, chap. Atmospheric chemistry and greenhouse gases, pp. 239–287, Cambridge: Cambridge University Press, Cambridge, UK.

Price, C., and D. Rind (1992), A simple lightning parameterization for calculating global lightning distributions, *J. Geophys. Res.*, *97*, 9919–9933.

Priestley, A. (1993), A quasi-conservative version of the semi-lagrangian advection scheme, *Mon. Weather Rev.*, *121*, 621–629.

Quaife, T., S. Quegan, M. Disney, P. Lewis, M. Lomas, and F. I. Woodward (2008), Impact of land cover uncertainties on estimates of biospheric carbon fluxes, *Global Biogeochem. Cycles*, *22*, GB4016, doi:10.1029/2007GB003097.

Racherla, P. N., and P. J. Adams (2006), Sensitivity of global tropospheric ozone and fine particulate matter concentrations to climate change, *J. Geophys. Res.*, *111*, D24,103, doi:10.1029/2005JD006939.

Racherla, P. N., and P. J. Adams (2008), The response of surface ozone to climate change over the eastern United States, *Atmos. Chem. Phys.*, *8*, 871–885.

Ramankutty, N., and J. A. Foley (1999), Estimating historical changes in global land cover: Croplands from 1700 to 1992, *Global Biogeochem. Cycles*, *13*, 997–1027.

Ramankutty, N., C. Delire, and P. Snyder (2006), Feedbacks between agriculture and climate: An illustration of the potential unintended consequences of human land use activities, *Global Planet. Change*, *54*, 79–93.

Rasmussen, R., and C. Jones (1973), Emission isoprene from leaf discs of hamamelis, *Phytochemistry*, *12*, 15–19.

Rasmussen, R. A. (1970), Isoprene: Identified as a forest-type emission to the atmosphere, *Environ. Sci. Technol.*, *4*, 667–671.

Rasmussen, R. A., and M. A. Khalil (1988), Isoprene over the Amazon basin, *J. Geophys. Res.*, *93*, 1417–1421.

Rasmussen, R. A., and F. W. Went (1965), Volatile organic carbon of plant origin in the atmosphere, *Proc. Natl. Acad. Sci. USA*, *53*, 215–220.

Rayner, N. A., D. E. Parker, E. B. Horton, C. K. Folland, L. V. Alexander, E. C. Rowell, D. P.and Kent, and J. Kaplan (2003), A global analyses of sea surface temperature, sea ice, and night marine air temperature since the late nineteenth century, *J. Geophys. Res.*, *108*, D14,4407, doi:10.1029/2002JD002670.

Ren, X., et al. (2008), HO_x chemistry during INTEX-A 2004: Observation, model calculation, and comparison with previous studies, *J. Geophys. Res.*, *113*, D05,310, doi:10.1029/2007JD009166.

Renewable Fuels Agency (Accessed 21 October, 2009), RTFO targets, Online: http://www.renewablefuelsagency.org/index.cfm.

Renewable Fuels Association (Accessed 15 September, 2009), Ethanol industry statistics, Online: http://www.ethanolrfa.org/industry/statistics/.

Riahi, K., A. Grbler, and N. Nakicenovic (2007), Scenarios of long-term socio-economic and environmental development under climate stabilization, *Technol. Forecast. Soc.*, *74*, 887–935.

Richardson, L. (1922), *Weather Prediction by Numerical Process*, Cambridge: Cambridge University Press.

Rinne, H. J. I., A. B. Guenther, J. P. Greenberg, and P. C. Harley (2002), Isoprene and monoterpene fluxes measured above amazonian rainforest and their dependence on light and temperature, *Atmos. Environ.*, *36*, 2421–2426.

Roelofs, G.-J., and J. Lelieveld (1995), Distribution and budget of O_3 in the troposphere calculated with a chemical general circulation model, *J. Geophys. Res.*, *100*, 20,983–20,998.

Roelofs, G.-J., and J. Lelieveld (2000), Tropospheric ozone simulation with a chemistry-general circulation model: Influence of higher hydrocarbon chemistry, *J. Geophys. Res.*, *105*, 22,697–22,712.

Romm, J. (2006), The car and fuel of the future, *Energy Policy*, *34*, 2609–2614.

Rosenstiel, T. N., M. J. Potosnak, K. L. Griffin, R. Fall, and R. K. Monson (2003), Increased CO_2 uncouples growth from isoprene emission in an agriforest ecosystem, *Nature*, *421*, 256–259.

Rowe, R. L., N. R. Street, and G. Taylor (2009), Identifying potential environmental impacts of large-scale deployment of dedicated bioenergy crops in the UK, *Renew. Sust. Energ. Rev.*, *13*, 271–290.

Ruppert, L., and K. Heinz-Becker (2000), A product study of the OH radical-initiated oxidation of isoprene: Formation of C_5-unsaturated diols, *Atmos. Environ.*, *34*, 1529–1542.

Sanadze, G. (1964), Light-dependent excretion of isoprene by plants, *Photosynthesis Research*, *2*, 701–707.

Sanadze, G. A. (1957), The nature of gaseous substances emitted by leaves of *Robina pseudoacacia*, *Soobshch. Akad. Nauk Gruz. SSR*, *19*, 83–86.

Sanderson, M. G., C. D. Jones, W. J. Collins, C. E. Johnson, and R. G. Derwent (2003), Effect of climate change on isoprene emissions and surface ozone levels, *Geophys. Res. Lett.*, *30*, 18,1936, doi:10.1029/2003GL017642.

Saunders, S. M., M. E. Jenkin, R. G. Derwent, and M. J. Pilling (1997), World wide web site of a master chemical mechanism (MCM) for use in tropospheric chemistry models, *Atmos. Environ.*, *31*, 1249–1249.

Saunders, S. M., M. E. Jenkin, R. G. Derwent, and M. J. Pilling (2003), Protocol for the development of the Master Chemical Mechanism, MCM v3 (Part a): Tropospheric degradation of non-aromatic volatile organic compounds, *Atmos. Chem. Phys.*, *3*, 161–180.

Savage, N. H., K. S. Law, J. A. Pyle, A. Richter, H. Nuss, and J. P. Burrows (2004), Using GOME NO_2 satellite data to examine regional differences in TOMCAT model performance, *Atmos. Chem. Phys.*, *4*, 1895–1912.

Scaife, A. A., N. Butchart, C. D. Warner, and R. Swinbank (2002), Impact of a spectral gravity wave parameterization on the stratosphere in the met office unified model, *J. Atmos. Sci.*, *59*, 1473–1489.

Schiermeier, Q., J. Tollefson, T. Scully, A. Witze, and O. Morton (2008), Energy alternatives: Electricity without carbon, *Nature*, *454*, 816–823.

Schilling, K. E., M. K. Jha, Zhang, You-Kuan, P. W. Gassman, and C. F. Wolter (2008), Impact of land use and land cover change on the water balance of a large agricultural watershed: Historical effects and future directions, *Water Resour. Res.*, *44*, W00A09, doi:10.1029/2007WR006644.

Schmidt, G. A., et al. (2006), Present-day atmospheric simulations using GISS ModelE: Comparison to in situ, satellite, and reanalysis data, *J. Climate*, *19*, 153–192.

Schumann, U., and H. Huntrieser (2007), The global lightning-induced nitrogen oxides source, *Atmos. Chem. Phys.*, *7*, 3823–3907.

Service, R. (2007), Cellulosic ethanol: Biofuel researchers prepare to reap a new harvest, *Science*, *315*, 1488 – 1491.

Service, R. F. (2009), ExxonMobil fuels Venter's efforts to run vehicles on algae-based oil, *Science*, *325*, 379.

Sharkey, T. D. (1996), Isoprene synthesis by plants and animals, *Endeavour*, *20*, 74–78.

Sharkey, T. D., and E. L. Singsaas (1995), Why plants emit isoprene, *Nature*, *374*, 769–769.

Shay, E. G. (1993), Diesel fuel from vegetable oils: Status and opportunities, *Biomass and Bioenergy*, *4*, 227–242.

Shepson, P. B., E. Mackay, and K. Muthuramu (1996), Henry's Law constants and removal processes for several atmospheric β-hydroxy alkyl nitrates, *Environ. Sci. Technol.*, *30*, 3618–3623.

Shevliakova, E., et al. (2009), Carbon cycling under 300 years of land use change: Importance of the secondary vegetation sink, *Global Biogeochem. Cycles*, *23*, GB2022, doi:10.1029/2007GB003176.

Shim, C., Y. Wang, Y. Choi, P. I. Palmer, D. S. Abbot, and K. Chance (2005), Constraining global isoprene emissions with Global Ozone Monitoring Experiment (GOME) formaldehyde column measurements, *J. Geophys. Res.*, *110*, D24301, doi:10.1029/2004JD005629.

Shindell, D., G. Faluvegi, A. Lacis, J. Hansen, R. Ruedy, and E. Aguilar (2006a), Role of tropospheric ozone increases in 20th-century climate change, *J. Geophys. Res.*, *111*, D08302, doi:10.1029/2005JD006348.

Shindell, D., J.-F. Lamarque, N. Unger, D. Koch, G. Faluvegi, S. Bauer, M. Ammann, J. Cofala, and H. Teich (2008), Climate forcing and air quality change due to regional emissions reductions by economic sector, *Atmos. Chem. Phys.*, *8*, 7101–7113.

Shindell, D. T., et al. (2006b), Multimodel simulations of carbon monoxide: Comparison with observations and projected near-future changes, *J. Geophys. Res.*, *111*, D19,306, doi:10.1029/2006JD007100.

Sillman, S. (1995), The use of NO_y, H_2O_2, and HNO_3 as indicators for ozone-NO_x-hydrocarbon sensitivity in urban locations, *J. Geophys. Res.*, *100*, 14,175–14,188.

Sillman, S. (1999), The relation between ozone, NO_x and hydrocarbons in urban and polluted rural environments, *Atmos. Environ.*, *33*, 1821–1845.

Sillman, S., and D. He (2002), Some theoretical results concerning O_3-NO_x-VOC chemistry and NO_x-VOC indicators, *J. Geophys. Res.*, *107*, D224,659, doi:10.1029/2001JD001123.

Sillman, S., and P. J. Samson (1995), Impact of temperature on oxidant photochemistry in urban, polluted rural and remote environments, *J. Geophys. Res.*, *100*, 11,497–11,508.

Sillman, S., and J. J. West (2009), Reactive nitrogen in mexico city and its relation to ozone-precursor sensitivity: results from photochemical models, *Atmos. Chem. Phys.*, *9*, 3477–3489.

Sillman, S., J. A. Logan, and S. C. Wofsy (1990), The sensitivity of ozone to

nitrogen oxides and hydrocarbons in regional ozone episodes, *J. Geophys. Res.*, *95*, 1837–1851.

Sims, R., A. Hastings, B. Schlamadinger, G. Taylor, and P. Smith (2006), Energy crops: current status and future prospects, *Global Change Biol.*, *12*, 2054–2076.

Sims, R., M. Taylor, J. Saddler, and W. Mabee (2008), From 1st- to 2nd-generation biofuel technologies: An overview of current industry and RD&D activities, *Tech. rep.*, International Energy Agency.

Sims, R. E., and R. N. Schock (Eds.) (2007), *Mitigation of Climate Change, Contribution of Working Group III to the Fourth Assessment Report of the Intergovernmental Panel on Climate Change*, chap. Energy Supply, pp. 251–322, Cambridge: Cambridge University Press.

Singh, H. B., and P. L. Hanst (1981), Peroxyacetyl nitrate (PAN) in the unpolluted atmosphere: An important reservoir for nitrogen oxides, *Geophys. Res. Lett.*, *8*, 941–944.

Sitch, S., V. Brovkin, W. von Bloh, D. van Vuuren, B. Eickhout, and A. Ganopolski (2005), Impacts of future land cover changes on atmospheric CO_2 and climate, *Global Biogeochem. Cycles*, *19*, GB2013, doi:10.1029/2004GB002311.

Solomon, B. D., and A. Banerjee (2006), A global survey of hydrogen energy research, development and policy, *Energy Policy*, *34*, 781–792.

Solomon, B. D., J. R. Barnes, and K. E. Halvorsen (2007a), Grain and cellulosic ethanol: History, economics, and energy policy, *Biomass and Bioenerg.*, *31*, 416–425.

Solomon, S., D. Qin, M. Manning, Z. Chen, M. Marquis, K. Averyt, M. Tignor, and H. Miller (Eds.) (2007b), *Climate Change 2007: The Physical Science Basis, Contribution of Working Group I to the Fourth Assessment Report of the*

Intergovernmental Panel on Climate Change, Cambridge: Cambridge University Press.

Sorteberg, A., and O. Hov (1996), Two parametrizations of the dry deposition exchange for SO_2 and NH_3 in a numerical model, *Atmos. Environ.*, *30*, 1823–1840.

Spivakovsky, C. M., et al. (2000), Three-dimensional climatological distribution of tropospheric OH: Update and evaluation, *J. Geophys. Res.*, *105*, 8931–8980.

Sprengnether, M., K. L. Demerjian, N. M. Donahue, and J. G. Anderson (2002), Product analysis of the OH oxidation of isoprene and 1,3-butadiene in the presence of NO, *J. Geophys. Res.*, *107*, D15,4268, doi:10.1029/2001JD000716.

Steiner, A. L., S. Tonse, R. C. Cohen, A. H. Goldstein, and R. A. Harley (2006), Influence of future climate and emissions on regional air quality in California, *J. Geophys. Res.*, *111*, D18,303, doi:10.1029/2005JD006935.

Steinkamp, J., L. N. Ganzeveld, W. Wilcke, and M. G. Lawrence (2009), Influence of modelled soil biogenic NO emissions on related trace gases and the atmospheric oxidizing efficiency, *Atmos. Chem. Phys.*, *9*, 2663–2677.

Stevenson, D., R. Doherty, M. Sanderson, C. Johnson, B. Collins, and D. Derwent (2005), Impacts of climate change and variability on tropospheric ozone and its precursors, *Faraday Discuss.*, *130*, 41–57.

Stevenson, D. S., C. E. Johnson, W. J. Collins, R. G. Derwent, and J. M. Edwards (2000), Future estimates of tropospheric ozone radiative forcing and methane turnoverthe impact of climate change, *Geophys. Res. Lett.*, *27*, 2073–2076.

Stevenson, D. S., et al. (2006), Multimodel ensemble simulations of present-day and near-future tropospheric ozone, *J. Geophys. Res.*, *111*, D08301, doi: 10.1029/2005JD006338.

Stott, P. A., G. S. Jones, J. A. Lowe, P. Thorne, C. Durman, T. C. Johns, and J.-C.

Thelen (2006), Transient climate simulations with the hadgem1 climate model: Causes of past warming and future climate change, *J. Climate*, *19*, 2763–2782.

Sustainable biofuels: prospects and challenges (2008), *Policy Document ISBN 978 0 85403 662 2*, The Royal Society.

Szopa, S., D. A. Hauglustaine, R. Vautard, and L. Menut (2006), Future global tropospheric ozone changes and impact on European air quality, *Geophys. Res. Lett.*, *33*, L14,805, doi:10.1029/2006GL025860.

Szybist, J. P., A. L. Boehman, J. D. Taylor, and R. L. McCormick (2005), Evaluation of formulation strategies to eliminate the biodiesel NO_x effect, *Fuel Process. Technol.*, *86*, 1109–1126.

Szybist, J. P., J. Song, M. Alam, and A. L. Boehman (2007), Biodiesel combustion, emissions and emission control, *Fuel Processing Technology*, *88*, 679–691.

Tagaris, E., K. Manomaiphiboon, K.-J. Liao, L. R. Leung, J.-H. Woo, S. He, P. Amar, and A. G. Russell (2007), Impacts of global climate change and emissions on regional ozone and fine particulate matter concentrations over the United States, *J. Geophys. Res.*, *112*, D14,312,, doi:10.1029/2006JD008262.

Talukdar, R. K., J. B. Burkholder, A.-M. Schmoltner, J. M. Roberts, R. R. Wilson, and A. R. Ravishankara (1995), Investigation of the loss processes for peroxyacetyl nitrate in the atmosphere: UV photolysis and reaction with OH, *J. Geophys. Res.*, *100*, 14,163–14,174.

Tao, Z., and A. K. Jain (2005), Modeling of global biogenic emissions for key indirect greenhouse gases and their response to atmospheric CO_2 increases and changes in land cover and climate, *J. Geophys. Res.*, *110*, D21309, doi:10.1029/2005JD005874.

Tao, Z., S. M. Larson, D. J. Wuebbles, A. Williams, and M. Caugh (2003), A summer simulation of biogenic contributions to ground-level ozone over

the continental United States, *J. Geophys. Res.*, *108*, D14,4404, doi:10.1029/2002JD002945.

Tao, Z., A. Williams, H.-C. Huang, M. Caughey, and X.-Z. Liang (2007), Sensitivity of U. S. surface ozone to future emissions and climate changes, *Geophys. Res. Lett.*, *34*, L08,811, doi:10.1029/2007GL029455.

Teyssèdre, H., et al. (2007), A new chemistry-climate tropospheric and stratospheric model MOCAGE-Climat: evaluation of the present-day climatology and sensitivity to surface processes, *Atmos. Chem. Phys.*, *7*, 5815–5860.

Thompson, A. M. (1992), The oxidizing capacity of the earth's atmosphere: Probable past and future changes, *Science*, *257*, 1157–1165.

Thompson, A. M., R. W. Stewart, M. A. Owens, and J. A. Herwehe (1989), Sensitivity of tropospheric oxidants to global chemical and climate change, *Atmos. Environ.*, *23*, 519–532.

Thompson, A. M., et al. (2003), Southern Hemisphere Additional Ozonesondes (SHADOZ) 1998-2000 tropical ozone climatology 2. Tropospheric variability and the zonal wave-one, *J. Geophys. Res.*, *108*, D2,8241, doi:10.1029/2002JD002241.

Tilman, D., J. Hill, and C. Lehman (2006), Carbon-Negative Biofuels from Low-Input High-Diversity Grassland Biomass, *Science*, *314*, 1598–1600.

Tilman, D., et al. (2009), Beneficial biofuels–the food, energy, and environment trilemma, *Science*, *325*, 270–271.

Tingey, D. T., M. Manning, L. C. Grothaus, and W. F. Burns (1979), The influence of light and temperature on isoprene emission rates from live oak, *Physiol. Plantarum*, *47*, 112–118.

Tingey, D. T., R. Evans, and M. Gumpertz (1981), Effects of environmental conditions on isoprene emission from live oak, *Planta*, *152*, 565–570.

Toenges-Schuller, N., et al. (2006), Global distribution pattern of anthropogenic nitrogen oxide emissions: Correlation analysis of satellite measurements and model calculations, *J. Geophys. Res.*, *111*, D05,312, doi:10.1029/2005JD006068.

Tribbia, J. J., and R. A. Anthes (1987), Scientific basis of modern weather prediction, *Science*, *237*, 493–499.

Turner, D. P., J. V. Baglio, A. G. Wones, D. Pross, R. Vong, B. D. McVeety, and D. L. Phillips (1991), Climate change and isoprene emissions from vegetation, *Chemosphere*, *23*, 37–56.

Turner, E. C., and W. A. Foster (2009), The impact of forest conversion to oil palm on arthropod abundance and biomass in Sabah, Malaysia, *J. Trop. Ecol.*, *25*, 23–30.

Unger, N., D. T. Shindell, D. M. Koch, M. Amann, J. Cofala, and D. G. Streets (2006), Influences of man-made emissions and climate changes on tropospheric ozone, methane, and sulfate at 2030 from a broad range of possible futures, *J. Geophys. Res.*, *111*, D12313, doi:10.1029/2005JD006518.

Unger, N., D. T. Shindell, and J. S. Wang (2009), Climate forcing by the on-road transportation and power generation sectors, *Atmos. Environ.*, *43*, 3077–3085.

United Kingdom Parliament (2007-2008 Session), Climate change bill, Available Online: http://services.parliament.uk/bills/2007-08/climatechangehl.html.

United Kingdom Statutory Instrument No. 3072 (26 October, 2007), Transport energy, sustainable and renewable fuels: The renewable transport fuel obligations order, London: The Stationery Office Limited.

United Nations Framework Convention on Climate Change (1992), Online: http://unfccc.int/essential_background/convention/background/items/1349.php.

United Nations Framework Convention on Climate Change (1997), Kyoto Protocol, Online: http://unfccc.int/essential_background/kyoto_protocol/items/1678.php.

United States Environmental Protection Agency (2002), A comprehensive analysis of biodiesel impacts on exhaust emissions, *Tech. Rep. EPA420-P-02-001*.

United States Environmental Protection Agency (2009), EPA proposes new regulations for the national renewable fuel standard program for 2010 and beyond, *Regulatory Annoucement EPA-420-F-09-023*, Office of Transportation and Air Quality.

U.S. Department of Energy: Energy efficiency and renewable energy (2009), States with renewable portfolio standards, Online: http://apps1.eere.energy.gov/states/maps/renewable_portfolio_states.cfm.

van der Werf, G., J. T. Randerson, G. J. Collatz, and L. Giglio (2003), Carbon emissions from fires in tropical and subtropical ecosystems, *Global Change Biol.*, *9*, 547–562.

van der Werf, G. R., J. T. Randerson, G. J. Collatz, L. Giglio, P. S. Kasibhatla, A. F. Arellano Jr., S. C. Olsen, and E. S. Kasischke (2004), Continental-scale partitioning of fire emissions during the 1997 to 2001 El Niño/La Niña period, *Science*, *303*, 73–76.

van Dingenen, R., F. J. Dentener, F. Raes, M. C. Krol, L. Emberson, and J. Cofala (2009), The global impact of ozone on agricultural crop yields under current and future air quality legislation, *Atmos. Environ.*, *43*, 604–618.

Vitousek, P. M., H. A. Mooney, J. Lubchenco, and J. M. Melillo (1997a), Human domination of earth's ecosystems, *Science*, *277*, 494–499.

Vitousek, P. M., J. D. Aber, R. W. Howarth, G. E. Likens, P. A. Matson, D. W.

Schindler, W. H. Schlesinger, and G. D. Tilman (1997b), Human alteration of the global nitrogen cycle: Sources and consequences, *Ecol. Appl.*, *7*, 737–750.

Voldoire, A., B. Eickhout, M. Schaeffer, J. F. Royer, and F. Chauvin (2007), Climate simulation of the twenty-first century with interactive land-use changes, *Clim. Dynam.*, *29*, 177–193.

von Kuhlmann, R., M. G. Lawrence, U. Pöschl, and P. J. Crutzen (2004), Sensitivities in the global scale modelling of isoprene, *Atmos. Chem. Phys.*, *4*, 1–17.

Wang, K.-Y., and D. E. Shallcross (2000), Modelling terrestrial biogenic isoprene fluxes and their potential impact on global chemical species using a coupled LSM-CTM model, *Atmos. Environ.*, *34*, 2909–2925.

Wang, M. (2009), The Greenhouse Gases, Regulated Emissions, and Energy Use in Transportation (GREET) Model, Online: http://www.transportation.anl.gov/modeling_simulation/GREET/.

Wang, M., M. W. Hong, and H. Huo (2007), Life-cycle energy and greenhouse gas emission impacts of different corn ethanol plant types, *Environ. Res. Let.*, *2*, 024,001.

Wang, M., M. Wu, H. Huo, and J. H. Liu (2008), Life-cycle energy use and greenhouse gas emission implications of Brazilian sugarcane ethanol simulated with the GREET model, *Int. Sugar J.*, *110*, 527.

Wayne, R. P. (2000), *Chemistry of Atmospheres*, third ed., Oxford: Oxford University Press, New York.

Webster, S., A. R. Brown, D. R. Cameron, and C. P. Jones (2003), Improvements to the representation of orography in the Met Office Unified Model, *Q. J. Roy. Meteor. Soc.*, *129*, 1989–2010, doi:10.1256/qj.02.133.

Weng, J.-K., X. Li, N. D. Bonawitz, and C. Chapple (2008), Emerging strategies of

lignin engineering and degradation for cellulosic biofuel production, *Curr. Opin. Biotech.*, *19*, 166–172.

Went, F. W. (1960), Organic matter in the atmosphere, and its possible relation to petroleum formation, *Proc. Natl. Acad. Sci. USA*, *46*, 212–221.

Wesely, M. L., and B. B. Hicks (2000), A review of the current status of knowledge on dry deposition, *Atmos. Environ.*, *34*, 2261–2282.

Wiedinmyer, C., A. Guenther, P. Harley, C. Hewitt, C. Geron, P. Artaxo, R. Steinbrecher, and R. Rasmussen (2004), *Emissions of Atmospheric Trace Compounds*, chap. Global organic emissions from vegetation, pp. 115 –170, Dordrecht, The Netherlands: Kluwer Academic Publishers.

Wiedinmyer, C., X. Tie, A. Guenther, R. Neilson, and C. Granier (2006), Future changes in biogenic isoprene emissions: How might they affect regional and global atmospheric chemistry?, *Earth Interactions*, *10*, Paper No. 3, doi: 10.1175/EI174.1.

Wild, O. (2007), Modelling the global tropospheric ozone budget: exploring the variability in current models, *Atmos. Chem. Phys.*, *7*, 2643–2660.

Wild, O., and M. J. Prather (2000), Excitation of the primary tropospheric chemical mode in a global three-dimensional model, *J. Geophys. Res.*, *105*, 24,647–24,660.

Wilkins, C. K., P. A. Clausen, P. Wolkoff, S. Larsen, M. Hammer, K. Larsen, V. Hansen, and G. D. Nielsen (2001), Formation of strong airway irritants in mixtures of isoprene/ozone and isoprene/ozone/nitrogen dioxide, *Environ. Health Persp.*, *109*, 937–941.

Wilkinson, M. J., R. K. Monson, N. Trahan, S. Lee, E. Brown, R. B. Jackson, H. W. Polley, P. A. Fay, and R. Fall (2009), Leaf isoprene emission rate as a function of atmospheric co2 concentration, *Global Change Biol.*, *15*, 1189–1200.

Williams, E. J., G. L. Hutchinson, and F. C. Fehsenseld (1992), NO_x and N_2O emissions from soil, *Global Biogeochem. Cycles*, *6*, 351–388.

Williams, R. (1995), Variants of low CO_2-emitting supply system (LESS) for the world: Prepared for the IPCC Second Assessment Report Working Group IIa, Energy Supply Mitigation Options, *Tech. Rep. PNL-IO851*, Pacific Northwest Laboratories.

Wilson, D., and S. Ballard (1999), A microphysically based precipitation scheme for the UK Meteorological Office Unified Model, *Q. J. Roy. Meteor. Soc.*, *125*, 1607–1636, doi:10.1256/smsqj.55706.

Woodward, F. I., T. M. Smith, and W. R. Emanuel (1995), A global land primary productivity and phytogeography model, *Global Biogeochem. Cycles*, *9*, 471–490.

World Meteorological Organization (Geneva, February 1979), The first world climate conference, 12-23 February 1979, Geneva, Switzerland, in *Confrence mondiale sur le climat: Confrence d'experts sur le climat et l'homme*.

Wu, M., M. Wang, and H. Huo (2006), Fuel-cycle assessment of selected bioethanol production pathways in the united states, *Tech. Rep. ANL/ESD/06-7*, Argonne National Laboratory, Energy Systems Division.

Wu, S., L. J. Mickley, D. J. Jacob, J. A. Logan, R. M. Yantosca, and D. Rind (2007), Why are there large differences between models in global budgets of tropospheric ozone?, *J. Geophys. Res.*, *112*, D05,302, doi:10.1029/2006JD007801.

Wu, S., L. J. Mickley, D. J. Jacob, D. Rind, and D. G. Streets (2008a), Effects of 2000–2050 changes in climate and emissions on global tropospheric ozone and the policy-relevant background surface ozone in the United States, *J. Geophys. Res.*, *113*, D18,312, doi:10.1029/2007JD009639.

Wu, S., L. J. Mickley, E. M. Leibensperger, D. J. Jacob, D. Rind, and D. G. Streets (2008b), Effects of 2000–2050 global change on ozone air quality in the United States, *J. Geophys. Res.*, *113*, D06,302, doi:10.1029/2007JD008917.

Yáñez Angarita, E. E., E. E. Silva Lora, R. E. da Costa, and E. A. Torres (2009), The energy balance in the palm oil-derived methyl ester (pme) life cycle for the cases in brazil and colombia, *Renewable Energy*, *34*, 2905–2913.

Yamamoto, H., J. Fujino, and K. Yamaji (2001), Evaluation of bioenergy potential with a multi-regional global-land-use-and-energy model, *Biomass & Bioenergy*, *21*, 185–203.

Yienger, J. J., and H. Levy II (1995), Empirical model of global soil-biogenic NO_x emissions, *J. Geophys. Res.*, *100*, 11,477–11,464.

Young, P., A. Arneth, G. Schurgers, G. Zeng, and J. A. Pyle (2009), The CO_2 inhibition of terrestrial isoprene emission significantly affects future ozone projections, *Atmos. Chem. Phys.*, *9*, 2793–2803.

Young, P. J. (2007), The influence of biogenic isoprene emissions of atmospheric chemistry: A model study for present and future atmospheres, Ph.D. thesis, University of Cambridge.

Zeldovich, Y. (1946), The oxidation of nitrogen in combustion and explosions, *Acta. Physiochim.*, *21*, 577–628.

Zeng, G., and J. A. Pyle (2003), Changes in tropospheric ozone between 2000 and 2100 modeled in a chemistry-climate model, *Geophys. Res. Lett.*, *30*, 1392, doi:10.1029/2002GL016708.

Zeng, G., and J. A. Pyle (2005), Influence of El Niño Southern Oscillation on stratosphere/troposphere exchange and the global tropospheric ozone budget, *Geophys. Res. Lett.*, *32*, L01814, doi:10.1029/2004GL021353.

Zeng, G., J. A. Pyle, and P. J. Young (2008), Impact of climate change on tropospheric ozone and its global budgets, *Atmos. Chem. Phys.*, *8*, 369–387.

Zhang, D., R. Zhang, and S. W. North (2003a), Experimental study of NO reaction with isoprene hydroxyalkyl peroxy radicals, *J. Phys. Chem. A*, *107*, 11,013–11,019.

Zhang, L., J. R. Brook, and R. Vet (2003b), A revised parametisation for gaseous dry deposition in air-quality models, *Atmos. Chem. Phys.*, *3*, 2067–2082.

Zhang, Y., X.-M. Hu, L. R. Leung, and W. I. Gustafson Jr. (2008), Impacts of regional climate change on biogenic emissions and air quality, *J. Geophys. Res.*, *113*, D18,310, doi:10.1029/2008JD009965.

Zhang, Y., X.-Y. Wen, K. Wang, K. Vijayaraghavan, and M. Z. Jacobson (2009), Probing into regional o3 and particulate matter pollution in the united states: 2. an examination of formation mechanisms through a process analysis technique and sensitivity study, *J. Geophys. Res.*, *114*, D22,305.

Ziemke, J. R., S. Chandra, B. N. Duncan, M. R. Schoeberl, O. Torres, M. R. Damon, and P. K. Bhartia (2009), Recent biomass burning in the tropics and related changes in tropospheric ozone, *Geophys. Res. Lett.*, *36*, L15,819, doi: 10.1029/2009GL039303.

Zimmer, W., R. Steinbrecher, C. Körner, and J.-P. Schnitzler (2003), The process-based SIM-BIM model: Towards more realistic prediction of isoprene emission from adult *Quercus petraea* forest trees, *Atmos. Environ.*, *37*, 1665–1671.

Zimmerman, P. R. (1979), Determination of emission rates of hydrocarbons from indigenous species of vegetation in the Tampa/St. Petersburg, Florida area. Appendix C. Tampa Bay area photochemical oxidant study, *Tech. rep.*, U.S. Environmental Protection Agency, Region IV, Atlanta, Georgia.